UNIVERSITY OF GENOVA

POLYTECHNIC SCHOOL

DIME

Department of Mechanical, Energy, Management and Transportation Engineering

MASTERS THESIS

IN

ENERGY ENGINEERING

Fuel Cell Applications in Land, Marine, and Aviation Sectors: An SOFC/GT System Case Study

Supervisor:

Chiar.mo Prof. Ing. Mario Luigi Ferrari

Co-Supervisor:

Dott. Ing. Dario Buzzola

Candidate:

Amir Hossein Forouzandeh

July 2026

UNIVERSITÀ DEGLI STUDI DI GENOVA

SCUOLA POLITECNICA

DIME

Dipartimento di Ingegneria Meccanica, Energetica, Gestionale e dei Trasporti

TESI DI LAUREA MAGISTRALE

IN

INGEGNERIA ENERGETICA

Applicazioni delle celle a combustibile nei settori terrestre, marino e aeronautico: un caso di studio su un sistema SOFC/GT

Relatore:

Chiar.mo Prof. Ing. Mario Luigi Ferrari

Correlatore:

Dott. Ing. Dario Buzzola

Allievo:

Amir Hossein Forouzandeh

luglio 2026

Fuel Cell Applications in Land, Marine, and Aviation Sectors: An SOFC/GT System Case Study

Abstract

The aim of this thesis is to develop and verify a physics-based numerical model of a hybrid Solid Oxide Fuel Cell–Gas Turbine (SOFC–GT) system for high-efficiency aerospace power generation under cruise operating conditions. The developed model integrates fuel processing, SOFC electrochemistry, combustion, heat exchangers, turbomachinery, and generator performance into a unified thermodynamic framework.

The model is formulated using mass, species, and energy conservation equations together with electrochemical relations for the SOFC stack, turbomachinery performance equations, heat-transfer models, and generator efficiency correlations to predict the coupled behaviour of the integrated hybrid system. The model was verified using three representative reference configurations covering different levels of system complexity. The first case reproduced a well-established baseline hybrid SOFC–GT architecture, the second evaluated the robustness of the methodology for a modified system configuration with different fuel representation and thermal integration, and the third assessed the model under a $1\ MW$ cruise-condition operating scenario representative of aerospace applications.

For all verification cases, the predicted thermodynamic, electrochemical, and overall system performance parameters agreed with the published reference data, with errors below 1%. Under cruise operating conditions, the verified model predicts a global electrical efficiency of approximately 70%, indicating that the improvement in overall performance is primarily achieved through effective waste-heat recovery and thermodynamic integration between the SOFC and gas turbine subsystems. The proposed framework therefore provides a reliable and physically consistent basis for the analysis and future optimization of hydrogen-fuelled hybrid SOFC–GT systems for aerospace applications.

Acknowledgements

I would like to express my sincere gratitude to everyone who supported me throughout the completion of this thesis. First and foremost, I am deeply grateful to my thesis advisor, Prof. Ing. Mario Luigi Ferrari, for his unwavering support, invaluable guidance, patience, and encouragement throughout every stage of this research. His expertise and constructive advice have been instrumental in the successful completion of this thesis.

I would also like to express my sincere appreciation to all the professors at the Department of Mechanical, Energy, Management and Transportation Engineering (DIME), University of Genoa, whose knowledge, academic rigor, and inspiring teaching have greatly contributed to my academic and professional development. Their guidance and challenging discussions have played a significant role in shaping my research skills and critical thinking abilities.

My sincere thanks also go to my family and friends for their unconditional love, patience, encouragement, and continuous support throughout my academic journey. Their belief in my abilities has been a constant source of strength and motivation.

Finally, I acknowledge the contributions of everyone who assisted me during this work. Any errors or omissions that remain are entirely my own responsibility.

به نام خداوند جان و خرد

کزین برتر اندیشه برنگذرد

خداوند نام و خداوند جای

خداوند روزی ده رهنمای

حکیم ابولقاسم فردوسی

Table of Contents

Abstract……………………………..……………..…………………….....**I**

Acknowledgement…………………….……………………………….…………**II**

List of figures & tables………………………………………….………………VI

1. Introduction..**1**

2. Fuel Cells: Toward Future Energy Solutions...**9**

2.1 Thermodynamic and Electrochemical Principles of Fuel Cells 12

2.2 Fuel Cell Performance Behaviour and Operating Conditions 14

3. Hybridization and System Integration of Fuel Cell Systems **16**

3.1 System-level Motivation for Hybridization..16

3.1.1 Role of Hybridization in Fuel Cell Systems 16

3.1.2 Definition Of Hybrid Architectures in Fuel Cell Systems..............................17

3.2 Functional Classification of Fuel Cell Hybrid Architectures 17

3.2.1 Electrochemical–Thermal Hybrid Systems 18

3.2.2 Electrochemical–Electrical Hybrid Systems 18

3.2.3 Electrochemical–Mechanical Coupling Systems..19

3.3 PEMFC Electrical Hybridization Power Flow and Operational Behaviour........20

3.3.1 Power Flow-Oriented System Representation..21

3.3.2 Limitations of PEMFC Hybridization 22

3.4 High-Temperature Fuel Cells for Hybrid Systems (MCFC vs SOFC)...............22

3.5 MCFC–Gas Turbine Hybrid Systems...23

3.5.1 Thermodynamic Limitations of MCFC–GT Hybrid Systems 25

3.5.2 Parametric Performance Analysis of MCFC–GT Systems.............................26

3.5.3 Operational and Control Challenges of MCFC–GT Hybrid Systems 27

3.6 SOFC–Gas Turbine Hybrid Systems configurations..28

3.6.1 Thermodynamic behaviour of SOFC-based hybrid systems 28

3.6.2 High-Temperature Operation and Exhaust Energy Potential 29

3.6.3 System-Level Integration, Design, and Performance of SOFC–GT Hybrid Systems 30

3.6.4 System Architecture and Configuration of SOFC–Gas Turbine Hybrids 31

3.6.5 Pressurization Strategies and Turbomachinery Integration 34

3.6.6 Thermodynamic Coupling and Energy Integration Mechanisms 36

3.6.7 System Performance, Efficiency, and Design Trade-offs...............................38

3.6.8 Application of SOFC–Gas Turbine Hybrid Systems in Transport 38

3.6.9 From Thermodynamic Advantage to System-Level Application of SOFC–GT and MCFC Hybrid Systems 50

3.6.10 Advanced SOFC Architectures and Emerging Concepts 52

4. Case-Study-Based Comparative Analysis of PEMFC and SOFC/GT Hybrid Systems in Marine and Aeronautical Applications **57**

4.1 Marine sector case studies 57

4.1.1 Case Study A -SF-BREEZE (high-speed PEMFC ferry as an extreme feasibility benchmark) 57

4.1.2 Case Study B -Methanol HT-PEMFC marine propulsion (a small-vessel architecture optimized around fuel logistics rather than maximum efficiency) 60

4.1.3 Case Study C – MCFC-Based Hybrid Propulsion Systems for Liquefied Hydrogen Tankers..63

4.1.4 Case Study D-SOFC/GT hybridization as the thermodynamic reference case for high-efficiency marine power 68
4.2 Comparative Discussion of Marine Systems 71
4.3 Aeronautical Case Studies 72
4.3.1 Case Study A - PEMFC-based Auxiliary Power Unit (APU) 73
4.3.2 Case Study B -SOFC/GT-based Auxiliary Power Unit (APU) 77
4.3.3 Case Study C –SOFC/GT Hybrid System for Primary Propulsion in Aircraft 80
4.4 Aeronautical Comparative Analysis PEMFC vs SOFC/GT Systems 83
4.4.1 Fuel Choice and configuration Trade-offs 84
4.5 Numerical Methodology and Simulation Framework 87
5. Numerical Methodology and System Modelling 89
5.1 Selection of the Reference Architecture and Verification Strategy 89
5.1.1 NASA SOFC–GT Architecture as the Primary Verification Reference 89
5.1.2 Distinction Between the Verification Reference and the Computational Tool of the Present Study 90
5.1.3 Role of the Wilson et al. Study in Model Extension and Trend Verification 90
5.2 System Architecture Definition and Overall Diagrams Used in This Study 91
5.2.1 Conceptual System Architecture Based on the NASA SOFC–GT Schematic 92
5.2.2 Application-Oriented SOFC–GT APU Layout Proposed by Eelman et al. 93
5.2.3 Process-Level System Representation Using the ProMax Flowsheet 94
5.3 Definition of Main Flow Paths and State Points 96
5.3.1 Definition of Main Flow Paths 97
5.3.2 Definition of State Points and Thermodynamic Variables 100
5.4 Modelling Assumptions and Simplifications 103
5.5 Governing Equations of System Components 104
5.5.1 Fuel Processing and Reformer Mass Balance 104
5.5.2 SOFC Anode Mass Balance and Fuel Utilization 106
5.5.3 SOFC Electrochemical Model 108
5.5.4 Combustor Energy Balance 113
5.5.5 Heat Exchanger Modelling 114
5.5.6 Gas Turbine Modelling and Performance Analysis 118
5.5.7 Generator Model and Electrical Power Output 121
6. Model Verification and Comparative Performance Analysis 124
6.1 Verification Against the NASA Baseline Configuration 124
6.1.1 NASA Verification Case and Operating Conditions 124
6.1.2 Electrochemical Verification 127
6.1.3 Component Thermodynamic Verification 128
6.1.4 Global System Performance Verification 129
6.1.5 Internal Consistency Verification 130
6.2 Verification Against the Eelman Hybrid SOFC–GT Model 131
6.2.1 Reformer Inlet Conditions and Fuel Representation 131
6.2.2 Electrochemical Performance Verification of the SOFC Stack 132
6.2.3 Turbomachinery Performance and System-Level Energy Closure under the Eelman Configuration 133
6.2.4 Structural Robustness of the Model under Modified Fuel Representation 135
6.3 Verification and System-Level Performance Evaluation of the 1-MW ProMax SOFC–GT Configuration under Cruise Conditions 136
6.3.1 Operating Scenario Definition and Boundary Conditions 136

6.3.2 Thermodynamic Reconstruction of the Gas Path 138
6.3.3 Electrochemical Operating State under ProMax Conditions 140
6.3.4 SOFC Stack Energy Balance under ProMax Conditions 141
6.3.5 Turbine–Generator Power Coupling under ProMax Cruise Conditions 142
6.3.6 System-Level Electrical Performance of the Hybrid Configuration 144
6.3.7 Verification and Physical Consistency Assessment of the Hybrid Model 144
6.3.8 Thermodynamic Hierarchy and Hybridization Insight 145
6.4 Comparative Performance Assessment 146
6.5 Overall System Performance and Physical Interpretation 148
7. Conclusions 149
8. Bibliography 151

List of figures

Figure 1-1 Global greenhouse gas emissions by sector [5]. 1

Figure 1-2 Global energy demand and fossil fuel consumption trends under the STEPS scenario [6]. 2

Figure 1-3 Overview of the global energy system, including energy supply, consumption sectors, and emissions under different scenarios [12]. 4

Figure 1-4 Projected evolution of low-emission electricity generation capacity by source from 2010 to 2050 [6]. 5

Figure 2-1 Fuel Cell Technologies Overview [21]. 12

Figure 2-2 Typical fuel cell polarization curve showing the contributions of activation, ohmic, and concentration losses to the overall voltage drop [24]. 13

Figure 2-3 Voltage–power characteristics of a fuel cell as a function of current density, illustrating the trade-off between electrical efficiency and power output [21]. 15

Figure 3-1 Power flow architecture of a PEMFC–battery hybrid system, including the fuel cell stack, lithium-ion battery, DC/DC converters, and energy management system (EMS), illustrating the distribution of power and control signals [36]. 21

Figure 3-2 Schematic Configuration and System Operation of MCFC–GT Hybrid Systems [43]. 24

Figure 3-3 Schematic representation of SOFC–gas turbine hybrid configurations: (a) bottoming cycle, where the gas turbine recovers energy from SOFC exhaust; (b) topping cycle, where compressed air from the compressor is supplied to the SOFC; (c) pressurized SOFC–GT system, where the fuel cell operates within the pressurized turbine loop [51-53]. 32

Figure 3-4 Pressurization Comparison of SOFC Configurations with Turbocharger and Microturbine [58, 59]. 34

Figure 3-5 Integrated SOFC-based trigeneration system for marine applications, including power generation, heat recovery, cooling, and freshwater production subsystems. The configuration illustrates the coupling between the SOFC stack, gas turbine, and auxiliary thermal cycles [70]. 41

Figure 3-6 Aircraft mission power profile highlighting steady cruise conditions for SOFC/GT hybrid operation [81]. 46

Figure 3-7 Power distribution between SOFC and gas turbine in a hybrid SOFC–GT system under a representative aeronautical mission profile [46]. 48

Figure 3-8 Efficiency profile of a hybrid SOFC–GT system under a representative aeronautical mission, highlighting high-efficiency operation during cruise and the impact of transient load variations on system performance [46]. 49

Figure 3-9 structural distinction between classical electrolyte-based SOFCs and emerging electrolyte-free architectures [84]. 52

Figure 3-10 Schematics of (a) dual-chamber SOFC, (b) single-chamber SOFC, and (c) no-chamber SOFC [84]. 53

Figure 3-11 Comparison of electrolyte-supported and anode-supported micro-tubular SOFC configurations [62]. 55

Figure 4-1 Propulsion power demand profile along the mission, showing different operating phases (legs) and corresponding load variations [87]. 60

Figure 4-2 Dynamic response of the HT-PEMFC system to step changes in current demand, compared with the reference signal [88]. 61

Figure 4-3 Schematic layouts of the MCFC-GT and MCFC-ST hybrid propulsion systems for an $LH2$ tanker [89]. 64

Figure 4-4 Thermal integration of the SOFC with the reformer and tail heat recovery system [82]. 69

Figure 4-5 Baseline aircraft mission profile showing the different flight phases and corresponding variations in auxiliary power demand [90]. 73

Figure 4-6 Load profile used for PEMFC APU simulation [90]. 74

Figure 4-7 Detailed PEMFC system architecture for aeronautical APU applications, including hydrogen supply, air compression, humidification, and thermal management subsystems [90]. 74

Figure 4-8 Variation of cell efficiency and power density as a function of current density, highlighting the optimal operating range of PEMFC systems [90]. 75

Figure 4-9 Representative configurations of SOFC-integrated hybrid propulsion systems for aeronautical applications, highlighting alternative strategies for coupling electrochemical energy conversion with Brayton-cycle processes: (a) baseline SOFC-integrated turbojet configuration; (b) thermally integrated configuration with extended exhaust energy utilization; (c) fuel-flexible configuration with distributed fuel injection and enhanced operational adaptability [91]. 78

Figure 4-10 SOFC/GT configuration represent by Mashamba [97]. 81

Figure 4-11 architecture-level mass breakdown as a function of mission duration for PEMFC and SOFC-based propulsion systems under different fuel options [47]. 85

Figure 5-1 NASA's NPSS SOFC/GT hybrid system architecture [93]. 92

Figure 5-2 SOFC-GT APU system design as presented by Eelman et al [95]. 93

Figure 5-3 SOFC-GT system flowsheet in ProMax [95]. 94

Figure 5-4 The Air Path of SOFC/GT Hybrid System [99]. 97

Figure 5-5 The Fuel and Reformate Path of SOFC-GT Hybrid System [99]. 98
Figure 5-6 Solid Oxide Fuel Cell Model [99]. 99
Figure 5-7 Heat Exchanger Network for Air and Water Preheating [99]. 100
Figure 5-8 Mass balance of the SOFC fuel processing subsystem [99]. 105
Figure 5-9 Schematic of the solid oxide fuel cell [99]. 106
Figure 5-10 Combustor control volume and associated inlet and outlet state points [99]. 113
Figure 5-11 Schematic representation of the air–air heat exchanger with inlet and outlet state points [99]. 115
5-12 Schematic representation of the air–Water heat exchanger with inlet and outlet state points [93]. 117
5-13 Schematic representation of the gas turbine and generator within the SOFC–GT hybrid system [93]. 118
Figure 6-1 Hierarchical distribution of fuel chemical energy under cruise conditions, normalized with respect to fuel lower heating value (LHV). 145
Figure 6-2 Comparison of the global electrical efficiency predicted by the present model with the ProMax reference (Wilson et al.) 146
Figure 6-3 Error of key performance indicators relative to the ProMax reference configuration. 147

List of Tables

Table 2-1 Comparative Technical Characteristics of Major Fuel Cell Technologies [21]. 10

Table 3-1 Comparative Evaluation of SOFC–GT Architectures [51-53]........33

Table 3-2 Engineering comparison of turbocharger-based and microturbine-based SOFC hybrid systems [50, 57, 61, 62]........36

Table 3-3 Comparison of Energy and Heat Integration Strategies in SOFC–GT Hybrid Systems [28, 64, 66]. 37

Table 3-4 Comparative assessment of fuel pathways for marine SOFC/GT hybrid systems based on efficiency, storage characteristics, and application suitability [69-71, 76]. .44

Table 3-5 Exergy-based comparative analysis of MCFC–GT and SOFC–GT hybrid systems [41, 81-83]........51

Table 3-6 Comparative Overview of SOFC Structural Configurations [84]........54

Table 4-1 Key design and operational parameters of the SF-BREEZE case study [86]. 59

Table 4-2 Main design and operating characteristics of the methanol HT-PEMFC marine propulsion system [87]........63

Table 4-3 Key performance characteristics of the MCFC-GT and MCFC-ST systems[89]. 66

Table 4-4 Performance characteristics of the SOFC/GT hybrid system [82].........70

Table 5-1 Definition of State Points and Associated Thermodynamic Variables for NASA's NPSS SOFC/GT hybrid system architecture [99]........102

Table 5-2 Electrochemical parameters used in the SOFC model [99]. 111

Table 6-1 Input operating conditions and calculated performance of the compressor and air–air heat exchanger pathway from combustor [93]. 125

Table 6-2 Heat duty distribution and outlet conditions of the air–water heat exchanger [93]. 125

Table 6-3 Operating conditions and performance of the gas turbine [93].........126

Table 6-4 Turbine shaft power and generator electrical output [93]. 126

Table 6-5 Electrochemical performance comparison with NASA reference. 127

Table 6-6 Thermodynamic components of compressor and turbine verification against NASA reference.........128

Table 6-7 Global electrical performance comparison with NASA reference.........129

Table 6-8 Reformer inlet conditions – Eelman case [95]. 131

Table 6-9 Electrochemical performance comparison under Eelman configuration. 132
Table 6-10 Turbomachinery and global performance under Eelman configuration. 134
Table 6-11 Operating conditions and boundary parameters for the 1-MW ProMax case. 137
Table 6-12 Thermodynamic reconstruction of the turbomachinery block (1-MW ProMax case). 139
Table 6-13 Electrochemical operating point of the SOFC under ProMax conditions. 141
Table 6-14 SOFC energy balance and performance indicators – ProMax case. 142
Table 6-15 Turbine and generator performance under ProMax cruise conditions. 143
Table 6-16 Overall hybrid system electrical performance at cruise condition. 144

Nomenclature

Symbol	Description	Unit
$\dot{m}$	Mass flow rate	$\frac{kg}{s}$
$\dot{Q}$	Heat transfer rate	kW
$\dot{W}$	Power	kW
h	Specific enthalpy	$\frac{kJ}{kg}$
C_p	Specific heat capacity	$\frac{kJ}{kg.K}$
$\dot{n}$	Molar flow rate	$\frac{mol}{s}$
T	Temperature	K
P	Pressure	bar
η	Efficiency	$[-]$
LHV	Lower heating value	$\frac{kJ}{kg}$
A	Active cell area	m^2
Ai, Bi, Ci, Di, E	Shomate polynomial coefficients	$[-]$
$C_{p,mix}$	Mixture specific heat capacity	$\frac{kJ}{kg.K}$
F	Faraday constant	$\frac{C}{mol}$
g	Gibbs free energy	$\frac{kJ}{mol}$
h_f°	Standard enthalpy of formation	$\frac{kJ}{mol}$

i	Current density	$\frac{A}{cm^2}$
I	Electric current	A
k	Specific heat ratio	$[-]$
M	Molecular weight	$\frac{kJ}{kmol}$
P_{el}	Electrical power	kW
R	Universal gas constant	$\frac{kJ}{kmol.K}$
R_{mix}	Mixture gas constant	$\frac{kJ}{kg.K}$
$S/_C$	Steam-to-carbon ratio	$[-]$
$O/_C$	Oxygen-to-carbon ratio	$[-]$
TIT	Turbine inlet temperature	K
U	Cell voltage	V
U_{rev}	Reversible voltage	V
x_i	Mole fraction	$[-]$
y_i	Mole fraction	$[-]$
z	Number of transferred electrons	$[-]$
η_t	Turbine isentropic efficiency	$[-]$
η_c	Compressor efficiency	$[-]$
η_{gen}	Generator efficiency	$[-]$

η_{SOFC}	Fuel-to-electric efficiency	$[-]$
$\eta_{overall}$	Overall stack efficiency	$[-]$
η_{global}	Global electrical efficiency	$[-]$
β	Pressure ratio	$[-]$
ε	Heat exchanger effectiveness	$[-]$
σ	Electrical conductivity	$\frac{S}{m}$

Acronyms

Proton Exchange Membrane Fuel Cells	PEMFCs
Solid Oxide Fuel Cells	SOFCs
Solid Oxide Fuel Cell–Gas Turbine	SOFC–GT
United Nations Framework Convention on Climate Change	UNFCCC
Nationally Determined Contributions	NDCs
Polymer Electrolyte Fuel Cells	PEFC
Alkaline Fuel Cells	AFC
Phosphoric Acid Fuel Cells	PAFC
Molten Carbonate Fuel Cells	MCFC
combined heat and power	CHP
yttria-stabilized zirconia	YSZ
internal combustion engines	ICEs
nitrogen oxides	$N0_x$
Direct Methanol Fuel Cells	DMFCs
International Maritime Organization	IMO
International Civil Aviation Organization	ICAO
sulfur oxide	S0x
liquefied natural gas	LNG
auxiliary power units	APUs
balance of plant	BOP
Low-Temperature PEMFCs	LT-PEMFCs
High-Temperature PEMFCs	HT-PEMFCs
sulfonated poly ether ether ketone	SPEEK
Computational fluid dynamics	CFD
uninterruptible power supplies	UPS
membrane–electrode assembly	MEA
perfluoro sulfonic acid	PFSA

$La_{0.6}Sr_{0.4}CO_{0.2}Fe_{0.8}$	LSCF
direct-flame fuel cell	DFFC
High-Temperature	HT-SOFCs
Intermediate-Temperature	IT-SOFCs
Low-Temperature	LT-SOFCs
scandia-stabilized zirconia	ScSZ
Lower Heating Value	LHV
Open circuit voltage	OCV
Lanthanum Strontium Manganite	LSM
Lanthanum Strontium Cobalt Ferrite	LSCF
Barium Strontium Cobalt Ferrite	BSCF
mixed ionic–electronic conductivity	MIEC
electrolyte-supported SOFC	ES-SOFC
Anode-Supported SOFCs	AS-SOFCs
Emission Control Areas	ECAs
Energy management systems	EMS
diesel generators	DGs
Organic Rankine Cycle	ORC
Levelized cost of electricity	LCOE
liquid hydrogen	LH_2
specific fuel consumption	SFC
gross take-off weight	GTOW
unmanned aerial vehicles	UAVs
multi-objective optimization	MOO
hybrid fuel cell–gas turbine	FC–GT
waste-heat-recovery	WHR
catalytic combustion burner	CCB
turbine inlet temperature	TIT
micro gas turbine	mGT

catalytic partial oxidation	CPOX
Energy Efficiency Design Index	EEDI
environmental control	ECS
partial oxidation	PrOx
air split ratio	As
fuel utilisation	Uf
Numerical Propulsion System Simulation	NPSS
Effectiveness–Number of Transfer Units method	ε–NTU
fuel-to-electric efficiency	FTE
gadolinium-doped ceria	GDC
energy storage systems	ESS
boil-off gas	BOG
Energy Efficiency Design Index	EEDI

1. Introduction

The global energy system is undergoing a significant transition driven by the urgent need to reduce greenhouse gas emissions and mitigate the increasing impacts of climate change. In this context, the transportation sector represents one of the largest sources of greenhouse gas emissions worldwide and is therefore under increasing pressure to transition toward more sustainable energy sources. Although electrification has made considerable progress in road transportation, battery-based systems still remain limited for applications requiring high energy density and long operational lifetimes [1, 2].

This limitation is particularly evident in heavy-duty land transport, maritime shipping, and aviation, where performance constraints make full electrification difficult to achieve, both technically and economically. In these sectors, efforts to reduce carbon emissions must balance strict operational requirements such as long range, reliability, and high power demand, while climate targets continue to become more ambitious. This has driven research toward alternative energy carriers, and advanced propulsion concepts have become a major focus in energy and transport, aiming to reduce emissions without compromising system performance [3, 4]. The distribution of greenhouse gas emissions across different sectors is illustrated in Figure 1-1 [5].

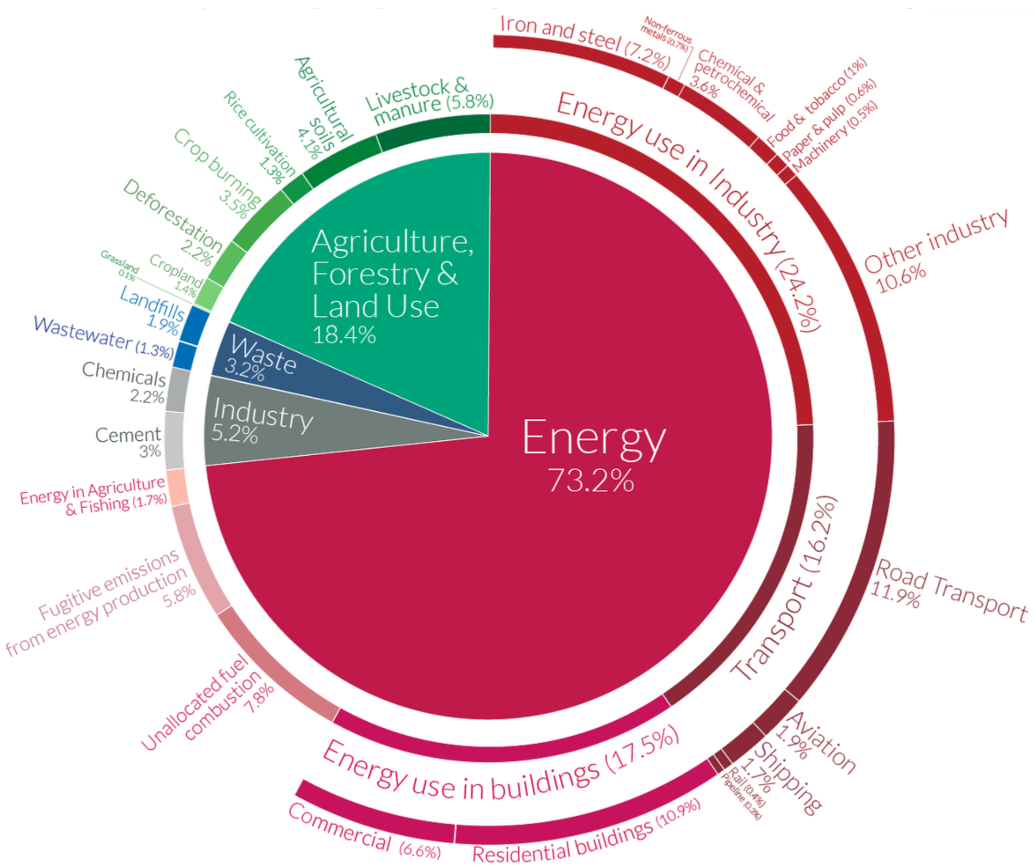

Figure 1-1 Global greenhouse gas emissions by sector [5].

Figure 1-1 illustrates the distribution of global greenhouse gas emissions by sector. The energy sector is the dominant contributor, accounting for approximately 73.2% of total global emissions. Within this sector, energy use in industry represents the largest share, followed by buildings (17.5%) and transport (16.2%). These results highlight the central role of energy systems in climate change mitigation and emphasize the importance of targeting energy-related emissions in order to achieve meaningful global reductions [5].

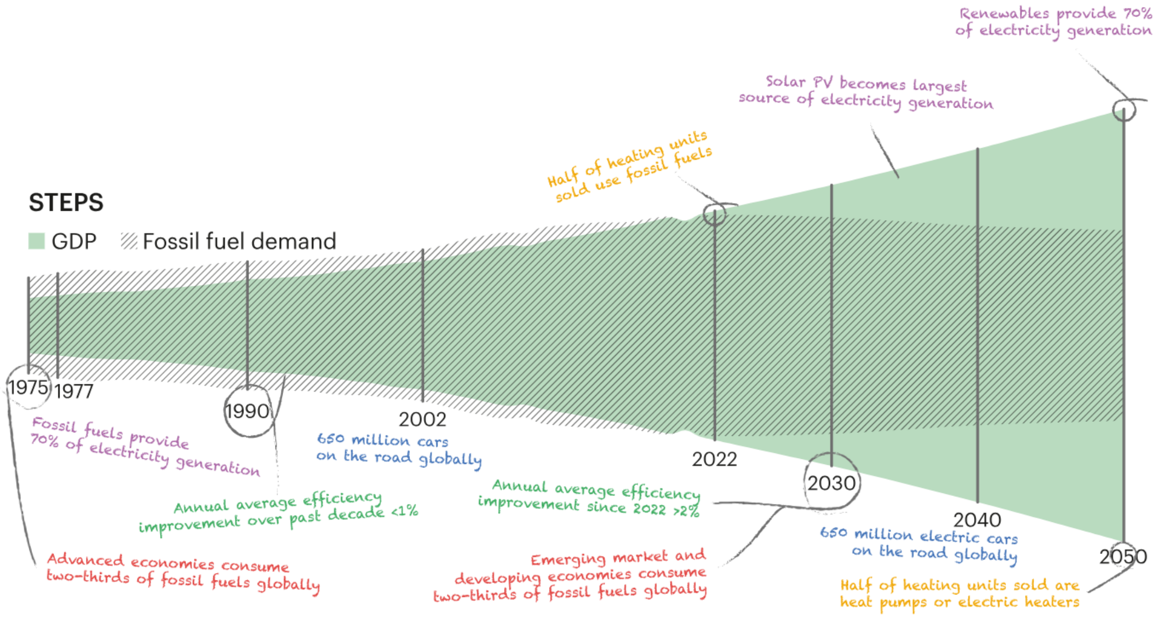

Figure 1-2 Global energy demand and fossil fuel consumption trends under the STEPS scenario [6].

Considering this situation, it is important to try to forecast future energy scenarios providing further insight into the expected evolution of the global energy system in the coming decades [6]. So, Figure 1-2 shows the projected trends of global energy demand, fossil fuel consumption, and economic growth under the Stated Policies Scenario (STEPS). In this context, Gross Domestic Product (GDP) is used as an indicator of global economic activity, reflecting the overall growth of the world economy. The figure highlights that, while continued economic growth, fossil fuel demand is expected to stabilize or gradually decline under current policy scenarios. This trend suggests a partial decoupling between economic growth and fossil fuel consumption, driven by improvements in energy efficiency and the increasing contribution of renewable energy sources [6].
To invert the environmental effect of fossil fuel utilization, over the past few decades, the architecture of international climate policy has gradually shifted from a system based mainly on binding commitments for industrialized countries toward a broader and more inclusive global framework. An important early milestone in this process was the Kyoto Protocol, adopted in 1997 under the United Nations Framework Convention on Climate Change (UNFCCC) and entering into force in 2005 after receiving the required number of ratifications [7]. The Protocol represented the first legally binding international agreement aimed at reducing greenhouse gas emissions. It introduced quantified emission reduction targets for industrialized countries and economies in transition, commonly referred to as

Annex I Parties. These countries were assigned binding emission reduction commitments under the Protocol, with more specific targets defined for those listed in Annex B [7]. The Kyoto Protocol was implemented through two commitment periods: the first (2008–2012), which required participating developed countries to reduce emissions by an average of approximately 5% compared to 1990 levels, and the second (2013–2020), which introduced more ambitious targets of at least 18% below 1990 levels. These targets could be achieved through both domestic mitigation measures and international flexibility mechanisms, including emissions trading [7].

Despite its foundational role, the effectiveness of the Kyoto framework was limited by its restricted geographical scope, as binding commitments applied only to developed countries. This significantly reduced its overall impact on global emissions, particularly in light of the increasing contribution of developing and emerging economies. To address these limitations and the evolving global emissions landscape, the Paris Agreement was adopted in 2015 and entered into force in 2016, marking a fundamental shift toward a more inclusive and flexible global climate governance framework [8]. In contrast to the Kyoto Protocol, the Paris Agreement established a universal structure in which all Parties commit to climate mitigation and adaptation efforts, taking into account their national circumstances and capabilities. Its long-term objectives include limiting the increase in global average temperature to well below 2 $°C$ above pre-industrial levels, while pursuing efforts to restrict warming to $1.5\ °C$ [8].

Additional objectives include enhancing adaptive capacity, strengthening climate resilience, aligning financial flows with low-emission development pathways, and improving transparency and accountability in climate action. A key innovation of the Paris Agreement is the introduction of Nationally Determined Contributions (NDCs), through which each country defines and periodically updates its climate action plan. These contributions follow a five-year cycle designed to progressively increase ambition over time, supported by a strengthened transparency framework and collective assessment mechanisms such as the Global Stocktake process. The implementation of this framework has been further detailed through the Paris Rulebook, adopted at COP24 and finalized at COP26, which establishes common guidelines for reporting, monitoring, and review. More recently, the first Global Stocktake, concluded at COP28, led to the adoption of the UAE Consensus, which emphasizes the need to transition away from fossil fuels while promoting near-term actions such as tripling renewable energy capacity and doubling the rate of energy efficiency improvements by 2030 [9-11].

However, despite these institutional advancements, substantial gaps persist between pledged commitments and observed emission trajectories. Recent assessments indicate that current NDCs remain collectively insufficient to achieve the temperature goals of the Paris Agreement, particularly the objective of limiting global warming to $1.5\ °C$. This shortfall reflects structural challenges within the global energy system, including the continued expansion and lock-in of fossil fuel systems in several major economies and the inertia associated with carbon-intensive infrastructure. Furthermore, geopolitical tensions, energy security concerns, and recent global crises have, in several instances, led to policy reversals or delays in decarbonization efforts, thereby complicating coordinated international action. Ultimately, the effectiveness of international climate frameworks depends on transformations within the global energy system. Therefore, understanding its structure, including energy supply, sectoral consumption, and associated emissions, is essential [9-11].

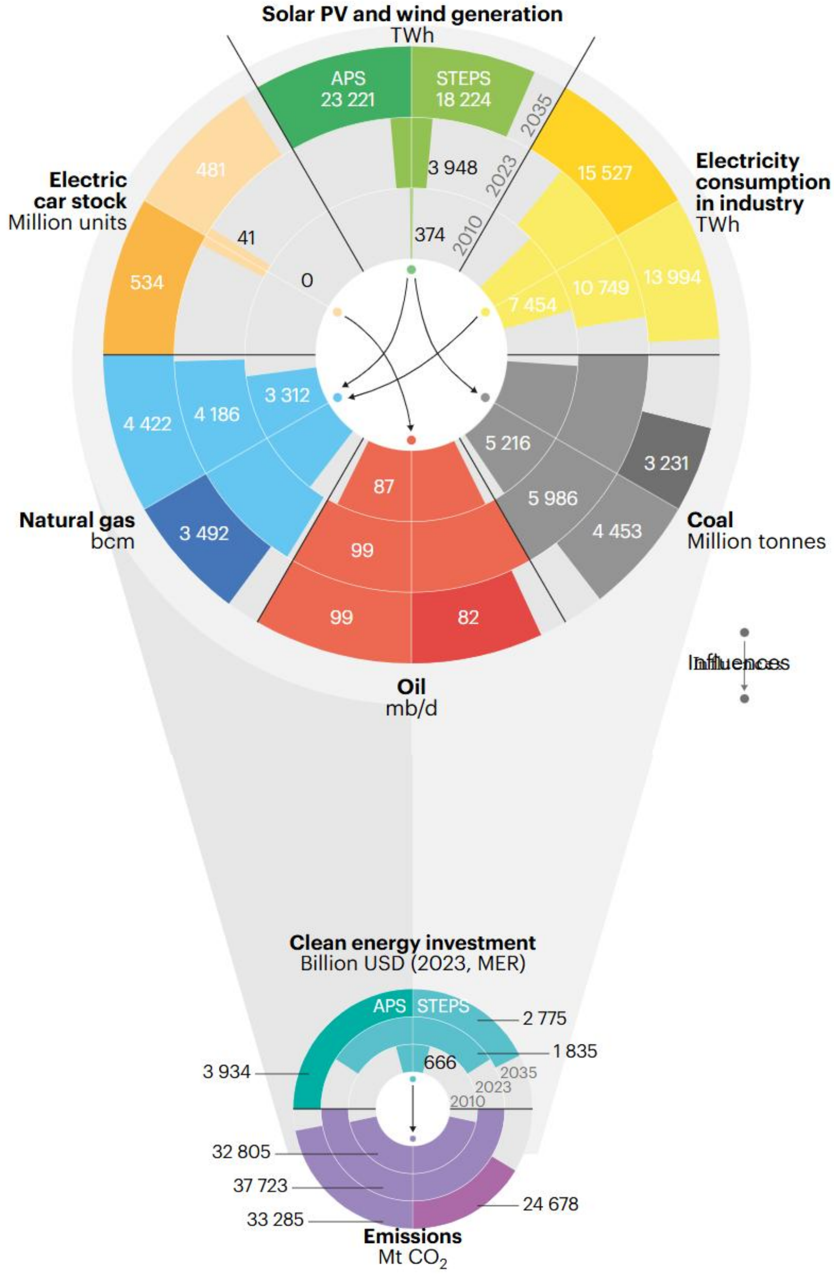

Figure 1-3 Overview of the global energy system, including energy supply, consumption sectors, and emissions under different scenarios [12].

Due to the impact of the different climate actions and restrictions, Figure 1–3 provides a comprehensive representation of the global energy system, systematically illustrating the interactions among primary energy sources, end-use sectors, and associated emissions. Within this framework, fossil fuels namely oil, natural gas, and coal continue to dominate the global energy supply, maintaining a central role particularly in energy-intensive sectors such as transportation and industry [12].

Although renewable energy technologies have expanded rapidly, their current share remains insufficient to fully replace fossil fuels in the short term. This limitation is driven not only by technological and infrastructural constraints, but also by the inherent complexity of the energy system itself. The global energy system is characterized by the coexistence of multiple energy carriers, extensive distribution networks, and strong interdependencies across sectors, making the transition toward deep decarbonization a multifaceted and systemic challenge [12].

Against this background, alternative energy carriers most notably hydrogen are increasingly recognized as strategic solutions for reducing greenhouse gas emissions. Hydrogen is particularly relevant for sectors where direct electrification is technically or economically challenging, including heavy-duty transport, aviation, and maritime applications. Fuel cell technologies, which enable the efficient conversion of hydrogen chemical energy into electricity, play a pivotal role in this transition and are widely regarded as key components of future sustainable energy systems. These aspects are further discussed in the following sections. Looking ahead, projections indicate that the global energy system is likely to undergo significant structural transformations. These changes are expected to include a substantial increase in the share of low-carbon energy sources, the development of advanced energy infrastructures, and a fundamental reconfiguration of consumption patterns across sectors [12].

Nevertheless, a substantial gap remains between declared climate ambitions and the pace of real-world implementation. This gap is particularly evident in sectors characterized by high energy demand, long asset lifetimes, and limited decarbonization options, underscoring the need for scalable and technically viable low-carbon solutions capable of delivering significant emissions reductions within the current decade [13, 14].

In response to these challenges, achieving deep decarbonization requires a broad portfolio of energy technologies capable of addressing the diverse characteristics of different sectors. In particular, transportation systems including ground mobility, maritime shipping, and aviation pose significant challenges due to their high energy demand, long operational ranges, and reliance on energy-dense fuels. In these sectors, decarbonization cannot rely on a single solution, but instead requires a combination of electrification, sustainable fuels, energy efficiency improvements, and advanced energy conversion technologies [15].

Although deep decarbonization remains complex at the system level, the electricity sector is expected to transition more rapidly toward low-emission energy sources. In this regard, Figure 1-4 illustrates the projected evolution of low-emission electricity generation capacity by source from 2010 to 2050 [6].

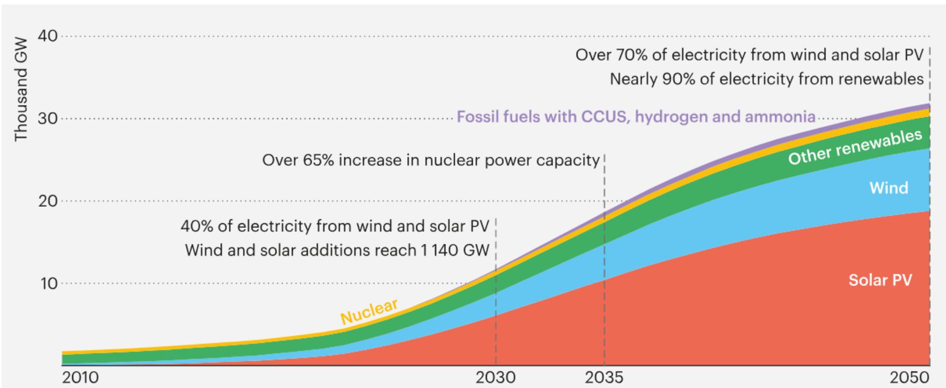

Figure 1-4 Projected evolution of low-emission electricity generation capacity by source from 2010 to 2050 [6].

Renewable energy technologies are expected to expand significantly, with solar photovoltaic (PV) and wind power emerging as the dominant contributors to future electricity generation. In particular, solar PV is projected to experience the most substantial growth, followed by wind energy, driven by ongoing cost reductions and large-scale deployment worldwide. Alongside renewables, nuclear energy continues to play a supporting role in providing low-carbon baseload power, while other emerging technologies such as hydrogen-based systems and fossil fuels with carbon capture, utilization, and storage (CCUS) contribute to the diversification of the low-emission energy mix. These trends indicate a progressive shift away from conventional fossil fuel-based electricity generation toward a more sustainable and decarbonized energy system [6]. This transition, however, remains uneven across sectors. While electrification can effectively decarbonize certain applications, several sectors particularly heavy transport, aviation, and maritime shipping continue to face significant limitations due to their high energy density requirements and operational constraints. Under these conditions, hydrogen-based energy systems, supported by fuel cell technologies, offer a promising pathway to complement electrification and enable deep decarbonization in sectors where the direct use of electricity is not feasible [6].

Building on this perspective, hydrogen has emerged as a central energy carrier for the energy transition. Rather than being a primary energy source, hydrogen acts as an energy vector, enabling the storage and transport of energy produced from other sources and supporting sector coupling through Power-to-X pathways that link electricity generation with transport and industrial applications. Hydrogen can be produced through multiple pathways, each with distinct environmental implications. When derived from fossil fuels, its climate performance depends strongly on the effectiveness of carbon capture technologies, whereas production via water electrolysis powered by renewable electricity enables a near-zero-carbon fuel cycle. At the same time, the variability of renewable energy sources introduces system-level challenges related to balancing, storage, and infrastructure integration [16].

A wide range of technologies support the utilization of hydrogen across the energy system, including combustion-based applications, synthetic fuel production, and electrochemical energy conversion. Among these, fuel cells offer an efficient pathway for converting hydrogen into electricity without combustion, making them particularly attractive for applications where conventional electrification is constrained. Their key advantages include high conversion efficiency, modularity, and the potential for low-emission operation when coupled with low-carbon hydrogen supply, supporting their growing relevance in future energy systems [15, 16].

From this perspective, hybrid energy systems combining fuel cells with batteries and advanced power management architectures have gained increasing attention as both a transitional and potentially long-term pathway. In such configurations, fuel cells can contribute not only to CO_2 emission reduction but also to improvements in overall system efficiency, operational flexibility, and energy diversification [11, 17]. Building on the previous discussion, fuel cell technologies have been widely investigated as efficient solutions for low-carbon energy conversion. Fuel cells convert the chemical energy of hydrogen directly into electricity through electrochemical reactions, avoiding combustion and thereby significantly reducing pollutant emissions. One important performance indicator of these systems is the fuel-to-electric efficiency, which represents the ratio between the electrical energy produced and the chemical energy contained in the fuel. Fuel cell systems were initially developed primarily for stationary power generation, where operating conditions are relatively stable and system integration can be optimized. In many stationary installations, fuel cells are integrated into combined heat and power (CHP) systems, allowing both electricity and useful heat to be recovered. This configuration can achieve high overall system efficiencies and has demonstrated the technical feasibility and reliability of fuel cell technologies in real energy infrastructures [18].

Building on this established foundation, fuel cells have increasingly attracted attention for energy and transport applications, where they enable high-efficiency electrochemical conversion with substantially lower pollutant emissions than combustion-based systems. In particular, their deployment has been widely explored in terrestrial and marine transport, where high energy demand and long operating durations require efficient and reliable power generation solutions. In such applications, fuel cells are typically integrated within advanced powertrains, combining electrochemical conversion with complementary energy storage or thermal systems to address load variability, reliability, and operational constraints. Both PEMFCs and SOFCs have been extensively investigated due to their complementary characteristics, including differences in operating temperature, dynamic response, efficiency, and fuel flexibility [19].

In terrestrial transport applications, fuel cells are primarily considered for heavy-duty vehicles and long-haul operations, where high energy demand and extended operating times favour electrochemical systems capable of continuous power generation. In this domain, low-temperature fuel cells offer advantages in terms of dynamic response and system integration, while high-temperature systems provide improved efficiency and fuel flexibility, albeit at the cost of increased system complexity [18, 19].

In marine applications, the relevance of fuel cells is further strengthened by long mission durations, predictable load profiles, and stringent emission regulations in coastal and port areas. Fuel-cell-based power systems can contribute to both propulsion assistance and onboard energy supply, benefiting from the high efficiency and low local emissions of electrochemical conversion. However, challenges related to fuel storage, thermal management, and integration with existing shipboard power architectures remain critical design considerations [20, 21].

The aeronautical sector presents the most restrictive operating environment for fuel cell deployment, due to stringent constraints on weight, volume, safety, and reliability. Unlike ground and marine transport, aviation applications impose severe limitations on energy storage solutions, significantly reducing the feasibility of purely battery-electric architectures beyond short-range or niche use cases. In this sector, fuel cells are not envisioned as standalone propulsion systems, but rather as components of hybrid architectures, where their high efficiency and low-emission characteristics can be leveraged in combination with complementary energy storage and power management systems. The effectiveness of such configurations is inherently dependent on optimized system integration and the availability of low-carbon hydrogen supply chains [20, 21].

Despite their demonstrated potential across these sectors, the large-scale adoption of fuel-cell-based systems remains constrained by system-level challenges, including the current dominance of fossil-derived hydrogen production, limited refuelling infrastructure, and unresolved issues related to cost, durability, and long-term operation under real-world conditions. Addressing these limitations requires coordinated advances in technology development, infrastructure deployment, and regulatory alignment [20, 21]. Within this broader context, the present work focuses on the application of fuel cell technologies in the aeronautical domain, with particular emphasis on their integration within hybrid power systems as a pathway toward achieving meaningful emission reductions in one of the most demanding transport sectors [20, 21]. While significant progress has been made in hydrogen-based propulsion systems, the integration of fuel cell technologies within hybrid propulsion architectures for aviation remains insufficiently explored. In particular, the performance and efficiency implications of hybrid SOFC–gas turbine systems under realistic operating conditions are not yet fully understood. This thesis aims to evaluate the feasibility and performance of hybrid Solid Oxide Fuel Cell–Gas Turbine (SOFC–GT) systems for aviation applications through thermodynamic modelling and system-level analysis. The study is based on models developed within NASA's NPSS environment and complemented by simulations performed in ProMax.

The remainder of this thesis is organized as follows. Chapter 2 introduces the main fuel cell technologies and discusses their thermodynamic and electrochemical operating principles, with particular attention to performance behaviour and operating limitations. Chapter 3 investigates the system-level integration and hybridization of fuel cell technologies for transportation applications. In particular, the chapter distinguishes between low-temperature PEMFC electrical hybrid systems and high-temperature SOFC-based thermodynamic hybrid architectures integrated with gas turbines. Chapter 4 presents a comparative review of selected marine and aeronautical case studies involving PEMFC and SOFC/GT hybrid systems. Chapter 5 describes the numerical modelling methodology and the architecture adopted for the SOFC–GT hybrid configuration developed in this work. Finally, Chapter 6 presents model verification and discusses the thermodynamic performance of the proposed hybrid system through comparative analysis.

2. Fuel Cells: Toward Future Energy Solutions

Fuel cells are commonly classified according to the type of their electrolyte, as the electrolyte determines the ionic charge carrier, defines the operating temperature range, and influences both material selection and fuel processing strategies. Based on this criterion, five principal types are typically identified: Polymer Electrolyte Fuel Cells (PEFC), Alkaline Fuel Cells (AFC), Phosphoric Acid Fuel Cells (PAFC), Molten Carbonate Fuel Cells (MCFC), and Solid Oxide Fuel Cells (SOFC) [10, 17]. Low-temperature fuel cells such as PEFCs, AFCs, and PAFCs operate below approximately in the $80°C - 200°C$ temperature range, where the electrolyte transports light ions (protons) in PEFCs and PAFCs, and hydroxide ions in AFCs [20, 21].

These systems offer advantages including fast start-up capability, compact balance-of-plant requirements, and the use of lightweight polymeric materials. However, their electrochemical performance is highly sensitive to fuel impurities. For example, platinum catalysts in PEFCs suffer severe degradation in the presence of trace amounts of carbon monoxide due to strong adsorption on catalytic sites. Similarly, the aqueous KOH electrolyte in AFCs readily reacts with CO_2 to form carbonates, reducing ionic conductivity and shortening system lifetime. Consequently, low-temperature fuel cells require high-purity hydrogen and strict gas clean-up procedures, which increase system cost and complexity [20, 21]. In contrast, high-temperature fuel cells such as MCFCs and SOFCs operate typically in the 600–1000 °C temperature range and utilize heavier ionic carriers carbonate ions (CO_3^{2-}) in MCFCs and oxide ions (O^{2-}) in SOFCs which become mobile only at elevated temperatures. These conditions enhance ionic conductivity, reduce ohmic losses, and enable the use of cost-effective nickel-based electrodes instead of noble metals. [17]. Furthermore, high operating temperatures allow internal reforming of hydrocarbon fuels such as methane, methanol, or syngas within the stack, eliminating the need for external reformers and increasing fuel flexibility [20, 21].

In addition to these electrochemical advantages, high-temperature fuel cells provide significant system-level benefits. Their elevated operating temperatures enable efficient integration with bottoming cycles, such as gas turbines, allowing additional power generation from high-temperature exhaust gases. Accordingly, electrical efficiencies exceeding 60% can be achieved, while combined heat and power (CHP) configurations can increase total system efficiency beyond 80%. However, these advantages are accompanied by important engineering challenges. High-temperature operation requires materials that can withstand harsh conditions, leading to issues such as corrosion in MCFCs and mechanical fragility in ceramic components of SOFCs, such as yttria-stabilized zirconia (YSZ). Thermal gradients, sealing difficulties, and long-term material degradation remain critical barriers to wide commercialization [10, 17].

Ultimately, classifying fuel cells by electrolyte type highlights a fundamental trade-off: low-temperature systems offer operational simplicity and fast response but require high-purity fuels and exhibit limited efficiency, whereas high-temperature systems provide superior efficiency and fuel flexibility but demand advanced materials, robust thermal management, and sophisticated mechanical integration. Table 2-1 summarizes the main characteristics of each type and illustrates how electrolyte chemistry shapes both electrochemical behaviour and broader system design considerations [20, 21].

Table 2-1 Comparative Technical Characteristics of Major Fuel Cell Technologies [21].

Types of FC	PEMFC	AFC	PAFC	MCFC	SOFC
Electrolyte	Hydrated Polymer Ion Exchange Membranes	KOH (mobilized or immobilize)in porous matrix	Immobilized phosphoric acid (SiC matrix)	Molten carbonate immobilized in $LiAlO_2$	Ceramic oxide (perovskite)
Electrodes	Carbon	Transition metals	Carbon	Nickel / nickel oxide	Perovskite–metal cermet
Catalyst	Platinum	Platinum	Platinum	Electrode material	Electrode material
Interconnect	Carbon or metal	Metal	Graphite	Stainless steel or Nickel	Nickel, ceramic, or steel
Operating Temperature	40 – 80°C	65– 220°C	205°C	650°C	600-1000°C
Charge Carrier	H^+	OH^-	H^+	CO_3^{-2}	O^{-2}
Prime cell component	Carbon-based	Carbon-based	Graphite-based	Stainless based	Ceramic
Product heat management	Process gas+ liquid cooling	Process gas + electrolyte circulation	Process gas + liquid cooling / steam generation	Internal reforming + process gas	Internal reforming+ process gas

Fuel cells differ fundamentally from internal combustion engines (ICEs), as they do not rely on combustion-driven thermodynamic cycles involving high-temperature gas expansion. In practice, they convert the chemical energy of the fuel directly into electrical energy through electrochemical reactions. This operating principle avoids the formation of major combustion-related pollutants such as nitrogen oxides (NO_x) and particulate matter, while hydrogen-fed systems generate only water vapor (H_2O) as the primary by-product along with recoverable heat [22]. Moreover, the absence of moving mechanical components such as pistons and flame fronts enables higher conversion efficiency, and near-zero local emissions when clean fuels are used. The performance and operating mechanisms of fuel cells are largely governed by the electrolyte type and the nature of the ionic species transported across it.

In Polymer Electrolyte Fuel Cells (PEFCs), a solid polymer membrane (e.g., Nafion) conducts protons (H^+). Hydrogen introduced at the anode dissociates into protons and electrons; the protons migrate through the membrane while the electrons flow through an external circuit to produce electrical work. At the cathode, oxygen reacts with the protons and electrons to form water [23]. PEFCs are widely used in transportation applications due to their high power density and rapid response. However, they rely on platinum-based catalysts that are extremely sensitive to carbon monoxide, requiring highly purified hydrogen stream. Another low-temperature fuel cell type, Phosphoric Acid Fuel Cells (PAFCs) employ concentrated phosphoric acid as the electrolyte and operate at intermediate temperatures ($150 - 200\ °C$). They are commercially mature and suitable for combined heat and power (CHP) systems, although their electrical efficiency is lower compared to high-temperature fuel cells.

A related technology, Direct Methanol Fuel Cells (DMFCs), also based on polymer electrolyte membranes, utilize liquid methanol directly at the anode, simplifying fuel storage and handling. However, their performance is limited by methanol crossover through the membrane, which reduces overall efficiency. While DMFCs are suited for portable and small-scale applications, MCFCs utilize molten lithium–potassium carbonate electrolytes that conduct carbonate ions ($CO_3{}^{2-}$), enabling high-temperature operation. Their main challenges include material corrosion and gradual electrolyte degradation [20, 21].

Solid Oxide Fuel Cells (SOFCs), by contrast, employ a ceramic electrolyte commonly yttria-stabilized zirconia (YSZ) which conducts oxygen ions (O^{2-}) at elevated temperatures ($600 - 1000°C$). At the cathode, oxygen is reduced to oxide ions, which migrate through the electrolyte to react with fuel at the anode. While high-temperature operation enhances electrochemical kinetics, it also introduces challenges such as mechanical stress, thermal cycling limitations, and slower start-up characteristics [20, 21, 23].

Alkaline Fuel Cells (AFCs) employ an aqueous potassium hydroxide (KOH) electrolyte, where hydroxide ions (OH^-) acts as charge carriers. AFCs can operate with non-precious metal catalysts and offer high electrical efficiency when supplied with purified reactants. However, they are highly sensitive to carbon dioxide, which reacts with the electrolyte to form carbonates, reducing ionic conductivity and system lifetime [20, 21]. Figure 2-1 provides a comparative overview of these technologies, highlighting differences in electrolytes, charge carriers, and typical operating temperature ranges [21].

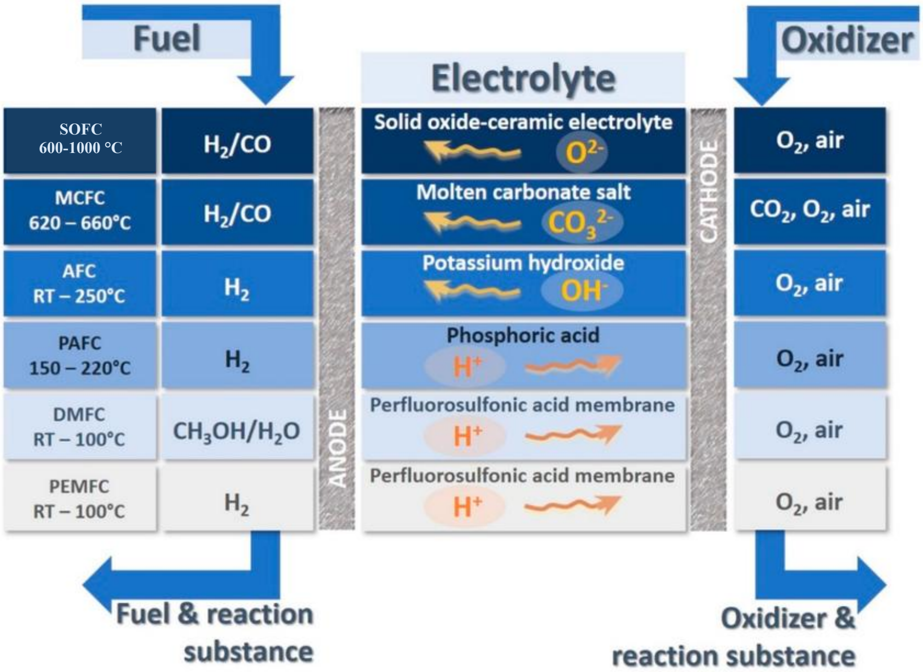

Figure 2-1 Fuel Cell Technologies Overview [21].

2.1 Thermodynamic and Electrochemical Principles of Fuel Cells

Fuel cells convert chemical energy directly into electrical energy through electrochemical reactions governed by fundamental thermodynamic principles. From a theoretical standpoint, their performance is largely determined by the characteristics of the overall electrochemical reaction, which defines the theoretical efficiency and cell voltage under ideal conditions. In particular, thermodynamic parameters such as the Gibbs free energy change and the electrochemical potential of the reacting species define the theoretical limits of fuel cell performance. Based on these principles, the maximum theoretical performance of a fuel cell can be described by the Gibbs free energy change of the overall electrochemical reaction, which determines the maximum electrical work obtainable from the system .

$$H_2 + \frac{1}{2} O_2 \rightarrow H_2O \tag{2.1}$$

For the hydrogen–oxygen system, the global reaction is (Eq.2-1): at standard reference conditions ($298\,K$,$1\,atm$) the enthalpy change ($\Delta H = -285.8\,kJ/mol$) represents the total energy released, while the Gibbs free energy ($\Delta G = -237.1\,kJ/mol$) defines the maximum useful electrical work obtainable. The ratio $\Delta G/\Delta H$ therefore expresses the upper bound of the first-law efficiency, which is approximately 83% for this reaction. The remaining fraction is released as thermal energy, which can be recovered in CHP or hybrid cycles [21]. The reversible open-circuit voltage (OCV) of a fuel cell is determined by the Nernst equation (Eq.2-2):

$$E = E^{\circ} + ln \frac{RT}{2F} \left(\frac{pO_2^{\frac{1}{2}} pH_2}{p\, H_2O} \right) \tag{2.2}$$

where E° is the standard reversible potential ($1.229\, V\, at\, 25°C$), R is the universal gas constant, T is the absolute temperature, F is the Faraday constant, and p_i are the partial pressures of the reacting species. This equation highlights [20, 21].

In practice, fuel cells do not operate under ideal reversible conditions, and the actual cell voltage is always lower than the theoretical value predicted by thermodynamic analysis. This deviation is primarily caused by irreversible losses within the cell, which can be broadly classified into three main categories: activation losses, ohmic losses, and concentration losses. Activation losses are associated with the kinetics of electrochemical reactions at the electrodes. In order for these reactions to proceed, an activation energy barrier must be overcome, resulting in a voltage drop that is particularly significant at low current densities. Ohmic losses arise from the resistance to the flow of ions through the electrolyte and electrons through the electrodes and interconnects. These losses are proportional to the current density and depend on both material conductivity and cell design. In high-temperature fuel cells, enhanced ionic conductivity leads to lower ohmic losses compared to low-temperature systems. Concentration losses, also referred to as mass transport losses, arise when the supply of reactants to the reaction sites becomes insufficient to sustain the electrochemical reaction. This typically occurs at high current densities, where the consumption of reactants exceeds their rate of transport, resulting in a sharp drop in cell voltage. The combined effect of these losses explains the deviation of real fuel cell performance from ideal behaviour and leads to the characteristic voltage decrease observed during operation [20, 21]. These different types of losses can be clearly visualized in the polarization curve shown in Figure 2-2.

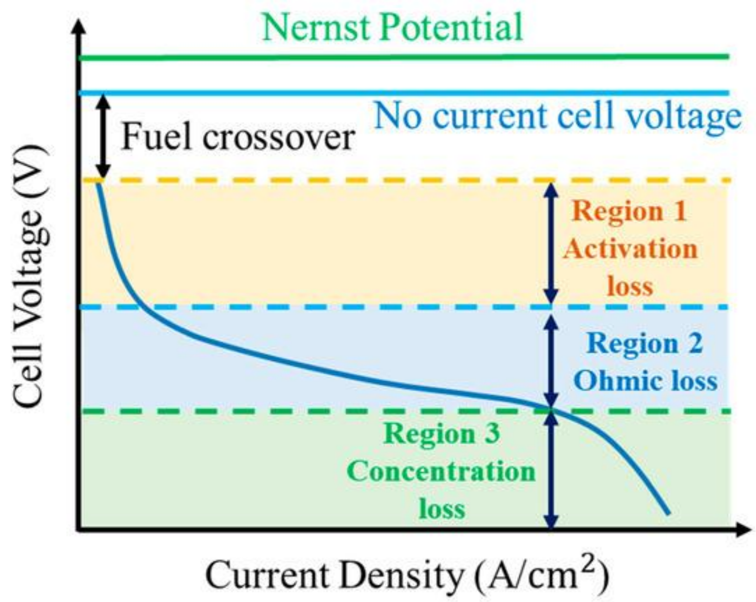

Figure 2-2 Typical fuel cell polarization curve showing the contributions of activation, ohmic, and concentration losses to the overall voltage drop [24].

2.2 Fuel Cell Performance Behaviour and Operating Conditions

Fuel cell performance under real operating conditions differs significantly from its ideal electrochemical behaviour, as it is governed by a range of interacting parameters that influence both efficiency and power output. Unlike theoretical models based on equilibrium assumptions, practical fuel cell systems are affected by operating variables such as current density, temperature, pressure, and reactant composition. Understanding the combined effect of these parameters is essential for identifying optimal operating conditions and ensuring stable system performance [20, 21]. Among these parameters, current density plays a central role in defining fuel cell behaviour. As current density increases, the cell voltage decreases due to the presence of irreversible losses, resulting in the characteristic polarization curve. At low current densities, fuel cells operate at higher voltages and therefore higher electrical efficiency (fuel-to-electric efficiency) but generate limited power output. In contrast, at higher current densities, the power density increases and reaches a maximum value, although this occurs at the expense of efficiency. Consequently, practical fuel cell systems are typically operated within an intermediate region that provides a compromise between efficiency and power density, while also avoiding instability issues associated with operation near peak power conditions [20, 21].

Temperature is another key factor affecting fuel cell performance. An increase in temperature generally enhances electrochemical reaction rates, thereby reducing activation losses and improving overall kinetics. Moreover, temperature can influence ohmic resistance, particularly in high-temperature fuel cells where ionic conductivity improves significantly. However, from a thermodynamic standpoint, increasing temperature leads to a reduction in the reversible cell voltage. Therefore, the net effect of temperature results from a balance between improved reaction kinetics and reduced theoretical potential [20, 21].

Operating pressure has a significant impact on fuel cell performance, as higher pressures increase the partial pressures of reactants, leading to an increase in the reversible cell voltage and improved mass transport processes. This generally results in improved cell performance and increased electrical efficiency. However, operating under elevated pressure conditions introduces additional complexity and cost, requiring more robust system components and pressurized infrastructure. Another important aspect is to the overall system pressure, the local composition and utilization of reactant gases within the cell also play a crucial role in determining performance. According to electrochemical principles, an increase in reactant availability leads to higher cell voltages. However, as the fuel is consumed along the flow path, the local concentration of reactants decreases, leading to a reduction in the effective cell voltage. This spatial variation in gas composition imposes a limitation on the maximum achievable performance and must be carefully managed in practical system design [21].

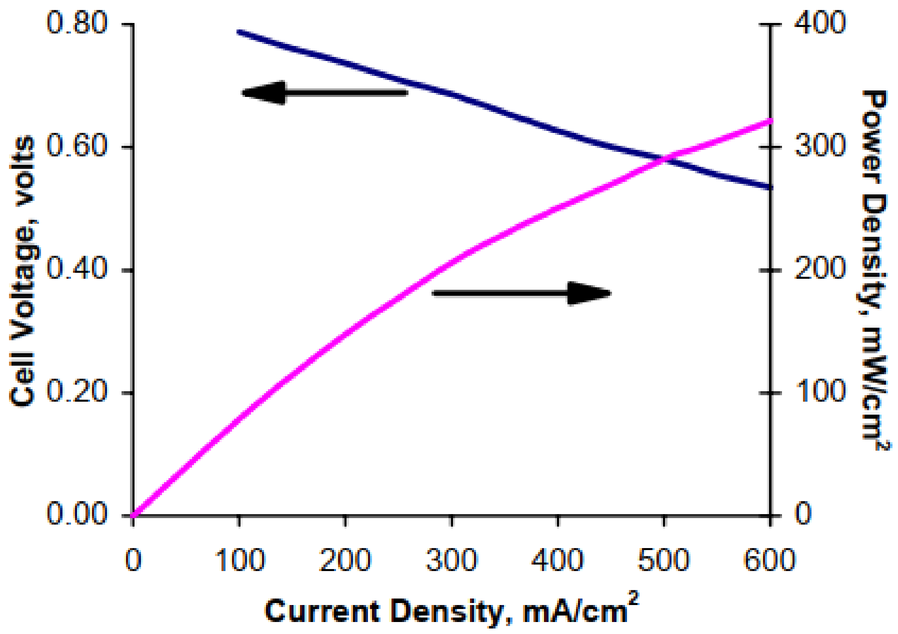

Figure 2-3 Voltage–power characteristics of a fuel cell as a function of current density, illustrating the trade-off between electrical efficiency and power output [21].

As illustrated in Figure 2-2 , the cell voltage decreases monotonically with increasing current density due to presence of irreversible losses, while the power density exhibits a peak before declining. This behaviour defines the practical operating window of fuel cells. In practice, fuel cells are typically operated in the intermediate current density region, located on the left side of the maximum power point. In this region, the cell maintains relatively high voltage levels, ensuring higher electrical efficiency, while still delivering sufficient power output. Operating at very high current densities, although associated with higher power density, leads to significant efficiency losses and may cause instability and accelerated degradation. Therefore, the intermediate operating region represents the optimal compromise between efficiency, power output, and system durability [21].

3. Hybridization and System Integration of Fuel Cell Systems

The transition toward practical fuel cell-based transport systems requires moving beyond component-level analysis toward system-level integration strategies. While the fundamental principles and individual characteristics of fuel cell technologies have been discussed in Chapter 2, their effective deployment in real transport applications depends on their ability to operate under dynamic conditions, meet varying power demands, and achieve high efficiency within complex energy systems. In this context, hybridization and system integration emerge as key enablers for bridging the gap between theoretical performance and practical implementation.

3.1 System-level Motivation for Hybridization

The motivation for using fuel cells in transport systems has already been discussed in Chapter One, where their role in emission reduction, clean-fuel utilization, and decarbonization of hard-to-electrify sectors was introduced. Therefore, this chapter does not repeat the general environmental justification of fuel cell technologies. In practice, it focuses on how fuel cells can be integrated at system level to meet the practical requirements of transport applications, where power demand, dynamic operation, fuel storage, reliability, and efficiency must be considered simultaneously. In real transport missions, a fuel cell rarely operates under perfectly steady conditions. Road vehicles are exposed to frequent acceleration, braking, start–stop operation, and rapid load changes. Marine vessels may experience long-duration operation with auxiliary loads, hotel loads, manoeuvring phases, and variable propulsion demand. Aircraft and UAV applications impose even stricter requirements, since power demand can vary significantly between taxiing, take-off, climb, cruise, and descent, while system mass and volume remain critical constraints. Under these conditions, standalone fuel cell systems may suffer from slow dynamic response, limited capability to follow sudden load variations, increased degradation under cycling operation, and additional parasitic losses caused by balance-of-plant components such as compressors, pumps, humidifiers, and thermal management units. For this reason, fuel cell systems are commonly hybridized with batteries, supercapacitors, photovoltaic systems, flywheels, or other energy conversion devices to improve transient performance, protect the fuel cell stack, stabilize the DC bus, and operate the fuel cell closer to its high-efficiency region [25, 26].

3.1.1 Role of Hybridization in Fuel Cell Systems

Hybridization in fuel-cell-based transport systems can be understood as a system integration strategy rather than a simple combination of components. To overcome the limitations of standalone operation, fuel cell systems are commonly integrated with complementary energy sources or storage technologies, enabling improved transient performance, better load matching, enhanced system flexibility, and higher overall efficiency. In fuel cell–battery and fuel cell–supercapacitor architectures, the storage device supplies short power peaks, absorbs regenerative energy when available, and reduces the exposure of the fuel cell to sharp current variations. In renewable-assisted configurations, such as PV–fuel cell systems, hybridization compensates for the intermittency of solar power and supports more continuous electricity generation through coordinated power management. In high-temperature systems, especially SOFC-based configurations, hybridization may also involve thermal integration with bottoming cycles or gas turbines, where the high-temperature exhaust of the fuel cell can be recovered to produce additional useful power. However, these hybrid approaches do not provide identical benefits, electrical hybridization mainly improves dynamic response and durability, renewable hybridization improves energy availability and autonomy, while thermodynamic hybridization aims primarily at increasing fuel-to-electric efficiency through waste heat recovery [25, 27].

3.1.2 Definition Of Hybrid Architectures in Fuel Cell Systems

Hybridization in fuel-cell-based energy systems should not be interpreted as a simple combination of multiple components or energy sources. In practice, it refers to a structured system-level integration in which different subsystems are deliberately combined to enhance the overall performance of the system. A configuration can be defined as a hybrid system only when its components operate in a coordinated manner and each element contributes to specific functions such as power supply, energy management, or efficiency improvement [25, 26]. From this perspective, hybrid systems are typically characterized by the integration of multiple energy sources or subsystems with complementary characteristics, allowing them to compensate for each other's limitations. For instance, in electrical hybrid configurations, the fuel cell acts as the primary energy source, while energy storage devices such as batteries or supercapacitors provide transient power support and absorb regenerative energy. This coordinated interaction reduces operational stress on the fuel cell, improves dynamic response, and enhances overall system durability. However, not all configurations involving fuel cells and auxiliary components can be classified as true hybrid systems. A fundamental distinction must be made between functional hybridization and auxiliary system optimization. In many cases, components such as compressors, turbochargers, or thermal management systems are integrated to improve the operation of the fuel cell stack. Nevertheless, these components typically consume power rather than contributing to net power generation [26, 28]. Therefore, such configurations should be interpreted as balance-of-plant (BoP) enhancements rather than genuine hybrid systems. In contrast, true hybrid systems are characterized by an integration that directly contributes to the overall energy conversion process. A representative example is the SOFC–gas turbine hybrid system, where high-temperature exhaust heat from the fuel cell is recovered within a thermodynamic cycle to generate additional useful power. This type of integration not only improves system efficiency significantly but also demonstrates a genuine interaction between subsystems at the energy conversion level [28]. Accordingly, the definition of hybrid systems in fuel-cell-based applications should be based on the functional role of each component and its contribution to overall system performance, rather than merely on the coexistence of multiple subsystems. This distinction is particularly important in the analysis and design of advanced transport energy systems, as it avoids ambiguity in system classification and enables a more rigorous evaluation of hybrid architectures.

3.2 Functional Classification of Fuel Cell Hybrid Architectures

Fuel cell hybrid architectures can be classified according to the dominant form of interaction between the fuel cell stack and the coupled subsystem. This classification is important because the term "hybrid" is sometimes used broadly for any system that includes a fuel cell and an additional component, while from a system-level perspective not all couplings provide the same functional contribution. In this thesis, hybrid architectures are therefore classified based on whether the additional subsystem contributes to energy conversion, power management, or only auxiliary operation. A useful reference for such classification is the critical review by Nikiforakis et al., where 399 studies on SOFC hybrid systems were reviewed and organized according to primary energy sources, component configurations, system outputs, and analysis methods. Their classification identifies several coupling families, including gas turbines, piston engines, wind systems, and solar systems, and shows that SOFC–GT configurations are the most prevalent among the reviewed SOFC hybrid designs. This supports the need to classify hybrid architectures not only by fuel cell type, but also by the role played by the coupled subsystem in the overall energy system [29].

3.2.1 Electrochemical–Thermal Hybrid Systems

Electrochemical–thermal hybrid systems are based on the integration of a fuel cell with a thermodynamic cycle. In these systems, the fuel cell is not simply assisted by an auxiliary device; instead, its thermal output is used as part of the energy conversion process. The most representative example is the SOFC–gas turbine hybrid system, where the high-temperature exhaust of the SOFC is recovered through a Brayton-based cycle to generate additional useful power. This architecture is fundamentally different from electrical buffering. In an electrical hybrid system, the secondary device mainly handles load variations. In an SOFC–GT system, the coupled turbine contributes directly to the net power output by converting thermal energy into mechanical or electrical power.

Ferrari et al. report that coupling SOFCs with micro gas turbines can increase the efficiency from the $25-30\%$ range of standalone microturbines to approximately $60-65\%$, mainly due to the thermodynamic contribution of the SOFC and the recovery of exhaust energy [28]. However, this overall efficiency gain comes with important integration challenges. SOFC–mGT coupling is not simply a matter of replacing the combustor of a gas turbine with a fuel cell. The integration requires matching pressure levels, air flow rates, turbine inlet conditions, recuperation strategy, and control of components that have different dynamic time scales.

This is why electrochemical–thermal hybrids are usually attractive for applications where efficiency and fuel utilization are more important than rapid transient response, such as stationary power generation, maritime auxiliary power, and future aviation propulsion concepts [28]. Recent aviation studies extend this idea further. Xu et al. proposed a dual-shaft SOFC hybrid propulsion system for aircraft, where the SOFC replaces the conventional turbine-driven compressor and the high- and low-pressure spools are independently controlled through a power distribution system. At the design point, the proposed system delivers 36.304 kN thrust, 15.931 MW SOFC power, and 54.76% SOFC overall efficiency. This is a useful example for this thesis because it shows that SOFC hybridization in transport is moving beyond simple SOFC–GT layouts toward more integrated propulsion architectures, where fuel cell power, compressor operation, thermal recovery, and thrust generation are treated as one coupled system [30].

3.2.2 Electrochemical–Electrical Hybrid Systems

Electrochemical–electrical hybrid systems are based on the integration of a fuel cell with an electrical energy storage device, most commonly a battery or a supercapacitor. In transport applications, this architecture is particularly relevant for PEMFC-based systems, where the

fuel cell provides the main energy supply while the storage device manages transient power demand and rapid load variations. The practical motivation for this configuration is demonstrated in PEMFC–battery vehicle studies, where hybridization allows the fuel cell to operate within a relatively stable power range while the battery supplies peak demand. This highlights a key design principle: the storage system acts as a dynamic buffer that decouples the fuel cell from fast load fluctuations and improves overall system operation. This decoupling is essential for avoiding frequent current cycling in the fuel cell, which is known to accelerate degradation and reduce system lifetime [25, 31]. From a system integration perspective, electrochemical–electrical hybridization also requires appropriate power electronics and control strategies. Voltage adaptation through DC/DC converters and coordinated energy management are essential to ensure efficient interaction between the fuel cell, storage system, and load [25, 31].
In practice, the energy management strategy determines the power split between the fuel cell and the storage device, making it a critical design variable in system performance. Similar load-sharing behaviour has been observed in aerial applications, where the fuel cell supplies the base load and the battery contributes only during high-demand conditions. This confirms that system design must consider both average power and transient peak requirements, particularly under constraints such as mass, volume, and mission duration [32]. However, this architecture also introduces design trade-offs, particularly in the sizing of the storage system, where increasing battery capacity improves dynamic response but adds weight, cost, and system complexity. Therefore, electrochemical–electrical hybrid systems are most effective in applications where dynamic load following and operational flexibility are more critical than maximizing thermodynamic efficiency [31, 32].

3.2.3 Electrochemical–Mechanical Coupling Systems

Electrochemical–mechanical coupling systems refer to configurations in which the fuel cell stack is integrated with mechanical subsystems such as compressors, turbochargers, or turbomachinery. However, this category must be critically distinguished from true hybrid energy systems, as not all mechanical couplings provide a net contribution to system-level energy conversion. In low-temperature fuel cell systems, particularly Proton Exchange Membrane Fuel Cells (PEMFCs), mechanical devices are primarily employed to enhance air supply conditions. As highlighted in the work of Kerviel et al., increasing the air pressure supplied to a PEMFC stack directly improves its output power and efficiency, with pressure ratio increases (e.g., from 1.0 to 1.7) leading to approximately 10% higher output power.
This improvement is achieved through better oxygen availability and enhanced electrochemical reaction kinetics. Consequently, boosting systems such as electric turbochargers or multi-stage compressors are widely implemented in fuel cell vehicles to improve power density and reduce stack size [33]. Despite these benefits, the thermodynamic role of such mechanical subsystems remains fundamentally different from that of conventional hybrid energy systems. Due to the relatively low operating temperature of PEMFCs , the exhaust stream does not contain sufficient thermal energy to drive a turbine effectively.
Consequently, even in turbocharged configurations, the compressor is primarily powered by electrical energy drawn from the fuel cell itself rather than by recovered waste heat [33]. This leads to a critical insight: in PEMFC-based systems, mechanical coupling devices are predominantly power-consuming auxiliaries, not power-generating subsystems. Even when an expander or turbine is present, its contribution is limited and cannot offset the compressor

power demand in a thermodynamically meaningful way. Therefore, such systems should not be classified as true PEMFC–gas turbine (PEMFC–GT) hybrid architectures. In practice, these configurations are more accurately described as advanced balance-of-plant (BoP) enhancements or air management strategies aimed at improving stack performance, reducing mass, and increasing vehicle range. For example, Kerviel et al. demonstrated that electric-assisted turbochargers can reduce compressor power consumption by up to 46% compared to single-stage compressors while improving system efficiency and driving range. However, this improvement results from better system integration and reduced auxiliary losses rather than from genuine hybridization through energy recovery [33]. In contrast, high-temperature fuel cell systems, particularly Solid Oxide Fuel Cells (SOFCs), exhibit fundamentally different behaviour when coupled with mechanical systems. Due to their high operating temperature, SOFC exhaust gases contain sufficient thermal energy to drive a turbine. In such configurations, the turbine can recover part of the waste heat and convert it into additional electrical or mechanical power, thus contributing directly to the total system output [34].

This distinction highlights a key classification criterion:

- **Power-consuming mechanical coupling (PEMFC systems):** auxiliary devices that enhance operating conditions but reduce net electrical output.
- **Power-producing thermodynamic coupling (SOFC systems):** integrated subsystems that recover waste energy and increase overall efficiency.

Therefore, the term "hybrid" should be applied selectively. While PEMFC systems with compressors or turbochargers are often labelled as hybrid in the literature, they do not satisfy the fundamental requirement of hybridization, which is the integration of multiple energy conversion pathways contributing to net power generation. In contrast, SOFC–GT systems represent true hybrid architectures due to their thermodynamic synergy and energy recovery capability. From a system design perspective, this refined classification is essential. It prevents conceptual ambiguity and enables a more rigorous comparison between different fuel cell hybrid configurations, particularly in transportation and aerospace applications where efficiency, weight, and system complexity must be carefully balanced [34].

3.3 PEMFC Electrical Hybridization Power Flow and Operational Behaviour

From a system-level perspective, the performance of PEMFC-based hybrid systems is not determined solely by their structural configuration, but rather by the dynamic interaction between multiple energy sources. In practical applications, the behaviour of these systems is governed by how power is distributed among the fuel cell, energy storage components, and the load. In this context, energy management systems (EMS) play a central role by continuously regulating power allocation based on load demand, system constraints, and operating conditions. Instead of viewing system components as independent units, PEMFC hybrid systems must be interpreted as dynamically coupled energy networks, where real-time power flow interactions define overall system behaviour [35]. Therefore, despite the presence of turbomachinery components in some PEMFC-based systems, these configurations cannot be classified as true hybrid energy systems, as they do not introduce an additional energy conversion pathway contributing to net power generation. In practice, they should be interpreted as advanced auxiliary or balance-of-plant configurations aimed at improving system performance.

3.3.1 Power Flow-Oriented System Representation

A useful way to represent PEMFC hybrid systems is through a power flow-oriented framework. Within this approach, the system is modeled as a network of interconnected energy sources linked through a common DC bus and coordinated via power electronic converters. This configuration enables continuous energy exchange between the fuel cell and the battery, rather than isolated operation. At the core of this architecture, the EMS determines the instantaneous contribution of each energy source. By processing inputs such as bus voltage, fuel cell current, and battery state-of-charge (SOC), the EMS dynamically adjusts the power split to satisfy load requirements while maintaining operational constraints. This coordinated control ensures load balancing, prevents component overloading, and enhances system reliability. Beyond operational control, hybridization introduces important design advantages. By shifting transient power demand to the battery, the fuel cell can be sized closer to average load conditions rather than peak demand. This reduces system cost and improves overall efficiency, while also mitigating degradation effects associated with rapid load fluctuations [36]. A representative PEMFC hybrid architecture is illustrated in Figure 3.1, highlighting the interaction between the fuel cell stack, battery system, and power electronic converters within a unified DC bus structure [36].

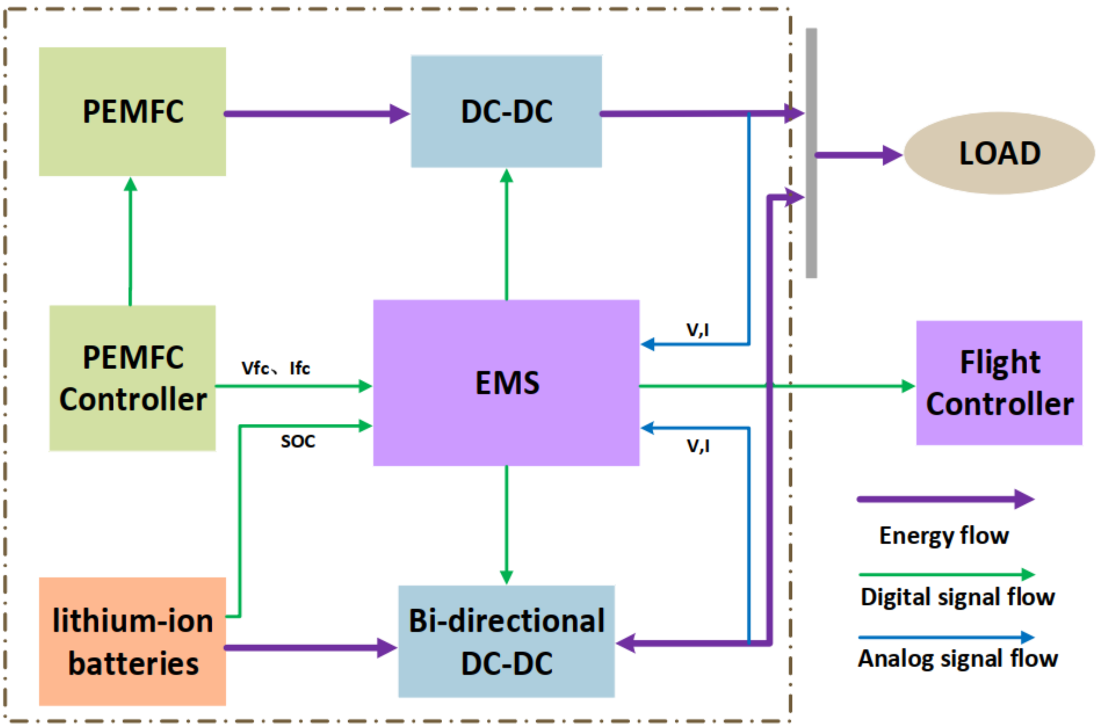

Figure 3-1 Power flow architecture of a PEMFC–battery hybrid system, including the fuel cell stack, lithium-ion battery, DC/DC converters, and energy management system (EMS), illustrating the distribution of power and control signals [36].

As shown in Figure 3.1, system-level coordination is achieved through continuous monitoring and control of key variables. The EMS processes real-time measurements and redistributes power accordingly, enabling stable operation under varying load conditions and transient events [36].

3.3.2 Limitations of PEMFC Hybridization

In spite of widespread adoption in transport applications, PEMFC-based hybrid systems exhibit inherent limitations that constrain their effectiveness in advanced energy conversion architectures. A key limitation arises from system dynamics. Although PEMFC stacks are capable of relatively fast response compared to high-temperature fuel cells, their operation within hybrid configurations remains strongly dependent on auxiliary energy storage components. In practice, batteries or supercapacitors absorb rapid load fluctuations, meaning that overall system dynamics are governed more by the storage subsystem than by the fuel cell itself [37]. From a thermodynamic standpoint, the low operating temperature of PEMFC systems (typically temperature below $100°C$) introduces a more fundamental constraint. In comparison, high-temperature fuel cells, PEMFCs produce low-grade waste heat that cannot be effectively utilized in downstream energy conversion processes such as turbine expansion or combined cycles. This limits the potential for thermodynamic integration and prevents the development of fully coupled hybrid systems.

Consequently, hybridization in PEMFC-based systems is primarily focused on power management rather than efficiency enhancement. While this approach improves load-following capability and operational flexibility, it does not significantly increase overall energy conversion efficiency. The absence of high-temperature heat recovery restricts the system to single-stage energy utilization, limiting its performance compared to thermodynamically integrated systems. This distinction becomes critical when comparing PEMFC systems with high-temperature alternatives. Whereas PEMFC hybridization is driven by electrical load balancing, high-temperature fuel cell systems enable deeper integration with thermodynamic cycles, allowing multi-stage energy conversion and higher system-level efficiency. Accordingly, the limitations of PEMFC-based hybrid systems motivate the exploration of high-temperature fuel cell technologies, particularly SOFCs, which provide a pathway toward more integrated, efficient, and thermodynamically optimized hybrid energy systems [37, 38].

3.4 High-Temperature Fuel Cells for Hybrid Systems (MCFC vs SOFC)

The integration of fuel cells with gas turbine systems is primarily governed by the thermochemical characteristics of the fuel cell technology. In this context, high-temperature fuel cells namely Molten Carbonate Fuel Cells (MCFC) and Solid Oxide Fuel Cells (SOFC) are widely recognized as the most suitable candidates for hybridization. From a thermodynamic standpoint, high-temperature fuel cells enable internal reforming of hydrocarbon fuels, eliminating the need for extensive external fuel processing. This intrinsic capability allows both MCFC and SOFC systems to operate on a wide range of fuels, including natural gas and syngas, thereby enhancing system-level fuel flexibility [39].A fundamental distinction between these two technologies arises from their electrolyte and charge transport mechanisms. As discussed in chapter 2 table 2.1 MCFC systems operate at

approximately $600 - 650°C$ using molten carbonate electrolytes with CO_3^{2-}ions as charge carriers, whereas SOFC systems function at higher temperatures (650–1000°C) with oxygen ion (O^{2-}) conduction through a solid ceramic electrolyte [40]. In light of these differences, the integration potential with gas turbines varies significantly. Due to their higher operating temperatures, SOFC systems generate exhaust streams with greater thermal quality, which can be more effectively utilized within gas turbine cycles. Consequently, SOFC-based hybrid systems tend to achieve higher overall efficiencies compared to MCFC-based configurations under similar operating conditions [39].
Furthermore, comparative thermoeconomic assessments indicate that although MCFC stacks may exhibit competitive electrochemical efficiencies, SOFC–GT systems offer superior global efficiency and significantly lower capital investment, reinforcing their attractiveness for large-scale applications [39]. Another distinguishing factor lies in system coupling requirements. MCFC systems often necessitate additional combustion stages to elevate turbine inlet temperatures, thereby introducing complexity and potential efficiency penalties. In contrast, SOFC systems can more directly interface with turbomachinery due to their inherently higher exhaust temperatures.
Collectively, these characteristics highlight that while both MCFC and SOFC technologies are viable for hybrid systems, SOFC demonstrates a more favorable balance between efficiency, integration simplicity, and economic feasibility. This distinction has driven the increasing research focus toward SOFC-based hybrid architectures in advanced energy systems [41]. Although MCFC systems present thermodynamic compatibility with gas turbines and represent an important step in hybrid system development, their practical implementation is constrained by lower exhaust temperature, the need for supplementary combustion, and more complex system integration. Therefore, their overall performance and efficiency are generally lower than those achievable with SOFC–GT systems. For this reason, while MCFC-based hybrids are discussed for completeness, the primary focus of this thesis is placed on SOFC–GT systems, which offer more favorable conditions for high-efficiency integrated hybrid architectures [39].

3.5 MCFC–Gas Turbine Hybrid Systems

The integration of Molten Carbonate Fuel Cells (MCFC) with gas turbines represents one of the earliest configurations explored in hybrid energy systems. These systems are designed to utilize the high-temperature exhaust of the fuel cell to drive a secondary power cycle, thereby improving overall energy conversion efficiency. From an energy cascade perspective, MCFC–GT systems operate by first extracting electrical power through electrochemical reactions, followed by the utilization of residual thermal energy within a gas turbine. This multi-stage conversion process significantly enhances fuel utilization compared to standalone systems [42]. Nevertheless, a critical limitation emerges from the relatively moderate operating temperature of MCFC systems. While the typical operating temperature ($\sim 650°C$) is sufficient for internal reforming, it is generally lower than the optimal turbine inlet temperature required for efficient gas turbine operation. As a result, additional combustion of unutilized fuel is often required to elevate the turbine inlet temperature, introducing efficiency trade-offs [43].

This thermodynamic mismatch necessitates careful system-level optimization. Specifically, the balance between fuel utilization within the fuel cell and the thermal requirements of the gas turbine becomes a key design constraint. Excessive fuel utilization may reduce the

available energy for the turbine, whereas insufficient utilization decreases overall system efficiency.
Moreover, system dynamics introduce further complexity. Variations in airflow or mass flow rate can lead to significant deviations in fuel cell temperature and turbine performance. For instance, insufficient cathode airflow may result in fuel cell overheating, whereas excessive airflow reduces turbine inlet temperature and overall system efficiency [43]. Despite these challenges, MCFC–GT systems offer several notable advantages. Their ability to internally reform hydrocarbons and utilize carbon monoxide enhances fuel flexibility. Additionally, MCFC systems inherently facilitate carbon dioxide management, making them suitable for carbon capture applications [42].

In terms of performance, hybrid MCFC–GT systems have demonstrated efficiencies exceeding 70% (LHV) in optimized configurations, significantly outperforming conventional power generation technologies [41]. However, when compared to SOFC-based systems, MCFC–GT configurations generally exhibit higher capital costs and lower integration efficiency, limiting their competitiveness in advanced applications [39]. Therefore, while MCFC–GT systems represent an important milestone in hybrid system development, their role is increasingly being complemented and, in some cases, replaced by SOFC-based hybrid architectures that offer improved thermodynamic compatibility and economic performance. Following the conceptual discussion of MCFC–GT hybrid systems, the schematic representation of a typical configuration is illustrated in Figure 3.2. The diagram highlights the main components and flow interactions within the system, including the compressor, fuel cell stack, heat exchangers, oxidizer, and gas turbine [43].

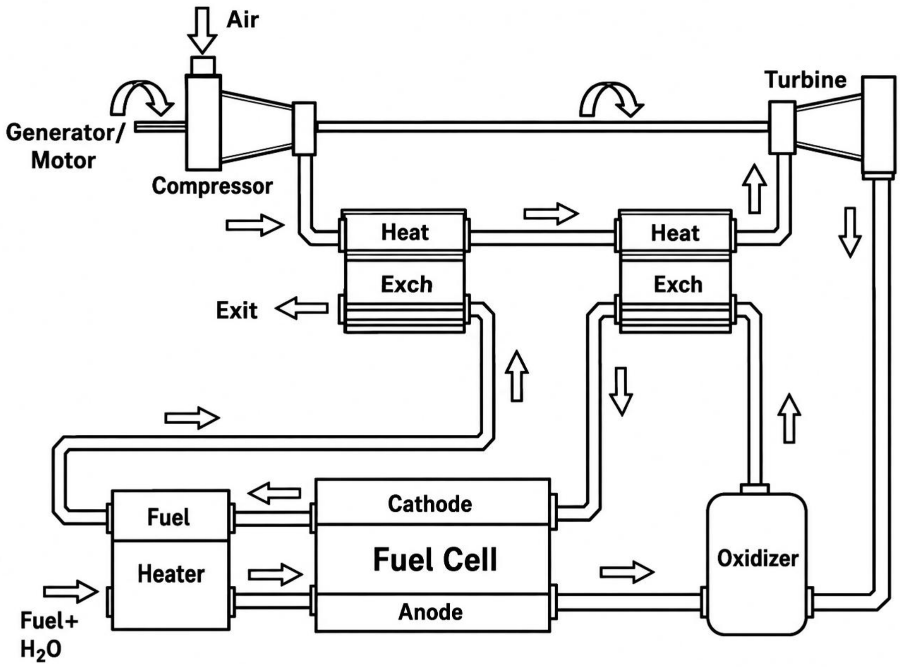

Figure 3-2 Schematic Configuration and System Operation of MCFC–GT Hybrid Systems [43].

As shown in Figure 3.2 compressed air from the compressor is preheated through heat exchangers before entering the cathode of the MCFC. Simultaneously, the fuel stream,

mixed with steam, is conditioned in the fuel heater and supplied to the anode side of the fuel cell. The electrochemical reactions occurring within the MCFC generate electricity while producing high-temperature exhaust gases. The remaining fuel and thermal energy in the exhaust stream are subsequently directed toward the gas turbine subsystem. In order to achieve the required turbine inlet temperature, additional combustion is typically performed in the oxidizer chamber. This step compensates for the relatively lower operating temperature of the MCFC compared to conventional gas turbine requirements [43].
Furthermore, the inclusion of heat exchangers in the system enables effective thermal integration by recovering waste heat and improving overall energy efficiency. This cascading utilization of energy from electrochemical conversion to thermomechanical power generation demonstrates the fundamental advantage of hybrid systems. However, the schematic also implicitly illustrates the inherent design trade-offs discussed earlier. The distribution of fuel between the fuel cell and the combustor directly influences both fuel cell efficiency and turbine performance. Consequently, precise control of airflow, fuel utilization, and thermal management is essential to ensure stable and efficient system operation [43]. This configuration serves as a basis for further comparison with alternative hybrid systems, particularly SOFC–GT architectures, which offer improved thermodynamic compatibility.

3.5.1 Thermodynamic Limitations of MCFC–GT Hybrid Systems

From a thermodynamic perspective, the integration of Molten Carbonate Fuel Cells (MCFC) with gas turbine systems is constrained by several inherent limitations related to operating temperature, heat quality, and system coupling. A primary limitation arises from the relatively moderate operating temperature of MCFC systems, typically in the range of 600–650°C. Although this temperature is sufficiently high to enable internal reforming of hydrocarbon fuels, it remains significantly lower than the optimal turbine inlet temperature required for efficient gas turbine operation. As a result, the thermal energy available in the MCFC exhaust is not always adequate to directly sustain high-efficiency turbine expansion [42].
To overcome this mismatch, most MCFC–GT hybrid configurations incorporate supplementary combustion processes, where unutilized fuel exiting the fuel cell is burned to increase the turbine inlet temperature. While this approach enables effective turbine operation, it introduces an additional irreversibility in the system, thereby reducing the overall thermodynamic efficiency. In addition to temperature limitations, the distribution of energy within the hybrid system further constrains performance. A portion of the fuel energy must be retained at the outlet of the fuel cell to support downstream combustion, which directly limits the achievable fuel utilization within the electrochemical process. Consequently, the system cannot simultaneously maximize both fuel cell efficiency and turbine performance, leading to a fundamental trade-off in hybrid system design [43].
Moreover, the lower exhaust temperature of MCFC systems reduces the quality of recoverable exergy compared to higher-temperature fuel cells such as SOFC. This limitation restricts the extent of thermodynamic integration and reduces the potential for multi-stage energy recovery within the hybrid cycle [41]. Parametric studies further highlight the sensitivity of MCFC–GT performance to operating temperature. Increases in fuel cell temperature lead to higher reaction rates and improved system efficiency; however, practical constraints related to material stability limit the extent to which operating temperature can be elevated. As a result, MCFC systems operate within a relatively narrow temperature

window, constraining their thermodynamic optimization potential [42].
Taken together, these limitations indicate that MCFC–GT hybrid systems are inherently restricted by their thermal characteristics. While they can achieve significant efficiency improvements compared to standalone systems, their performance is ultimately bounded by the mismatch between fuel cell operating conditions and gas turbine requirements. This constraint represents a key factor in the transition toward higher-temperature fuel cell technologies, particularly SOFC-based hybrid systems, which offer improved thermodynamic compatibility and integration potential [41].

3.5.2 Parametric Performance Analysis of MCFC–GT Systems

Beyond the inherent thermodynamic limitations discussed in the previous section, the performance of MCFC–GT hybrid systems is strongly influenced by key operating parameters, which govern the interaction between electrochemical and thermodynamic processes. Among these parameters, operating temperature plays a dominant role in determining system efficiency. Increasing the MCFC operating temperature enhances electrochemical reaction kinetics and improves ionic conductivity, leading to higher power output and improved overall system performance.
In parallel, higher temperatures increase the thermal energy available for downstream turbine expansion, thereby improving the effectiveness of the hybrid cycle [42]. In contrast, the influence of operating pressure is comparatively less pronounced. While moderate pressurization can improve gas turbine performance and increase overall system efficiency, studies indicate that MCFC systems exhibit limited sensitivity to pressure variations due to constraints associated with electrolyte stability and system design [42].
Fuel utilization represents another critical parameter affecting system performance. Higher fuel utilization within the fuel cell increases electrochemical efficiency; however, it simultaneously reduces the amount of unreacted fuel available for combustion in the turbine. As a result, an optimal balance must be achieved between maximizing fuel cell efficiency and maintaining sufficient energy input for the gas turbine subsystem [43]. The steam-to-carbon ratio (S/C ratio) also plays a significant role in hybrid system operation. Increasing the S/C ratio improves reforming reactions and reduces the risk of carbon deposition within the fuel cell. However, excessive steam addition leads to energy penalties due to increased heat demand and dilution effects, which can negatively impact overall system efficiency. Therefore, the S/C ratio must be carefully optimized to balance chemical stability and thermodynamic performance [41].

From a system-level perspective, these parameters are strongly interdependent. Variations in one parameter often influence multiple aspects of system behaviour, including temperature distribution, reaction rates, and turbine performance. For instance, increasing fuel utilization may improve electrochemical efficiency but simultaneously reduce turbine output due to lower exhaust energy. Similarly, changes in airflow distribution affect both fuel cell cooling and turbine inlet conditions, highlighting the coupled nature of the hybrid system [43]. Parametric studies consistently demonstrate that optimal system performance is achieved within a narrow operating window, where temperature, fuel utilization, and airflow are simultaneously controlled. Outside this range, system efficiency declines due to thermal imbalance, reduced exergy recovery, or increased irreversibilities. These findings emphasize that MCFC–GT hybrid systems cannot be effectively optimized through independent parameter adjustment. In practice, a multi-variable optimization approach is required, in which thermodynamic, electrochemical, and fluid dynamic interactions are considered simultaneously. This complexity represents a key challenge in the design and operation of MCFC-based hybrid systems and further motivates the transition toward alternative technologies with more favorable integration characteristics [41].

3.5.3 Operational and Control Challenges of MCFC–GT Hybrid Systems

While parametric analyses provide valuable insight into system performance, the practical implementation of MCFC–GT hybrid systems introduces additional challenges related to operation, control, and system stability. These challenges arise primarily from the strong coupling between electrochemical and thermodynamic subsystems. A defining characteristic of MCFC–GT hybrid systems is the interdependence between the fuel cell and the gas turbine. Variations in operating conditions such as airflow rate, fuel supply, or load demand do not affect individual components independently, but instead propagate throughout the entire system. For instance, a reduction in cathode airflow may increase fuel cell temperature due to insufficient cooling, whereas excessive airflow can lower turbine inlet temperature, reducing turbine efficiency [44]. From a control perspective, this coupling significantly complicates system operation. Unlike conventional power systems, where subsystems can often be regulated independently, MCFC–GT configurations require coordinated control strategies to maintain thermal balance, fuel utilization, and pressure stability simultaneously. Failure to achieve this coordination can lead to thermal runaway, efficiency degradation, or even system instability [44].

Another critical challenge relates to load-following capability. MCFC systems exhibit relatively slow dynamic response due to their high operating temperature and associated thermal inertia. Therefore, rapid changes in power demand common in real-world applications cannot be immediately accommodated by the fuel cell. In hybrid configurations, this limitation must be compensated by the gas turbine or auxiliary systems, adding complexity to system control and design [45]. Thermal management represents an additional operational constraint. The exothermic nature of electrochemical reactions, combined with internal reforming processes, generates significant heat within the fuel cell. Maintaining uniform temperature distribution is essential to prevent thermal stresses, material degradation, and performance loss. However, achieving such uniformity becomes increasingly difficult under transient operating conditions, particularly when airflow or fuel distribution fluctuates [45].

Furthermore, the requirement for supplementary combustion in MCFC–GT systems introduces additional control variables. The amount of fuel directed toward combustion must be carefully regulated to ensure sufficient turbine inlet temperature without compromising fuel cell efficiency. This introduces a multi-variable control problem involving fuel distribution, airflow regulation, and turbine operation [41]. Operational stability is also influenced by system start-up and shut-down processes. Due to the high operating temperature of MCFC systems, start-up times are relatively long and require controlled heating to avoid thermal shock.

Similarly, shut-down procedures must be carefully managed to prevent damage to system components, further complicating operational protocols. Collectively, these challenges highlight that the performance of MCFC–GT hybrid systems is not solely determined by thermodynamic efficiency, but by the ability to maintain stable, coordinated operation under varying conditions. The need for advanced control strategies, combined with sensitivity to operating parameters, represents a major barrier to large-scale deployment. These limitations further reinforce the motivation for exploring alternative high-temperature fuel cell technologies, such as SOFC, which offer improved integration characteristics and more favorable dynamic behaviour [45].

3.6 SOFC–Gas Turbine Hybrid Systems configurations

In hybrid energy system configurations for transport applications, the role of Solid Oxide Fuel Cells (SOFCs) must be examined from a system-oriented perspective, with particular emphasis on how their operating characteristics influence integration with other subsystems. Within this context, three aspects become especially critical for hybrid and aeronautical applications: the thermodynamic behaviour of SOFCs and its impact on system dynamic performance, the role of high-temperature operation in enabling energy recovery and coupling with thermodynamic cycles, and the development of advanced cell architectures aimed at increasing power density, structural compactness, and adaptability to system-level constraints.

Based on these considerations, the following subsections are organized to address these aspects in a progressive manner. Section 3.6.1 focuses on the thermodynamic characteristics of SOFCs from a system integration perspective, with emphasis on dynamic limitations and their implications for hybrid operation. Section 3.6.2 examines the high-temperature nature of SOFCs and the associated potential for exhaust energy utilization, providing the basis for integration with gas turbine cycles. Finally, Section 3.6.3 addresses emerging high power density SOFC technologies, with particular attention to compact configurations and design approaches relevant to aeronautical applications.

3.6.1 Thermodynamic behaviour of SOFC-based hybrid systems

The thermodynamic behaviour of SOFC-based hybrid systems is fundamentally governed by the interaction between electrochemical energy conversion and high-temperature heat flows within an integrated system architecture. compared to isolated fuel cell operation, where thermal effects are often treated as secondary outputs, the performance of SOFCs in hybrid configurations is strongly dependent on how thermal energy is redistributed and reutilized across the entire system.

In such systems, the energy conversion process is inherently coupled: a portion of the fuel chemical energy is directly converted into electrical power, while the remaining fraction is released as high-temperature exhaust. Rather than being rejected, this thermal energy is actively integrated into the system through heat recovery and preheating mechanisms, forming a closed thermodynamic loop that links the SOFC with downstream or parallel subsystems. This integration is particularly evident in configurations where exhaust gases are used to preheat incoming air or fuel streams, or to supply energy to additional thermodynamic cycles such as gas turbines [46].

In practice, this thermodynamic coupling is realized through a network of heat exchange pathways and interacting flow streams across the system. High-temperature sources, including SOFC exhaust gases, combustion products, and turbine outlet flows, are utilized through heat exchangers to condition incoming reactants, stabilize operating conditions, and reduce overall energy losses. The arrangement of these components, including the positioning of heat exchangers, the configuration of combustion units, and the routing of flow streams, directly defines the thermodynamic structure of the system. Therefore, the performance of each subsystem cannot be evaluated independently, since local variations in temperature or flow conditions propagate throughout the system and influence the global energy balance [46].

From a system design perspective, the effectiveness of this thermodynamic integration depends on the ability to maintain consistent temperature levels across different components. The requirement for elevated inlet temperatures necessitates the implementation of internal heat exchange networks, where multiple high-temperature streams are utilized to preheat both air and fuel. Consequently, the thermodynamic architecture is not only defined by energy conversion processes, but also by the configuration and effectiveness of heat recovery pathways within the system. However, this approach introduces inherent trade-offs. Increasing the degree of thermal recovery improves overall system efficiency, but also leads to higher system complexity, increased component size, and stricter integration constraints. This trade-off becomes particularly critical in aeronautical applications, where additional heat exchangers or increased stack sizes directly impact system weight and volumetric constraints. Therefore, thermodynamic optimization in SOFC-based hybrid systems involves balancing energy efficiency with system compactness, component sizing, and operational feasibility [46].

Furthermore, the thermodynamic behaviour of these systems is highly sensitive to operating conditions, especially in aeronautical environments. Variations in ambient pressure, inlet temperature, and flight conditions lead to changes in fluid density, mass flow rates, and heat transfer characteristics throughout the system. For instance, reduced ambient pressure at higher altitude decreases air density, affecting compressor performance and the available oxidant supply to the SOFC, which in turn influences reaction rates and temperature distribution within the stack. Similarly, changes in ambient temperature and flight conditions alter heat exchanger effectiveness and the degree of preheating achievable within the system [47].

Beyond this, variations in electrical load during different mission phases such as take-off, cruise, and maneuvering result in changes in fuel consumption rates, reaction intensities, and heat generation within the SOFC. These variations must be managed through coordinated adjustment of fuel-to-air ratios, mass flow rates, and heat exchange processes to prevent excessive thermal gradients or deviation from stable operating conditions. Components such as heat exchangers, compressors, combustion chambers, and flow routing networks play a critical role in maintaining thermodynamic balance, as any mismatch between these elements can lead to efficiency degradation, thermal instability, or operational limitations [48].

3.6.2 High-Temperature Operation and Exhaust Energy Potential

Building upon the thermodynamic framework introduced in Section 3.6.1, the high-temperature operation of SOFC systems enables a distinct mode of energy utilization, in which the exhaust stream serves as an active input to secondary power generation processes. In this configuration, the SOFC functions not only as an electrochemical converter, but also as a source of a high-energy working fluid capable of driving thermodynamic cycles. A defining characteristic of SOFC operation is the generation of exhaust gases with sufficiently high temperature and enthalpy to sustain expansion processes without requiring significant additional heating. This enables the exhaust stream to act as the primary carrier of residual energy between the electrochemical stage and downstream turbomachinery. Therefore, SOFC systems can be directly coupled with Brayton-type cycles, where the thermal energy of the exhaust is converted into mechanical work through controlled expansion in a turbine. From a system integration perspective, this coupling is established through the direct transfer of mass and energy from the SOFC outlet to the turbine inlet. The exhaust gases comprising reaction products and excess oxidant are routed either directly or after supplementary combustion into the turbine stage. In both cases, the thermodynamic state of this stream, defined by its temperature, pressure, and composition, determines the boundary conditions of the expansion process. The turbine extracts mechanical work from the enthalpy drop of the flowing gas, which can be utilized for compressor operation or converted into additional electrical power [46].

This configuration forms a sequential energy conversion pathway in which the initial electrochemical process extracts a portion of the fuel chemical energy, while the remaining energy retained in the exhaust stream is subsequently recovered through mechanical expansion. In contrast to conventional systems where residual thermal energy is dissipated, the SOFC-GT architecture enables direct utilization of this energy, thereby extending the effective conversion chain and improving overall system performance. The effectiveness of this coupling depends strongly on the matching between SOFC outlet conditions and turbine operating requirements.

Key parameters such as fuel utilization factor, exhaust temperature, pressure level, and mass flow rate directly influence the expansion ratio and efficiency of the turbine stage. Variations in these parameters arising from changes in load demand, operating strategy, or environmental conditions affect the distribution of energy between electrical and mechanical outputs and may lead to deviations from optimal performance [49].From a thermodynamic analysis perspective, the SOFC-GT system can be interpreted as a coupled control volume in which mass and energy flows are continuously exchanged between the electrochemical and turbomachinery subsystems.

The exhaust stream acts as the primary carrier of residual enthalpy, and its state at the SOFC outlet defines the available work potential for the turbine. The overall energy balance is governed by the conservation of mass and energy, where the total input comprising fuel chemical energy and oxidant flow is distributed among electrical power, mechanical work, and thermal losses. Maintaining this balance requires coordinated control of flow rates, fuel distribution, and operating conditions across the system [49].

In aeronautical applications, this interaction becomes increasingly sensitive due to variations in ambient conditions. Changes in altitude and pressure affect compressor performance and turbine inlet conditions, while variations in flight regime modify the required power output and system operating point. These factors alter the thermodynamic state of the exhaust stream and, consequently, the efficiency of the expansion process. Therefore, the design of SOFC-GT hybrid systems must ensure compatibility between electrochemical and turbomachinery subsystems across a wide range of operating conditions, particularly in applications characterized by continuously varying load and environmental parameters [49].

3.6.3 System-Level Integration, Design, and Performance of SOFC–GT Hybrid Systems

The integration of SOFC systems within hybrid architectures is examined from a system design perspective, where the configuration of components and the selection of operating parameters define the interaction and functional compatibility between subsystems. Within this framework, the coupling of SOFC with gas turbine systems represents one of the most advanced hybrid configurations, enabling the direct combination of electrochemical energy conversion with turbomachinery-based energy extraction. This integration is achieved through the linkage of flow streams and alignment of operating conditions between components, requiring coordinated control of mass flow rates, pressure levels, and temperature distributions across the system. Consequently, overall performance is not solely determined by the efficiency of individual components, but also by the degree of functional matching between them [50].

In such configurations, fuel energy is utilized in a staged manner. The SOFC converts a portion of the fuel's chemical energy into electrical and thermal energy, while the remaining energy contained in the exhaust stream characterized by high enthalpy is transferred to the gas turbine. Through controlled expansion, this energy is converted into mechanical power and subsequently into additional electrical output. This sequential energy conversion pathway enhances overall fuel utilization and significantly improves system efficiency [50, 51].

Accordingly, this section focuses on the analysis of SOFC–GT system architectures and the arrangement of energy conversion pathways. Various configurations are considered, ranging from systems based on exhaust-driven energy recovery to fully integrated hybrid cycles capable of simultaneous electrical and mechanical power generation. In this context, pressurization strategies play a key role in defining system behaviour and integration performance. From this perspective, the SOFC–GT system is treated as an integrated energy conversion architecture, in which system-level design decisions directly influence efficiency, operational stability, and overall feasibility [51].

3.6.4 System Architecture and Configuration of SOFC–Gas Turbine Hybrids

The architecture of solid oxide fuel cell–gas turbine (SOFC–GT) hybrid systems is defined by the manner in which electrochemical and thermodynamic processes are physically integrated within a unified cycle. Various configurations have been proposed in the literature, each representing a different level of coupling between subsystems and a distinct approach to energy utilization and flow management [46, 51].

As illustrated in Figure 3.3, the degree of system integration is highest in pressurized SOFC–GT configurations, followed by topping cycles, and decreases further in bottoming architectures, reflecting the progressive decoupling of thermodynamic interactions between subsystems [51-53].

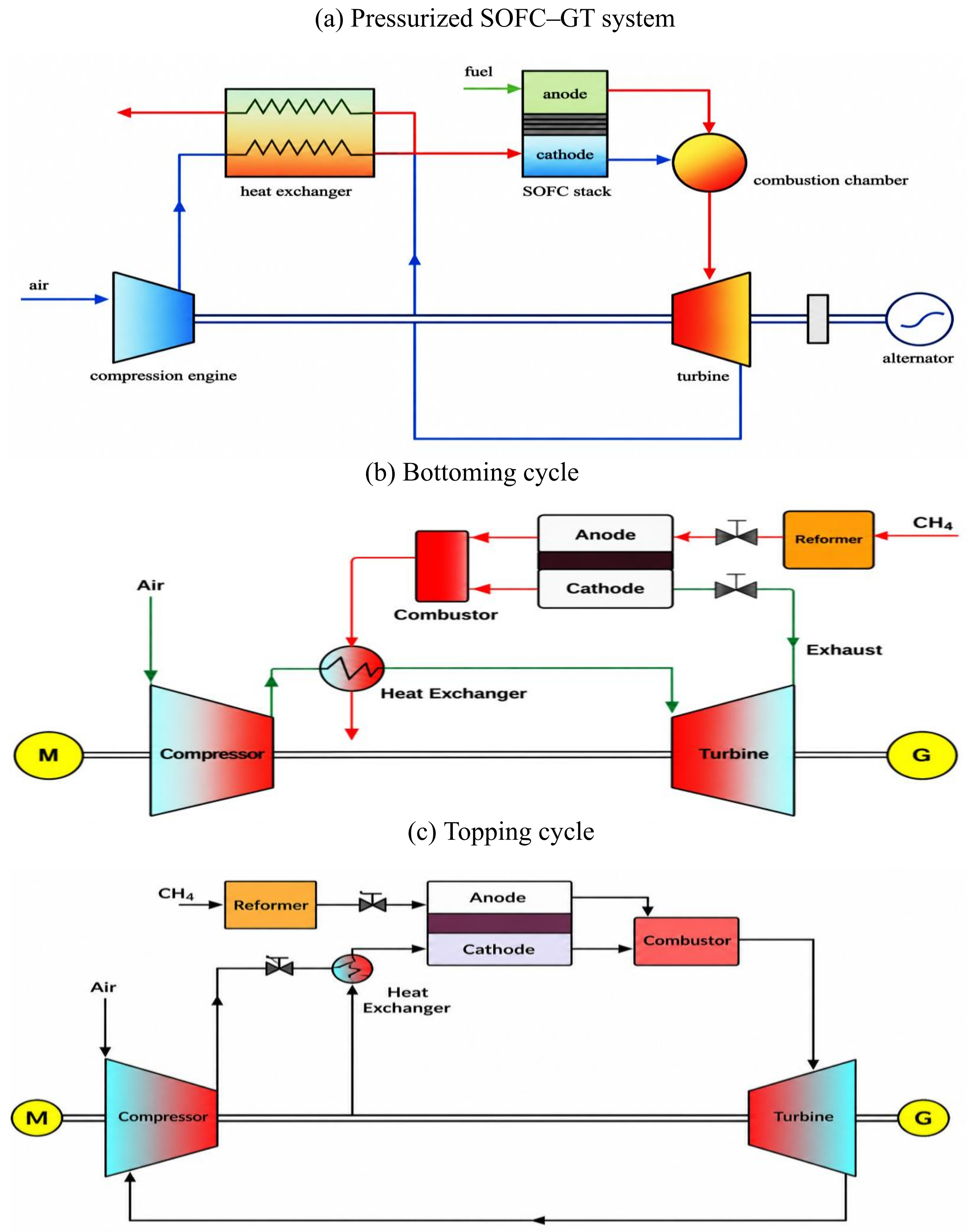

Figure 3-3 Schematic representation of SOFC–gas turbine hybrid configurations: (a) bottoming cycle, where the gas turbine recovers energy from SOFC exhaust; (b) topping cycle, where compressed air from the compressor is supplied to the SOFC; (c) pressurized SOFC–GT system, where the fuel cell operates within the pressurized turbine loop [51-53].

The simplest configuration is the bottoming cycle (b), where the SOFC operates as the primary power generator and the gas turbine is positioned downstream to recover residual thermal energy from the exhaust gases. In this arrangement, SOFC determines the operating conditions of the turbine, and the interaction between subsystems remains relatively weak. Therefore, although the system benefits from structural simplicity and ease of control, a significant portion of the thermodynamic potential is not fully exploited due to the lack of coordinated matching between the SOFC exhaust conditions and turbine requirements [50]. An intermediate level of integration is achieved in topping cycle configurations, where the gas turbine compressor is placed upstream of the SOFC and supplies pressurized air directly to the fuel cell stack. In this case, SOFC operates under elevated pressure, which enhances electrochemical performance by increasing reactant partial pressures and improving reaction kinetics [54]. The gas turbine, therefore, assumes a more active role by conditioning the inlet flow to the SOFC, rather than merely recovering energy. Notwithstanding this improvement, the interaction between subsystems remains partially decoupled, as the thermal and fluid dynamic conditions are not fully optimized across the entire cycle. In particular, the requirement to control inlet temperature and avoid thermal gradients within the SOFC introduces additional constraints that limit the flexibility of system operation [55]. The most advanced configuration is the pressurized SOFC–GT hybrid system, in which the SOFC is fully integrated into the gas turbine cycle and operates under compressor-induced pressure. In this architecture, the SOFC effectively replaces the conventional combustion chamber, producing high-temperature and high-pressure exhaust gases that directly drive the turbine. Experimental and modelling studies have demonstrated that such configurations enable strong thermodynamic coupling and significantly improve overall system efficiency and fuel utilization [46, 56]. To better highlight the differences between the proposed SOFC–GT hybrid configurations, a comparative evaluation is presented in Table 3.1. This comparison focuses not only on structural distinctions, but also on system-level implications, including the degree of integration, operational complexity, and the effectiveness of energy utilization.

Table 3-1 Comparative Evaluation of SOFC–GT Architectures [51-53].

Design Criteria	Bottoming	Topping	Pressurized
Level of Integration	Low	Medium	High
Type of Coupling	Weak (downstream)	Semi-coupled	Fully coupled
Role of Gas Turbine	Energy recovery	Air supply / conditioning	Core cycle component
Thermodynamic Matching	Limited	Moderate	High
Energy Utilization	Limited	Improved	Maximized
System Control Complexity	Low	Medium	High
Subsystem Dependency	Low	Moderate	High
Sensitivity Operate Conditions	Low	Moderate	High
Design Risk	Low	Moderate	High
Optimization Potential	Limited	Moderate	High

The comparison highlights that increasing the level of integration from bottoming to pressurized configurations enhances energy utilization and overall efficiency but simultaneously intensifies system complexity and interdependency. To this purpose, no single architecture is universally optimal; In practice, the preferred configuration depends on the required balance between efficiency, controllability, and system-level constraints [51, 52].

3.6.5 Pressurization Strategies and Turbomachinery Integration

The selection of a pressurization strategy in SOFC–gas turbine hybrid systems extends beyond a purely mechanical design decision and directly influences system efficiency, cost, and integration complexity. Two principal approaches are typically considered: turbocharger-based pressurization and microturbine-based hybridization, each representing a distinct level of energy system integration. Beyond their conceptual differences, extensive research has been conducted to evaluate their dynamic behaviour, control requirements, and system-level trade-offs [57]. To better understand the impact of balance-of-plant configurations on SOFC performance, two common approaches are compared: turbocharger-assisted and microturbine-based systems in Figure 3.4.

From energy recovery to power generation

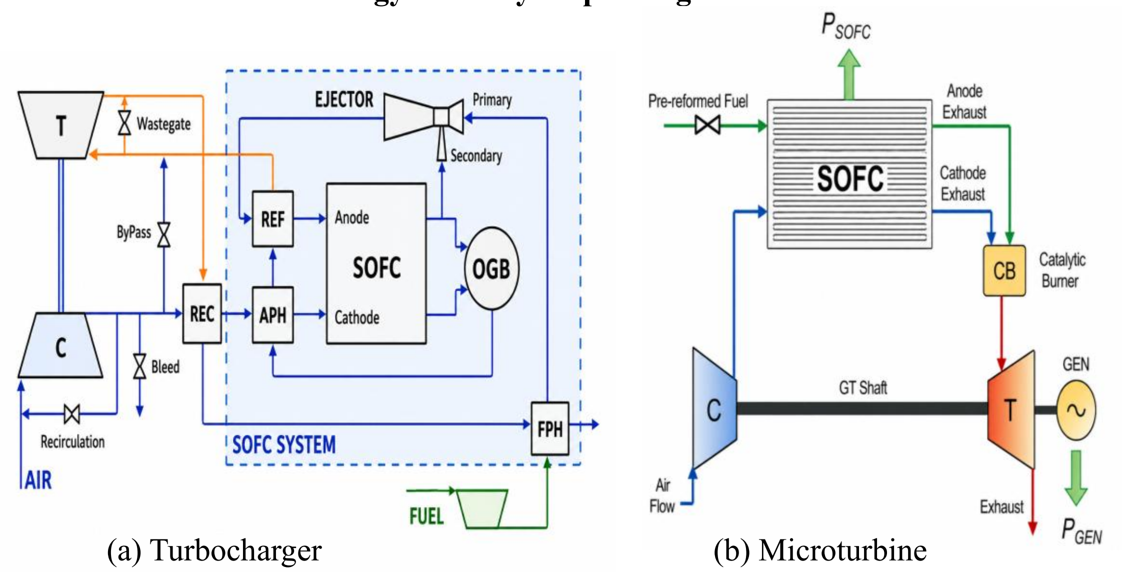

Figure 3-4 Pressurization Comparison of SOFC Configurations with Turbocharger and Microturbine [58, 59].

As demonstrated in Figure 3.4 Turbocharger-based configurations rely on exhaust-driven compression, where the turbine extracts only sufficient energy from the SOFC exhaust stream to sustain compressor operation without producing net power. This enables pressurized SOFC operation while maintaining a relatively simple and cost-effective architecture. Studies conducted by the Thermochemical Power Group (TPG) at the University of Genoa have demonstrated that turbochargers offer significant economic advantages due to mass production and reduced capital cost, making them attractive for distributed energy applications [50, 60]. Additionally, the relatively weak coupling between subsystems allows for improved operational robustness and simplified control strategies. However, experimental and modelling studies also indicate that such systems are still subject to dynamic challenges, particularly related to thermal stress and transient response, requiring careful control design even in partially integrated configurations [50]. Nevertheless, these advantages, the fundamental limitation of turbocharger-based systems lies in their inability to extend the energy conversion chain beyond the electrochemical stage. The thermal energy of the SOFC exhaust is only partially utilized, resulting in moderate overall efficiencies. To this purpose, these systems are generally regarded as intermediate solutions that enhance SOFC performance through pressurization but do not fully realize the potential of hybrid cycle energy recovery [53, 57]. In contrast, microturbine-based configurations introduce an active thermodynamic conversion stage, transforming the system into a fully integrated hybrid cycle. In these architectures, the turbine not only drives the compressor but also generates additional power through expansion of high-temperature exhaust gases, establishing a strong coupling between electrochemical and thermodynamic processes. Foundational studies by McLarty, Brouwer, and Samuelsen have shown that such hybrid systems can theoretically achieve fuel-to-electricity efficiencies exceeding 70%, provided that appropriate thermodynamic matching between the SOFC and turbomachinery is achieved [61].

Subsequent review and experimental studies further confirm that microturbine-based SOFC systems are particularly well-suited for hybridization due to the compatibility of operating temperature and pressure levels between the two subsystems [61].

Demonstration projects, such as the Siemens Westinghouse SOFC–microturbine hybrid system, have validated the feasibility of this approach, achieving electrical efficiencies above 50% and demonstrating the benefits of pressurized operation in real systems [62]. In advanced configurations, system efficiencies exceeding 60% have been widely reported, highlighting the effectiveness of multi-stage energy conversion and heat recovery [61].

However, the increased level of integration introduces substantial design and operational challenges. The strong interdependency between the SOFC and turbomachinery requires precise matching of pressure ratios, turbine inlet temperature, and mass flow distribution. Deviations from optimal conditions can propagate through the system, affecting both electrochemical performance and turbine operation. Studies have shown that issues such as compressor surge, thermal gradients, and fuel utilization variations significantly impact system stability, particularly under transient operating conditions.

From a system engineering perspective, the distinction between turbocharger and microturbine strategies reflects a fundamental trade-off between cost, complexity, and energy utilization. Turbocharger-based systems offer a cost-effective and robust solution with limited integration, while microturbine-based architectures enable deep hybridization and superior efficiency at the expense of increased system complexity and stricter control requirements. This transition represents a shift from assisted pressurization toward fully integrated hybrid energy conversion systems, which are particularly relevant for advanced applications such as distributed generation and high-efficiency power systems [50, 57].

Table 3-2 Engineering comparison of turbocharger-based and microturbine-based SOFC hybrid systems [50, 57, 61, 62].

Design Aspect	Turbocharger-Based System	Microturbine-Based System
Role in System	Auxiliary compression device	Active energy conversion unit
Power Output	No net power generation	Produces additional mechanical/electrical power
Level of Integration	Partial (weak coupling)	Full hybrid (strong coupling)
Energy Utilization	Limited (no expansion work recovery)	High (multi-stage energy conversion)
System Efficiency	Moderate improvement	Significant improvement
Control Complexity	Relatively simple	Highly complex (tight parameter matching)
Dynamic Response	More stable, less sensitive	Sensitive to transients (surge, thermal gradients)
System Cost	Lower (mature technology)	Higher (complex turbomachinery)
Design Risk	Low to moderate	High (integration constraints)
Hybridization Level	Assisted pressurization	True hybrid cycle

From a system engineering perspective, Table 3.2 highlights a clear transition from auxiliary pressurization toward fully integrated hybrid energy conversion. While turbocharger-based systems prioritize simplicity and cost-effectiveness, microturbine-based configurations maximize energy utilization through strong coupling, at the expense of increased system complexity and control requirements [50, 57].

3.6.6 Thermodynamic Coupling and Energy Integration Mechanisms

What emerges from the literature is not simply that heat recovery improves efficiency, but that each integration strategy fundamentally reshapes the role of the SOFC within the energy conversion chain. In early heat-recovery-oriented approaches (e.g., Lin et al.), the SOFC behaves essentially as a high-temperature heat source, where the primary objective is to extract residual thermal energy through external devices such as heat exchangers or secondary cycles. In these configurations, integration remains externally imposed, meaning that the thermodynamic structure of the system is not altered only extended. To this purpose, although efficiency improves, the SOFC and the downstream processes remain functionally decoupled, and a large fraction of exergy destruction still occurs during indirect heat transfer [63]. In contrast, studies such as Chinda & Brault shift the perspective by treating the SOFC not merely as a heat source, but as an active thermodynamic component embedded within the Brayton cycle. Here, the coupling is no longer external but structural: the SOFC effectively replaces or modifies the combustor, allowing direct interaction between electrochemical conversion and turbine expansion. This transition marks a critical change energy is no longer "recovered" after conversion, but rather co-converted across stages, reducing the thermodynamic penalty associated with sequential processes [64].

This distinction becomes more pronounced in the work of Ferrari et al., where hybrid systems are interpreted as cascade energy systems, in which electrochemical and thermodynamic processes are deliberately interlinked to maximize energy utilization. In such architectures, the increase in efficiency (up to $\sim 60 - 65\%$) is not merely due to heat recovery, but due to the elimination of intermediate irreversibilities between conversion stages . However, this gain comes at a cost: the system loses modularity, and performance becomes highly sensitive to operating conditions such as pressure ratio and mass flow matching [28].

More recent investigations (e.g., Köhler et al.) reveal an additional layer of trade-off: not all integration pathways are thermodynamically equivalent, even if they recover similar amounts of heat. For instance, turbine-exhaust-based preheating maximizes efficiency by preserving high-grade energy for expansion, whereas SOFC-exhaust-based recovery sacrifices thermodynamic quality for architectural simplicity [65]. This highlights a critical insight often overlooked: The location of heat recovery in the cycle is more important than the amount of heat recovered. Finally, multi-generation studies (Cao et al.) push integration even further, demonstrating that extending the cascade beyond electricity (e.g., to cooling or hydrogen production) can improve overall exergy utilization, but introduces diminishing returns due to increased system-level irreversibilities and economic penalties [66]. Across the literature, integration strategies can be interpreted as a progressive shift in system philosophy:

Table 3-3 Comparison of Energy and Heat Integration Strategies in SOFC–GT Hybrid Systems [28, 64, 66].

Integration Level	Configuration Type	System Role of SOFC	Energy Utilization	Main Advantage	Key Limitation
Low	External Heat Recovery	Heat source	Indirect heat exchange (preheating air/fuel)	Simple design, high robustness	High exergy losses due to indirect transfer
Medium	Hybrid SOFC–GT Cycle	Active thermodynamic component	Direct coupling with turbine	Significant efficiency improvement	Strong interdependency between subsystems
High	Cascade / Multi-generation Systems	Integrated energy hub	Multi-level energy utilization	Maximum energy exploitation	Increased complexity and diminishing returns

Table 3.3 summarizes the evolution of energy and heat integration strategies in SOFC–gas turbine hybrid systems, highlighting the transition from externally coupled heat recovery

configurations to fully integrated cascade systems. The comparison illustrates that increasing integration enhances energy utilization efficiency but introduces higher system complexity and stronger coupling constraints [28, 64, 66].

3.6.7 System Performance, Efficiency, and Design Trade-offs

The performance advantage of SOFC–gas turbine hybrid systems cannot be reduced to efficiency improvement alone; rather, it emerges from a fundamental reconfiguration of where and how irreversibilities occur within the system. Literature consistently shows that hybridization does not eliminate losses but redistributes them across the energy conversion chain. In standalone SOFC systems, a significant portion of exergy destruction is associated with thermal management and exhaust heat rejection, whereas in conventional gas turbines, major losses occur during combustion and high-temperature expansion. Hybrid configurations alter this distribution by partially replacing combustion with electrochemical conversion, thereby reducing entropy generation in high-temperature regions while shifting losses toward auxiliary components such as heat exchangers and afterburners [66].This redistribution explains why hybrid systems outperform standalone configurations not by eliminating losses, but by relocating them within the cycle. However, this advantage introduces a critical system-level constraint: performance becomes dependent on subsystem interaction rather than individual component efficiency. As shown in hybrid modelling studies, the turbine no longer operates independently but is strongly constrained by SOFC outlet conditions. Consequently, improving one subsystem (e.g., increasing fuel utilization in the SOFC) may negatively affect another (e.g., reducing turbine inlet temperature), creating inherent trade-offs within the system [64].

Further complexity arises with deeper thermal integration. Studies indicate that while advanced integration strategies improve overall energy utilization, they reduce the system's tolerance to off-design conditions. Small deviations in pressure ratio, temperature, or flow distribution can propagate across the system and degrade performance or stability [28]. This behaviour contrasts with loosely coupled systems, where subsystems retain greater operational independence. Recent multi-generation and system-level analyses reveal an additional limitation: beyond a certain level of integration, performance gains are constrained by non-thermodynamic factors such as system complexity, auxiliary losses, and economic considerations. While additional recovery subsystems can increase exergy utilization, they also introduce new sources of irreversibility and cost, leading to diminishing returns in system optimization [66, 67]. From an engineering perspective, the key advantage of SOFC–GT systems lies in their ability to redistribute energy conversion processes across multiple stages. However, this benefit inherently introduces stronger coupling between subsystems, shifting the design problem from maximizing efficiency to balancing efficiency, stability, and system complexity.

3.6.8 Application of SOFC–Gas Turbine Hybrid Systems in Transport

Following the detailed discussion of integration principles and system design in Section 3.6.3, this section shifts the focus toward evaluating SOFC–gas turbine hybrid systems from an application-oriented perspective. The intention is not to repeat configuration-level descriptions, but to examine how these systems perform when subjected to the practical constraints and operational demands of different transport environments. To maintain conceptual consistency, the discussion is confined to SOFC–GT architectures. Although PEMFC-based systems are occasionally referenced for context, they are not treated as parallel solutions, as their hybridization mechanisms differ fundamentally from those based on thermodynamic coupling. In practice, the analysis highlights how SOFC–GT systems leverage high-temperature operation to enable deeper integration and more effective energy utilization across various applications. The section is structured around three key domains, each representing a distinct operational framework. Stationary systems are first considered as a benchmark, given their technological maturity and relatively stable operating conditions. Marine applications are then examined, where system design is shaped by prolonged operation, fuel flexibility, and onboard integration constraints. Within this context, limited comparisons with PEMFC systems are provided, while emphasis is placed on the suitability of SOFC–GT configurations and their interaction with different fuel pathways.

The final part of the section focuses on aeronautical applications, which impose the most stringent requirements on system design. Here, factors such as specific power, weight, and mission profile become dominant, requiring a more integrated and adaptive system approach. This includes the consideration of advanced SOFC technologies, particularly those capable of achieving higher power density and improved responsiveness, which are essential for UAVs and long-endurance flight platforms. In this way, the section establishes a clear progression from controlled operating environments to highly dynamic ones, demonstrating how system-level integration strategies must be tailored to meet the unique demands of each application domain [47, 68].

3.6.8.1 SOFC/GT Hybrid Systems for Ground and Stationary Applications

Stationary power systems represent one of the most favorable environments for the deployment of SOFC–gas turbine hybrid configurations. Unlike mobile or aeronautical applications, these systems are not constrained by strict limitations on weight and volume, which enables the adoption of more complex and highly integrated designs. Under such conditions, pressurized and strongly coupled SOFC–GT architectures become particularly attractive, as they allow for enhanced fuel utilization and improved overall efficiency [53, 66].

A major factor contributing to this suitability is the operational stability typically observed in stationary applications. As reported by Ferrari et al. [28] , power plants in this sector generally operate under relatively constant load conditions, in contrast to the highly transient behaviour seen in aviation systems. This stability allows the system to remain close to its optimal operating point, thereby minimizing efficiency losses associated with off-design operation and reducing the burden on control systems. At the same time, the availability of installation space facilitates the integration of advanced heat recovery units, large-scale heat exchangers, and more sophisticated fuel processing technologies, all of which contribute to improved system performance [28, 66].

Different research approaches in the literature reflect varying priorities in the design of stationary SOFC–GT systems. Early work by McLarty, Brouwer, and Samuelsen primarily focuses on maximizing thermodynamic efficiency through tightly integrated and pressurized configurations, highlighting the theoretical limits of hybrid cycle performance [61]. In contrast, studies by Ferrari, Magistri, and co-workers emphasize practical considerations such as cost, durability, and operational feasibility, often proposing simplified or turbocharger-assisted configurations as more realistic implementation pathways [28, 58].

This divergence highlights a fundamental trade-off in system design. Increasing the level of thermal and mechanical integration tends to improve energy utilization; however, it simultaneously introduces greater sensitivity to operating conditions. Parameters such as pressure ratio, temperature gradients, and mass flow distribution play a critical role in determining system stability, and deviations from optimal values can significantly affect performance [53, 61]. As a consequence, highly integrated systems require more sophisticated control strategies and careful system tuning. Beyond performance considerations, practical challenges remain a key factor in the deployment of these systems. High system complexity, extended start-up durations, and vulnerability to thermal stresses continue to limit widespread implementation. In addition, economic factors become increasingly important in stationary applications. Capital investment, component lifetime, and maintenance requirements often outweigh purely efficiency-driven considerations. Notably, auxiliary components such as heat exchangers and reformers have been shown to exert a significant influence on both system cost and reliability, potentially reducing the net benefit of higher efficiency configurations [28, 66]. Taken as a whole, stationary applications provide a suitable platform for exploiting the full potential of SOFC–GT hybrid systems. Nevertheless, achieving an optimal design requires a balanced approach, in which efficiency gains are evaluated alongside considerations of cost, controllability, and long-term operational stability.

3.6.8.2 Hybrid SOFC/GT Systems in Marine Applications

The maritime sector constitutes one of the most demanding environments for the deployment of advanced energy systems, due to the simultaneous requirements of high power output, extended operating duration, and strict reliability standards. in contrast stationary or aeronautical applications, shipboard energy systems must sustain continuous operation under harsh environmental conditions while maintaining performance over long voyages and varying load profiles. These factors fundamentally influence the design philosophy of hybrid energy systems. Within this framework, SOFC–gas turbine hybrid systems are better understood not merely as efficiency-enhancing solutions, but as integrated energy platforms capable of addressing multiple operational requirements simultaneously. The thermodynamic coupling between SOFCs and gas turbines, previously described in Section 3.6.6, enables multi-stage energy conversion and supports the development of tightly integrated energy systems [69]. A notable trend in marine system architecture is the transition toward multi-functional energy platforms. Rather than focusing solely on electricity generation, these systems are designed to simultaneously support propulsion, thermal management, and auxiliary onboard services. In line with the energy integration mechanisms also discussed in Section 3.6.6 , coupling SOFC–GT units with bottoming cycles and advanced thermal subsystems enables cascade energy utilization. For large vessels such as cruise ships and container carriers, this approach has been shown to achieve overall system efficiencies exceeding 80% [70].

The suitability of SOFC–GT systems for maritime applications is closely linked to the operational characteristics of marine transport. Long cruising periods at near-constant load conditions reduce the impact of the limited dynamic response typically associated with SOFC systems. Under such steady operating regimes, the fuel cell can function close to its optimal efficiency point. Meanwhile, the gas turbine provides the necessary flexibility for load adjustment and contributes to overall system stability. This complementary interaction not only enhances efficiency but also mitigates thermal cycling effects, which are a primary contributor to fuel cell degradation [69]. In spite of these advantages, the deployment of

SOFC–GT systems in marine environments is constrained by several sector-specific challenges. Continuous long-duration operation with limited maintenance opportunities places strong emphasis on durability and long-term performance stability. Degradation mechanisms such as thermal fatigue, corrosion, and gradual performance decay become critical design considerations, as even small efficiency losses accumulated over extended periods can significantly affect fuel consumption and economic viability. System integration is further complicated by the physical constraints of vessel design. The adoption of alternative fuels such as hydrogen and ammonia introduces additional challenges related to storage volume and onboard layout. Due to their lower volumetric energy density compared to conventional marine fuels, these alternatives require larger storage systems, which directly impact cargo capacity and vessel range. Techno-economic analyses indicate that this trade-off between fuel storage and payload is a key factor influencing the feasibility of fuel cell-based marine systems [69]. Another defining feature of SOFC–GT hybrid systems in marine applications is their capability for multi-output energy generation. By integrating bottoming cycles and auxiliary thermal subsystems such as Organic Rankine Cycles (ORC), supercritical CO_2 cycles, and absorption chillers, these systems can operate as trigeneration units, simultaneously producing electricity, heat, and cooling. In such configurations, high-temperature exhaust from the SOFC is first utilized for turbine expansion and subsequently recovered for secondary thermal applications, thereby enabling cascade energy utilization and reducing exergy losses relative to conventional single-output systems [70].

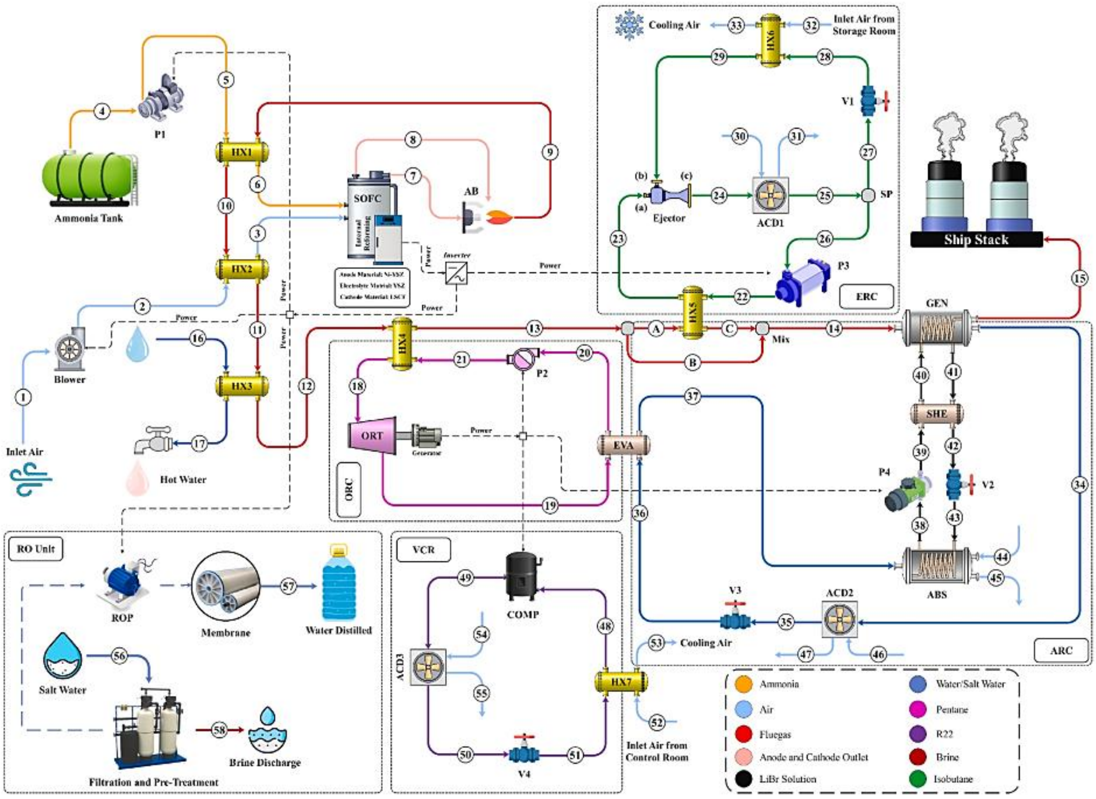

Figure 3-5 Integrated SOFC-based trigeneration system for marine applications, including power generation, heat recovery, cooling, and freshwater production subsystems. The configuration illustrates the coupling between the SOFC stack, gas turbine, and auxiliary thermal cycles [70].

As illustrated in Figure 3-5, the integration of multiple subsystems allows energy to be utilized in a sequential manner across different temperature levels. The SOFC stack acts as the primary energy conversion unit, while the gas turbine and auxiliary subsystems redistribute energy across propulsion, thermal management, and onboard services. The inclusion of additional components, such as absorption cooling and desalination units, further demonstrates the ability of SOFC-based hybrid systems to satisfy diverse energy demands within a unified framework. This configuration reflects a broader transition toward integrated energy systems, in which multiple energy carriers are managed simultaneously to maximize resource utilization under complex operating conditions [70]. Finally, fuel selection represents a critical design parameter in marine SOFC–GT systems. Different fuels including hydrogen, ammonia, methanol, and LNG present distinct trade-offs in terms of storage requirements, efficiency, emissions, and system complexity. Therefore, system design must be approached as a multi-objective optimization problem, where performance is balanced against onboard integration constraints, cost considerations, and lifecycle emissions. Consequently, no single fuel pathway can be considered universally optimal, and the choice of fuel and system configuration must be aligned with the specific vessel type and operational profile [70, 71].

3.6.8.2.1. Operational and Regulatory Drivers of SOFC–GT Systems in Marine Applications

Marine energy systems operate under a set of constraints that fundamentally distinguish them from terrestrial applications. Unlike land-based systems, where design is often driven primarily by efficiency considerations, maritime applications require simultaneous consideration of long-duration operation, vessel integration, and strict regulatory compliance. These combined factors define a distinct design space for SOFC–gas turbine hybrid systems. A defining characteristic of marine operation is the prevalence of extended steady-state conditions. Commercial vessels typically operate continuously for days or even weeks, with limited opportunities for shutdown or maintenance. Under such conditions, the limited dynamic response of SOFC systems previously identified as a constraint due to thermal inertia becomes less critical. In practice, system performance is governed by durability, thermal stability, and long-term efficiency retention. Consequently, degradation mechanisms such as thermal fatigue, corrosion, and gradual electrochemical performance decay emerge as dominant design drivers. Unlike short-duration systems, where transient losses are critical, marine applications accumulate small inefficiencies over time, resulting in significant impacts on fuel consumption and lifecycle cost. This shifts the optimization focus from instantaneous efficiency toward long-term performance and durability [72].

Evidence from techno-economic studies further highlights the importance of system-level integration with vessel architecture. The adoption of alternative fuels, including hydrogen and ammonia, introduces substantial challenges related to storage volume, safety, and onboard layout. Due to their lower volumetric energy density compared to conventional marine fuels, these alternatives require significantly larger storage tanks, which directly affects cargo capacity and vessel range. Therefore, the trade-off between fuel storage and payload has been identified as a key barrier to the large-scale implementation of fuel cell-based marine systems [73]. In parallel, regulatory frameworks play an increasingly influential role in shaping system design. International Maritime Organization (IMO) regulations, including MARPOL Annex VI and the IGF Code, impose stringent limits on greenhouse gas emissions and define safety requirements for low-flashpoint fuels. These regulations not only promote the adoption of low-carbon technologies such as SOFC–GT systems, but also introduce additional constraints related to fuel handling, system redundancy, and onboard safety architecture [74].

From a system-level perspective, the interaction of these operational and regulatory constraints leads to a fundamentally different optimization problem compared to terrestrial applications. While deep thermal integration and pressurized hybridization enable high efficiency, their practical implementation in marine systems is constrained by spatial limitations, safety requirements, and the need for robust long-term operation. Consequently, the optimal system configuration is not necessarily the one that maximizes thermodynamic efficiency, but rather the one that achieves the best balance between efficiency, reliability, and integration feasibility. Taken together, these considerations underline a critical insight: in marine SOFC–GT systems, performance cannot be assessed solely based on peak efficiency. Instead, system viability depends on the ability to sustain stable, safe, and economically viable operation over extended time scales. For this reason, system design must be approached as a multi-objective optimization problem, where energy efficiency, durability, regulatory compliance, and vessel-level integration are evaluated simultaneously. Under such conditions, the feasibility of SOFC–GT systems are governed less by maximum efficiency and more by their capacity to deliver reliable and integrated performance within strict operational and regulatory boundaries [73].

3.6.8.2.2. Fuel Pathways and Comparative Assessment for Marine SOFC/GT Hybrid Systems

Fuel selection represents one of the most influential design variables in marine SOFC–gas turbine hybrid systems, as it simultaneously affects system efficiency, onboard integration, and long-term environmental performance. In contrast to conventional marine propulsion systems, which rely predominantly on diesel fuels, SOFC–GT configurations offer a significantly higher degree of fuel flexibility. However, this flexibility introduces additional complexity, as the effectiveness of energy recovery and system integration is strongly dependent on the physicochemical properties of the selected fuel [19]. A key distinction among alternative fuels lies in the trade-off between energy density, system complexity, and environmental impact. Hydrogen provides the most direct route toward zero-emission operation at the point of use, since its electrochemical conversion produces only water. Nevertheless, its low volumetric energy density imposes substantial storage constraints, requiring either high-pressure compression or cryogenic liquefaction. These requirements have direct implications for vessel layout and cargo capacity, thereby limiting the practical applicability of hydrogen-based systems primarily to short-range or coastal vessels [69].

Ammonia, by contrast, offers a more balanced compromise between storage feasibility and environmental performance. Its higher volumetric energy density and the possibility of storage in liquid form under moderate conditions make it more suitable for long-haul maritime applications. This advantage, however, is offset by increased system complexity, as ammonia must be cracked or reformed prior to utilization in SOFC systems. In addition, the potential formation of NO_x emissions during downstream processes introduces further operational constraints. As a result, ammonia-based systems shift the design challenge from storage limitations toward reaction control and emission management [70, 75]. Methanol and LNG can be interpreted as transitional fuel options within the broader decarbonization pathway of maritime transport. Methanol combines relatively simple storage characteristics with the ability to be reformed onboard into hydrogen-rich fuel streams, enabling comparatively straightforward system integration. LNG, although still fossil-based, benefits from an established global infrastructure and offers reduced emissions relative to conventional marine fuels. Despite these advantages, both fuels remain associated with carbon emissions and therefore cannot be considered long-term zero-carbon solutions [71].

From a system-level perspective, the choice of fuel leads to fundamentally different distributions of irreversibilities within the hybrid cycle. Hydrogen-based systems tend to shift exergy losses toward compression and storage processes, whereas ammonia-based systems concentrate losses in fuel processing and reaction stages. In contrast, methanol and LNG systems exhibit a more distributed pattern of exergy destruction across reforming and heat recovery units. This observation highlights that fuel selection does not only influence efficiency but also determines where complexity and thermodynamic losses are introduced within the system. Taken together, these differences indicate that fuel selection must be treated as a multi-objective optimization problem, rather than a single-parameter decision. Efficiency, storage feasibility, system complexity, emissions, and operational constraints must be evaluated simultaneously to identify the most suitable configuration. As maritime decarbonization progresses, it is unlikely that a single fuel pathway will dominate across all vessel categories. In practice, a portfolio of fuels tailored to specific operational profiles from short-range vessels to long-haul deep-sea shipping is expected to provide the most practical and scalable solution[70, 71]. To better compare the characteristics of different fuel options for marine SOFC/GT hybrid systems, a summary is provided in Table 3-4.

Table 3-4 Comparative assessment of fuel pathways for marine SOFC/GT hybrid systems based on efficiency, storage characteristics, and application suitability [69-71, 76].

Fuel	**Key Advantages**	**Main Limitations**	**Typical Efficiency (SOFC/GT)**	**Marine Suitability**
Hydrogen	Zero emissions, high electrochemical performance	Low volumetric energy density, storage complexity	$50-60\%$	Short-range / coastal
Ammonia	Carbon-free, better storage than H_2	Cracking requirement, NO_X formation risk	$55-65\%$	Long-haul / deep-sea
Methanol	Liquid fuel, easy storage, reforming capability	CO_2 emissions, lower efficiency than NH_3	$50-60\%$	Medium-range
LNG	Mature infrastructure, lower emissions than diesel	Fossil-based, CO_2 emissions	$45-55\%$	Transitional fuel

The comparison presented in Table 3-4 clearly indicates that no single fuel pathway simultaneously satisfies all design criteria. Hydrogen maximizes environmental performance but introduces severe storage challenges, ammonia improves storage feasibility while increasing system complexity, and methanol and LNG offer practical integration advantages at the expense of long-term sustainability. This reinforces a central insight: fuel selection in marine SOFC–GT systems is not an isolated choice, but a system-level decision that directly shapes overall architecture, performance, and feasibility.

3.6.8.3 Application of SOFC–GT Hybrid Systems in Aeronautical Applications

Aeronautical applications impose a fundamentally different operational framework on SOFC–gas turbine hybrid systems compared to terrestrial and marine environments. In this context, system behaviour is not governed solely by steady-state efficiency, but by the ability to operate under continuously varying conditions such as altitude, ambient pressure, and mission phase [77, 78]. From a comparative perspective, the suitability of high-temperature fuel cell technologies for hybridization with gas turbine cycles becomes particularly relevant. Among these, both Molten Carbonate Fuel Cells (MCFC) and Solid Oxide Fuel Cells (SOFC) offer the potential for thermodynamic integration due to their elevated operating temperatures. However, their applicability to aeronautical systems differs significantly [43]. As discussed in detail in section 3.5 about MCFC systems, they are capable of hybridization with gas turbines in aviation applications but operate at comparatively lower temperatures and have limits the quality of exhaust heat available for turbine expansion. Therefore, MCFC–GT configurations generally require supplementary combustion to achieve adequate turbine inlet temperatures, introducing additional system complexity and reducing overall efficiency [42].
Furthermore, the relatively lower thermal grade of the exhaust restricts the depth of thermodynamic integration, making MCFC-based hybrids less suitable for weight-sensitive and performance-critical aeronautical applications [39]. In contrast, SOFC-based systems operate at significantly higher temperatures which make them more attractive choice for aviation applications, enabling direct coupling with gas turbine cycles without the need for additional firing. This allows more effective utilization of high-grade thermal energy, improved integration between electrochemical and turbomachinery subsystems, and higher overall system efficiency. Consequently, SOFC–GT hybrid systems are better aligned with the requirements of endurance-oriented aeronautical missions, where sustained operation under quasi-steady conditions is dominant [79, 80]. A further distinction emerges when comparing these technologies with low-temperature fuel cells like PEMFC Electrical hybrid with battery or coupling turbocharger in UAV applications. Based on these considerations and take into account SOFC–GT hybrid systems constraint in aviation applications, SOFC–GT hybrid systems represent the most suitable configuration for aeronautical applications requiring high efficiency, deep energy integration, and sustained operation under mission-driven constraints [79].

3.6.8.3.1. System Characteristics and Integration

From an integration standpoint, SOFC–GT systems are defined by strong thermodynamic and fluid dynamic coupling between subsystems. Mass flow, energy exchange, and thermal interactions are tightly interconnected, forming a unified energy conversion network. Under aeronautical conditions, this coupling becomes more pronounced, as variations in flight conditions continuously shift system operation away from nominal design points. Unlike stationary systems, where quasi-steady operation dominates, aircraft systems must maintain performance across a wide range of off-design conditions, requiring coordinated control of airflow, fuel utilization, and turbine operation [79, 80].

This level of interdependency implies that subsystem-level analysis is insufficient. Variations in airflow rate, fuel utilization, or turbine inlet temperature directly influence stack temperature, electrochemical efficiency, and overall system stability. Consequently, SOFC–GT hybrid systems in aviation must be evaluated at the aircraft level, where propulsion, electrical generation, and thermal management are inherently coupled [79].

3.6.8.3.2. Aeronautical Design Drivers

In contrast to stationary and marine applications, the design of hybrid systems in aviation is dominated by weight, volume, and integration constraints. Under these conditions, system performance cannot be evaluated based on efficiency alone, as even moderate increases in mass or volume can significantly affect aerodynamic performance and mission capability.

One of the primary limitations of SOFC-based systems is their relatively low specific power. While SOFCs achieve high fuel-to-electric efficiency, the presence of compressors, heat exchangers, and auxiliary components reduces the overall power-to-weight ratio. Hybridization with gas turbines provides a partial solution by combining high-efficiency electrochemical conversion with the high specific power of turbomachinery, enabling a more balanced distribution of power generation [77, 79].

Another critical driver is the rapid increase in onboard electrical demand. Modern aircraft rely extensively on electrically powered subsystems, and future platforms are expected to further increase electrification levels. Under these conditions, efficient onboard power generation becomes essential. Fuel cell systems offer clear advantages in this regard, although their integration introduces additional penalties in terms of system mass and complexity. Mission-dependent operation introduces an additional layer of complexity. Aircraft must operate across highly dynamic flight phases, including take-off, climb, cruise, and descent.

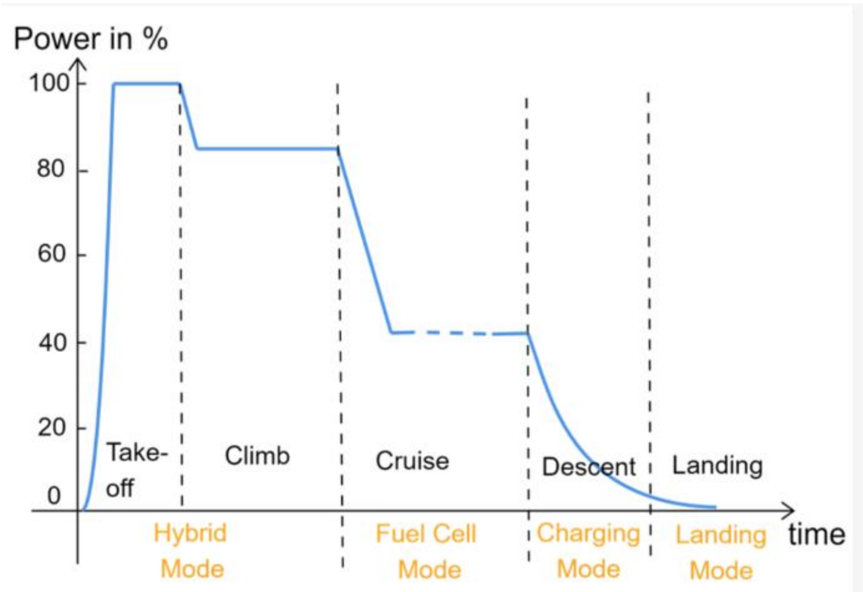

Figure 3-6 Aircraft mission power profile highlighting steady cruise conditions for SOFC/GT hybrid operation [81].

As illustrated in Figure 3-6, power demand is highly non-uniform, with peak requirements during take-off and climb, followed by relatively stable conditions during cruise. High-temperature SOFC systems are inherently sensitive to such variations, as thermal gradients can induce material stress and reduce system lifetime. Maintaining stable operation therefore requires advanced control strategies capable of coordinating fuel utilization, airflow distribution, and thermal management [77]. Finally, integration constraints play a decisive role. Unlike stationary systems, aircraft architectures impose strict spatial limitations. The inclusion of fuel processing units, heat recovery systems, and auxiliary components increases system complexity and introduces additional integration challenges. As a result, system performance depends not only on component efficiency but also on the effectiveness of overall architectural integration [79].

3.6.8.3.3. SOFC–GT Systems for Endurance-Critical Aircraft and UAVs

Endurance-oriented missions have been identified as promising application domains for SOFC–GT hybrid systems in aviation. Although these missions are not fully steady-state, they are typically characterized by a dominant cruise phase with relatively stable power demand, despite the presence of transient operating phases such as take-off, climb, and descent. Typical examples proposed in the literature include high-altitude pseudo-satellites, surveillance UAVs, and communication relay platforms, where long-duration operation under quasi-stationary conditions is required. Under such operating regimes, several conceptual studies, feasibility analyses, and early-stage prototype demonstrations indicate that SOFC–GT hybrid architectures have the potential to provide high-efficiency continuous power generation. In these proposed configurations, the SOFC is generally operated near its optimal efficiency point, while the gas turbine supports pressurization and thermal management within the integrated system. The primary objective of these architectures is to shift system operation from transient-driven behaviour toward efficiency-oriented performance during the dominant cruise phase. Nevertheless, it should be emphasized that SOFC–GT systems for aviation applications remain largely at the research and technology demonstration stage. Most existing investigations rely on numerical simulations, system-level assessments, or laboratory-scale demonstrators, while significant challenges related to thermal management, weight, durability, system integration, and certification still limit large-scale practical implementation in aircraft and UAV platforms [77, 80].

Despite these advantages, system performance remains highly sensitive to variations in operating conditions. Changes in altitude, ambient temperature, and pressure directly affect fuel reforming reactions, airflow distribution, and turbine behaviour. Aircraft-level simulations have shown that parameters such as compressor flow split and the oxygen-to-carbon ratio in the reformer significantly influence both fuel cell output and turbine thrust. These interactions demonstrate that stable operation cannot be achieved through independent subsystem control, but requires coordinated management of airflow, fuel utilization, and turbine operation across the entire system [77]. Fuel flexibility introduces additional system-level trade-offs. While the use of hydrocarbon fuels reduces storage penalties compared to liquid hydrogen, it also introduces challenges related to reforming stability and carbon management. For instance, propane-fueled SOFC–GT systems optimized for UAV applications can achieve efficiencies of approximately 62% with a power-to-weight ratio near 0.57 kW/kg, but only under carefully controlled operating conditions [46].

These observations indicate that fuel selection influences not only energy density, but also system mass, thermal integration, and overall mission endurance. Consequently, the primary limitation of SOFC–GT systems in aeronautical applications is not thermodynamic efficiency, but controllability under off-design and transient conditions. Factors such as thermal inertia, slow start-up, and sensitivity to temperature gradients restrict the system ability to respond rapidly to changing flight conditions. From a system modelling perspective, these effects are reflected in the strong coupling between propulsion, electrical generation, and aerodynamic integration. Aircraft-level analyses further indicate that system integration, including component placement within the fuselage or nacelle, can influence aerodynamic drag and overall fuel consumption by several percent. This reinforces the importance of integrated, aircraft-level design approaches rather than isolated component optimization [80].

To further illustrate the internal power distribution within SOFC–GT hybrid systems, Figure 3.7 presents the contribution of the fuel cell and gas turbine under a representative mission profile. As shown, the SOFC provides a relatively stable power output throughout the mission, particularly during the cruise phase, operating close to its optimal efficiency point. In contrast, the gas turbine exhibits a more dynamic response, adjusting its output to accommodate variations in load demand, especially during transient phases such as climb and descent. This distribution highlights a key advantage of SOFC–GT hybrid architectures: the functional decoupling between steady-state efficiency and dynamic response. The fuel cell serves as the primary energy conversion unit, maximizing efficiency under quasi-steady conditions, while the gas turbine compensates for transient power requirements and supports system stability. Such a coordinated power-sharing strategy is particularly well aligned with aeronautical mission profiles, where prolonged cruise operation is combined with short-duration high-power demands.

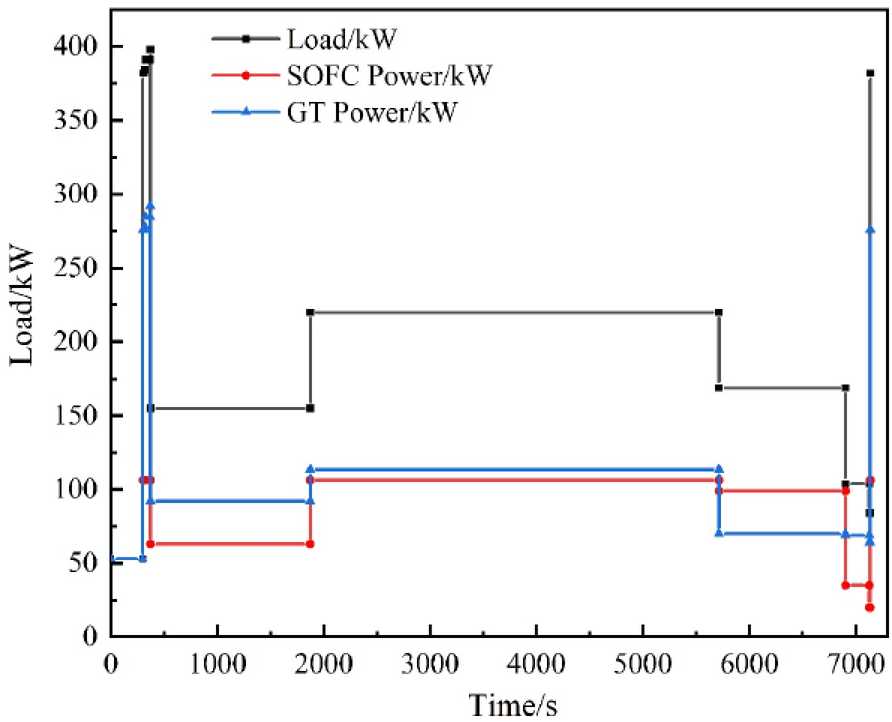

Figure 3-7 Power distribution between SOFC and gas turbine in a hybrid SOFC–GT system under a representative aeronautical mission profile [46].

From a design perspective, this distribution of power emphasizes the importance of balancing efficiency and responsiveness within the hybrid system. While maximizing the contribution of the SOFC improves overall efficiency, it reduces the system ability to respond to rapid load changes. Conversely, increasing the reliance on the gas turbine enhances dynamic performance but may reduce efficiency due to additional thermodynamic losses. This trade-off highlights a central design challenge in SOFC–GT systems: achieving an optimal balance between steady-state efficiency and transient performance. In aeronautical applications, where both long-duration cruise and high-power transient phases are critical, this balance becomes a key factor in determining system feasibility [46]. This behaviour demonstrates that hybridization is not merely a combination of components, but a functional separation of roles between efficiency-oriented and response-oriented subsystems. From a performance standpoint, this coordinated operation translates into improved overall system efficiency during cruise, where the SOFC dominates energy conversion under near-optimal conditions. At the same time, the contribution of the gas turbine during transient phases ensures that system efficiency is not severely compromised by rapid load changes. This combined behaviour allows SOFC–GT systems to maintain relatively high efficiency across the full mission profile, rather than only at design point conditions.

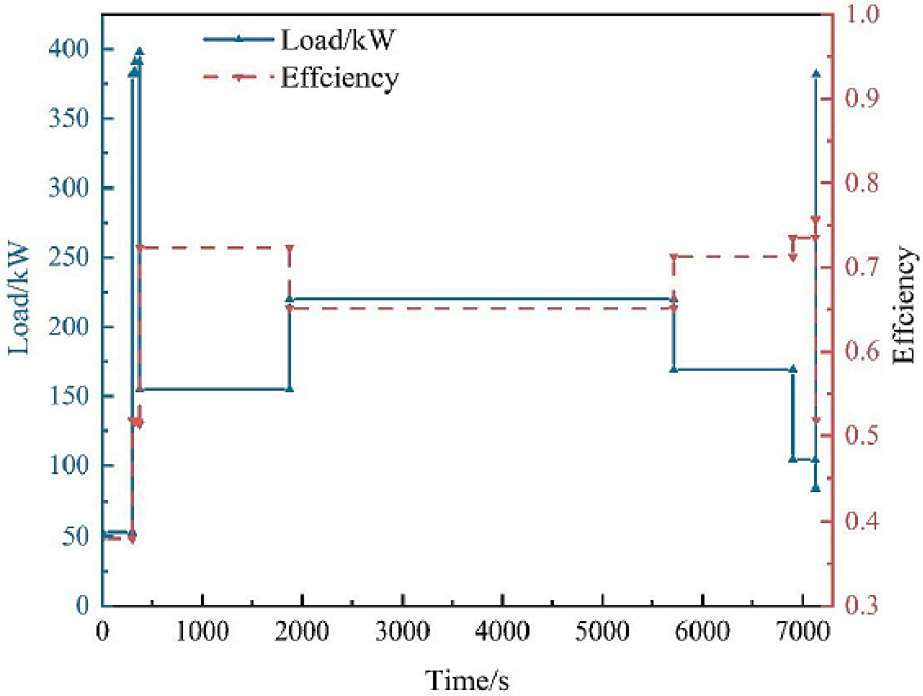

Figure 3-8 Efficiency profile of a hybrid SOFC–GT system under a representative aeronautical mission, highlighting high-efficiency operation during cruise and the impact of transient load variations on system performance [46].

The efficiency profile presented in Figure 3.8 provides a qualitative representation of the operational behaviour of SOFC–GT hybrid systems under representative aeronautical mission conditions. It should be emphasized that the efficiency values reported in the figure are intended primarily to illustrate general performance trends and relative variations across different flight phases, rather than absolute achievable efficiencies. In practical SOFC–GT architectures, additional losses associated with auxiliary subsystems, balance-of-plant components, thermal management requirements, and off-design operation would reduce the net system efficiency. Despite these limitations, the figure highlights several important system-level characteristics. One key observation is that the hybrid architecture maintains relatively stable and comparatively higher efficiency during the cruise phase, where the SOFC operates near its optimal design condition and contributes most of the energy conversion process. This behaviour is consistent with the expectation that the primary thermodynamic advantage of SOFC-based hybrid systems is realized most effectively during extended quasi-steady operation rather than under highly transient conditions [46].

By contrast, the efficiency variations observed during take-off, climb, and descent illustrate the influence of dynamic load fluctuations and the increased reliance on the gas turbine subsystem. During these transient phases, the turbine compensates for rapid changes in power demand and enhances operational flexibility. However, this adaptability is accompanied by additional thermodynamic irreversibilities and off-design losses, resulting in a temporary reduction in overall efficiency. This behaviour further highlights the inherent trade-off between efficiency optimization and transient responsiveness in hybrid propulsion architectures. When interpreted together with the power-sharing behaviour presented in Figure 3.8, the results suggest a possible functional separation of roles within the integrated system. Under relatively steady operating conditions, the SOFC appears to provide high-efficiency base-load power generation, while the gas turbine primarily supports transient response capability and operational adaptability. This coordinated interaction enables the hybrid architecture to maintain acceptable performance across the overall mission profile rather than optimizing operation around a single design point. From an aeronautical system design perspective, these observations suggest that the feasibility of SOFC–GT hybrid architectures depends not only on achieving high peak efficiency, but also on sustaining efficient operation across mission-relevant flight conditions while effectively managing transient power demands. Accordingly, future optimization strategies for SOFC–GT systems should focus not only on maximizing peak thermodynamic efficiency, but also on extending stable high-efficiency operating regions under realistic mission profiles and integrated system constraints [46].

3.6.9 From Thermodynamic Advantage to System-Level Application of SOFC–GT and MCFC Hybrid Systems

Having established the thermodynamic superiority of SOFC–GT hybrid systems from an exergy perspective, the discussion now moves beyond comparative analysis toward system-level implementation and application-driven design considerations for both MCFC–GT and SOFC–GT Hybrid Systems. While conventional comparisons between hybrid fuel cell systems often focus on energy efficiency, a more rigorous evaluation can be achieved through exergy analysis, which accounts for the quality of energy and the irreversibilities within the system. From an exergy perspective, the fundamental difference between MCFC–GT and SOFC–GT hybrid systems lies in the temperature level at which energy is released and subsequently recovered. MCFC systems operate at moderate temperatures, resulting in exhaust streams with limited exergy content. Consequently, a significant portion of the available energy cannot be effectively converted into useful work within the gas turbine subsystem, leading to increased exergy destruction in downstream components such as combustors and heat exchangers [41, 81]. In contrast, SOFC systems operate at substantially higher temperatures, producing high-grade thermal energy that can be directly utilized within the gas turbine cycle. This enables a more efficient conversion of thermal exergy into mechanical work through turbine expansion, thereby reducing the reliance on supplementary combustion and minimizing associated irreversibilities [41, 82]. The distribution of exergy destruction within the hybrid cycle further highlights the distinction between the two technologies. In MCFC–GT systems, a considerable fraction of exergy loss is associated with combustion processes required to elevate turbine inlet temperature. Additional losses occur in heat recovery units due to the lower temperature gradients available for effective heat exchange. Conversely, in SOFC–GT systems, exergy destruction is more evenly distributed and mainly due to electrochemical processes, which are inherently more efficient than combustion-based energy conversion [82, 83]. Another critical aspect is the degree of exergy recovery achievable through system integration. MCFC-based hybrids are generally limited to partial recovery of exhaust energy, whereas SOFC-based systems enable multi-stage energy utilization, including internal reforming, turbine expansion, and advanced heat recovery. This cascaded use of energy significantly improves overall system effectiveness and reduces total exergy losses [83]. Table 3.5 presents an exergy-based comparison of MCFC–GT and SOFC–GT hybrid systems, highlighting key differences in energy quality, loss mechanisms, and integration potential.

Table 3-5 Exergy-based comparative analysis of MCFC–GT and SOFC–GT hybrid systems [41, 81-83].

Exergy Criterion	MCFC–GT Hybrid System	SOFC–GT Hybrid System	Engineering Insight
Exergy Level of Exhaust	Medium	High	Determines ability for direct turbine expansion
Exergy Utilization Efficiency	Medium	High	SOFC enables deeper conversion of thermal exergy
Combustion Dependency	High (required)	Low (often unnecessary)	Major source of irreversibility in MCFC
Primary Exergy Loss Location	Combustor + Heat Exchangers	Electrochemical + Minor thermal losses	Losses more controllable in SOFC
Heat Recovery Effectiveness	Limited by temperature	Highly effective	SOFC supports cascade energy use
Exergy Destruction Mechanism	Chemical + thermal mismatch	Mostly electrochemical irreversibility	Different optimization strategies required
Integration Depth	Partial	Full (multi-stage)	SOFC enables tighter coupling with GT
Cycle Irreversibility Level	Higher	Lower	Impacts total system efficiency
System-Level Exergy Efficiency	Lower	Higher	Key driver for technology selection

From a broader perspective, the inclusion of MCFC–GT systems in this analysis is not intended to position them as a direct alternative to SOFC–GT configurations for advanced transport applications. Rather, MCFC systems serve as a comparative benchmark within the class of high-temperature fuel cells, highlighting the impact of operating temperature on exergy utilization and hybrid system performance. While MCFC-based hybrids demonstrate the feasibility of thermodynamically integrated configurations, their comparatively lower exhaust exergy limits the extent of system integration and reduces their effectiveness in applications requiring high specific power and deep energy recovery. Consequently, their role within this study is primarily analytical, supporting the identification of SOFC–GT systems as the more suitable platform for advanced hybrid energy systems. Overall, the exergy analysis confirms that the superiority of SOFC–GT hybrid systems is not solely a matter of higher efficiency, but rather a consequence of more effective utilization of available energy resources. This distinction reinforces the suitability of SOFC technology for advanced hybrid energy systems and provides a thermodynamic basis for its selection in subsequent sections of this work [41, 81-83].

3.6.10 Advanced SOFC Architectures and Emerging Concepts

Building upon the exergy-based evaluation presented in the previous section, the focus now shifts toward the architectural evolution of SOFC systems, where these thermodynamic advantages are translated into practical design improvements and system-level performance enhancements. While conventional classifications of SOFC systems based on temperature, geometry, and support configuration have been extensively discussed, recent research has increasingly focused on advanced architectures aimed at overcoming key limitations such as interfacial resistance, fabrication complexity, and system integration constraints [84].This shift reflects a broader transition from traditional multi-layer structures toward more integrated and functionally optimized designs. One of the most notable developments is the emergence of electrolyte-free SOFCs, also referred to as single-component or homogeneous fuel cells. In contrast to conventional electrolyte-based configurations, these systems employ a single mixed ionic–electronic conducting material that simultaneously fulfills the roles of electrolyte, anode, and cathode [84].

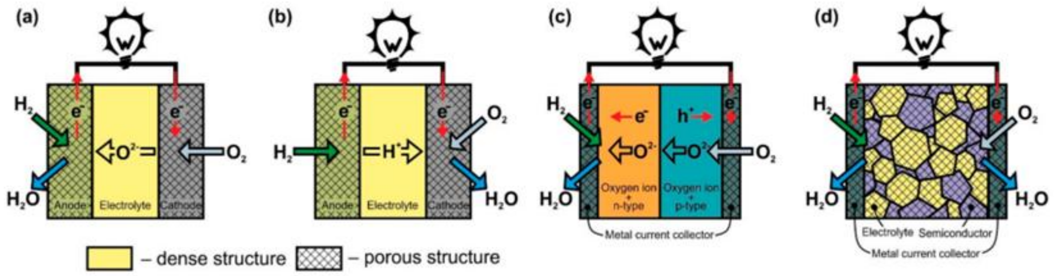

Figure 3-9 structural distinction between classical electrolyte-based SOFCs and emerging electrolyte-free architectures [84].

As illustrated in Figure 3-10, this architecture eliminates distinct functional layers and interfacial boundaries, thereby reducing polarization losses and mitigating thermal mismatch effects [84]. From a manufacturing perspective, the absence of a discrete electrolyte layer simplifies fabrication and enables compatibility with scalable techniques such as cosintering and additive manufacturing. In addition, operation at intermediate temperatures (typically between 500–700 °C) reduces thermal stress and improves start-up characteristics, although challenges related to parasitic electronic conduction and material optimization remain critical research topics [84].

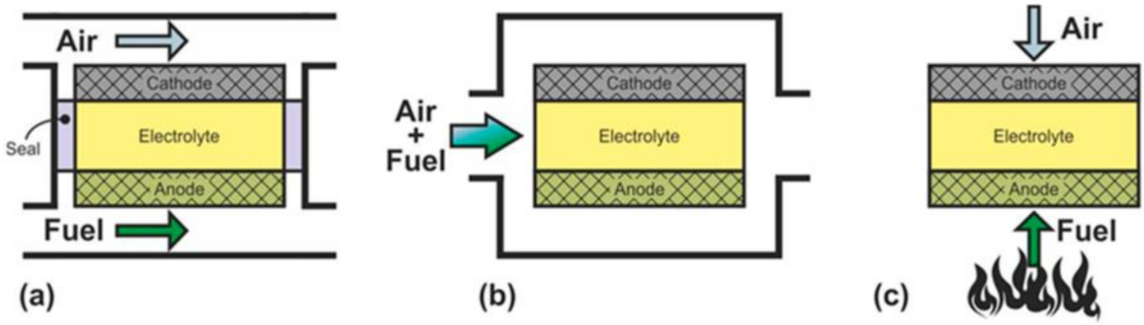

Figure 3-10 Schematics of (a) dual-chamber SOFC, (b) single-chamber SOFC, and (c) no-chamber SOFC [84].

In parallel, alternative gas management concepts have been explored to address sealing and system integration challenges. Conventional dual-chamber SOFCs rely on strict separation of fuel and oxidant streams, requiring gas-tight sealing under high-temperature conditions. As shown in Figure 3-11, emerging configurations such as single-chamber and no-chamber (direct-flame) SOFCs aim to simplify system architecture by allowing reactants to coexist within a shared environment [84]. While these designs reduce mechanical complexity and improve robustness, they typically suffer from lower open-circuit voltage and limited controllability of reaction conditions, restricting their application to niche systems where compactness is prioritized over peak efficiency.

From a structural standpoint, significant advances have been achieved through the optimization of cell support strategies. Modern designs, particularly anode-supported and metal-supported SOFCs, enable thinner electrolytes, resulting in reduced ohmic losses and improved thermal responsiveness. As summarized in Table 3-6, the evolution of SOFC architectures reflects a transition from mechanically robust but performance-limited configurations toward designs that prioritize electrochemical efficiency and system-level integration [84]. Anode-supported SOFCs have emerged as the dominant architecture due to their superior power density and operational flexibility, while metal-supported configurations offer improved mechanical strength and rapid start-up capability, albeit with challenges related to oxidation resistance and long-term degradation [84].

Table 3-6 Comparative Overview of SOFC Structural Configurations [84]

Configuration	Key Feature	Advantage	Limitation
ES-SOFC	Thick electrolyte	Stability	High resistance
AS-SOFC	Thin electrolyte	High performance	Ni degradation
CS-SOFC	Cathode support	Good ORR	Weak structure
MS-SOFC	Metal support	Fast start-up	Corrosion

3.6.10.1 High Power Density SOFC Technologies for Aeronautical Applications

In aeronautical applications, system feasibility is governed not only by efficiency but also by stringent constraints on weight, volume, and specific power. Conventional planar SOFC configurations, although suitable for stationary systems, are generally limited in terms of power density and thermal responsiveness when applied to airborne platforms [47]. These limitations have driven the development of high power density SOFC technologies, particularly micro-tubular SOFC (mSOFC) architectures. Micro-tubular cells, typically characterized by millimeter-scale diameters, provide a high surface-area-to-volume ratio, enabling enhanced electrochemical reaction rates and compact stack configurations [44]. Furthermore, their reduced characteristic dimensions improve internal heat transfer, resulting in better thermal uniformity and reduced temperature gradients during operation [44].

From a mechanical perspective, tubular geometries offer inherent advantages in terms of structural integrity and thermal resilience. The cylindrical configuration accommodates thermal expansion more effectively, reducing mechanical stresses associated with temperature variations and improving resistance to thermal cycling and vibration. These characteristics are particularly relevant in aeronautical environments, where structural stability and reliability are critical design constraints. Experimental studies have demonstrated the feasibility of micro-tubular SOFC systems in UAV applications, achieving compact configurations with power outputs on the order of hundreds of watts while maintaining acceptable system mass [85]. To further illustrate the impact of cell support configurations on micro-tubular SOFC design, schematic representations of electrolyte-supported and anode-supported architectures are presented in Figure 3.12.

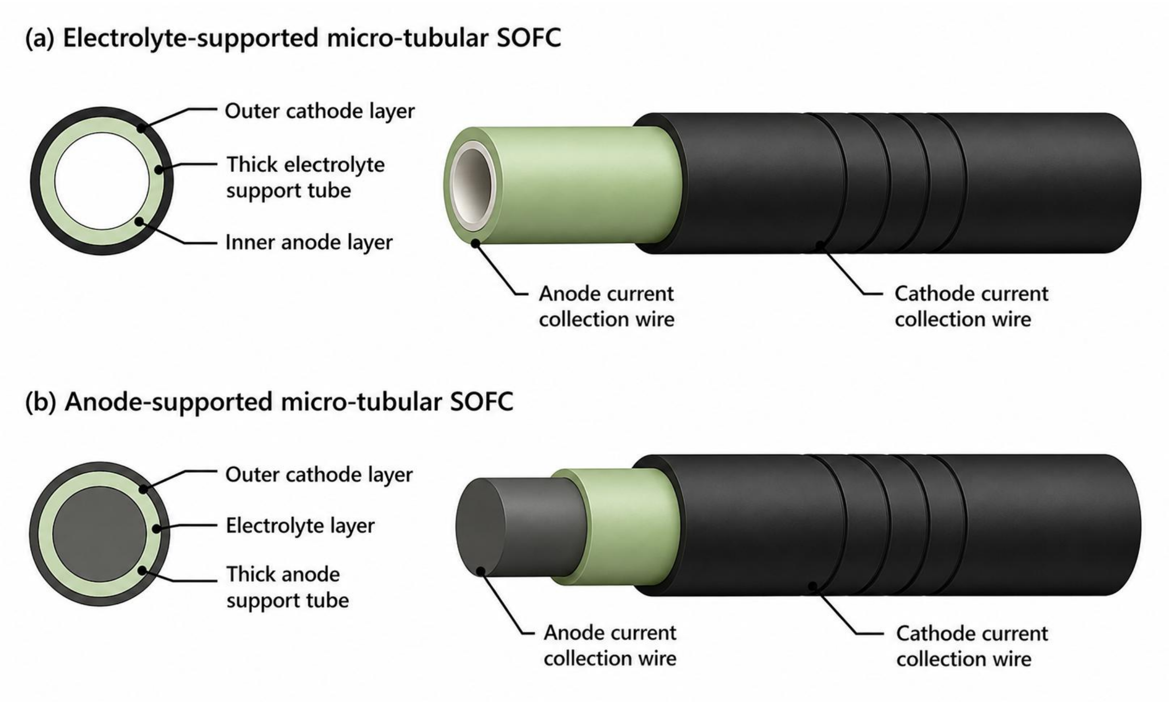

Figure 3-11 Comparison of electrolyte-supported and anode-supported micro-tubular SOFC configurations [62].

As shown in Figure 3.12, the reduction in electrolyte thickness in anode-supported designs significantly decreases ohmic resistance, enabling higher current densities and improved power output. In parallel with geometric optimization, advancements in materials and cell support structures have significantly contributed to enhancing power density. Anode-supported and metal-supported SOFC configurations enable thinner electrolytes and reduced ohmic resistance, leading to higher current densities and improved power output. These developments have resulted in substantial increases in cell-level specific power, indicating the potential of SOFC technologies for high-performance applications [54].
Even though these advancements, achieving high power density at the system level remains a major challenge. A significant portion of system mass is associated with balance-of-plant components, including thermal insulation, heat exchangers, fuel processing units, and structural elements. These subsystems are essential for stable operation but do not directly contribute to power generation, thereby limiting overall system-level specific power [56].

From a system integration perspective, the deployment of SOFC systems in aeronautical applications requires balancing efficiency, power density, and dynamic response. While SOFCs provide high efficiency under steady-state conditions, their high operating temperature introduces thermal inertia, limiting transient response capability [55]. To address this limitation, hybrid architectures are employed, combining SOFC systems with energy storage units for rapid load-following capability and with turbomachinery for thermodynamic energy recovery [46, 55].
This multi-level hybridization enables functional decoupling between subsystems but also introduces critical trade-offs. Increasing reliance on energy storage improves dynamic response but adds mass and system complexity, whereas maximizing thermodynamic integration enhances efficiency at the expense of operational flexibility. Overall, advanced SOFC architectures, particularly micro-tubular designs, represent a promising pathway

toward meeting the stringent requirements of aeronautical applications, where compactness, specific power, and system responsiveness are critical design drivers [47, 56]. These advancements indicate that the evolution of SOFC architectures is not only a matter of improving cell performance, but a critical enabler for their integration into advanced applications such as hybrid aeronautical systems, where power density, compactness, and thermal responsiveness are essential.

4. Case-Study-Based Comparative Analysis of PEMFC and SOFC/GT Hybrid Systems in Marine and Aeronautical Applications

The objective of this chapter is not to revisit the general technological characteristics of PEMFC and SOFC systems discussed in Chapter 3, but to assess their performance under application-specific operating conditions. The analysis is structured around two key questions: how PEMFC-based and SOFC/GT-based architectures behave under realistic operational constraints in marine and aeronautical environments, and under what conditions one configuration outperforms another in relation to mission profile, integration strategy, and boundary conditions.

For this purpose, the evaluation is conducted using mission-relevant indicators, including efficiency, weight implications, dynamic response, and design limitations. In the marine context, the selected cases include a high-speed liquid-hydrogen PEMFC ferry, a methanol-based HT-PEMFC propulsion system for a small vessel, and a representative SOFC/GT hybrid demonstrator illustrating the thermodynamic basis of high-efficiency integrated cycles. In the aeronautical context, the analysis focuses on PEMFC-based APU concepts and SOFC/GT auxiliary and propulsion architectures, with particular emphasis on efficiency–weight trade-offs, which are further examined in the aeronautical case studies. The chapter follows a three-step analytical structure. First, representative case studies are selected for marine and aeronautical applications. Second, the systems are compared using sector-specific performance criteria. Finally, the results are used to identify the most relevant hybrid architecture and to support the modelling approach developed in Chapter 5.

4.1 Marine sector case studies

This section presents representative case studies illustrating the application of PEMFC-based and SOFC/GT hybrid systems in marine environments. The selected cases are intended to capture distinct design philosophies and operational contexts within the maritime sector, rather than to provide an exhaustive overview of all possible configurations. The analysis includes hydrogen-based PEMFC propulsion systems, methanol-fuelled HT-PEMFC configurations for small-scale vessels, and high-efficiency SOFC/GT hybrid architectures, representing different power ranges, fuel pathways, and mission requirements, ranging from short-range transport to steady-state power generation. For each case study, the system architecture and key performance characteristics are examined to identify the main technical drivers and limitations.

4.1.1 Case Study A –SF-BREEZE (high-speed PEMFC ferry as an extreme feasibility benchmark)

The ***SF-BREEZE*** project is one of the most useful marine references for this thesis because it does not study a low-demand leisure craft or a symbolic demonstrator, but a deliberately demanding transport mission: a 150-passenger high-speed ferry designed for San Francisco Bay service, with a target top speed of 35 $knots$ and four daily 50 nautical mile round trips, allowing one midday refueling event. In other words, the project was intentionally framed as a "stress test" for zero-emission hydrogen marine propulsion. That makes it analytically valuable here, because it allows PEMFC technology to be assessed under a mission profile where power density, vessel weight, route length, turnaround constraints, and regulatory feasibility all become binding design variables [86].

The final conceptual configuration adopted PEM fuel cells because of their favourable weight and volume characteristics relative to alternative fuel-cell options, their commercial maturity, and their fast response under load variation. The designed vessel required a total installed power of $4.92\ MW$, of which about $4.4\ MW$ was allocated to propulsion at top speed, using forty-one $120\ kW$ PEMFC racks based on ***Hydrogenics HD-30*** modules. Liquid hydrogen was selected as the onboard fuel because compressed gas storage would have imposed an unacceptable volume and weight penalty for a ferry operating at this speed and range. The vessel carried approximately $1{,}200\ kg$ of LH_2, enough for two $50\ nm$ round trips with a remaining margin of $200 - 400\ kg$. This is a critical result, even within the PEMFC family, the feasibility of the architecture depended not simply on cell performance but on the shift from compressed hydrogen to cryogenic storage [86].

From a system-engineering perspective, the ***SF-BREEZE*** is best interpreted not as proof that PEMFCs are universally ideal for marine propulsion, but as proof that they remain technically viable even when imposed on one of the least forgiving civilian ferry missions in the literature. The project concluded that such a zero-emission ferry and its associated fuelling infrastructure were technically and regulatorily feasible, with no identified show-stoppers, but the design also revealed the central weakness of PEMFC-based marine propulsion at high speed: the vessel becomes energetically and economically sensitive to mass growth. The study quantified this sensitivity explicitly, showing that a 1% increase in vessel weight caused approximately a 1.1% increase in required power, and that an additional $7{,}500\ lb$ could require one extra $120\ kW$ PEMFC rack. This matters because PEMFC vessels do not merely "**carry**" a powertrain; the mass of the fuel-cell system recursively increases the propulsive power demand, which then further enlarges the fuel-cell system [86].

This recursive mass penalty is also visible in the comparison with the conventional diesel ferry Vallejo. The *SF-BREEZE* required about $4.8\ MW$ of installed propulsive power for 150 passengers, corresponding to roughly $32\ kW$ per passenger, whereas the ***Vallejo*** used about $3.4\ MW$ for 300 passengers, corresponding to roughly $11.3\ kW$ per passenger. Therefore, although the *SF-BREEZE* demonstrated point-of-use zero emissions and superior manoeuvring response, it was less transport-efficient on a per-passenger basis than the diesel benchmark used in the study. PEMFC systems can be technically attractive in high-speed vessels because of responsiveness and low-temperature operation, but they are not intrinsically optimal when the mission is strongly speed-driven and payload-limited [86].

The environmental interpretation of *SF-BREEZE* is also more nuanced than a simple "zero-emission" label suggests. At the point of use, the ferry eliminated greenhouse gas and criteria pollutant emissions. However, the study well-to-waves analysis showed that when the LH_2 was produced through non-renewable pathways, the total pathway greenhouse gas emissions could become higher than those of the diesel reference ferry on a per-passenger basis, precisely because the high-speed PEMFC vessel was heavy and energy-intensive.

By contrast, when the hydrogen was produced from renewable electricity, the study reported a 75.8% reduction in well-to-waves GHG emissions relative to the diesel ferry, together with a 99.1% reduction in NO_x, a 99.2% reduction in hydrocarbons, and a 98.6% reduction in particulate matter. This makes *SF-BREEZE* highly relevant to the thesis argument: PEMFC marine performance cannot be judged at stack level alone; the environmental superiority of the concept is conditional on both mission profile and hydrogen production pathway [86].
The key design and operational parameters of the *SF-BREEZE* case study are summarized in Table 4.1 in order to provide a structured reference for the subsequent comparative analysis.

Table 4-1 Key design and operational parameters of the SF-BREEZE case study [86].

Parameter	Value
Passenger capacity	150 passengers
Maximum speed	35 knots
Mission profile	4 round trips per day, each 50 nautical miles
Installed PEMFC power	4.92 MW
Propulsion power	4.4 MW
Fuel type	Liquid hydrogen (LH_2)
Onboard LH_2 mass	1200 kg
Refuelling strategy	Single refuelling event during midday
Main technical advantage	Fast dynamic response and zero emissions at point of use
Main technical limitation	Strong sensitivity to system mass and recursive increase in power demand

As shown in Table 4.1, the *SF-BREEZE* system is characterized by high installed power and demanding operational conditions, which highlight both the feasibility and the limitations of PEMFC-based propulsion in high-speed marine applications [86].

In summary of this case study, the SF-BREEZE project demonstrates that PEMFC-based propulsion is technically feasible even for demanding high-speed ferry operations, owing to the favourable weight and volume characteristics, commercial maturity, and rapid dynamic response of PEMFC technology. The study also highlights the crucial role of liquid hydrogen storage in achieving operational feasibility, while revealing the strong sensitivity of the system to vessel mass growth, which can significantly increase power demand and overall system size. Although the concept achieves zero emissions at the point of use, its transport efficiency on a per-passenger basis remains lower than that of conventional diesel ferries. Furthermore, the environmental advantages of the system are highly dependent on the hydrogen production pathway, with substantial reductions in greenhouse gas and pollutant emissions only achievable when renewable hydrogen is utilized.

4.1.2 Case Study B –Methanol HT-PEMFC marine propulsion (a small-vessel architecture optimized around fuel logistics rather than maximum efficiency)

The second marine case shifts the analysis from high-speed hydrogen transport to a much smaller commercial vessel intended for protected marine areas near Capri Island. Here, the propulsion system is based on reformed methanol feeding two $5\,kW$ HT-PEMFC units, supported by a lithium-ion battery pack and an electric propulsion motor. Unlike the *SF-BREEZE* case, where the technological challenge is extreme installed power at high speed, this architecture is shaped by a different optimization problem; low-speed operation, compatibility with spatial constraints on a $10\,m$ vessel, and the need to avoid hydrogen bunkering dependence in local maritime service. This difference is important because it shows that within the PEMFC family, the preferred fuel pathway and architecture are operating context, not technology-intrinsic [87].

The analysed mission profile involved speeds of 7 knots for transit and 4.5 knots in a protected zero-emission area. The propulsion system used reformed methanol HT-PEMFC modules, a battery pack acting as an energy buffer, and a central $48\,V$ DC bus. The study emphasized that the fuel-cell system itself was not expected to supply every transient peak directly; instead, the battery compensated for the limited dynamic response of the HT-PEMFC system during peak propulsion demand and in full-electric operating zones. This is one of the most useful lessons of the case for Chapter 4; once the fuel cell moves away from low-temperature hydrogen PEMFC operation and toward reformed-fuel HT-PEMFC, the architecture tends to become hybrid not only in the broad sense, but functionally hybrid, because electrochemical efficiency is preserved by offloading transients to storage [87]. The propulsion power demand along the mission profile is illustrated in Figure 4.2, where different operational phases (legs) are associated with varying load conditions.

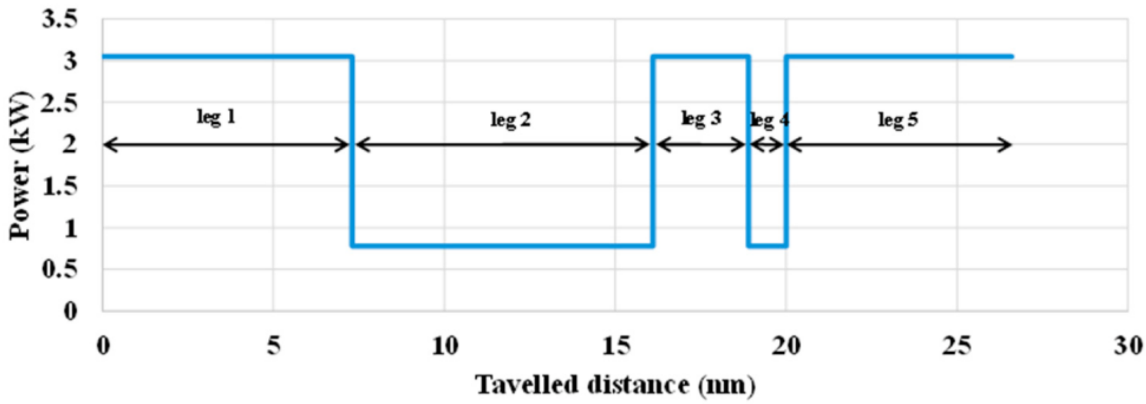

Figure 4-1 Propulsion power demand profile along the mission, showing different operating phases (legs) and corresponding load variations [87].

As shown in Figure 4.2, the propulsion system is subjected to multiple operating phases characterized by distinct power levels. High power demand is observed during legs 1, 3, and 5, corresponding to transit conditions, while significantly lower power levels occur in leg 2 and leg 4, which can be associated with reduced-speed or manoeuvring operations.
This variation in load demand highlights that the propulsion system does not operate under steady-state conditions but rather experiences frequent transitions between different power levels. Such behaviour imposes significant constraints on the fuel cell system, particularly in terms of its ability to follow rapid load changes. Consequently, the variable nature of the mission profile justifies the need for a hybrid architecture in which the battery system supports transient power demands, while the HT-PEMFC operates closer to stable and efficient operating conditions [87]. The dynamic response of the HT-PEMFC system to load variations is presented in Figure 4.3.

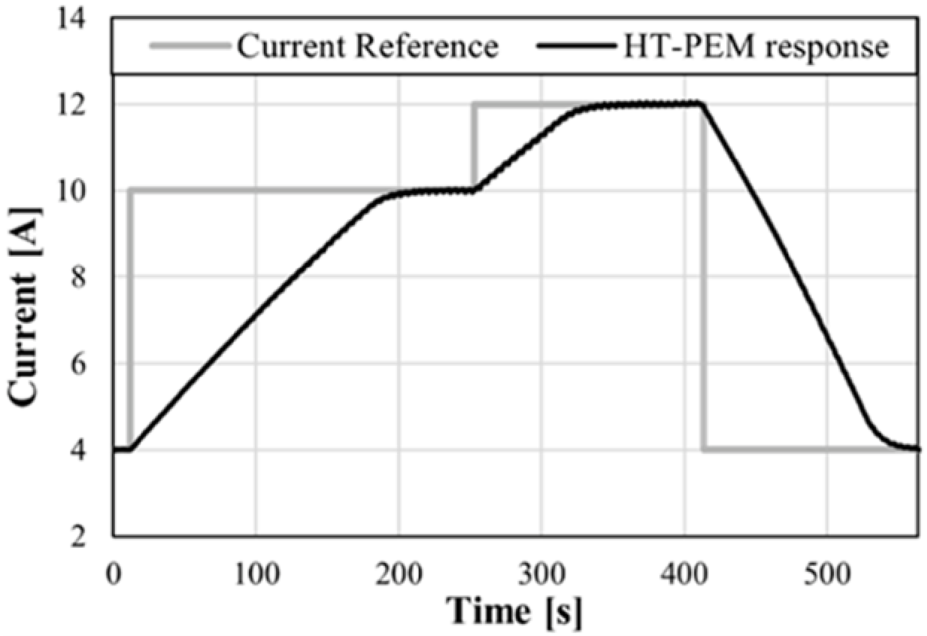

Figure 4-2 Dynamic response of the HT-PEMFC system to step changes in current demand, compared with the reference signal [88].

As shown in Figure 4.2, the HT-PEMFC system exhibits a delayed response when tracking rapid increases in current demand. While the reference signal changes abruptly, the system output follows a gradual trajectory, requiring a significant amount of time to reach steady-state conditions. This behaviour is primarily attributed to the dynamics of the fuel processing unit, particularly the reformer, as well as limitations in hydrogen supply to the fuel cell stack during transient operation.

In contrast, when the load decreases, the system response is faster, indicating an asymmetric dynamic behaviour. This confirms that the HT-PEMFC system is not well-suited to directly handle rapid load variations, especially during increasing demand conditions. Therefore, the integration of a battery system is not only beneficial, but necessary, as it compensates for the slow transient response of the fuel cell and ensures stable operation under realistic mission conditions.

A quantitative assessment of the system performance further highlights the operational characteristics of the HT-PEMFC-based propulsion architecture [87]. Quantitatively, the vessel energy requirement could be satisfied with two 5 kW HT-PEMFC units; the full daily cruise consumed $12.7\ kg$ of fuel, while methanol consumption during $7 - knot$ cruising was about 1.88 kg/h. The study further reported that the maximum system efficiency reached about 44% at partial load around $2.1\ kW$, whereas the efficiency at the high-power operating point of roughly $4.2\ kW$ was about 41%. This load-dependent behaviour is analytically important, because it shows that the HT-PEMFC system is most efficient not when maximally loaded, but in a moderated operating band. Therefore, for marine applications with fluctuating demand, the presence of a battery is not merely helpful for transient smoothing; it is part of the strategy for keeping the fuel-cell subsystem closer to its favourable efficiency window [87].

The fuel logistics dimension is where this case becomes particularly valuable in comparison with *SF-BREEZE*. By using methanol as a hydrogen carrier, the system avoids the storage-volume and infrastructure penalties associated with compressed or liquid hydrogen, while also benefiting from cleaner combustion characteristics and easier onboard handling. At the same time, these gains are purchased through reformer-related complexity, additional thermal integration requirements, and lower absolute efficiency than what is achievable in a thermally integrated SOFC/GT cycle. The point is not simply that methanol HT-PEMFC is "worse" than SOFC/GT, but that it solves a different problem; it trades some efficiency for implement ability in smaller vessels and near-term fuel availability [87].

The feasibility assessment reinforces this interpretation. The study reported that the propulsion package was compatible with the vessel in both dimensions and mass. The main component weights included $2 \times 65\ kg$ for the HT-PEMFC units, $37\ kg$ for the battery pack, $76\ kg$ for the electric motor, and $63.5\ kg$ for the $70\ L$ fuel tank. The total system therefore remained manageable within a ship displacement of 3,698 kg. This is a decisive difference from *SF-BREEZE*; in the small-vessel case, the fuel-cell propulsion package fits comfortably inside the vessel design envelope, whereas in the high-speed ferry case, the propulsion system itself becomes one of the dominant drivers of vessel-level performance penalties. Thus, the methanol HT-PEMFC case should be interpreted as a fuel-logistics-optimized marine architecture rather than an efficiency-maximized one. It is well suited to vessels operating at modest speeds, especially in protected or near-shore areas where zero-emission operation, compact packaging, and compatibility with existing liquid-fuel handling practices are more valuable than maximum thermodynamic efficiency.

Its main limitation is not that the cell technology fails, but that once reforming, auxiliary equipment, and battery support are included, the architecture becomes less attractive for applications demanding sustained high power or large-scale heat recovery [87]. The main design and operational characteristics of the methanol HT-PEMFC propulsion system are summarized in Table 4.2.

Table 4-2 Main design and operating characteristics of the methanol HT-PEMFC marine propulsion system [87].

Parameter	Value
Vessel length	10 m
Mission speed(s)	$7\ knots\ (transit), 4.5\ knots\ (zero - emission\ zone)$
Fuel	Methanol (reformed to hydrogen)
Number of HT-PEMFC units	2
Nominal power per unit	$5\ kW$
Battery role	Energy buffer for transient load compensation
Methanol consumption at cruise	1.88 kg/h
Total fuel consumption per mission	12.7 kg
Peak system efficiency	$44\%\ (at\ partial\ load\ {\sim}2.1\ kW)$
Efficiency at high load	$41\%\ (at\ {\sim}4.2\ kW)$
Feasibility conclusion	Suitable for small vessels with moderate power demand and limited infrastructure availability

As shown in Table 4.2, the system is characterized by moderate power output and relatively high efficiency at partial load, confirming its suitability for small-scale marine applications with variable operating conditions. In summary of this case study, the methanol-fuelled HT-PEMFC propulsion system demonstrates that fuel-cell technology can be effectively adapted to small marine vessels by prioritizing fuel logistics, compact integration, and operational flexibility over maximum efficiency and power density.

The study highlights the advantages of methanol as an easily stored and readily available fuel, while emphasizing the necessity of battery support to compensate for the slow transient response associated with methanol reforming and to maintain operation within the fuel cell most efficient load range. Although this approach introduces additional system complexity and slightly lower efficiency compared with hydrogen-based or SOFC/GT systems, it provides a practical and feasible solution for low- to medium-speed vessels operating in near-shore and protected areas, where ease of implementation, fuel availability, and zero-emission operation are key priorities.

4.1.3 Case Study C – MCFC-Based Hybrid Propulsion Systems for Liquefied Hydrogen Tankers

While the previous case studies focused on PEMFC-based marine applications, MCFC-based hybrid propulsion systems represent an alternative high-temperature fuel cell approach for large-scale maritime transportation. Owing to their elevated operating temperature, molten carbonate fuel cells offer opportunities for internal fuel reforming and waste-heat utilization that are not available in low-temperature fuel cell technologies. The study conducted by Ahn et al. investigated two MCFC-based hybrid propulsion architectures for a 140,000 m^3 liquefied hydrogen (LH_2) tanker, namely an MCFC-GT system incorporating a gas turbine bottoming cycle and an MCFC-ST system utilizing a steam turbine bottoming cycle. The objective was to evaluate how different heat-recovery configurations influence overall system performance and environmental compliance in large marine applications. Figure 4-3 presents the schematic layouts of the two hybrid propulsion systems investigated by Ahn et al. [89], namely the MCFC-GT and MCFC-ST configurations. These schematics provide an overview of the system components and energy flow pathways discussed in the following sections.

(a) MCFC-GT

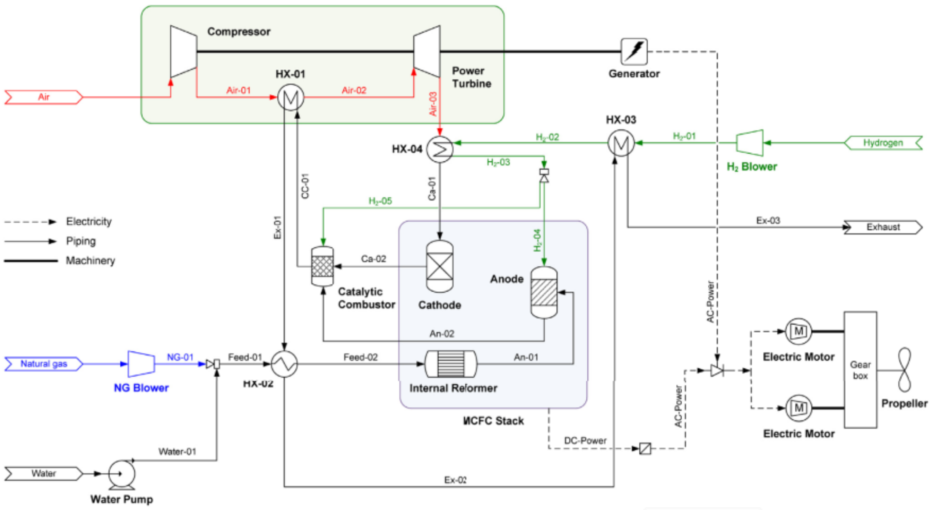

(b) MCFC-ST

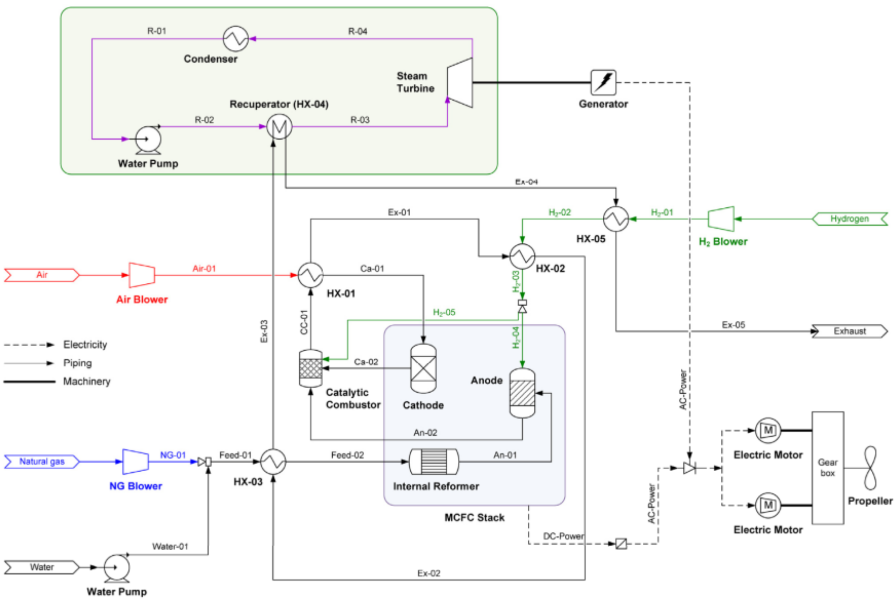

Figure 4-3 Schematic layouts of the MCFC-GT and MCFC-ST hybrid propulsion systems for an LH_2 tanker [89].

Although both architectures employ the same MCFC stack, internal reformer, and fuel supply arrangement, they differ in the method used for exhaust heat recovery.

The MCFC-GT configuration utilizes a Brayton-cycle gas turbine, whereas the MCFC-ST system employs a Rankine-cycle steam turbine. This architectural distinction forms the basis for the performance differences discussed in the following sections [89].
Both propulsion concepts are based on utilizing the thermal energy contained in the high-temperature exhaust gases leaving the MCFC stack. In each configuration, the fuel cell serves as the primary power-generating unit, while a secondary thermodynamic cycle recovers part of the exhaust energy and converts it into additional useful power. The systems operate using a combination of natural gas and hydrogen boil-off gas (BOG) generated during cargo storage. Natural gas is internally reformed within the fuel cell system, while hydrogen BOG is supplied directly to the anode and partially utilized in a catalytic combustor. This fuel strategy is particularly attractive for LH_2 carriers because it enables productive utilization of unavoidable hydrogen boil-off while simultaneously reducing the consumption of conventional marine fuels [89].

A defining characteristic of MCFC technology is its operating temperature of approximately $923\ K\ (650°C)$, which enables internal steam methane reforming and effective thermal integration. The thermodynamic analysis shows that as the reforming temperature approaches $923\ K$, methane concentration decreases from approximately 25% to nearly 1%, while the hydrogen concentration increases to roughly 55%, indicating effective fuel conversion and extensive utilization of internally generated thermal energy. The calculated reforming efficiencies were 70.13% for the MCFC-GT configuration and 69.68% for the MCFC-ST configuration ,demonstrating that both architectures achieve similar fuel-processing performance [89].
The electrochemical performance of the MCFC stack was evaluated at an operating temperature of $923\ K$ and a current density of $150\ {}^{mA}/_{cm^2}$. Under these conditions, the open-circuit voltage was approximately $1.026\ V$, while the operating voltage decreased to $0.879\ V$ due to activation, ohmic, and concentration losses. The resulting power density reached approximately $0.132\ {}^{W}/_{cm^2}$. To satisfy the propulsion requirements of the LH_2 tanker, the MCFC-GT system required approximately $18{,}500\ m^2$ of total active cell area, whereas the MCFC-ST configuration required $20{,}700\ m^2$. This difference indicates that the steam-turbine-based architecture requires a larger electrochemical subsystem to achieve a comparable net power output [89].

Although the intrinsic MCFC stack efficiency remained nearly identical in both configurations (approximately 52.7%), the overall performance of the hybrid systems differed significantly due to the characteristics of the bottoming cycles and auxiliary power requirements. The MCFC-GT configuration generated approximately $23.2\ MW$ from the fuel cell stack and recovered an additional $5.0\ MW$ through the gas turbine, resulting in a net power output of $28.1\ MW$. By comparison, the MCFC-ST system generated approximately $25.9\ MW$ from the stack and recovered only $4.1\ MW$ through the steam turbine, producing a similar net output of approximately $28.0\ MW$. Despite these comparable power levels, the overall electrical efficiency of the MCFC-GT system reached 53.87%, whereas the MCFC-ST configuration achieved only 50.11%, indicating that system-level integration rather than fuel-cell performance was the primary source of the efficiency difference [89].

These results suggest that the MCFC-ST configuration may be less attractive from a practical perspective, since the additional steam-cycle components increase system complexity, weight, capital cost, and maintenance requirements while providing only limited energy recovery benefits. Since the resulting overall efficiency remains below the intrinsic stack efficiency, the thermodynamic advantages of the steam cycle appear insufficient to compensate for the associated integration penalties.

The primary reason for this performance difference lies in the treatment of auxiliary power requirements. In the MCFC-GT architecture, the air-compression process is integrated into the gas turbine cycle, allowing part of the compressor work to be recovered through turbine expansion. In contrast, the MCFC-ST system requires a dedicated air compressor consuming approximately $1.9\ MW$ of electrical power. Therefore, a larger portion of the generated electricity is consumed by balance-of-plant components rather than being delivered to the propulsion system. This finding highlights an important design consideration for high-temperature fuel-cell applications: overall system performance depends not only on fuel-cell efficiency but also on the effectiveness of auxiliary system integration [89].

From a thermodynamic perspective, the superiority of the MCFC-GT configuration can be explained through the quality of the exhaust energy available for recovery. The exhaust gases leaving the MCFC possess sufficiently high temperature and pressure to be effectively utilized within a Brayton-cycle gas turbine. Consequently, the gas turbine is able to recover a larger fraction of the available exhaust exergy and convert it into useful mechanical work than the steam-turbine alternative. This improved utilization of waste heat ultimately translates into higher overall efficiency and better energy conversion performance [89].
Environmental performance was assessed using both NO_x emissions and the Energy Efficiency Design Index (EEDI). The results indicate that both hybrid systems satisfy IMO Tier III NO_x requirements, with emissions of $1.62\ g/kWh$ for the MCFC-GT system and $1.14\ g/kWh$ for the MCFC-ST system. Furthermore, the attained EEDI values of 13.28 and $13.20\ g - CO_2/ton - NM$, respectively, comply with the Phase 2 regulatory requirements applicable to large merchant vessels. However, neither configuration fully satisfies the more stringent future targets, indicating that further reductions in hydrocarbon fuel consumption will be required for long-term compliance [89].

Table 4-3 Key performance characteristics of the MCFC-GT and MCFC-ST systems[89].

Parameter	MCFC-GT	MCFC-ST
Stack power output (MW)	23.17	25.92
Turbine power output (MW)	5.02	4.11
Net power output (MW)	28.07	28
MCFC efficiency (%)	52.74	52.72
Global electrical efficiency (%)	53.87	50.11
NO_x emissions (g/kWh)	1.62	1.14
EEDI ($g - CO_2/ton - NM$)	13.28	13.20

As summarized in Table 4-3, both configurations deliver similar net power outputs, whereas the MCFC-GT system achieves higher overall electrical efficiency due to more effective waste-heat recovery and reduced auxiliary power consumption. These results indicate that system-level integration plays a more significant role in determining performance than the electrochemical efficiency of the MCFC stack alone.

From a marine engineering perspective, this case study demonstrates that MCFC technology provides an attractive compromise between efficiency, fuel flexibility, environmental performance, and practical implementation. The ability to utilize both natural gas and hydrogen boil-off gas, combined with effective waste-heat recovery, makes MCFC-based hybrid systems particularly suitable for large commercial vessels operating under relatively steady load conditions. Furthermore, the comparison between MCFC-GT and MCFC-ST clearly shows that the selection of the secondary power cycle can significantly influence overall system performance, even when the fuel cell stack itself remains unchanged [89].

Despite the attractive thermodynamic performance demonstrated by the MCFC-based configurations, several technological and operational limitations continue to constrain the large-scale adoption of MCFC systems in marine propulsion. The elevated operating temperature (approximately 923 K) imposes stringent requirements on thermal insulation, material durability, and start-up/shutdown procedures, resulting in reduced operational flexibility compared with lower-temperature fuel-cell technologies. Furthermore, the molten carbonate electrolyte promotes corrosion phenomena and accelerates degradation mechanisms within stack components and metallic interconnects, creating additional challenges for long-term reliability and maintenance planning [89].

From a system-integration perspective, MCFC installations require extensive balance-of-plant subsystems, including fuel-processing units, thermal management equipment, gas recirculation loops, and exhaust-energy recovery devices. Consequently, the overall plant architecture becomes significantly more complex than that of PEMFC-based systems, leading to increased installation volume, higher capital expenditure, and greater maintenance demands. These factors are particularly relevant in marine applications, where machinery-space constraints, operational reliability, and lifecycle cost often represent critical design drivers. Moreover, despite the favourable electrical efficiencies reported for MCFC hybrid systems, the relatively low power density of MCFC stacks generally results in larger and heavier installations than competing fuel-cell technologies. This characteristic may limit their suitability for weight-sensitive vessels or missions requiring high power-to-weight ratios. Therefore, although MCFC technology offers substantial efficiency advantages and effective waste-heat utilization, its practical deployment remains largely confined to conceptual studies and demonstration projects, with relatively limited evidence of commercial-scale marine implementation to date [89].

In summary, the study demonstrates that the integration of an MCFC with a gas turbine constitutes the most effective hybrid configuration among the alternatives considered. The superior performance of the MCFC-GT system originates not only from enhanced waste-heat recovery but also from the effective integration of auxiliary equipment and the reduction of parasitic power consumption. However, the results also indicate that the practical attractiveness of MCFC-based marine systems cannot be assessed solely on the basis of efficiency gains. Factors such as high operating temperatures, system complexity, material durability, maintenance requirements, and overall plant integration must also be considered when evaluating their suitability for real-world maritime applications. More broadly, the study highlights that the performance and viability of marine fuel-cell systems depend not only on the intrinsic characteristics of the fuel-cell stack, but also on the effectiveness with which the overall energy-conversion architecture manages waste heat, auxiliary loads, operational constraints, and lifecycle considerations [89].

4.1.4 Case Study D-SOFC/GT hybridization as the thermodynamic reference case for high-efficiency marine power

While the previous marine case studies highlighted different approaches to balance fuel logistics, operational flexibility, thermal integration, and vessel-level constraints, the SOFC/GT hybrid system represents the thermodynamic upper benchmark among the architectures examined in this chapter. Rather than prioritizing rapid dynamic response or simplified onboard integration, the design philosophy of the SOFC/GT concept is centred on maximizing fuel utilization and electrical efficiency through the integration of high-temperature electrochemical conversion with gas-turbine power recovery. The NFCRC/Siemens-Westinghouse demonstrator is particularly significant because it was the first operational SOFC/gas turbine hybrid system and provides quantitative evidence of the performance benefits achievable through advanced thermodynamic integration.

The system integrated a pressurized SOFC module with a microturbine-generator and delivered a total output of about $220\ kW$, of which roughly $180\ kW$ came from the SOFC and $40\ kW$ from the turbine-generator [82]. The thermodynamic logic of the configuration is straightforward but decisive. The SOFC stack operated at about 1000°C, and when pressurized to approximately $3\ atm$, it produced a hot, pressurized exhaust stream that could directly drive the turbine expander. In this architecture, the gas turbine compressor supplies the pressurized air needed by the fuel cell, while the SOFC effectively replaces the conventional combustor as the high-temperature core of the cycle. The result is not just an add-on turbine but an integrated dry hybrid cycle in which electrochemical conversion and Brayton-cycle power recovery reinforce each other. This is precisely the kind of cycle synergy that Chapter 3 described conceptually, and that Chapter 4 must now demonstrate through case evidence.

The demonstration reported approximately 53% fuel-to-electric efficiency in this size class, which was described as a world record for natural-gas-fueled fuel-cell operation at the time. More importantly for forward-looking interpretation, the same source indicated that efficiencies around 58% could be achieved at capacities as low as $250\ kW$, around 60% at approximately $1\ MW$, and 70% or more in the $2-3\ MW$ range with larger and more sophisticated gas turbines.
This scaling trend matters strongly for marine applications. Ships, unlike aircraft APUs or small local boats, often offer long periods of quasi-steady operation and sufficient packaging space to justify high-efficiency thermal integration. Therefore, SOFC/GT systems become more attractive as vessel scale and base-load character increase.
Another important aspect is the effect of pressurization itself.
The demonstrator noted that operating the SOFC at $3\ atm$ increased power output by around 10%. On its own, this increment would not necessarily justify the additional compression

work. The real justification emerges only when pressurization is embedded in a fully integrated SOFC/GT architecture, where the turbine recovers the exergy of the pressurized, high-temperature exhaust.
This point is analytically critical because it distinguishes “hybridization” from mere pressurization. The performance benefit of the SOFC/GT system does not arise simply because the cell is pressurized; it arises because pressurization enables a cycle architecture in which the compressor, SOFC, recuperator, and turbine become interdependent components of one thermodynamic system [82]. The thermodynamic coupling between the SOFC, reformer, and heat recovery system can be further understood through a detailed representation of heat flows within the system, as illustrated in Figure 4.4.

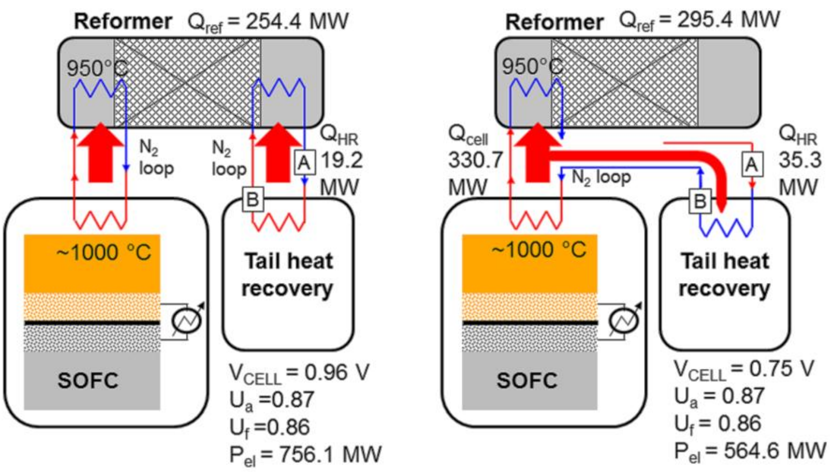

Figure 4-4 Thermal integration of the SOFC with the reformer and tail heat recovery system [82].

As shown in Figure 4.4, the high-temperature operation of the SOFC enables a significant portion of the generated thermal energy to be directly utilized for the reforming process, reducing the need for external heat input. In the ideal configuration, the heat produced by the SOFC is sufficient to sustain the reformer, while excess heat is recovered through the tail heat recovery unit. However, under more realistic operating conditions, a reduction in cell voltage leads to increased heat generation within the fuel cell. This additional heat modifies the thermal balance of the system, requiring more complex heat management strategies, but also increasing the potential for energy recovery. This behaviour highlights a key advantage of SOFC-based systems compared to low-temperature fuel cells: the ability to internally redistribute and reuse high-grade thermal energy. Such thermal integration is not achievable in PEMFC systems, where the lower operating temperature limits the recovery and utilization of waste heat. Therefore, the effectiveness of SOFC/GT hybrid systems is not solely a consequence of electrochemical efficiency, but rather of the strong coupling between electrochemical conversion and thermal energy management, which enables enhanced overall system performance [82].

For marine interpretation, this case should not be considered as a direct shipboard implementation in the same sense as the *SF-BREEZE* or the methanol *HT-PEMFC* vessel. In practice, it serves as a thermodynamic reference that illustrates the potential of SOFC/GT hybrid systems when operating under conditions that favour steady-state performance and high-efficiency energy conversion. The analysis indicates that such systems are particularly suitable for applications where continuous operation and high fuel utilization are prioritized, rather than rapid startup or simplified system integration. However, these advantages are accompanied by significant technical challenges, including high operating temperatures, extended warm-up times, material durability concerns, and increased system complexity. Therefore, the relevance of SOFC/GT systems in marine applications is strongly dependent on the operational context, particularly the ability of the vessel to accommodate the constraints associated with high-temperature operation while benefiting from improved overall efficiency [82]. The key performance and operating characteristics of the SOFC/GT hybrid demonstrator are summarized in Table 4.4.

Table 4-4 Performance characteristics of the SOFC/GT hybrid system [82].

Parameter	Value
Stack pressure	$3\ atm$
SOFC power output	$180\ kW$
Gas turbine output	$40\ kW$
Total system output	$220\ kW$
SOFC operating temperature	$1000\ °C$
Demonstrated electrical efficiency	53%
Efficiency at ~250 kW scale	58%
Efficiency at ~1 MW scale	60%
Efficiency at ~2–3 MW scale	70% ≤
Fuel flexibility	Hydrogen, natural gas, and reformable fuels
Main technical advantage	High efficiency through thermodynamic integration and waste heat recovery
Main technical limitation	High operating temperature, slow startup, and system complexity

As shown in Table 4.4, the SOFC/GT system exhibits a strong dependence on system scale, with efficiency increasing significantly at higher power levels. This behaviour reinforces its suitability for large-scale marine applications operating under steady-state conditions. In summary of this case study, the SOFC/GT hybrid system represents a high-efficiency power-generation architecture that leverages the strong thermodynamic integration between electrochemical conversion and gas-turbine power recovery.

The high operating temperature of SOFCs enables the effective utilization of high-grade waste heat for reforming and energy recovery, resulting in significantly higher efficiencies than those achievable with PEMFC-based systems, with reported efficiencies exceeding 70% at multi-megawatt scales. In addition, the architecture benefits from fuel flexibility and enhanced performance under pressurized operation. However, these advantages are accompanied by increased system complexity, high operating temperatures, extended start-up times, and material durability challenges. Consequently, SOFC/GT systems are particularly attractive for large-scale marine applications characterized by long operating periods and stable load profiles, where maximizing fuel efficiency and overall system performance is prioritized over rapid dynamic response and simplified integration.

4.2 Comparative Discussion of Marine Systems

The four marine case studies do not support a simplistic ranking in which one technology can be considered universally superior. In practice, they demonstrate that the suitability of a marine fuel-cell system depends strongly on mission profile, vessel scale, fuel logistics, dynamic requirements, and the extent to which waste heat can be converted into useful power. In the *SF-BREEZE* case, PEMFC technology succeeds because it offers low-temperature operation, fast response, and an architecture that can be scaled to megawatt power without the severe startup and thermal-cycling penalties of SOFC systems. Yet the same case also reveals the principal weakness of PEMFCs in demanding marine propulsion: once high speed is imposed, the fuel-cell system and cryogenic tankage increase vessel mass, and that mass increase directly raises the power needed to sustain speed. Hence the system becomes trapped in a mass–power feedback loop that reduces transport efficiency and worsens economics [86].

By contrast, the HT-PEMFC methanol case performs better not because it is more efficient than SF-BREEZE or SOFC/GT, but because the mission requirements are fundamentally softer and the architecture is optimized around operational practicality. For a $10\ m$ vessel moving at $7\ knots$, the decisive parameter is not maximum cycle efficiency but whether a compact system can satisfy the mission while fitting the available volume and avoiding hydrogen infrastructure dependency. In that context, liquid methanol becomes a system advantage, and the battery-supported hybrid layout becomes an enabling feature rather than a compromise. The architecture therefore performs better than a pure-hydrogen PEMFC solution would in similar local-service conditions , because it minimizes the infrastructure barrier and preserves acceptable onboard integration [87].

The MCFC-based hybrid propulsion case occupies an intermediate position between low-temperature PEMFC systems and highly integrated SOFC-based concepts. The study demonstrated that the use of an MCFC enables internal reforming and effective waste-heat utilization while maintaining fuel flexibility through the combined use of natural gas and hydrogen boil-off gas. Among the configurations evaluated, the MCFC-GT architecture achieved higher electrical efficiency than the MCFC-ST alternative because the gas turbine recovered a larger fraction of the exhaust exergy and reduced auxiliary power consumption associated with air compression. Consequently, MCFC systems become particularly attractive for large commercial vessels operating under relatively steady load conditions, where efficiency, fuel flexibility, and environmental performance are simultaneously important .Nevertheless, these efficiency advantages should be interpreted together with the technological and operational limitations previously discussed in Section 4.1.3, which continue to influence the practical viability of MCFC-based marine systems [89].

The SOFC/GT concept outperforms the PEMFC-, HT-PEMFC-, and MCFC-based marine cases when the primary evaluation criterion is thermodynamic efficiency under sustained operation. The reason is not merely that SOFCs operate at higher temperature, but that this temperature creates usable exergy at a level that justifies turbine integration. In a PEMFC vessel, the exhaust is too low-grade to support a comparably beneficial bottoming or integrated gas-turbine cycle. In an SOFC/GT system, by contrast, the fuel cell acts as a high-temperature electrochemical topping cycle, and the turbine recovers the pressure and temperature potential of the exhaust stream. This is the core physical reason why SOFC/GT architectures can reach efficiency bands beyond those of PEM-based marine systems [82].

However, that higher efficiency is only valuable if the mission actually allows the system to exploit it. Ships with long steady-state segments and relatively modest transient requirements can benefit from the slow but efficient behaviour of SOFC/GT systems. High-speed ferries, harbour craft, and vessels facing frequent manoeuvring cycles are much less favourable environments for them. This is why PEMFCs remain competitive, and sometimes preferable, although their lower thermodynamic ceiling; they align better with rapid power variation, lower startup time, and simpler thermal management. Therefore, one system performs better than another not because of an abstract superiority of one fuel-cell type, but because transport missions reward different combinations of exergy recovery, responsiveness, storage practicality, and packaging tolerance.

This logic can be summarized as follows. PEMFC systems perform better in marine missions where rapid response, modularity, and operational flexibility are more important than maximum efficiency. HT-PEMFC systems perform better when hydrogen infrastructure is unavailable and liquid-fuel logistics become the dominant design criterion. MCFC-based hybrid systems perform better in large commercial vessels requiring a balance between efficiency, fuel flexibility, and practical implementation, particularly when waste-heat recovery can be effectively utilized. Finally, SOFC/GT systems perform best when vessel scale, duty cycle, and operating conditions are sufficient to exploit their superior thermodynamic integration and efficiency potential [82, 86, 87, 89].

4.3 Aeronautical Case Studies

This section presents representative case studies of PEMFC-based and SOFC/GT hybrid systems in aeronautical applications, with a particular focus on auxiliary power units (APUs) and emerging propulsion concepts. Unlike marine systems, where space and weight constraints are relatively relaxed, aeronautical applications impose strict limitations on mass, volume, and system integration, making the evaluation of fuel cell technologies strongly dependent on weight penalties, transient response, and overall system efficiency. The selected case studies include PEMFC-based APU systems and SOFC/GT hybrid architectures investigated for both auxiliary and propulsion purposes. These cases are analysed in terms of system configuration, operating conditions, and performance metrics in order to identify the main drivers influencing their suitability for aviation applications.

4.3.1 Case Study A – PEMFC-based Auxiliary Power Unit (APU)

The integration of Proton Exchange Membrane Fuel Cell (PEMFC) systems as auxiliary power units in aircraft represents a transition from conventional subsystem replacement toward a reconfiguration of the onboard energy architecture. In traditional aircraft, auxiliary power is supplied by gas turbine-based APUs, which operate intermittently and primarily support ground operations, engine start, and limited in-flight services, typically with efficiencies in the range of $20-30\%$. In contrast, PEMFC-based APUs enable continuous electrical power generation across a broader portion of the flight mission, thereby extending their functional role within the aircraft energy system [90]. The operational relevance of this transition can be better understood by considering the aircraft mission profile. Auxiliary systems are required to operate across multiple phases, including ground operations, taxi, takeoff, climb, cruise, descent, and landing, each characterized by different power demands (Fig.4-6).

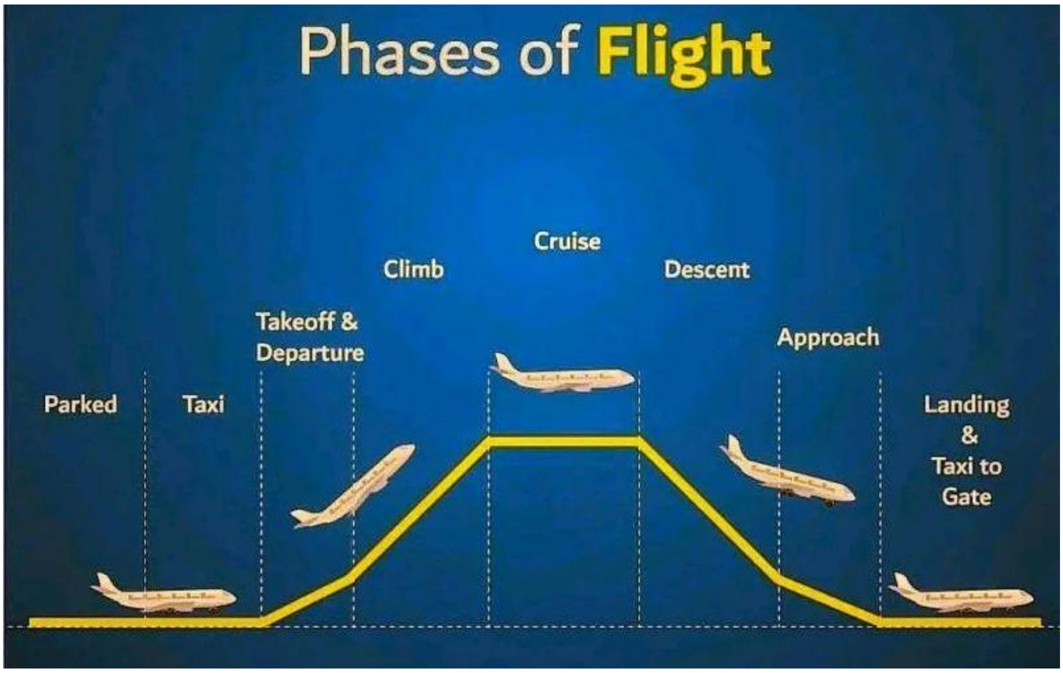

Figure 4-5 Baseline aircraft mission profile showing the different flight phases and corresponding variations in auxiliary power demand [90].

As shown in Figure 4.5, the auxiliary power demand is inherently non-uniform, with frequent transitions between low and moderate load levels depending on the flight phase. This variability imposes strict requirements on the dynamic response of the APU system. Unlike propulsion systems, which operate near steady-state conditions during cruise, auxiliary systems must respond to intermittent and rapidly changing loads. This operational characteristic strongly favours PEMFC technology due to its relatively fast transient response compared to high-temperature fuel cells.

In order to further relate the above observations to the present work, the aircraft mission profile considered in this study is adapted to define the load requirements of the proposed PEMFC-based APU system. This allows for a direct assessment of how the system responds to realistic operational conditions, bridging the gap between literature-based analysis and the modelling approach developed in Chapter 5. The corresponding load profile used in the present study is shown in Figure 4.6.

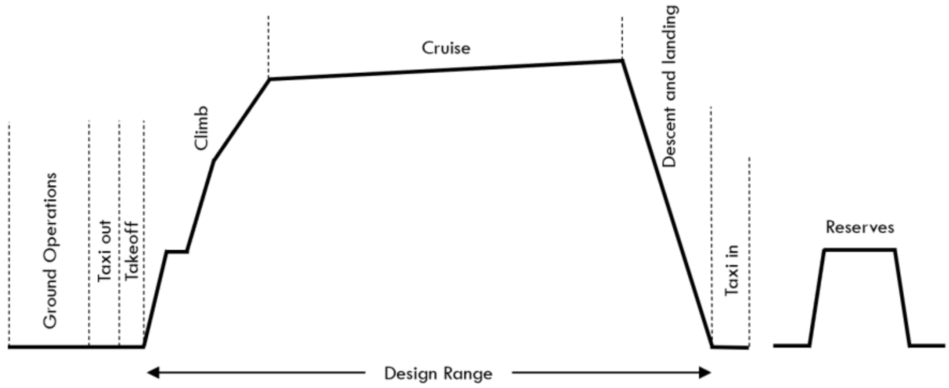

Figure 4-6 Load profile used for PEMFC APU simulation [90].

While the mission-based load profile defines the external power demand, the actual capability of the PEMFC-based APU to satisfy this demand depends strongly on its internal system architecture and the interaction between its main components. In particular, the PEMFC system cannot be considered as a standalone electrochemical device. In practice, it operates as an integrated energy conversion system, where the fuel cell stack is supported by multiple balance-of-plant subsystems, including air compression, hydrogen supply, humidification, and thermal management units. The configuration of these components directly affects both the dynamic response and the overall system efficiency [90].

A detailed configuration of the PEMFC-based APU system considered in this study is illustrated in Figure 4.7.

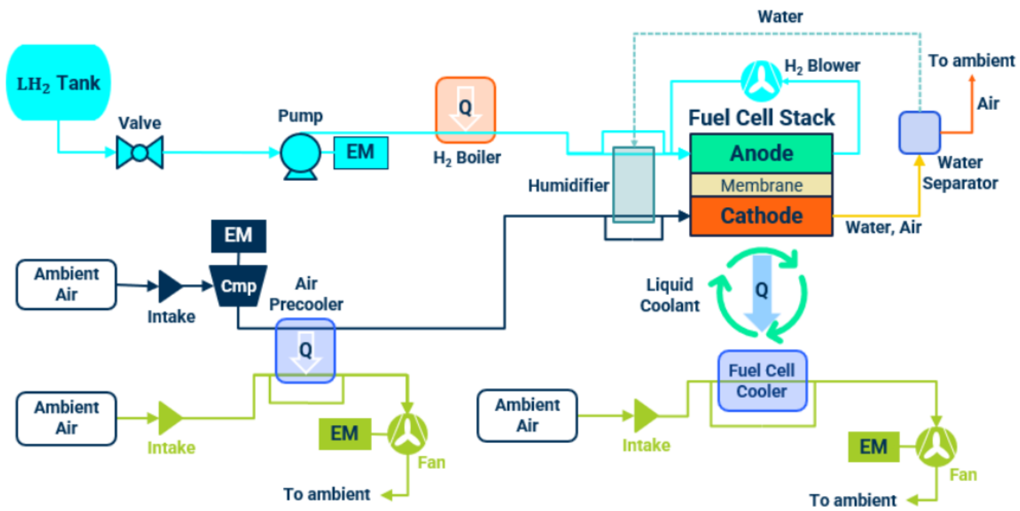

Figure 4-7 Detailed PEMFC system architecture for aeronautical APU applications, including hydrogen supply, air compression, humidification, and thermal management subsystems [90].

As illustrates in Figure 4.7, the system includes several auxiliary subsystems that are essential for operation but introduce non-negligible parasitic power consumption. In particular, the air compressor required to supply pressurized oxidant to the cathode, as well as the thermal management system needed to maintain the stack within its optimal temperature range, consume a portion of the generated electrical power. Additionally, hydrogen conditioning processes, including pumping, vaporization, and humidification, further contribute to the overall energy demand of the system. Thus, the net power delivered by the APU is significantly lower than the gross power produced by the fuel cell stack. This distinction between stack-level performance and system-level performance is critical for accurate evaluation, especially in aeronautical applications where efficiency, weight, and system integration penalties must be assessed simultaneously [90]. The performance of the PEMFC system is also strongly dependent on its operating point, as illustrated by the characteristic relationship between efficiency and current density. Figure 4.8 illustrates the characteristic relationship between cell efficiency and power density as a function of current density for a PEMFC.

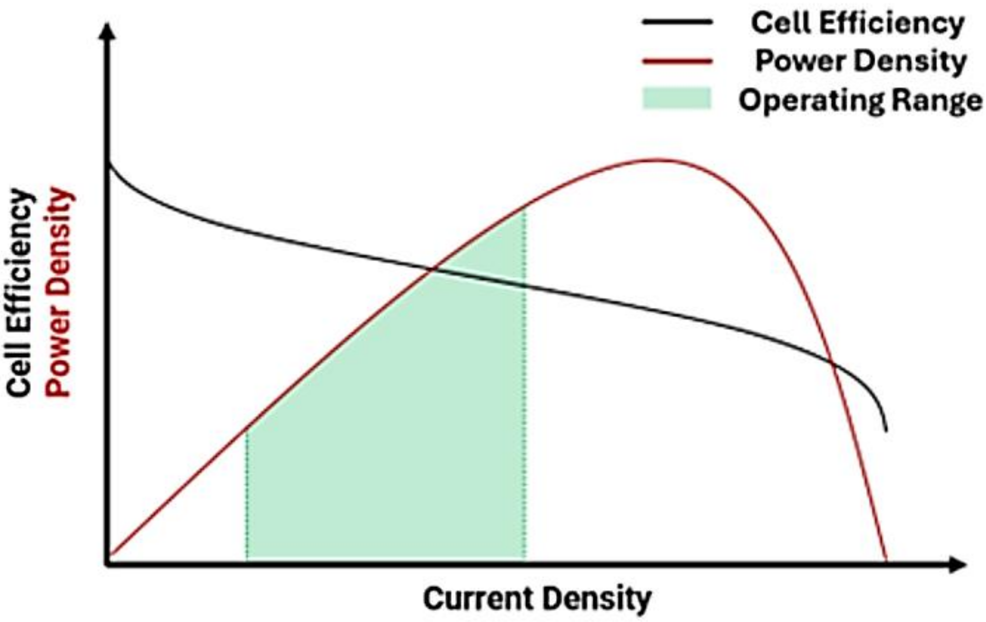

Figure 4-8 Variation of cell efficiency and power density as a function of current density, highlighting the optimal operating range of PEMFC systems [90].

As in Figure 4.8, fuel cell efficiency decreases with increasing current density, while power density follows an opposite trend. This creates an inherent trade-off between maximizing efficiency and maximizing power output. From an operational perspective, this behaviour implies that the PEMFC system cannot continuously operate at maximum power without sacrificing efficiency.

In practice, an optimal operating region exists in which the system achieves a balance between variable costs (linked with efficiency) and power output [90].

The mismatch between the highly dynamic load profile of the aircraft auxiliary systems and the optimal operating characteristics of the PEMFC stack inherently necessitates the adoption of a hybrid system architecture.

In particular, while PEMFC systems exhibit relatively fast transient response compared to high-temperature fuel cells, their electrochemical performance remains most efficient within a limited and relatively stable operating range. To reconcile this discrepancy, a secondary energy storage system typically a lithium-ion battery is integrated to decouple transient power demand from steady-state fuel cell operation. Under rapid load variations, such as those encountered during taxiing, system activation, or auxiliary subsystem engagement, the battery supplies the required peak power, thereby preventing the fuel cell from operating outside its optimal efficiency region.

Conversely, during low-demand phases, excess fuel cell output can be utilized to recharge the battery, enabling energy buffering across the mission profile. This operational strategy transforms the PEMFC-based APU from a purely electrochemical device into a functionally hybrid energy system, in which electrochemical conversion and electrical energy storage are synergistically coupled. Therefore, system performance is no longer governed solely by fuel cell characteristics, but by the coordinated interaction between generation and storage subsystems [90]. Therefore , the performance of PEMFC-based APU systems in aeronautical applications is governed by a complex interplay between mission-driven load variability, system architecture, and operational constraints [90].

While the fuel cell stack provides high-efficiency energy conversion under quasi-steady conditions, the presence of auxiliary subsystems and the requirement for transient load management introduce additional layers of complexity that significantly influence net system performance. In this context, the evaluation of PEMFC APUs cannot be limited to intrinsic efficiency metrics. Instead, it requires a system-level perspective that accounts for parasitic losses, hybridization strategies, and integration penalties associated with weight, volume, and fuel storage [90].

The effectiveness of the system is therefore determined by its ability to maintain operation within a constrained efficiency envelope while satisfying highly variable load demands imposed by the aircraft mission. This analysis reinforces a central theme of the present chapter: the relative performance of competing energy systems is not an inherent property of the technology itself, but rather a consequence of its compatibility with application-specific requirements.

In aeronautical environments, where dynamic operation, strict weight limitations, and integration complexity dominate design considerations, PEMFC-based hybrid architectures emerge as a balanced solution rather than an optimal one in absolute thermodynamic terms [90].
The key performance and design characteristics of the PEMFC-based APU system are summarized in Table 4.5 based on the analysed case study.

Table 4-5 Case-specific performance characteristics of PEMFC-based APU systems [90].

Parameter	Value	Engineering implication
Application	Aircraft APU	Variable, system constraints load
Net efficiency	$40-55\%$	Higher than GT APU, reduced by BOP losses
Conventional APU efficiency	$20-30\%$	Baseline efficiency reference
Operating temperature	$60-80\ ^{\circ}C$	Fast startup, low thermal stress
Air supply	Compressor-driven	Enables altitude operation, adds parasitic load
Parasitic losses	$10-20\%$	Reduces net usable power
Dynamic response	Limited (battery-assisted)	Cannot follow fast transients alone
Fuel	H_2 (compressed / LH_2)	High energy density, high integration penalty
System architecture	FC + battery hybrid	Decouples load and generation
Operating regime	Partial load optimal	Efficiency drops at high load
Main limitation	Weight + complexity	Critical for aircraft integration
Main advantage	Efficiency + zero emissions	Suitable for MEA architectures

Table 4.5 highlights that the performance of the PEMFC-based APU is governed by the trade-off between efficiency and system-level penalties. While the fuel cell provides a clear efficiency advantage, parasitic losses and hydrogen design limitations reduce its net benefit. Furthermore, the inability of the fuel cell to directly follow rapid load variations confirms that hybridization is not optional but a fundamental design requirement. Thus, the system must be interpreted as a hybrid energy architecture rather than a standalone fuel cell unit [90].

4.3.2 Case Study B –SOFC/GT-based Auxiliary Power Unit (APU)

In contrast to the PEMFC-based APU discussed in the previous section, the SOFC/GT hybrid configuration represents a fundamentally different approach to onboard energy generation in aeronautical systems. Rather than prioritizing dynamic response and low-temperature integration, this architecture is designed to maximize thermodynamic efficiency through the recovery and utilization of high-temperature exhaust energy. The relevance of this case study lies not in its maturity for immediate aircraft deployment, but in its role as a thermodynamic reference for high-efficiency onboard power generation. In this context, the SOFC/GT system is an integrated energy conversion cycle, where electrochemical and thermodynamic processes are tightly coupled [49].

The conceptual configurations of SOFC-based hybrid propulsion systems for aeronautical applications are illustrated in Figure 4.9. It should be noted that these configurations originate from thermodynamic cycle analyses reported in the literature, where various SOFC-integrated Brayton cycle concepts are systematically evaluated in terms of performance characteristics. However, the purpose of including these configurations in the present study is not to reproduce detailed thermodynamic cycle analyses, but rather to highlight the range of possible architectural integrations of SOFC systems within aeronautical propulsion frameworks [91].

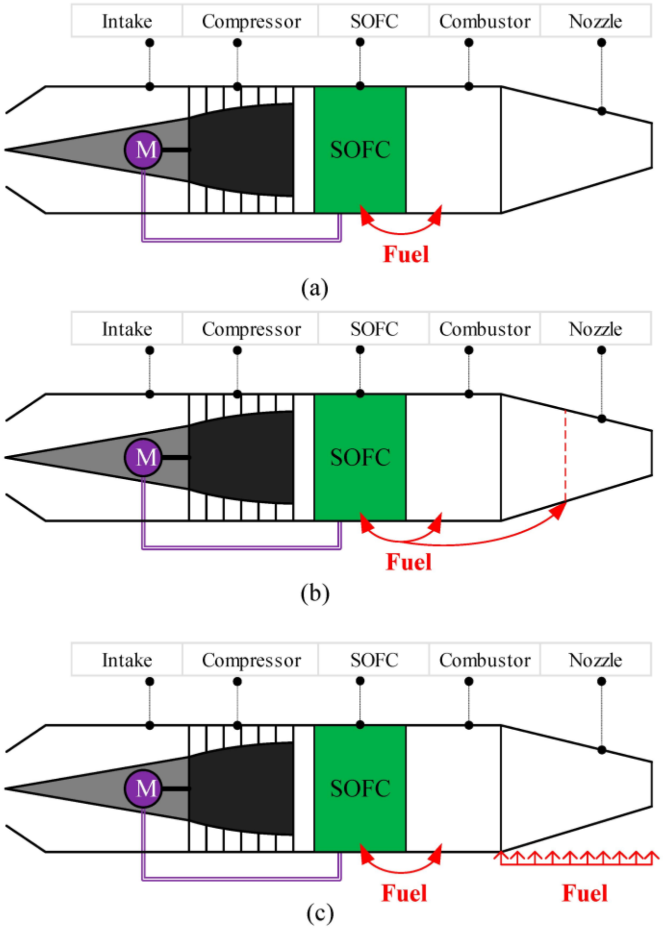

Figure 4-9 Representative configurations of SOFC-integrated hybrid propulsion systems for aeronautical applications, highlighting alternative strategies for coupling electrochemical energy conversion with Brayton-cycle processes: (a) baseline SOFC-integrated turbojet configuration; (b) thermally integrated configuration with extended exhaust energy utilization; (c) fuel-flexible configuration with distributed fuel injection and enhanced operational adaptability [91].

As shown in Figure 4.9, multiple system architectures can be identified depending on how the SOFC unit is integrated within the propulsion system. In all configurations, the fuel cell is positioned downstream of the compressor, allowing operation under pressurized conditions and enabling efficient electrochemical energy conversion.

The role of downstream components, particularly the combustor and nozzle, varies significantly across configurations. In the baseline configuration (a), the SOFC primarily functions as an electrochemical power generator, while the combustor provides the additional thermal energy required for expansion. In configuration (b), the utilization of exhaust thermal energy is extended. Configuration (c) introduces additional fuel injection strategies, reflecting a transition toward fuel-flexible and performance-optimized operation [91]. These variations demonstrate that the performance of SOFC-based aeronautical systems is not governed solely by fuel cell characteristics, but is strongly dependent on system-level integration, including the management of residual fuel and high-temperature exhaust energy [91].

4.3.2.1 Trade-offs Under Aeronautical Constraints

When interpreted within an aeronautical context, the differences between configurations become more pronounced. Configuration (b) increases flexibility. This may limit its applicability in weight-sensitive aircraft applications. Configuration (a), although less efficient, benefits from a simpler architecture and reduced integration requirements, making it more compatible with applications where system robustness and lower mass are prioritized over maximum efficiency. Configuration (c) occupies an intermediate position, offering improved operational flexibility at the cost of increased control complexity. Its suitability therefore depends on the extent to which variable operating conditions must be accommodated [91].

4.3.2.2 Mission-Oriented Interpretation

The comparison between configurations demonstrates that no single SOFC/GT architecture can be considered universally optimal for aeronautical applications. In practice, system performance must be evaluated in relation to mission requirements. For steady-state, endurance-driven missions, such as high-altitude platforms or long-endurance UAVs, configurations emphasizing thermal integration (such as configuration (b)). In contrast, for missions involving variable load demand, configurations with greater operational flexibility (such as configuration (c)) may provide better overall performance. in aeronautical applications, the performance of advanced energy systems is governed not only by thermodynamic efficiency, but by the alignment between system architecture and mission profile [91]. To enable a more meaningful interpretation of the SOFC/GT case study, the configurations presented in Figure 4.9 are compared in terms of their system-level behaviour rather than individual component performance.

4.3.2.3 Thermodynamic Scaling and Integration Penalty

The thermodynamic potential of SOFC/GT systems is often reported in terms of high fuel-to-electric efficiency; however, this metric alone does not capture the fundamental limitations that emerge when the system is translated from an idealized cycle to an aeronautical platform. A more rigorous interpretation of this case study requires examining how efficiency gains scale with system integration requirements. In thermodynamic cycle analyses, configurations with deeper heat recovery and stronger coupling between the SOFC and the Brayton cycle can achieve efficiencies exceeding 60%, with projections approaching 70% under optimized conditions. These gains are primarily driven by the ability of the system to convert high-temperature exhaust energy into additional useful work through turbine expansion and recuperation processes. However, the same mechanisms that enable these gains introduce non-negligible integration penalties [49, 91]. One of the most critical constraints arises from heat exchanger scaling. High-efficiency configurations rely on extensive thermal coupling, which requires large heat transfer surfaces to maintain effective temperature gradients between the SOFC exhaust, compressor outlet air, and recirculated flows. Thus, the size and mass of heat exchangers increase disproportionately with attempts to maximize efficiency. In some configurations, the required heat exchanger capacity can be several times larger than that of more compact architectures, directly impacting system weight and volume.

In addition to geometric scaling, thermodynamic optimization imposes stricter constraints on operating conditions. Parameters such as pressure ratio, mass flow distribution, and temperature gradients become tightly interdependent. For example, while increasing pressure enhances SOFC performance, it is limited by temperature differences across the cycle and by the allowable thermal stresses within system components. Consequently, the operational envelope of high-efficiency configurations becomes narrower, reducing tolerance to off-design conditions and increasing control complexity [49, 91].

From a system design perspective, these effects lead to a non-linear relationship between efficiency and feasibility. Initial increases in thermal integration yield substantial efficiency improvements, but beyond a certain point, additional gains require disproportionately higher integration effort. This results in diminishing returns at the aircraft level, where the benefits of reduced fuel consumption may be offset by penalties in mass, volume, and system complexity. This behaviour fundamentally distinguishes SOFC/GT systems from low-temperature fuel cell architectures. While PEMFC systems are primarily constrained by energy density and storage, SOFC/GT systems are constrained by the scalability of thermal integration. This leads to, their performance advantage is conditional rather than absolute. Therefore, the SOFC/GT architecture should be interpreted not as a universally superior solution, but as a configuration whose effectiveness depends on whether its thermodynamic advantages can be realized without exceeding aeronautical integration limits. This insight is critical for the subsequent comparative analysis, where the relative performance of PEMFC and SOFC/GT systems is evaluated in the context of operating system constraints [49, 91].

4.3.3 Case Study C –SOFC/GT Hybrid System for Primary Propulsion in Aircraft

The third case study explores the design and analysis of a high-performance SOFC/GT hybrid system intended not only for auxiliary power but also for partial propulsion in next-generation aircraft. Conducted by Mashamba and co-workers in 2024 [77], this study represents one of the most advanced numerical investigations of a hybrid SOFC-based power system integrated with a gas turbine engine for aviation applications. Unlike previous analyses, this work examined the potential of the SOFC/GT concept as a primary propulsion source, capable of simultaneously producing thrust and electrical energy for the aircraft's onboard systems.

The motivation behind this research derived from the increasing pressure to decarbonise aviation and to improve the overall energy efficiency of aircraft propulsion. Gas turbines alone, even in their most efficient configurations, typically achieve thermal efficiencies below 40 %, whereas the high operating temperature of SOFCs allows direct conversion of hydrocarbon fuels into electricity with efficiencies exceeding 60 %. By coupling an SOFC with a micro gas turbine, the system can recover high-temperature exhaust energy and utilise it for expansion work, achieving overall efficiencies well beyond those of traditional engines. The study thus investigated whether this hybridisation could provide a feasible path toward carbon-neutral propulsion without resorting entirely to hydrogen fuel [77].

The hybrid configuration developed by Mashamba et al. was composed of a CPO_X reformer, an SOFC stack, an afterburner, a heat exchanger, and a small-scale turbofan engine. The system was fuelled with conventional Jet-A, modelled as dodecane ($C_{12}H_{26}$), and the fuel was reformed within the $CPOx$ reactor to generate a mixture of hydrogen, carbon monoxide, and carbon dioxide suitable for electrochemical oxidation in the SOFC stack. The electrochemical model employed standard Nernst and Butler–Volmer formulations to describe the cell voltage and current characteristics, incorporating ohmic, activation, and concentration losses. The SOFC operated at 900 °C and 1.5 bar, with a fuel utilisation rate of approximately 85 %, a current density of $0.4\ \frac{A}{CM^2}$, and a mean cell voltage of $0.75\ V$. Thermodynamically, the system was structured so that the SOFC exhaust supplied both heat and unreacted fuel to the gas turbine, where the remaining energy content was converted to mechanical work. The turbine itself was linked to a generator and a fan stage, enabling dual-mode operation: electrical power generation and direct thrust production. The heat exchanger recovered residual energy from the exhaust stream to preheat the incoming air and fuel mixture, increasing overall cycle efficiency. The reformer, SOFC stack, and turbine were modelled in thermal equilibrium to ensure realistic heat coupling, while mass and energy balances were solved simultaneously for all components [77].

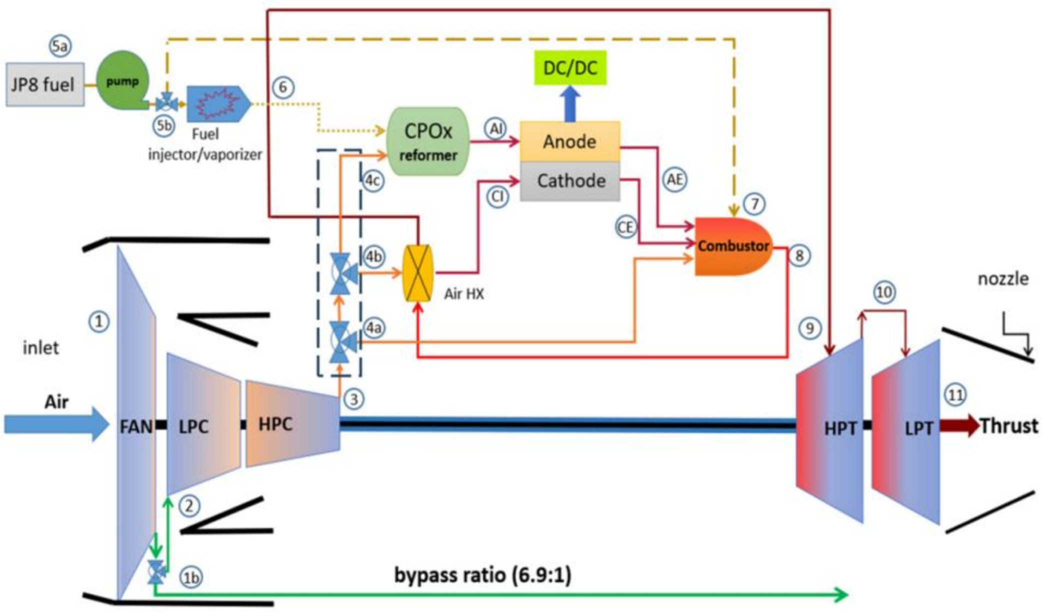

Figure 4-10 SOFC/GT configuration represent by Mashamba [97].

One of the key features of the analysis was the systematic evaluation of the three most influential operational parameters: the oxygen-to-carbon (O/C) ratio, the fuel utilisation (Uf), and the air split ratio (As). These parameters determined the balance between reforming reaction rates, electrochemical efficiency, and turbine work output. Sensitivity analysis revealed that the hybrid system was most responsive to variations in the air split ratio, which directly affected the fuel cell's temperature and the turbine inlet conditions. At low air split ratios, the turbine received hotter exhaust gases and generated higher mechanical power but at the risk of thermal stress in the SOFC stack. Conversely, higher air split ratios reduced turbine power and improved stack temperature uniformity, suggesting the need for an optimal trade-off between electrochemical stability and propulsion efficiency. At the design point, corresponding to a flight condition equivalent to 30,000 ft, the hybrid system achieved a total power output of $1.96\ MW$, distributed as $1.86\ MW$ of thrust power and $102.5\ kW$ of electrical power [77].

The overall efficiency of the integrated system reached approximately $56\ \%$, representing a significant improvement over conventional turbofan engines of similar scale. The hybrid configuration also demonstrated reduced specific fuel consumption and a substantial reduction in carbon emissions, highlighting the potential of SOFC-based propulsion systems as transitional technologies toward fully electric aviation. The dynamic simulation results further indicated that the system could sustain stable operation under transient conditions, with the SOFC stack temperature varying within $\pm 20\ °C$ during rapid load transitions. This stability was primarily attributed to the thermal inertia of the stack and the effective recuperation strategy embedded in the system. The exhaust stream from the turbine was sufficiently clean and hot to drive additional processes, such as cabin heating or dehumidification, without requiring complex after-treatment [77].

From an engineering perspective, the integration of SOFC and gas turbine subsystems required careful balancing of thermodynamic and structural constraints. The authors highlighted challenges related to material durability under cyclic loading, thermal expansion mismatches, and the control of reformer exhaust composition. In particular, maintaining a constant $\mathrm{O/C}$ ratio during throttle changes was critical to prevent carbon deposition and to ensure stable reforming. Advanced control strategies and variable-geometry components were proposed as potential solutions for future experimental prototypes. The analysis concluded that the hybrid $\mathrm{SOFC/GT}$ propulsion system could serve as a viable alternative for regional or medium-range aircraft if material advances and control techniques continue to progress. Its combined efficiency, reduced emissions, and potential for fuel flexibility make it a promising architecture for sustainable aviation [77].

However, the high operating temperatures and mechanical integration complexity remain significant barriers to near-term implementation. Within the scope of this thesis, the Mashamba et al. study represents a key reference for high-temperature fuel-cell applications in aircraft, complementing the PEM-based APU studies presented earlier. While the PEMFC configurations excel in auxiliary power and transient response, the $\mathrm{SOFC/GT}$ hybrid demonstrates the capability to contribute directly to propulsion, offering higher efficiency and lower specific emissions. The comparative insights from this study thus provide a critical foundation for evaluating the trade-offs between low-temperature and high-temperature fuel-cell technologies in the aviation sector [77].

4.4 Aeronautical Comparative Analysis PEMFC vs SOFC/GT Systems

Building on the previously discussed hybrid configurations and application-specific requirements, it becomes evident that the performance of fuel-cell-based propulsion systems in aviation cannot be assessed solely based on efficiency or power output. Instead, system-level performance is strongly governed by the interaction between energy conversion efficiency, fuel storage characteristics, and overall system weight. In this context, a more comprehensive evaluation framework can be established by decomposing the total system weight into fixed and variable contributions. The fixed weight includes components such as the fuel cell stack, turbomachinery, heat exchangers, and auxiliary systems, while the variable weight is mainly due to the fuel mass and storage system. This distinction provides a more rigorous basis for comparing different propulsion architectures, particularly when considering varying mission durations [47, 92].

For low-temperature fuel cell systems such as PEMFC-based configurations, the relatively high fuel consumption leads to a dominant contribution of variable weight. Accordingly, system performance becomes highly sensitive to hydrogen storage requirements, which significantly increase total system mass, especially for long-range missions. In contrast, high-temperature systems such as SOFC/GT configurations are characterized by higher fixed weight due to the integration of turbomachinery and thermal management components. However, their superior electrical efficiency results in lower fuel consumption, leading to a reduced variable weight contribution [77]. This trade-off leads to the concept of a break-even flight duration, beyond which high-efficiency systems can outperform lighter but less efficient alternatives in terms of total system mass. Therefore, the relative performance of PEMFC and SOFC-based systems cannot be defined independently of mission profile and must be evaluated within an operating context framework [47, 92]. To further refine the comparison between PEMFC and SOFC/GT systems, it is necessary to move beyond qualitative architectural differences and examine the underlying factors governing configuration performance. In particular, total system weight can be decomposed into fixed and variable contributions, providing a more rigorous basis for evaluating performance across different mission conditions.

Table 4-6 Fixed vs Variable Weight Contribution [47, 92].

Parameter	PEMFC Systems	SOFC/GT Systems
Fixed Weight Contribution (Stack + BoP + Turbine)	Low–Moderate	High
Variable Weight Contribution (Fuel + Storage)	High	Low
Dominant Limitation	Fuel storage	System complexity
Sensitivity to Mission Length	High	Moderate
Efficiency Impact	Moderate	High
Integration Complexity	Moderate	High

As shown in Table 4.6, PEMFC and SOFC/GT systems exhibit fundamentally different weight distributions. PEMFC-based systems are dominated by variable weight associated with hydrogen storage, making their performance highly sensitive to mission duration. In contrast, SOFC/GT systems are characterized by higher fixed weight due to turbomachinery and thermal integration but benefit from lower fuel consumption. This distinction leads to different performance scaling behaviours. PEMFC systems experience a continuous increase in total system weight with mission length, whereas SOFC/GT systems exhibit a more stable weight profile due to reduced fuel requirements.

While the weight-based comparison presented in Table 4.6 provides valuable insight into mission-dependent performance, recent investigations of SOFC/GT propulsion systems reveal additional factors that influence architecture selection. The study by Mashamba et al. [77] demonstrated that SOFC/GT systems can contribute directly to aircraft propulsion, producing approximately $1.86\,MW$ of thrust power while simultaneously generating electrical power for onboard systems. In addition, the high operating temperature of SOFC technology enables fuel flexibility and superior fuel utilisation compared with PEMFC systems. Conversely, PEMFC architectures as we discussed in chapter 2 and 3 offer faster transient response, lower operating temperatures, and reduced integration complexity. Therefore, the selection of a suitable fuel-cell architecture depends not only on weight distribution and mission duration, but also on propulsion requirements, fuel flexibility, thermal management constraints, and dynamic operational characteristics [47, 92].

Beyond weight considerations, the recent SOFC/GT investigation conducted by Mashamba et al. demonstrated that high-temperature fuel-cell systems can provide not only electrical power but also a substantial contribution to aircraft propulsion. The hybrid configuration achieved an overall efficiency of approximately 56% while producing 1.86 MW of thrust power and 102.5 kW of electrical power at cruise-equivalent conditions. These results highlight an additional dimension of comparison between PEMFC and SOFC-based architectures. Whereas PEMFC systems are generally better suited to auxiliary power generation and applications requiring rapid transient response, SOFC/GT systems offer superior fuel utilisation, fuel flexibility, and propulsion capability [77]. Consequently, the selection of an appropriate fuel-cell architecture depends not only on mission duration and system weight, but also on propulsion requirements, thermal management constraints, operational flexibility, and aircraft integration objectives [47, 92].

4.4.1 Fuel Choice and configuration Trade-offs

The influence of fuel selection on system-level performance becomes more explicit when interpreted through operating regime weight scaling, as illustrated in Figure 4.11. Rather than acting as a secondary design parameter, fuel choice fundamentally reshapes the balance between fixed and variable system mass, thereby altering the dominant performance limitation of each architecture. To further quantify the impact of fuel selection on architecture-level performance, Figure 4.11 presents the variation of total system mass as a function of mission duration.

it is necessary to move beyond qualitative discussion and examine how different fuel options influence the evolution of total system mass over mission duration. In particular, the relative contribution of fixed system components (such as the fuel cell stack and balance-of-plant) and variable components (fuel and storage) can be directly visualized as a function of flight time. This provides a more rigorous basis for comparing PEMFC and SOFC-based architectures under realistic operational conditions.

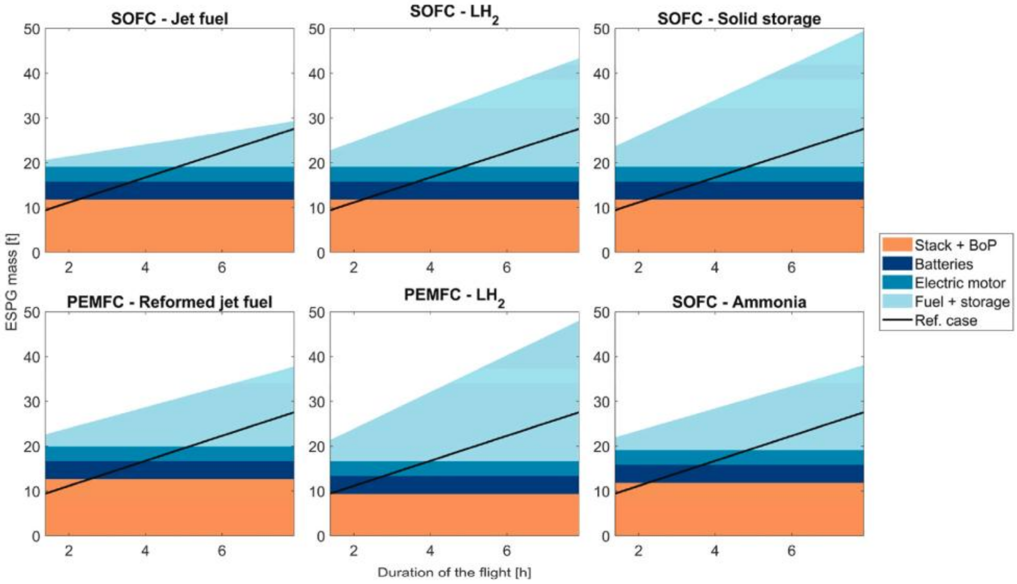

Figure 4-11 architecture-level mass breakdown as a function of mission duration for PEMFC and SOFC-based propulsion systems under different fuel options [47].

As shown in Figure 4.11, the influence of fuel selection becomes significantly more pronounced when evaluated over increasing mission duration. In PEMFC-based configurations, particularly in the PEMFC–LH_2 case, the total system mass increases rapidly due to the dominant contribution of fuel and storage. This reflects the inherent limitation associated with hydrogen storage, where low volumetric energy density leads to a steep growth in variable weight. In contrast, SOFC-based configurations demonstrate a more gradual increase in total system mass.

In cases such as SOFC–Jet fuel and SOFC–Ammonia, the higher energy density of the fuel results in a reduced rate of weight increase, effectively mitigating the impact of mission length on system performance. Therefore, the relative importance of fixed system components becomes more pronounced. This behaviour confirms that fuel selection fundamentally alters the scaling characteristics of the system. While PEMFC architectures remain constrained by storage-driven weight growth, SOFC systems shift the design limitation toward integration-related penalties. Therefore, the performance comparison between these systems cannot be decoupled from mission duration, as fuel choice directly governs the transition between competing system constraints [47].

The trends observed in Figure 4.11 naturally lead to the concept of a break-even mission duration, at which the total system mass of competing architectures becomes equivalent. This point represents a critical threshold beyond which the relative advantage of each system reverses. For short-duration missions, PEMFC-based systems typically exhibit lower total mass due to their reduced fixed weight and simpler system architecture. In these operating conditions, the penalty associated with hydrogen storage remains limited, allowing the system to benefit from its structural simplicity and lower integration requirements. However, as mission duration increases, the rapid growth of the variable weight component in PEMFC systems becomes dominant [47]. In contrast, SOFC-based systems, while their higher initial mass, benefit from lower fuel consumption and higher energy density fuels, resulting in a slower rate of mass increase. Accordingly, beyond a certain mission duration, SOFC configurations can achieve a lower total system mass compared to PEMFC systems. This transition defines the break-even point, which is not fixed but depends on fuel type, storage technology, and system configuration. This behaviour demonstrates that system superiority is not absolute, but emerges as a function of mission duration and weight scaling characteristics [47].

Table 4-7 Mission-dependent comparative assessment of PEMFC and SOFC/GT systems in aeronautical applications [47].

Criterion	PEMFC Systems	SOFC/GT Systems	Analytical Interpretation
Dominant limitation	Hydrogen storage	Thermal integration	Different governing constraints
Weight scaling behaviour	Rapid increase with mission	Gradual increase	Storage-driven vs integration-driven scaling
Efficiency utilization	Moderate	High (steady-state)	Efficiency only valuable in stable operation
Dynamic response	Fast	Slow	Hybridization requirement differs
Fuel flexibility	Low (hydrogen only)	High	Affects system feasibility
Best mission range	Short–medium	Medium–long	Break-even dependent
System role	Hybrid with buffering	Steady-state generator	Functional differentiation
Overall advantage	Flexibility & simplicity	Efficiency & endurance	operating regime superiority

The comparison presented in Table 4.7 consolidates the key findings of this section, highlighting that the relative performance of PEMFC and SOFC/GT systems is governed by fundamentally different scaling mechanisms and system constraints. Rather than identifying a universally superior technology, the analysis demonstrates that each architecture is optimized for a specific operational envelope. PEMFC systems perform more effectively in applications requiring dynamic response and operational flexibility, whereas SOFC-based systems become advantageous in endurance-driven missions where efficiency and fuel economy dominate. This interpretation reinforces a central conclusion of this study: the performance of fuel cell systems in aeronautical applications is not an intrinsic property of the technology itself, but an emergent characteristic defined by the interaction between system architecture, fuel selection, and mission profile. Ultimately, the comparison between PEMFC and SOFC/GT systems highlights that system performance in aviation is not determined by a single parameter such as efficiency or power density, but by the interaction between energy conversion, fuel storage, and mission characteristics. This perspective enables a more realistic assessment of advanced propulsion technologies and provides a framework for selecting the most suitable architecture based on operational requirements.

4.5 Numerical Methodology and Simulation Framework

The comparative evaluation presented in Chapter 4 revealed the progressive development of hybrid solid oxide fuel cell (SOFC) and gas turbine (GT) systems for aviation applications, illustrating how the conceptual studies of the early 2000s evolved into the high-fidelity thermodynamic simulations of recent years. Within this chronological and technical continuum, two studies the pioneering numerical model by Freeh et al.[93] and the advanced simulation work by Wilson et al. [94] emerge as the methodological cornerstones upon which the present numerical investigation is constructed. Both studies address the same fundamental challenge: the accurate coupling of electrochemical conversion and turbomachinery processes under flight-representative conditions. Yet, they do so at different levels of model maturity and fidelity, providing complementary perspectives that, when combined, form a comprehensive foundation for the current research.

The NASA Glenn model developed by Freeh and colleagues was the first to implement a physics-based SOFC/GT hybrid within the NPSS environment. This framework introduced a rigorous formulation of electrochemical performance, incorporating the Nernst potential, activation and ohmic losses, fuel utilisation, and temperature-dependent kinetics into a thermodynamic engine model. The model's primary strength lay in its ability to resolve the bidirectional coupling between the SOFC stack and gas turbine subsystem capturing how variations in pressure ratio, mass flow rate, and turbine expansion affect the cell voltage and overall system efficiency. Despite being developed nearly two decades ago, the NASA model remains a reference benchmark for hybrid-cycle thermodynamics and has been validated against laboratory-scale fuel-cell experiments with less than two percent deviation. Its analytical structure, based on conservation of mass, energy, and charge, provides the theoretical foundation adopted in the present work for the electrochemical and thermodynamic sub models[93].

In contrast, the study by Wilson et al.[94] represents a new generation of hybrid system simulations carried out using the ProMax process-simulation environment. Rather than focusing solely on the fuel cell stack, this model achieved a full thermodynamic coupling of the SOFC, gas turbine, reformer, and recuperative heat exchangers within a unified flowsheet. It successfully replicated the NASA NPSS results with less than one percent error in predicted voltage and efficiency, validating the numerical consistency of the ProMax-based methodology. However, it further expanded the model to include additional physical processes absent from the NASA baseline, such as anode-gas recirculation, internal steam reforming of n-dodecane, dynamic heat recovery, and altitude-dependent compressor/turbine performance maps for a flight condition of 36,000 feet. The result was a high-fidelity thermodynamic model capable of exploring configuration-dependent efficiency, fuel consumption, and temperature stability across multiple hybrid layouts[94].

Together, these two works define the computational boundaries for the current thesis. The NASA model contributes the mathematical and electrochemical formulation, offering a first-principles basis for voltage prediction, current density mapping, and reaction equilibrium under pressurised conditions. The Wilson model, on the other hand, provides a systems-integration perspective, combining process-level interactions, flow recirculation, and altitude corrections to simulate the complete hybrid cycle as an integrated thermodynamic entity. By merging the physical accuracy of the NPSS approach with the process flexibility of ProMax, the present study develops a hybrid numerical framework capable of both detailed component-level analysis and holistic cycle optimisation[93, 94].

Accordingly, the methodology presented in the next chapter draws directly from these two validated studies. The NASA framework is used to establish the electrochemical sub model defining governing equations for cell voltage, current density, fuel utilisation, and internal losses while the other framework provides the thermodynamic boundary conditions and inter-component coupling for the full hybrid system. These two methodological pillars serve as the reference against which the new model is constructed, calibrated, and validated. The implementation extends both prior works by introducing parametric flexibility in compressor pressure ratio, turbine inlet temperature, and anode-recycle fraction, allowing for comprehensive sensitivity analysis under varying altitude conditions [93, 94].
Therefore, Chapter 5 presents the numerical methodology and simulation framework developed for this thesis. It details the governing electrochemical and thermodynamic equations, defines the boundary conditions for steady and cruise operation, and describes the calibration process employed to ensure consistency with the NASA NPSS and ProMax reference models. This approach ensures that the subsequent numerical results not only maintain physical fidelity to the established literature but also extend it toward a more generalised, multi-physics representation of hybrid SOFC/GT systems for electric aviation [93, 94].

5. Numerical Methodology and System Modelling

This chapter presents the numerical modelling framework developed for the hybrid SOFC–GT system. While the previous chapters focused on the technological background and review of relevant literature, the emphasis here shifts toward the formulation of the governing equations and the implementation of a fully coupled system-level model. The aim is to construct a thermodynamically and electrochemically consistent computational framework in which the SOFC stack, combustor, heat exchangers, gas turbine, and generator are solved in an integrated manner under steady-state operating conditions. In doing so, particular attention is given to mass conservation, energy balance closure, and the physical consistency of the coupling between electrochemical and thermodynamic processes. The modelling sequence begins with the definition of the overall system architecture and identification of the principal mass and energy flow paths. This is followed by the formulation of component-level governing equations for each subsystem. The chapter concludes with a Verification of the developed model against well-established reference configurations, providing confidence in its suitability for subsequent performance evaluation and parametric analysis.

5.1 Selection of the Reference Architecture and Verification Strategy

Given the strong thermodynamic and electrochemical coupling within hybrid SOFC–GT systems, verification of the developed numerical model is a prerequisite before conducting any parametric or performance analysis. Due to the multi-physics nature of the system and the tight interaction between electrochemical reactions, heat transfer, and turbomachinery processes, even small inconsistencies in one subsystem may propagate and affect overall system predictions. For this reason, a structured verification strategy is adopted in the present study. First, the developed model is benchmarked against a well-established reference architecture with documented numerical results. Subsequently, an extended reference case is employed to verify that the model correctly captures performance trends under varying operating conditions. This two-level verification approach ensures both numerical consistency and physical credibility of the developed framework.

5.1.1 NASA SOFC–GT Architecture as the Primary Verification Reference

The hybrid SOFC–GT model developed by Freeh et al. [93] within NASA's Numerical Propulsion Systems Simulation (NPSS) framework represents one of the most comprehensive system-level models developed for aerospace applications.

In this work, detailed models of the solid oxide fuel cell, fuel processing unit, heat exchangers, and gas turbine components are implemented within the NPSS framework and solved in a fully integrated manner. A major strength the reference model lies in the integration of a physically based SOFC electrochemical model with the gas turbine cycle, together with verification against experimental fuel cell data, providing a high level of credibility for both component-level and system-level predictions [93].

As illustrated in the NASA system architecture, compressed air is first preheated in an air heat exchanger before entering the SOFC cathode. On the fuel side, liquid fuel and steam are supplied to an external reformer, where a hydrogen- and carbon-monoxide-rich syngas is produced and fed to the SOFC anode. The anode off-gas, containing unreacted fuel species, is directed to a downstream combustor, where the remaining chemical energy is released to raise the turbine inlet temperature. The exhaust heat from the turbine is subsequently recovered through heat exchangers to preheat the incoming air and water streams. The primary motivation for selecting the NASA architecture as the initial verification reference is its structural clarity and physical transparency. The configuration avoids secondary system complexities such as extensive anode recycling loops or water condensation units, focusing instead on the fundamental interactions between the SOFC and the gas turbine. This makes the architecture particularly well suited for verifying the correctness of mass and energy balance formulations and ensuring that the coupled electrochemical–thermodynamic behaviour is captured accurately in the developed model. Accordingly, in this thesis, the NASA SOFC–GT configuration is not treated as a final design target, but rather as a benchmark architecture against which the independently developed model is validated. Agreement with the published NASA results serves as the foundation for confidence in the physical consistency of the modelling approach.

5.1.2 Distinction Between the Verification Reference and the Computational Tool of the Present Study

It is important to clearly distinguish between the reference architecture used for verification and the computational platform employed in this research. Although the NASA study implements the SOFC–GT model within the NPSS environment, the present thesis does not rely on NPSS as a simulation tool. In this work, NPSS serves solely as a source of a validated SOFC–GT architecture, published benchmark results, and a widely recognized aerospace reference framework. All mass balance, energy balance, and electrochemical calculations are performed independently using a spreadsheet-based environment (Excel). Each governing equation is explicitly implemented, and all intermediate variables remain fully traceable throughout the computational procedure. This approach ensures transparency, reproducibility, and independence from proprietary simulation software, while maintaining strong alignment with a validated aerospace-grade reference model. The clear separation between the use of NASA results for verification and the independent development of the computational framework provides a transparent and defensible methodological foundation for the remainder of the study.

5.1.3 Role of the Wilson et al. Study in Model Extension and Trend Verification

Following the initial verification against the NASA reference architecture, the study by Wilson et al [95]. is employed as a secondary reference to support model extension and performance trend evaluation. This work addresses the SOFC–GT system at two distinct levels, each serving a specific purpose in the present thesis.

a) Baseline Architecture and System Complexity Assessment

In the first part of the Wilson et al. study, an SOFC–GT system architecture is proposed for APU applications. The overall layout closely resembles the NASA configuration, including an external reformer, a high-temperature SOFC stack with separate anode and cathode flow paths, a downstream combustor, and a gas turbine cycle. As shown in the corresponding schematic, the main distinction relative to the NASA architecture lies in the inclusion of anode exhaust recycling and advanced water management. By recycling part of the anode off-gas and recovering water from the exhaust, the system significantly reduces or eliminates the need for external water supply after startup. In this thesis, this baseline configuration is used to examine the impact of additional system complexity on overall performance, relative to the simpler NASA-based architecture.

b) ProMax-Based Model and Power–Altitude Analysis

In the second part of the Wilson et al. study, the same baseline architecture is implemented in the ProMax process simulation environment and extended to investigate system behaviour at higher power levels and under varying flight altitudes. This section of the study moves beyond architectural verification and focuses on realistic aerospace operating constraints. In comparison with the simplified NASA architecture, the ProMax-based implementation introduces additional process-level refinements that enhance physical realism without altering the fundamental thermodynamic structure of the hybrid cycle. These refinements include the incorporation of recycle split and mixer blocks to enable partial recirculation of anode off-gas, the introduction of a flash separator and condenser unit for water recovery from the exhaust stream, and the addition of a fuel atomization stage prior to reforming. The inclusion of anode gas recycling modifies the reformer inlet composition by reintroducing residual steam and carbon-containing species, thereby influencing the steam-to-carbon ratio and hydrogen production potential. Similarly, the condenser and water recovery unit reduce the dependence on external water supply by extracting and reutilizing water formed during electrochemical and combustion processes. Although the present thesis does not rely on ProMax as a computational tool, the process-level clarity offered by its flowsheet representation provides valuable insight into control-volume boundaries and thermal integration pathways. Within the scope of this thesis, this portion of the Wilson et al. work is used primarily for trend verification rather than direct numerical comparison. The objective is not to reproduce the ProMax results numerically, but rather to verify that the independently developed model captures the correct physical trends in system performance under varying power demands and ambient flight conditions.

5.2 System Architecture Definition and Overall Diagrams Used in This Study

In the present study, three different diagrams are employed to describe the SOFC–GT system architecture from complementary perspectives. Each diagram serves a distinct purpose in clarifying the system structure, component interactions, and flow paths. Together, they provide a complete and unambiguous representation of the system considered in this research. To avoid confusion, the system description proceeds in a structured manner. First, the overall architecture and component interactions are introduced using a conceptual schematic. Subsequently, a more detailed and application-oriented layout is discussed. Finally, the system is viewed from a process modelling perspective, focusing on unit boundaries and control volumes.

5.2.1 Conceptual System Architecture Based on the NASA SOFC–GT Schematic

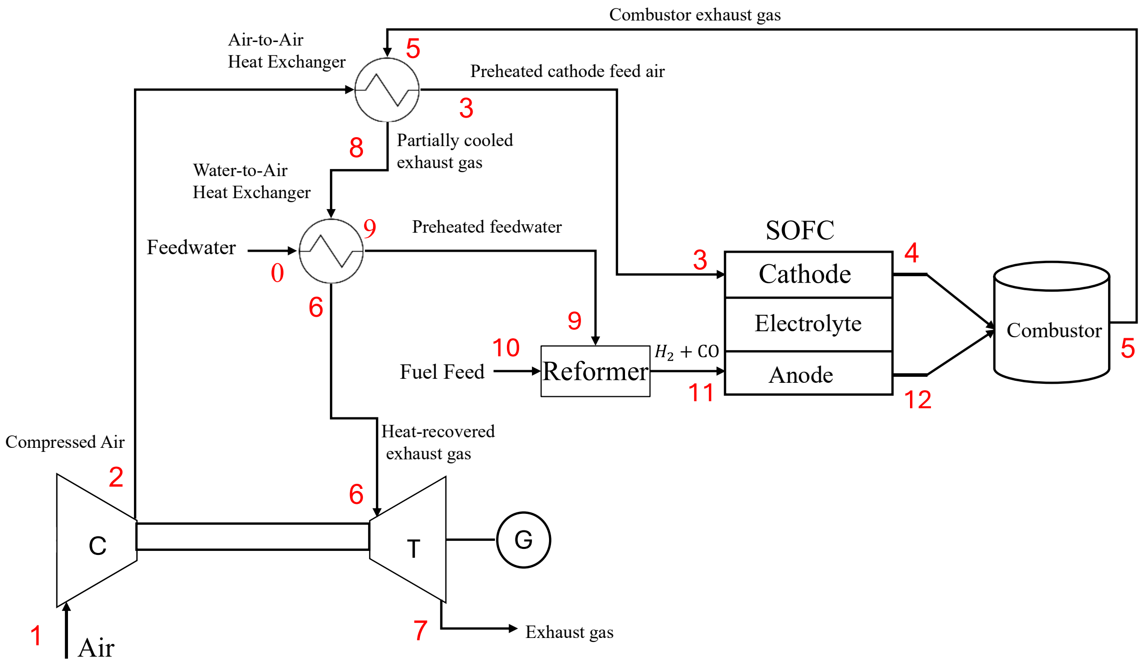

Figure 5-1 NASA's NPSS SOFC/GT hybrid system architecture [93].

The system description (Fig.5-1) begins with the SOFC–GT schematic developed by NASA, which is used as a conceptual reference architecture. As demonstrated , This schematic provides a clear and physically intuitive representation of the main system components and the primary mass and energy flow paths, without introducing unnecessary architectural complexity [93]. In the NASA schematic, ambient air is compressed and subsequently preheated in an air heat exchanger before entering the SOFC cathode. On the fuel side, liquid fuel is mixed with steam and processed in an external reformer to produce a hydrogen- and carbon-monoxide-rich syngas, which is supplied to the SOFC anode. The electrochemical reactions within the SOFC generate electrical power, while high-temperature exhaust streams are produced at both the anode and cathode outlets [93]. The anode off-gas, containing unreacted fuel species, is directed to a downstream combustor, where the remaining chemical energy is released to increase the turbine inlet temperature. The hot exhaust gases then expand through the turbine to generate additional mechanical and electrical power. Finally, the turbine exhaust is routed through heat exchangers to recover thermal energy for preheating the incoming air and water streams. This schematic is intentionally simple and focuses on the fundamental coupling mechanisms between the SOFC and the gas turbine. As such, it is particularly well suited for introducing the system architecture and establishing a clear baseline understanding of component roles and flow interactions [93].

5.2.2 Application-Oriented SOFC–GT APU Layout Proposed by Eelman et al.

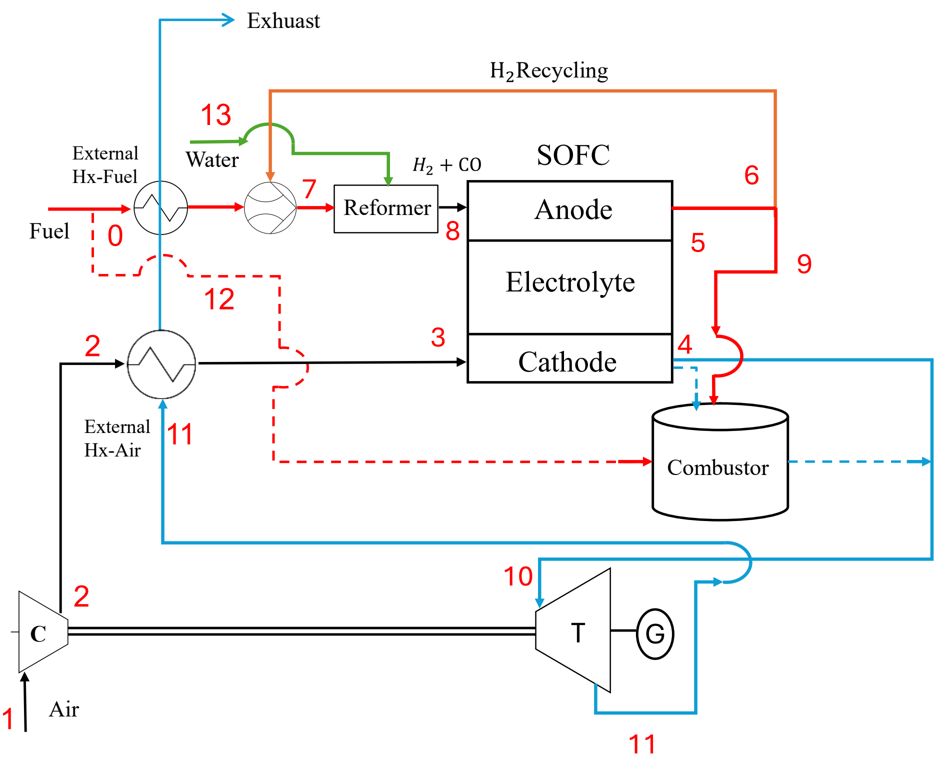

Figure 5-2 SOFC-GT APU system design as presented by Eelman et al [95].

After establishing the conceptual architecture using the NASA schematic, the system description is extended using the SOFC–GT APU layout proposed by Eelman *et al.* As shown in the Figure 5-2, This schematic represents a more application-oriented configuration and reflects additional design considerations relevant to aerospace auxiliary power units. While the overall structure remains consistent with the NASA architecture, several important features are added. These include anode exhaust gas recycling, enhanced water management strategies, and a more detailed arrangement of heat exchangers [95].In the Eelman et al. reference layout, the anode exhaust recirculation is driven by a jet pump/ejector located upstream of the reformer. In the present thermodynamic model, this device is not modelled as an independent component; In practice, the recycle stream is imposed according to the reference recycle fraction. Therefore, pressure losses, entrainment behaviour, and ejector performance are neglected. This assumption preserves consistency with the system-level verification objective of this work, while acknowledging that a detailed ejector design would be required for a final engineering implementation.

In particular, approximately 70% of the anode off-gas is recycled back to the reformer, allowing the system to retain water and residual fuel species within the fuel processing loop. This significantly reduces or eliminates the need for external water supply after startup. This layout provides valuable insight into how the baseline SOFC–GT architecture can be adapted to meet practical operational requirements. In this study, the Eelman configuration is used to illustrate the impact of added system complexity on mass and energy flow paths, while maintaining consistency with the underlying physical principles introduced through the NASA schematic [95].

5.2.3 Process-Level System Representation Using the ProMax Flowsheet

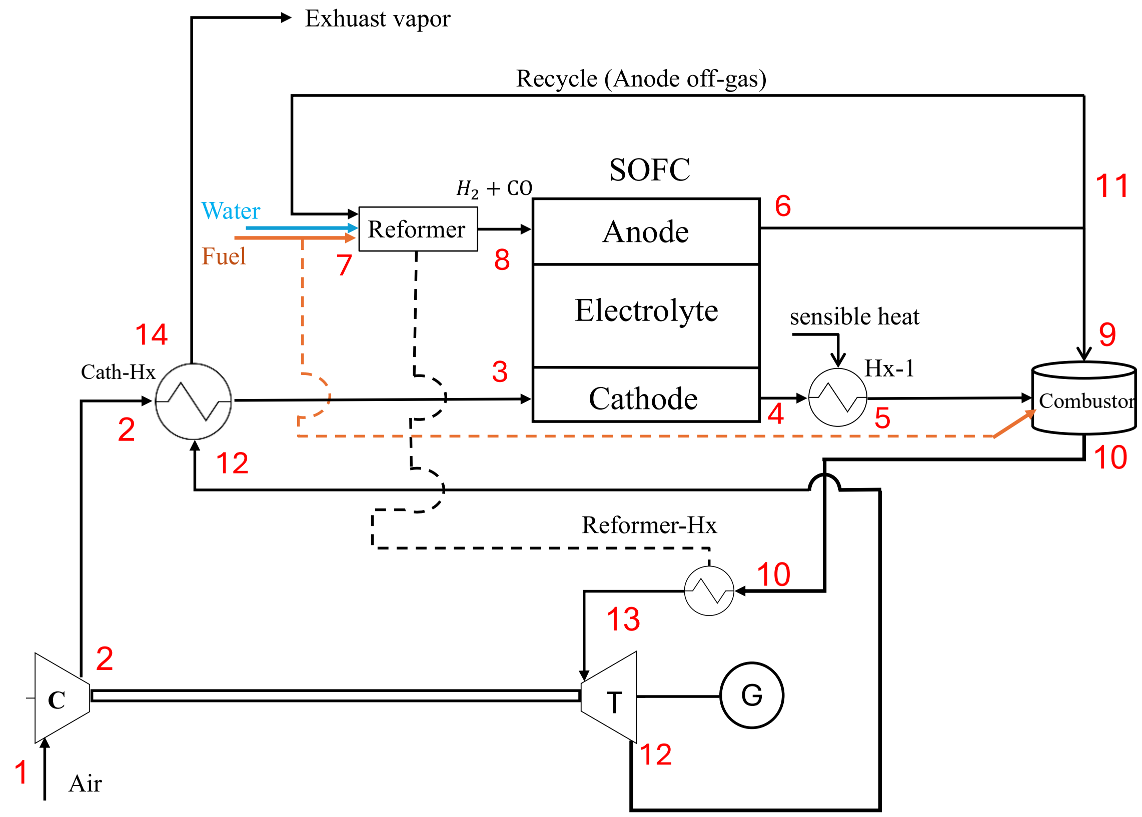

Figure 5-3 SOFC-GT system flowsheet in ProMax [95].

The third diagram employed in this study is the process flowsheet implemented in the ProMax simulation environment, as shown in the Figure 5-3 Unlike the previous two schematic , this representation does not merely reorganize the same architecture but instead introduces a higher level of process-level refinement through the explicit addition of several functional unit operations. In the ProMax model, the baseline SOFC–GT architecture is augmented with dedicated process blocks that enable detailed modelling of anode off-gas recycling, water recovery, steam management, and fuel preparation. These additions allow the physical behaviour of the system particularly within the fuel processing loop to be represented more realistically [95].

In the ProMax representation, the anode off-gas recirculation is implemented using a numerical recycle block with a prescribed recycle fraction, rather than by modelling a separate blower or ejector. Therefore, the recycle device is considered implicitly, and its pressure losses and auxiliary power consumption are neglected. This simplification is consistent with the available reference data, where the recycle fraction is specified but no separate operating parameters for a blower, ejector, or jet pump are reported.

5.2.3.1 Newly Introduced Components Relative to the Baseline Architectures

Compared to the NASA schematic and the simplified SOFC–GT APU layout, the ProMax implementation introduces the following key components [95]:

1. **Recycle Split and Recycle Mixer Blocks**
   These units enable controlled recycling of the anode off-gas back to the reformer inlet. The recycled stream contains steam and carbon dioxide, both of which play an important role in stabilizing reforming reactions and reducing external resource requirements.
2. **Steam Line and Mixer at the Reformer Inlet**
   Steam supplied to the reformer is no longer provided by an external water feed. Instead, steam originating from two internal sources recycled anode gas and condensed water is mixed and fed to the reformer. As a result, the freshwater inlet required in earlier configurations is eliminated.
3. **Fuel Spray (Atomization) Unit**
   In contrast to earlier models where liquid fuel enters the reformer directly, the ProMax model introduces a fuel spray block in which the fuel is pumped and injected as a fine mist**.** This modification has a direct impact on the reformer energy balance.

5.2.3.2 Implications for Reformer Inlet Conditions and Energy Balance

With these additions, the reformer inlet now includes water from two primary sources [95]:

1. Steam contained in the recycled anode off-gas (steam and CO_2).
2. Water recovered via condensation of the exhaust stream.

Furthermore, the introduction of fuel atomization fundamentally alters the thermal treatment of the fuel. The heat required for fuel vaporization and preheating is supplied internally within the reformer. Consequently [95]:

- External heat losses are minimized and may be reasonably neglected (assuming $Q_{\text{loss}} \approx 0$).
- The reformer energy balance explicitly accounts for the enthalpy of the atomized fuel entering the system.
- Heat transfer within the reformer becomes an intrinsic part of the fuel preparation process.

5.2.3.3 Role of the ProMax Flowsheet in the Present Study

Although all calculations in this thesis are carried out independently using a spreadsheet-based framework Excel, the ProMax flowsheet presented by Eelman *et al.* plays a critical role as a reference for verification under realistic aerospace operating conditions. In particular, this flowsheet corresponds to a 1-MW hybrid SOFC–GT system operating at a cruise altitude of 36,000 ft (10,973 m)**,** where variations in ambient pressure and temperature significantly influence system behaviour. The ProMax-based representation explicitly captures the impact of reduced ambient pressure, altered compressor operating conditions, and changes in mass flow rates associated with high-altitude operation. As such, it provides a physically consistent benchmark for assessing whether the independently developed model reproduces the correct system response to these environmental constraints [95].

Within the scope of this thesis, the ProMax flowsheet is therefore used to [95]:

- examine the effect of cruise-altitude pressure and temperature on the coupled SOFC–GT system;
- support verification of performance trends at the 1-MW power level;
- and verify that the modelled interactions between air compression, fuel processing, water management, and turbine expansion remain physically consistent under flight-relevant conditions.

By incorporating insights from this high-altitude, high-power operating scenario without directly relying on the ProMax software the present study ensures that the developed model is not only internally consistent, but also representative of realistic aerospace operating environments. This approach allows the model to maintain computational transparency while remaining anchored to an industry-grade process representation validated for flight conditions [95].

5.3 Definition of Main Flow Paths and State Points

In order to ensure clarity and consistency in the definition of flow paths and state points, it is necessary to explicitly identify a reference diagram for this section. Although multiple system schematics are introduced in this study, a single diagram must serve as the primary basis for flow identification and state point labelling. In this thesis, the NASA SOFC–GT system schematic is selected as the reference diagram for the initial definition of the main flow paths and state points. This choice is motivated by the fact that the NASA schematic provides a clear, uncluttered, and physically intuitive representation of the SOFC–GT architecture. The diagram emphasizes the fundamental mass and energy interactions between the fuel cell, gas turbine, reformer, and heat exchangers, without introducing secondary process-level details. By starting from the NASA schematic, the main air, fuel, and exhaust paths can be defined in a systematic and transparent manner. This establishes a consistent baseline framework for identifying state points and assigning thermodynamic properties such as pressure, temperature, mass flow rate, and gas composition. The more detailed schematics presented by Eelman et al., as well as the ProMax process flowsheet, are subsequently used to refine and extend this baseline definition. In particular, these diagrams are employed to account for additional features such as anode gas recycling, water recovery, and altitude-dependent operating conditions. However, to avoid ambiguity and excessive complexity at this stage, the formal definition of flow paths and state points in Section 5-3 is anchored to the NASA schematic. This approach ensures that the system description progresses from a conceptually clear architecture to more detailed and application-oriented representations, while maintaining consistency in flow identification and state point notation throughout the modelling process [93].

5.3.1 Definition of Main Flow Paths

Based on the reference system schematic introduced in the previous section, the hybrid SOFC–GT system can be described in terms of several distinct flow paths. Each flow path represents a physically meaningful stream of mass and energy and plays a specific role in the overall system operation. Defining these flow paths explicitly is a necessary step prior to the formulation of mass and energy balance equations and the assignment of state points. For clarity, the main flow paths considered in this study are grouped into five categories: the air path, the fuel and reformate path, the anode recycle loop, the cathode exhaust path, and the water and steam loop [93].

5.3.1.1 Air Path

The air path begins at the system inlet, where ambient air is drawn into the compressor. The air is compressed to the required pressure level and subsequently preheated through heat exchange with high-temperature exhaust gases. This preheating process improves the overall thermal efficiency of the hybrid cycle by recovering energy that would otherwise be lost with the exhaust stream. After preheating, the air is supplied to the cathode side of the solid oxide fuel cell. Within the SOFC, oxygen from the air participates in electrochemical reactions, contributing to electrical power generation. The cathode air stream therefore acts as the oxidant supply for the electrochemical reactions occurring within the fuel cell. The remaining cathode exhaust exits the fuel cell at elevated temperature and flows downstream toward the exhaust and heat recovery components [93]. The high temperature of the cathode exhaust makes it a valuable source of recoverable thermal energy within the hybrid system. The air flow path of the hybrid SOFC–GT system is schematically illustrated in Figure 5-4.

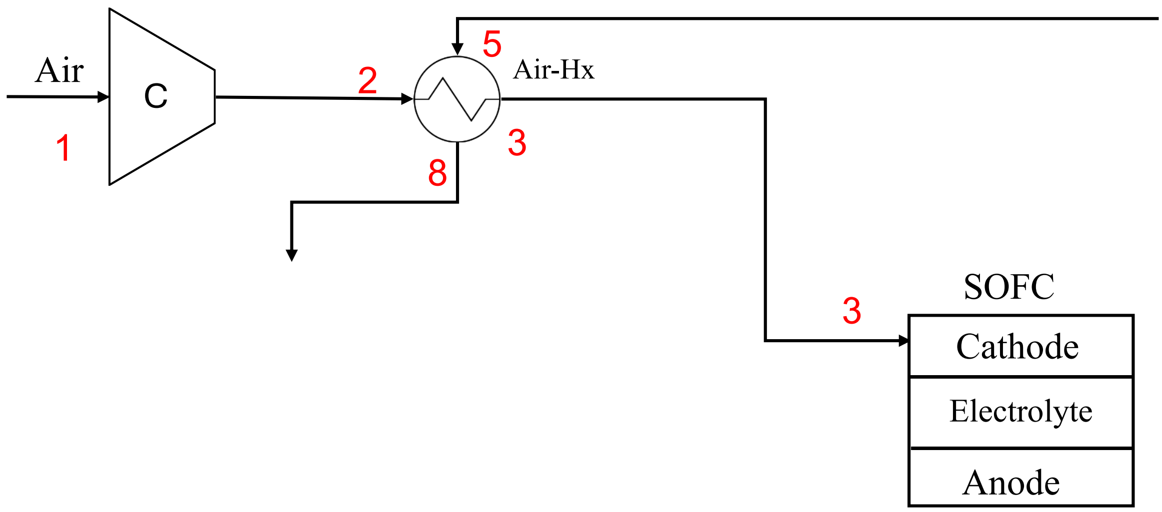

Figure 5-4 The Air Path of SOFC/GT Hybrid System [99].

5.3.1.2 Fuel and Reformate Path

The fuel and reformate path starts with the introduction of liquid fuel into the fuel processing section of the system. The fuel is mixed with steam and routed to an external reformer, where hydrocarbon reforming reactions produce a hydrogen- and carbon-monoxide-rich reformate gas. Hydrogen and carbon monoxide constitute the primary electrochemically active fuel species utilized by the SOFC anode. The addition of steam is essential for promoting reforming reactions and preventing carbon deposition within the fuel processing section. This reformate stream is then delivered to the anode side of the SOFC. Inside the fuel cell, hydrogen and carbon monoxide are electrochemically oxidized, generating electrical power and releasing thermal energy [93]. The fuel and reformate flow path is schematically illustrated in Figure 5-5. The reformer therefore serves as the critical interface between the hydrocarbon fuel supply and the electrochemical conversion process occurring within the SOFC.

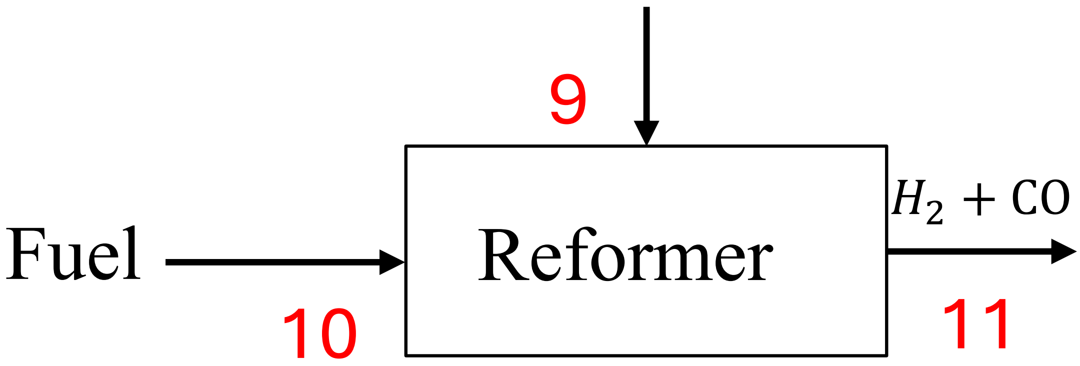

Figure 5-5 The Fuel and Reformate Path of SOFC-GT Hybrid System [99].

5.3.1.3 SOFC and Coupling of Anode and Cathode Exhausts to the Combustor

The solid oxide fuel cell constitutes the core electrochemical component of the system, where chemical energy is directly converted into electrical power. The SOFC operates with two separate flow paths: the cathode side, supplied with preheated compressed air, and the anode side, supplied with reformate gas rich in hydrogen and carbon monoxide. At the SOFC outlet, the exhaust streams from the anode and cathode sides are treated distinctly but are thermally and energetically coupled downstream [93]. The anode exhaust, which contains unreacted fuel species, is directed toward the combustor, where the remaining chemical energy is released through complete oxidation.

The cathode exhaust, consisting primarily of oxygen-depleted air at elevated temperature, provides a high-enthalpy stream that supports stable combustion and contributes to achieving the desired turbine inlet temperature. The combustor therefore acts as a critical junction where the two SOFC exhaust streams are effectively combined and utilized [93]. This configuration enables recovery of both residual chemical energy and sensible thermal energy, thereby increasing the overall efficiency of the hybrid SOFC–GT cycle, ensuring that the SOFC and gas turbine operate as a tightly integrated hybrid system rather than as isolated components [93]. The coupling between the SOFC anode and cathode exhaust streams and the downstream combustor is illustrated schematically in Figure 5-6.

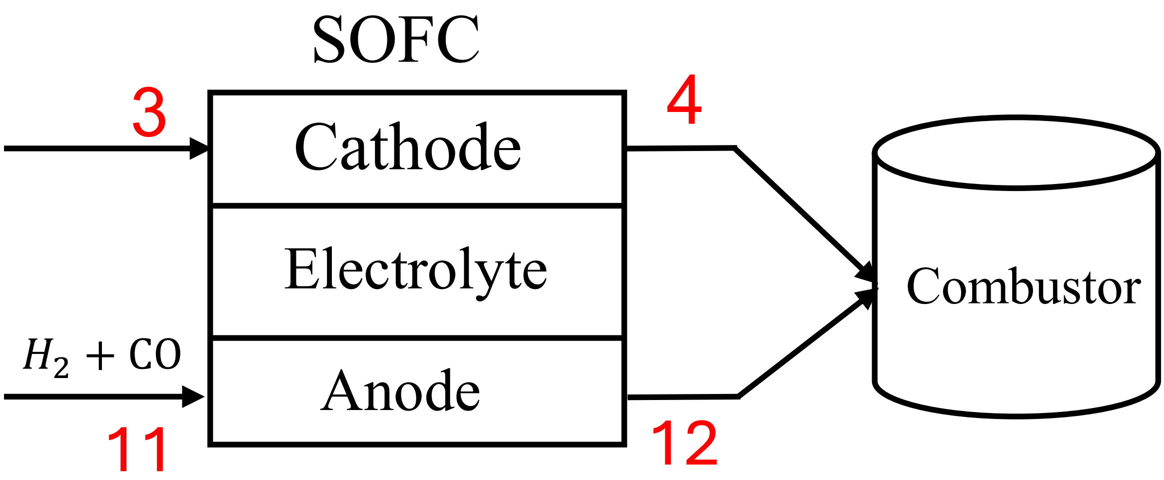

Figure 5-6 Solid Oxide Fuel Cell Model [99].

5.3.1.4 Heat Exchanger Network for Air and Water Preheating

Downstream of the combustor, the high-temperature exhaust gas forms the primary heat source for the system thermal management. Before entering the turbine, the hot gas transfers a portion of its thermal energy to the incoming air and water streams through a series of heat exchangers [93]. In the air heat exchanger, thermal energy from the combustor exhaust is used to preheat the compressed air supplied to the SOFC cathode. This preheating step is essential for maintaining the high operating temperature required by the SOFC and for reducing the overall thermal load on the fuel cell stack. In parallel, a water heat exchanger recovers heat from the same exhaust stream to raise the temperature of the incoming water prior to fuel processing [93].

This recovered thermal energy supports steam generation and improved the overall thermal efficiency of the system. The heat exchanger network therefore plays a central role in reducing external thermal requirements and enhancing overall cycle energy utilization. After passing through the heat exchanger network, the exhaust gas now at a reduced temperature enters the turbine, where it expands to produce mechanical power. By integrating the air and water heat exchangers upstream of the turbine, the system maximizes energy recovery from the combustor exhaust while ensuring appropriate inlet conditions for both the SOFC and the gas turbine [93].

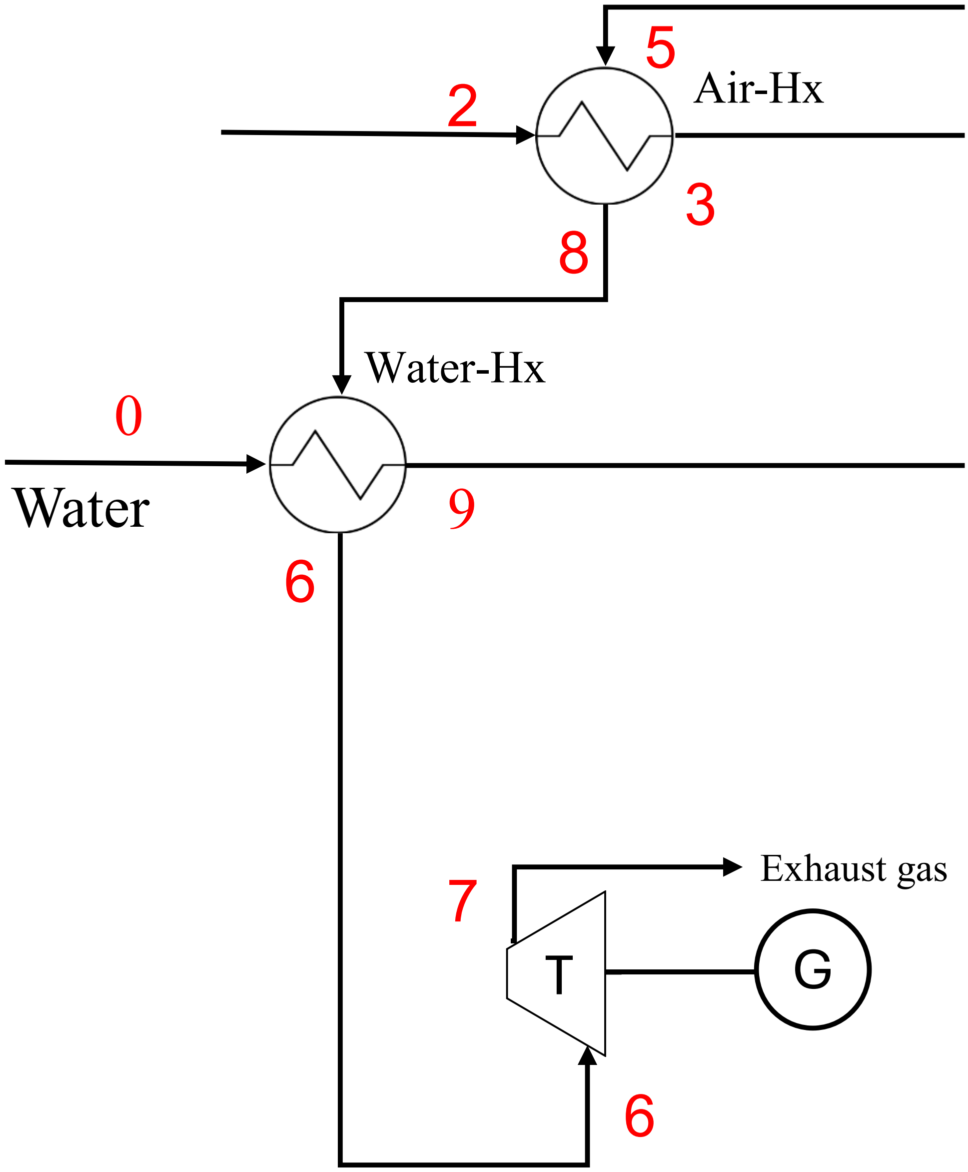

Figure 5-7 Heat Exchanger Network for Air and Water Preheating [99].

As shown in Figure 5-7, the heat exchanger network recovers thermal energy from the turbine exhaust to preheat both the cathode air stream and the steam supplied to the reformer. This arrangement represents a waste heat recovery strategy that contributes significantly to the high efficiency of hybrid SOFC–GT systems. The sequential use of exhaust heat for both air and water preheating increases the overall effectiveness of thermal integration within the hybrid cycle.

5.3.2 Definition of State Points and Thermodynamic Variables

In order to formulate the governing mass and energy balance equations of the hybrid SOFC–GT system, a consistent definition of state points is required. State points represent discrete locations along the main flow paths at which thermodynamic properties are evaluated and tracked throughout the system. In this study, the definition and numbering of state points are based on the NASA SOFC–GT system schematic, which serves as the reference architecture for flow identification. This choice ensures clarity and consistency in the system description and provides a physically intuitive framework for assigning thermodynamic variables [93].

The state points are defined sequentially along the direction of flow, from system inlets to outlets and from upstream components to downstream components. Each state point corresponds to a unique thermodynamic state characterized by a set of primary variables. For all flow streams, pressure, temperature, mass flow rate, and the corresponding thermodynamic properties required for energy balance calculations are defined [93].

Liquid streams, such as fuel and water, are characterized by their thermodynamic state, while gaseous streams are additionally defined by their species composition. On the air side, state points are defined at the compressor inlet, compressor outlet, cathode inlet, and cathode outlet, allowing the effects of compression, heat exchange, and electrochemical consumption of oxygen to be quantified. On the fuel side, state points are introduced at the reformer inlet, anode inlet, and anode outlet, enabling the evaluation of fuel processing, reforming reactions, and electrochemical fuel utilization within the SOFC. Downstream of the fuel cell, additional state points are defined at the combustor inlet and outlet to capture the coupling between the SOFC exhaust streams and the gas turbine cycle.

These state points are critical for determining the turbine inlet conditions and for assessing the efficiency of thermal and chemical energy recovery. Finally, state points are assigned at the turbine outlet and system exhaust to complete the thermodynamic description of the cycle. By defining the state points in this structured manner, all major thermodynamic states of the hybrid system are uniquely identified. This provides a clear and consistent basis for the formulation of component-level models and ensures that the subsequent analysis of system performance remains traceable and reproducible [93]. Table 5.1 summarizes the definition of all state points and associated thermodynamic variables used in the hybrid SOFC–GT system.

Table 5-1 Definition of State Points and Associated Thermodynamic Variables for NASA's NPSS SOFC/GT hybrid system architecture [99].

State Point	Description	Pressure (p)	Temperature (T)	Mass Flow Rate ($\dot{m}$)	Composition
1	Ambient air at compressor inlet	p_1	T_1	$\dot{m}_{Air}$	Air (O_2, N_2)
2	Compressed air at compressor outlet	p_2	T_2	$\dot{m}_{Air}$	Air (O_2, N_2)
3	Preheated air at SOFC cathode inlet	p_3	T_3	$\dot{m}_{Air}$	Air (O_2, N_2)
4	Cathode exhaust at SOFC outlet	p_4	T_4	$\dot{m}_{cath}$	O_2, N_2, H_2O
5	Combustor outlet	p_5	T_5	$\dot{m}_{gas}$	CO_2, N_2, H_2O, O_2
6	Turbine inlet	p_6	T_6	$\dot{m}_{gas}$	CO_2, N_2, H_2O, O_2
7	Turbine outlet	p_7	T_7	$\dot{m}_{gas}$	CO_2, N_2, H_2O, O_2
8	Air-Hx outlet	p_8	T_8	$\dot{m}_{gas}$	CO_2, N_2, H_2O, O_2
9	Preheated water/steam entering reformer	p_9	T_9	$\dot{m}_{H_2O}$	H_2O
10	Fuel at reformer inlet	p_{10}	T_{10}	$\dot{m}_{Fuel}$	Fuel
11	Reformate gas at SOFC anode inlet	p_{11}	T_{11}	$\dot{m}_{an}$	H_2, CO
12	Anode exhaust at SOFC outlet	p_{12}	T_{12}	$\dot{m}_{an}$	CO_2, H_2O H_2, CO

5.4 Modelling Assumptions and Simplifications

To develop a system-level model of the hybrid SOFC–GT configuration that is both physically meaningful and computationally manageable, several modelling assumptions are introduced. These assumptions are intended to simplify the analysis while retaining the dominant mechanisms that govern the overall performance of the system. The adopted assumptions are aligned with those commonly used in the literature and are consistent with the reference studies employed throughout this work. The analysis is conducted under steady-state operating conditions, with the focus placed on nominal design-point and cruise operation. Transient phenomena such as startup, shutdown, and dynamic load variations are not considered. This approach is appropriate for evaluating the baseline performance of the hybrid system, where steady operation represents the dominant mode during typical mission profiles. All gaseous streams within the system, including air, reformate gas, and exhaust products, are modelled as ideal gas mixtures. Thermodynamic properties are evaluated as functions of temperature, pressure, and chemical composition. Given the elevated operating temperatures and moderate pressure levels characteristic of SOFC–GT systems, the ideal gas assumption provides a reasonable balance between accuracy and simplicity [93].

Thermal interactions between system components and the surrounding environment are neglected. Accordingly, the solid oxide fuel cell stack, reformer, combustor, compressor, turbine, and heat exchangers are treated as adiabatic control volumes. This assumption is widely adopted in system-level studies and allows the energy balance of each component to be expressed in a consistent and transparent manner without introducing additional uncertainty associated with heat losses. Pressure losses in piping and manifolds are neglected. However, representative pressure drops across the cathode channel and heat exchangers are incorporated based on values reported in the reference study. Unless otherwise specified, the pressure at the outlet of each component is assumed to be equal to the pressure at the inlet of the subsequent component after accounting for the prescribed component pressure losses [93].

Neglecting pressure losses in piping and manifolds reduces the number of unknown variables in the model and is considered acceptable for a first-order assessment of system performance. Changes in kinetic and potential energy are neglected throughout the system, as they are small relative to the thermal and chemical energy terms governing SOFC–GT performance. Fuel processing within the reformer is assumed to proceed to chemical equilibrium at the outlet conditions [93]. Detailed reaction kinetics and finite-rate effects are not considered. This assumption is consistent with the high operating temperatures typically encountered in reforming processes and is commonly employed in system-level analyses of SOFC-based hybrid systems. The electrochemical behaviour of the solid oxide fuel cell is represented using a lumped, system-level model. The fuel cell stack is assumed to operate at a uniform temperature and current density, and spatial variations along the cell geometry are neglected. Electrochemical losses are incorporated through aggregate loss terms, enabling the SOFC to be modelled as a single control volume while capturing the essential performance characteristics [93].

The anode recycle loop is modelled as an ideal recirculation path with a prescribed recycle fraction. The jet pump/ejector required to sustain this recirculation is included conceptually in the system architecture but is not modelled as a separate component. Therefore, its pressure loss and auxiliary power consumption are neglected in the present energy balance.

The anode exhaust stream entering the combustor is assumed to undergo complete oxidation. All remaining combustible species are fully consumed, and chemical equilibrium within the combustor is not explicitly enforced. Under this assumption, the turbine inlet temperature is determined directly from the energy balance of the combustor, providing a clear linkage between the SOFC exhaust conditions and the gas turbine cycle. Ambient pressure and temperature are prescribed according to the operating scenario under consideration, including cruise-altitude conditions where applicable. Environmental conditions are treated as fixed inputs to the model rather than dynamic variables, allowing their influence on system performance to be evaluated in a controlled and systematic manner [93]. By clearly stating these assumptions, the scope and limitations of the developed model are explicitly defined. This provides a coherent foundation for the governing equations presented in the following section and ensures that the resulting performance predictions can be interpreted with clarity and confidence [93].

5.5 Governing Equations of System Components

In this section, the governing equations of the main components of the hybrid SOFC–GT system are presented. The equations are formulated based on mass and energy conservation principles and are structured to follow the physical flow of the system. The modelling procedure begins with the fuel processing unit and the reformer, as this component defines the composition and molar flow rates of the reformate supplied to the SOFC anode. Subsequent subsections address the solid oxide fuel cell, the combustor, heat exchangers, and turbomachinery components. This structured approach ensures that the interdependence between system components is clearly established and that the resulting model remains physically consistent and traceable [93].

5.5.1 Fuel Processing and Reformer Mass Balance

Prior to the electrochemical modelling of the solid oxide fuel cell, a detailed stoichiometric analysis is performed to determine the composition of the reformate gas supplied to the SOFC anode. Since the hybrid system operates on a hydrocarbon-based fuel, the hydrogen required for electrochemical conversion is generated upstream through an external reforming process coupled with water–gas shift reactions. Consequently, an accurate representation of the fuel processing stage is essential for maintaining physical consistency throughout the system-level model [93]. The reformer therefore serves as the upstream boundary condition for the SOFC model, linking fuel chemistry to electrochemical performance. The control volume of the fuel processing subsystem and the corresponding inlet and outlet state points considered in the reformer mass balance are illustrated in Figure 5-8.

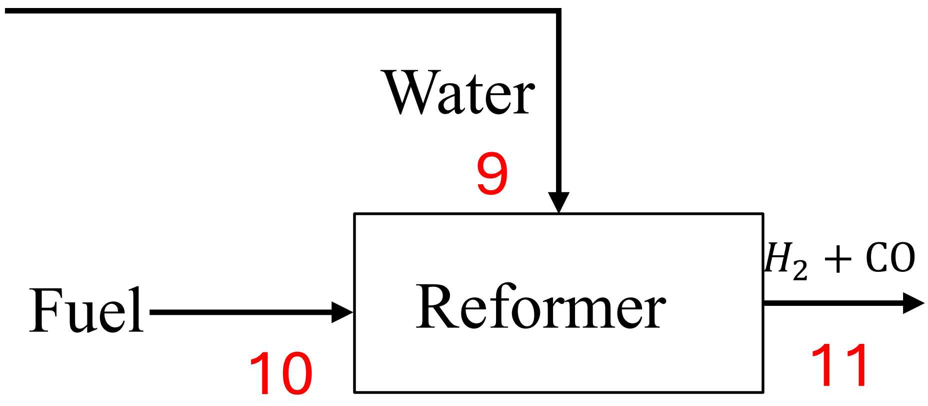

Figure 5-8 Mass balance of the SOFC fuel processing subsystem [99].

In the present study, the formulation of the governing equations begins with the fuel processing unit and the reformer, as this subsystem establishes the molar flow rates and chemical composition of the species entering the SOFC anode. The reformer is modelled as a steady-state control volume, and its formulation is aligned with the boundary conditions reported in the NASA hybrid SOFC–GT reference framework, ensuring consistency with the validated system architecture [99]. The fuel is represented by a Jet-A surrogate with the chemical formula $\mathrm{C_{12}H_{23}}$, consistent with the reference studies. Steam is supplied to the reformer according to a specified steam-to-carbon ratio $\left(\frac{S}{C}\right)$, while the oxygen-to-carbon ratio $\left(\frac{O}{C}\right)$ is set to zero. Therefore, partial oxidation and autothermal reforming pathways are not considered, since their inclusion would require additional oxygen boundary conditions not provided in the reference dataset [93]. The inlet mass flow rates of fuel and steam are first converted to molar flow rates using their respective molecular weights according to (Eq.5-1):

$$\dot{n}_i = \frac{\dot{m}_i}{M_i} \tag{5-1}$$

These molar flow rates serve as the inlet boundary conditions for the reformer control volume and form the basis for the subsequent stoichiometric calculations. Fuel conversion within the reformer is modelled using steam reforming as the primary reaction mechanism, followed by the water–gas shift (WGS) reaction [93]. The main steam reforming reaction for the Jet-A surrogate is defined as (Eq.5-2):

$$C_{12}H_{26} + 12\,H_2O \rightarrow 12\,CO + 25\,H_2 \tag{5-2}$$

This reaction defines the theoretical hydrogen production potential of the supplied hydrocarbon fuel and directly determines the electrochemical driving force available at the SOFC anode. Following the steam reforming step, the water–gas shift reaction is applied to account for the equilibrium-driven conversion of carbon monoxide (Eq.5-3):

$$\mathrm{CO} + \mathrm{H_2O} \rightleftharpoons \mathrm{CO_2} + \mathrm{H_2} \tag{5-3}$$

The stoichiometric coefficients in Eqs. (5.2) and (5.3) are applied to the inlet fuel molar flow rate to determine the molar production and consumption rates of hydrogen, carbon monoxide, carbon dioxide, and steam. Equation (5-2) and (5-3) represent the maximum theoretical hydrogen yield obtainable from the surrogate fuel under ideal steam-reforming conditions. The reforming process is modelled sequentially, with steam reforming applied first, followed by the WGS reaction to the extent permitted by the remaining steam. This approach reflects the equilibrium-driven behaviour of the reformate under high-temperature operating conditions and enables maximization of hydrogen production while preserving mass conservation [93]. The outlet molar flow rates of all reformer species are obtained by summing the individual species contributions. These molar flow rates are subsequently converted back into mass flow rates, and conservation of mass across the reformer control volume is verified by enforcing the overall mass balance (Eq.5-4):

$$\sum \dot{m}_{in} = \sum \dot{m}_{out} \tag{5-4}$$

The agreement between the total inlet and outlet mass flow rates confirms the physical consistency of the reformer model. The resulting reformate composition defines the inlet conditions for the SOFC anode and is used directly as input to the anode mass balance and electrochemical sub-model presented in the following section. By explicitly coupling the stoichiometric reforming calculations with the electrochemical model, the developed methodology ensures that the SOFC performance is evaluated based on a fuel composition derived from first-principles mass conservation rather than prescribed hydrogen fractions, thereby preserving the thermodynamic and chemical integrity of the hybrid SOFC–GT system [93].

5.5.2 SOFC Anode Mass Balance and Fuel Utilization

Following the determination of the reformate composition at the reformer outlet, the mass balance of the SOFC anode is formulated to quantify fuel consumption and the composition of the anode exhaust stream. The reformate entering the anode consists primarily of hydrogen and carbon monoxide, which are treated as the electrochemically active fuel species [93]. Figure 5-9 illustrates the SOFC control volume and the anode and cathode inlet and outlet state points considered in the mass balance formulation.

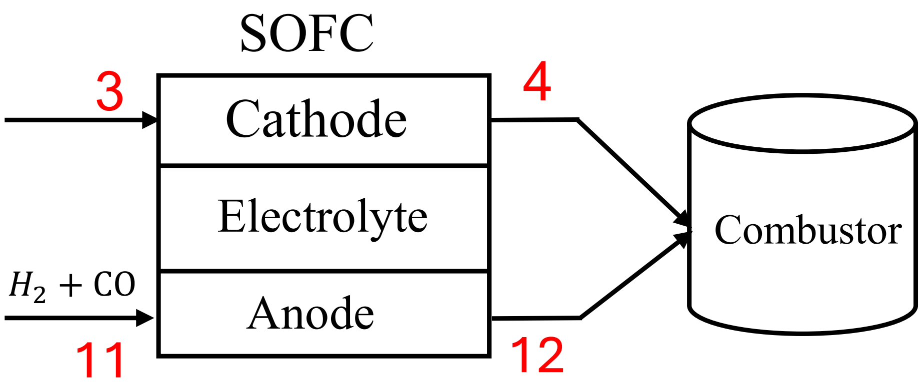

Figure 5-9 Schematic of the solid oxide fuel cell [99].

Fuel utilization is introduced as a global modelling parameter to represent the fraction of the inlet fuel that is electrochemically consumed within the anode [93]. The fuel utilization factor, U_f, is defined as the ratio of the molar flow rate of fuel species consumed in the anode to the total molar flow rate of electrochemically active species entering the anode, expressed as (Eq.5-5):

$$U_f = \frac{\dot{n}_{fuel,consumed}}{\dot{n}_{fuel,in}} \quad (5\text{-}5)$$

where the total inlet molar flow rate of fuel species is given by the sum of the hydrogen and carbon monoxide molar flow rates at the anode inlet (Eq.5-6),

$$\dot{n}_{fuel,in} = \dot{n}_{CO,in} + \dot{n}_{H_2,in} \quad (5\text{-}6)$$

Based on the specified fuel utilization factor, the total molar flow rate of fuel consumed within the anode can be expressed as (Eq.5-7):

$$\dot{n}_{fuel,\text{consumed}} = U_f \times \dot{n}_{fuel,in} \quad (5\text{-}7)$$

The consumption of hydrogen and carbon monoxide is assumed to occur proportionally to their respective molar fractions in the inlet reformate [93]. Accordingly, the individual molar consumption rates of hydrogen and carbon monoxide are calculated as (Eqs.5-8, 5-9):

$$\dot{n}_{consumed,H_2} = \dot{n}_{fuel,consumed} \times \frac{\dot{n}_{H_2,in}}{\dot{n}_{fuel,in}} \quad (5\text{-}8)$$

$$\dot{n}_{consumed\,,CO} = \dot{n}_{fuel,consumed} \times \frac{\dot{n}_{CO,in}}{\dot{n}_{fuel,in}} \quad (5\text{-}9)$$

The remaining unconsumed fractions of hydrogen and carbon monoxide constitute the fuel content of the anode exhaust stream. In addition to fuel consumption, water is produced at the anode as a result of the electrochemical oxidation of hydrogen. The molar production rate of water is directly linked to the molar consumption of hydrogen through the electrochemical reaction stoichiometry, such that (Eq.5-10):

$$\dot{n}_{\text{consumed,H}_2} = \dot{n}_{produced,H_2O} \quad (5\text{-}10)$$

The outlet molar flow rates of hydrogen, carbon monoxide, and water are obtained by subtracting the consumed fuel species and adding the produced water to the inlet species flow rates. These molar flow rates are subsequently converted to mass flow rates using the corresponding molecular weights. To ensure physical consistency, the conservation of mass across the anode control volume is verified by comparing the total mass flow rate at the anode inlet with that at the anode outlet. The resulting anode exhaust stream, containing unreacted fuel species and produced steam, is then directed to the combustor, thereby providing the thermal coupling between the electrochemical and thermodynamic subsystems of the hybrid SOFC–GT system. While the cathode is electrochemically involved in oxygen reduction within the SOFC stack, the thermodynamic treatment of the cathode air stream is addressed later as part of the air flow path and turbomachinery modelling [93].

5.5.3 SOFC Electrochemical Model

Following the formulation of the anode mass balance and fuel utilization, the electrochemical model of the solid oxide fuel cell is developed to relate the chemical energy of the fuel to electrical power generation. The electrochemical model establishes the connection between fuel consumption, charge transfer, and cell voltage, thereby providing the basis for predicting SOFC performance at the system level [93]. The operating cell voltage is evaluated by starting from the reversible thermodynamic (Nernst) potential and sequentially accounting for the dominant irreversible voltage losses that arise during operation. This formulation enables a transparent coupling between the mass balance of the fuel processing subsystem and the electrical performance of the SOFC, ensuring consistency between the chemical and electrochemical descriptions of the hybrid system [93].

5.5.3.1 Electrochemical Reactions

Within the SOFC, hydrogen is electrochemically oxidized at the anode, while oxygen is reduced at the cathode. The half-cell reactions are expressed as (Eqs.5-11 - 5-13):

- **Anode reaction:**

$$\mathrm{H_2 + O^{2-} \rightarrow H_2O + 2e^-} \tag{5-11}$$

- **Cathode reaction:**

$$\frac{1}{2}O_2 + 2e^- \rightarrow O^{2-} \tag{5-12}$$

- **The overall electrochemical reaction within the SOFC is therefore given by:**

$$\mathrm{H_2} + \frac{1}{2}\mathrm{O_2} \rightarrow \mathrm{H_2O} \tag{5-13}$$

These reactions define the stoichiometric relationship between hydrogen consumption, oxygen consumption, and electron transfer [93].

5.5.3.2 Relationship Between Fuel Consumption and Electric Current

The electrochemical oxidation of hydrogen releases two electrons per mole of hydrogen consumed [93]. Accordingly, the electric current generated by the SOFC stack is directly related to the molar consumption rate of hydrogen at the anode through Faraday's law (Eq.5-14):

$$I = 2F \times \dot{n}_{H_2,consumed} \tag{5-14}$$

where I is the stack current and F is Faraday's constant. This relation provides the direct coupling between the anode mass balance and the electrical output of the SOFC. The corresponding molar consumption rate of oxygen at the cathode is obtained from the overall reaction stoichiometry as (Eq.5-15):

$$\dot{n}_{O_2,consumed} = \frac{1}{2}\,\dot{n}_{H_2,consumed} \tag{5-15}$$

This formulation ensures closure of the electrochemical circuit and consistency between the anode and cathode processes [93].

5.5.3.3 Reversible (Nernst) Voltage

The maximum theoretical voltage of the SOFC is determined by the reversible electrochemical potential, commonly referred to as the Nernst voltage [93]. This voltage represents the upper thermodynamic limit of cell performance in the absence of any irreversible losses and is expressed as (Eq.5-16):

$$V_{rev} = \frac{\Delta G_f^{\circ}}{nF} + \frac{RT}{nF} l\,n\left(\frac{p_{H_2}\, p_{O_2}^{\frac{1}{2}}}{p_{H_2O}}\right) \tag{5-16}$$

In this equation , ΔG_f° represents the standard Gibbs free energy of formation, n is the number of electrons transferred per mole of fuel , F is Faraday's constant $(96{,}485\ \frac{C}{mol})$, R is the universal gas constant $(8.314\ \frac{J}{mol.K})$, T is the SOFC operating temperature (K), and $p_{\mathrm{H_2}}$, $p_{\mathrm{H_2O}}$, and $p_{\mathrm{O_2}}$ denote the partial pressures of hydrogen, steam, and oxygen respectively. This expression defines the thermodynamic limit of the cell voltage as a function of both temperature and reactant composition, with the partial pressures evaluated based on the mass balance results of the anode and cathode streams [93].

5.5.3.4 Voltage Loss Mechanisms

In practical SOFC operation, the actual cell voltage is reduced from its reversible value due to irreversible processes occurring within the cell. In the present system-level model, three dominant voltage losses are considered: activation, ohmic, and concentration losses [93].

I. Activation Loss

The activation overpotential accounts for the kinetic limitations of the electrochemical reactions at the electrode–electrolyte interfaces [93]. This loss is evaluated using a logarithmic expression derived from the Butler–Volmer equation (Eq.5-17):

$$V_{act} = \frac{RT}{n\alpha F} l\,n\left(\frac{i + i_n}{i_0}\right) \tag{5-17}$$

where i is the operating current density, i_0 is the exchange current density representing the intrinsic catalytic activity of the electrodes, i_n is a small leakage (parasitic) current density accounting for internal losses such as gas crossover, and α is the charge transfer coefficient [93]. The activation loss is most significant at low current densities and decreases as electrode kinetics improve [93].

II. Ohmic Loss

The ohmic voltage loss arises from resistance to ionic and electronic charge transport within the SOFC components, including the electrolyte, electrodes, and electrical contacts. This loss is modelled as a linear function of the total current density (Eq.5-18):

$$V_{ohm} = r\,(i + i_n) \tag{5-18}$$

where r denotes the area-specific resistance of the cell. This parameter implicitly captures the temperature-dependent conductivity of the electrolyte and electrode materials.

$$r = \sum_j r_j \tag{5-19}$$

The total area-specific resistance, r, is defined by (Eq.5-19) as the sum of the ionic and electronic resistances. Its temperature dependence is evaluated from the contributions of the anode, cathode, electrolyte, and interconnect using the empirical correlations reported in the NASA reference model [93] .

III. Concentration Loss

At high current densities, mass transport limitations can restrict the supply of reactants to the electrode surfaces, leading to concentration polarization. This effect is represented by the concentration overpotential (Eq.5-20):

$$V_{conc} = \frac{RT}{nF} ln\left(1 - \frac{i + i_n}{i_L}\right) \tag{5-20}$$

is the limiting current density corresponding to the maximum sustainable current before reactant depletion occurs at the electrode interface. Concentration losses become increasingly important as the operating current approaches this limiting value [93].

IV. Operating Cell Voltage

The operating voltage of the SOFC is obtained by subtracting all irreversible losses from the reversible voltage (Eq.5-21):

$$V_{op} = V_{rev} - V_{act} - V_{ohm} - V_{conc} \tag{5-21}$$

This stepwise formulation ensures that each physical loss mechanism is explicitly accounted for and allows the contribution of individual loss terms to be quantified and analysed [93].

5.5.3.5 Electrochemical Parameters

The electrochemical parameters required for evaluating the voltage losses are summarized in These values were selected in accordance with the NASA hybrid SOFC–GT reference model to ensure consistency and enable direct verification of the electrochemical performance (Tab.5-2) [93].

Table 5-2 Electrochemical parameters used in the SOFC model [99].

Parameter	Description	Value	Unit
$\boldsymbol{i}$	Operating current density	500	$\frac{mA}{cm^2}$
$\boldsymbol{i_l}$	Limiting current density	900	$\frac{mA}{cm^2}$
$\boldsymbol{i_n}$	Leakage current density	2	$\frac{mA}{cm^2}$
$\boldsymbol{i_0}$	Exchange current density	300	$\frac{mA}{cm^2}$
$\boldsymbol{\alpha}$	Charge transfer coefficient	1.68	$-$
$\boldsymbol{r}$	Area-specific resistance	0.5	$\Omega \cdot cm^2$

5.5.3.6 Electrical Power Output

The electrical power generated by the SOFC stack is obtained from the product of the stack voltage and the total current produced by the electrochemical reactions (Eq.5-22):

$$P_{\text{stack}} = \frac{V_{oper}\, i\, A_{cell}}{1000} \tag{5-22}$$

where A_{cell} represents the active area of an individual cell and N_{cell} the total number of cells within the stack. The corresponding fuel-to-electric efficiency (FTE) of the SOFC is defined as [93] (Eq.5-23):

$$\eta_{SOFC} = \frac{P_{stack}}{\dot{m}_{fuel}\, LHV_{fuel}} \tag{5-23}$$

in which $\dot{m}_{\text{fuel}}$ is the fuel mass flow rate and LHV_{fuel} the lower heating value of the fuel. This expression is introduced here to define the performance metric used later for system-level evaluation and comparison under different operating conditions. A detailed analysis of efficiency trends is presented in the results and verification sections.

5.5.3.7 Heat Generation within the SOFC Stack

In addition to electrical power production, the electrochemical reactions occurring within the SOFC stack also release thermal energy. The heat generated in the stack results from the difference between the chemical energy of the fuel consumed and the electrical energy extracted from the electrochemical process. The total heat generation rate within the SOFC stack can therefore be expressed as (Eq.5-24):

$$\dot{Q}_{gen} = \dot{\Delta H} - P_{SOFC} \tag{5-24}$$

where $\dot{Q}_{gen}$represents the rate of heat generated in the fuel cell stack (kW) , $\dot{\Delta H}$ is the rate of chemical energy release by the electrochemical reaction (kW), and $P_{SOFC}$is the electrical power output of the stack (kW). This heat is partly transferred to the surrounding system components and partly carried by the exhaust gases leaving the anode and cathode channels. The generated heat plays an important role in maintaining the high operating temperature of the SOFC and in providing thermal energy for downstream components such as the combustor and heat exchangers within the hybrid system.

5.5.3.8 Electrochemical Efficiency

The electrochemical efficiency of the SOFC represents the fraction of the theoretical reversible voltage that is effectively converted into electrical work during operation. Due to activation, ohmic, and concentration losses, the actual operating voltage of the fuel cell is lower than the reversible thermodynamic voltage. The electrochemical efficiency can therefore be defined as (Eq.5-25):

$$\eta_{electrical} = \frac{V_{opr}}{V_{rev}} \tag{5-25}$$

where V_{oper} is the operating cell voltage obtained after accounting for all irreversible losses, and V_{rev} is the reversible (Nernst) voltage. This efficiency provides an indication of how closely the real electrochemical performance approaches the theoretical thermodynamic limit of the fuel cell.

5.5.3.9 Fuel Utilization Factor

An important parameter governing SOFC performance is the fuel utilization factor, which quantifies the fraction of the fuel entering the anode that is electrochemically consumed within the stack. The fuel utilization factor is defined as (Eq.5-26):

$$U_f = \frac{\Delta_{(in-out)}(\dot{N}_{H_2} + \dot{N}_{CO})}{(\dot{N}_{H_2} + \dot{N}_{CO})_{in}} \tag{5-26}$$

where $\dot{N}_{H_2}$ and $\dot{N}_{CO}$, represent the molar flow rates of hydrogen and carbon monoxide, respectively. The numerator represents the net fuel consumption across the stack, while the denominator corresponds to the total fuel entering the anode channel. Fuel utilization is a critical operating parameter since excessively high values can lead to fuel starvation, while low values reduce overall system efficiency. Although the fuel utilization factor is specified as an input parameter in the present model, Eq.5-26 provides an equivalent mass-balance-based definition that can be used to verify consistency between the prescribed fuel utilization and the resulting anode inlet and outlet compositions.

5.5.4 Combustor Energy Balance

The combustor plays a key integrative role in the hybrid SOFC–GT system by thermally coupling the electrochemical subsystem with the gas turbine cycle. While the SOFC converts a large fraction of the fuel chemical energy directly into electricity, the remaining chemical energy contained in the anode off-gas, together with the sensible heat of the cathode exhaust, is recovered in the combustor and utilized to drive the gas turbine. In the present configuration, the combustor receives two primary inlet streams: (i) the anode exhaust gas exiting the SOFC, containing unreacted fuel species and steam, and (ii) the cathode exhaust air stream, which provides the oxidant required for combustion. The combustor outlet stream then supplies high-temperature combustion products to the turbine inlet. Figure 5-10 illustrates the combustor control volume and the associated inlet and outlet state points used for the energy balance formulation [93].

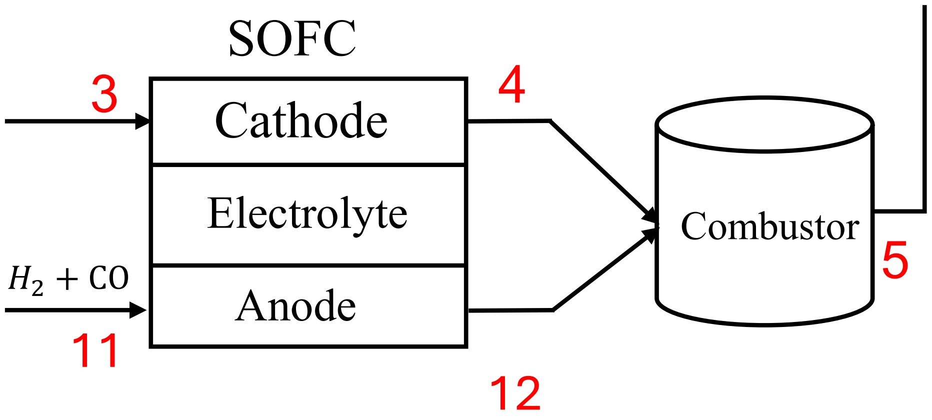

Figure 5-10 Combustor control volume and associated inlet and outlet state points [99].

5.5.4.1 Combustor Modelling Assumptions

Consistent with the system-level modelling approach adopted throughout this thesis, the combustor is modelled under steady-state conditions. Complete combustion of all remaining combustible species in the anode off-gas is assumed, and heat losses to the surroundings are neglected. Pressure losses across the combustor are assumed to be negligible unless otherwise stated. These assumptions are consistent with the reference hybrid SOFC–GT studies and allow the combustor behaviour to be represented through a simplified but physically meaningful energy balance. The anode and cathode exhaust streams are assumed to be perfectly mixed prior to combustion. This assumption allows the combustor inlet to be represented by a single, uniform thermodynamic state, thereby simplifying the energy balance formulation.

5.5.4.2 Combustor Energy Balance Formulation

The combustor is treated as a single control volume. Under steady-state and adiabatic conditions, the energy balance of the combustor can be written as (Eq.5-27):

$$\sum \dot{m}_{out} h_{out} = \sum \dot{m}_{in}\, h_{in} + \dot{Q}_{comb} \quad (5\text{-}27)$$

where $\dot{m}$ denotes mass flow rate, h is the specific enthalpy of the corresponding stream, and $\dot{Q}_{comb}$ represents the heat released by chemical combustion within the combustor.

The combustion heat release is obtained from the oxidation of the residual combustible species leaving the SOFC anode together with the injected fuel spray. Since the residual gaseous species are treated on a molar basis whereas the injected liquid fuel is treated on a mass basis, the total combustion heat release is expressed as (Eq.5-28):

$$\dot{Q}_{comb} = \sum_{i} \dot{n}_{i,res}\, LHV_i + \dot{m}_{spray}\, LHV_{spray} \tag{5-28}$$

where $\dot{n}_{i,\,res}$ denotes the molar flow rate of the residual combustible species (primarily H_2 and CO) leaving the SOFC anode, expressed in ${}^{mol}/_{s}$, and LHV_i is their lower heating value expressed in $(\frac{kJ}{mol})$. The injected fuel spray is represented by its mass flow rate, $\dot{m}_{spray}$ $\left(\frac{kg}{s}\right)$, while its lower heating value, LHV_{spray} is expressed in $\left(\frac{kJ}{kg}\right)$.Consequently, each contribution in Eq. (5-28) has units of kW, and their sum represents the total chemical heat released in the combustor.

5.5.4.3 Determination of Turbine Inlet Temperature

The primary output of the combustor model is the turbine inlet temperature (TIT), which is a critical parameter governing gas turbine performance. By rearranging the combustor energy balance, the outlet enthalpy of the combustion products is obtained and subsequently converted to temperature using appropriate thermodynamic property relations (Eq.5-29):

$$h_{comb\,,out} = \frac{\dot{Q}_{comb} + \sum \dot{m}_{in} h_{in}}{\dot{m}_{out}} \tag{5-29}$$

The resulting combustor outlet temperature defines the turbine inlet condition used in the subsequent gas turbine modelling. By converting the remaining chemical energy of the SOFC exhaust into sensible thermal energy, the combustor enables effective energy recovery within the hybrid system. This thermal coupling allows the gas turbine to operate at elevated inlet temperatures while maintaining high overall system efficiency. As such, the combustor serves as the key interface between the electrochemical and thermomechanical subsystems of the hybrid SOFC–GT architecture.

5.5.5 Heat Exchanger Modelling

The heat exchanger subsystem is introduced to enable thermal integration within the hybrid SOFC–GT system by recovering high-temperature exhaust energy and redistributing it to upstream components. Due to the high operating temperatures of both the SOFC stack and the downstream combustion process, a significant portion of the chemical energy of the fuel exits the system as thermal energy carried by the exhaust gases. In the present configuration, this energy is not rejected to the environment but is instead recovered through a network of heat exchangers to improve overall system efficiency and reduce external heating requirements. Two heat exchangers are considered in this study. This configuration maximizes waste-heat recovery and reduces the external thermal energy required by the fuel-processing subsystem. The first is an air–air heat exchanger that preheats the compressed air supplied to the SOFC cathode. The second is an air–water heat exchanger that utilizes exhaust heat to generate superheated steam required by the fuel processing and reforming subsystem. Although both components serve the purpose of heat recovery, their thermodynamic behaviour differs fundamentally due to the nature of the working fluids involved. Consequently, each heat exchanger is modelled using a formulation consistent with its physical operating conditions [93].

5.5.5.1 Air–Air Heat Exchanger (Recuperator)

The air–air heat exchanger operates as a recuperator, transferring thermal energy from the high-temperature exhaust gas downstream of the combustor to the compressed air stream entering the SOFC cathode. A schematic representation of the air–air heat exchanger, including the associated inlet and outlet state points, is shown in Figure 5-11.

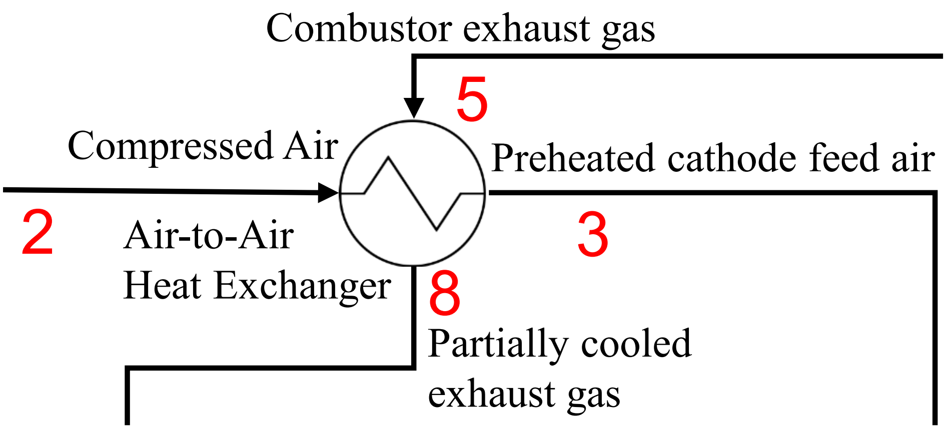

Figure 5-11 Schematic representation of the air–air heat exchanger with inlet and outlet state points [99].

Since both the hot exhaust gas and the compressed air remain in the gaseous phase throughout the heat exchange process, the air–air heat exchanger operates under single-phase conditions. Under steady-state operation and neglecting heat losses to the surroundings, the thermal performance of this component is described using an effectiveness-based formulation [93].

The effectiveness of the air–air heat exchanger is defined as the ratio of the actual heat transfer rate to the maximum thermodynamically possible heat transfer rate (Eq.5-30):

$$\varepsilon_{AA} = \frac{\dot{Q}_{AA}}{\dot{Q}_{AA,max}} \tag{5-30}$$

The actual heat transfer rate is obtained from the sensible enthalpy change of the hot or cold stream. On the hot side, this is expressed as (Eq.5-31):

$$\dot{Q}_{AA} = \dot{m}_h \times C_{p,h} \times \left(T_{h,in} - T_{h,out}\right) \tag{5-31}$$

where $\dot{m}_h$ is the mass flow rate of the hot exhaust gas, $C_{p,h}$ is its specific heat, and $T_{h,\mathrm{in}}$ and $T_{h,\mathrm{out}}$ are the inlet and outlet temperatures of the hot stream, respectively. An equivalent expression can be written for the cold air stream, ensuring consistency of the energy balance [93].

The maximum possible heat transfer rate is defined as (Eq5-32):

$$\dot{Q}_{AA,max} = C_{min} \times \left(T_{h,in} - T_{c,in}\right) \quad (5\text{-}32)$$

where the minimum heat capacity rate is given by (Eq.5-33):

$$C_{min} = min\left(\dot{m}_h C_{p,h}, \dot{m}_c c_{p,c}\right) \quad (5\text{-}33)$$

This formulation establishes a direct relationship between the combustor outlet temperature and the SOFC cathode inlet temperature, which is essential for maintaining appropriate thermal conditions within the fuel cell stack [93].

To accurately represent the thermophysical behaviour of the gas streams, the specific heat capacities are not assumed to be constant. Instead, the molar specific heat capacity of each gas species is evaluated as a function of temperature using the Shomate polynomial formulation (Eq.5-34):

$$C_{p,i}^{\circ}(T) = A_i + B_i t + C_i t^2 + D_i t^3 + \frac{E_i}{t^2} \;,\; t = \frac{T}{1000} \quad (5\text{-}34)$$

where the coefficients A_i–E_i are obtained from standard thermodynamic databases. The specific heat of the gas mixture is then calculated using a mole-fraction-weighted average (Eq.5-35):

$$c_{p,mix} = \sum_i y_i \; c_{p,i}(T) \quad (5\text{-}35)$$

The calculated preheated cathode-air temperature is used as the inlet boundary condition for the SOFC cathode and therefore affects both the stack thermal management and electrochemical performance. The corresponding numerical results will be presented and discussed in Chapter 6.

5.5.5.2 Air–Water Heat Exchanger (Steam Generator)

The second heat exchanger is an air–water heat exchanger employed to recover exhaust heat for steam generation upstream of the reformer. A schematic diagram of this component, illustrating the phase-change process experienced by the water stream, is shown in Figure 5-12 [93].

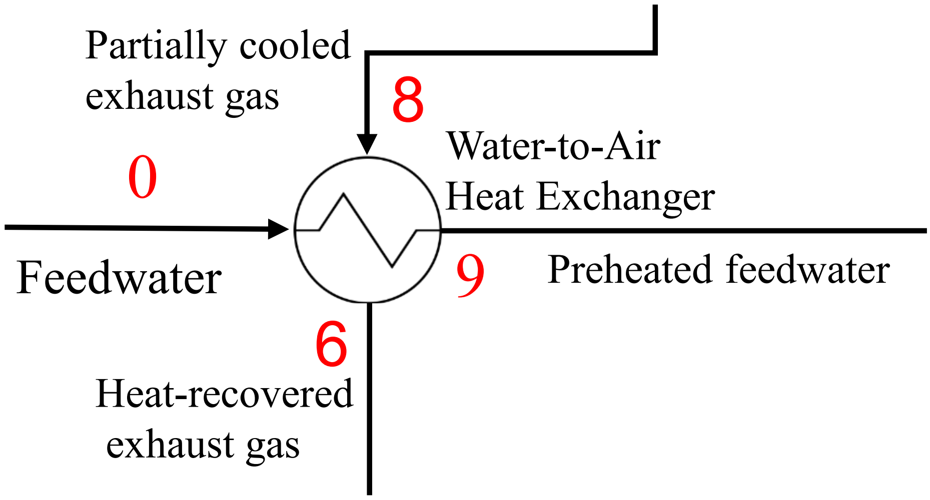

5-12 Schematic representation of the air–Water heat exchanger with inlet and outlet state points [93].

Unlike the air–air heat exchanger, the water stream in this component undergoes a phase change. Liquid water is first heated from its inlet temperature to the saturation temperature, then completely vaporized, and finally superheated to the desired outlet temperature. Due to the presence of phase change, the effectiveness-based formulation is not applicable. Instead, the air–water heat exchanger is modelled using an enthalpy-based energy balance [93]. It is important to distinguish between sensible heating and phase-change heating within the two heat exchangers.

While the air–air recuperator involves temperature variation of gaseous streams only, the air–water heater includes liquid heating, phase change, and potential superheating. Therefore, the energy balance for the water side must account separately for each thermodynamic stage to preserve physical consistency. This approach ensures accurate estimation of the steam enthalpy supplied to the reformer, which directly affects the steam-to-carbon ratio and reforming performance. Under steady-state conditions, the energy balance is written as (Eq.5-37):

$$\dot{m}_{air} \times c_{p,air} \times \left(T_{air,in} - T_{air,out}\right) = \dot{m}_{water} \times (h_{out} - h_{in}) \tag{5-36}$$

where the left-hand side represents the sensible heat released by the hot exhaust gas, and the right-hand side represents the total enthalpy increase of the water stream. For clarity, the enthalpy rise of the water stream is decomposed into three contributions as (Eq.5-38):

$$h_{out} - h_{in} = c_{p,l}(T_{sat} - T_{in}) + h_{fg} + c_{p,v}(T_{out} - T_{sat}) \tag{5-37}$$

The three terms correspond to sensible heating of liquid water, latent heat of vaporization, and sensible heating of superheated steam, respectively. Thermodynamic properties of water and steam are evaluated at the corresponding pressure levels, and the outlet steam temperature is determined iteratively to satisfy the overall energy balance. The resulting heat duty distribution and outlet conditions are employed as inputs to the integrated system model. Their numerical values will be presented and discussed in chapter 6. The adopted heat exchanger modelling approach is fully consistent with the formulations applied to other system components, including the SOFC stack, combustor, and gas turbine. By employing an effectiveness-based formulation for single-phase heat exchange and an enthalpy-based formulation for phase-change processes, thermodynamic consistency is preserved across the integrated SOFC–GT system. This approach ensures reliable prediction of SOFC inlet conditions, steam generation requirements, and turbine inlet temperature, thereby supporting accurate system-level performance analysis [93].

5.5.6 Gas Turbine Modelling and Performance Analysis

The gas turbine constitutes the final power conversion component of the hybrid SOFC–GT system and plays a critical role in recovering the remaining thermal energy of the high-temperature exhaust gases leaving the combustion chamber. After the completion of electrochemical reactions within the solid oxide fuel cell and the subsequent oxidation of unreacted fuel species in the combustor, the exhaust gas mixture still possesses substantial thermal and pressure potential. This energy is partially converted into mechanical power within the turbine, which is then transformed into electrical power by the coupled generator. The turbine is thermodynamically linked to the upstream components, particularly the combustor and the heat exchanger network, through the turbine inlet temperature (TIT), inlet pressure, and mass flow rate. Consequently, the turbine performance cannot be evaluated independently, and its modelling must remain fully consistent with the system-level mass and energy balances established in the preceding sections. Therefore, the gas turbine does not operate as an independent subsystem, but as a thermodynamically coupled component whose performance is directly influenced by SOFC fuel utilization, combustor energy release, and heat exchanger effectiveness. The turbine receives the hot exhaust gases from the combustor, as shown in Figure 5-13 [93].

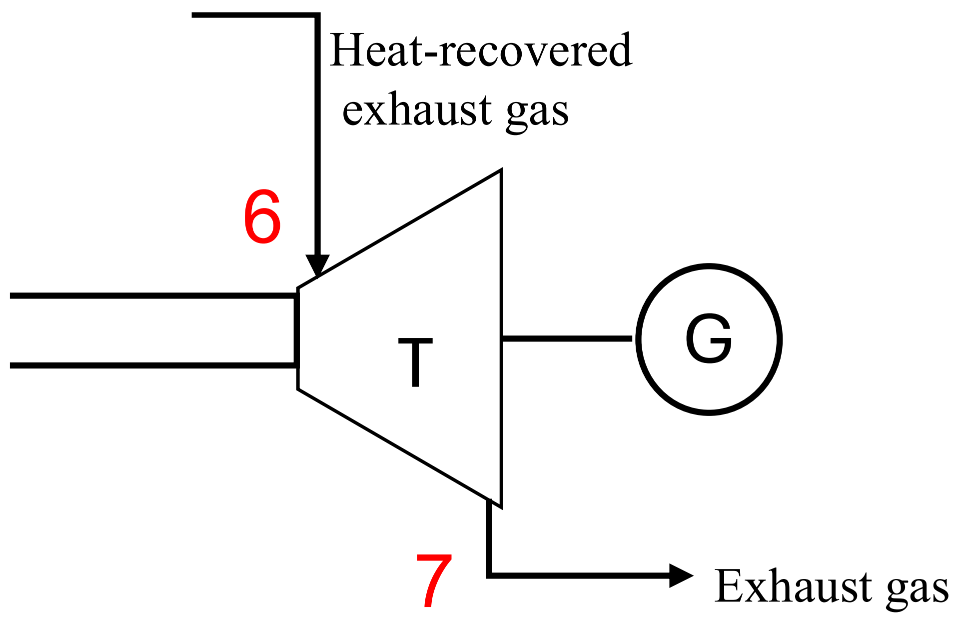

5-13 Schematic representation of the gas turbine and generator within the SOFC–GT hybrid system [93].

5.5.6.1 Modelling Assumptions and Governing Equations of the Gas Turbine

To establish a tractable yet physically consistent turbine model, the following assumptions are adopted: the turbine operates under steady-state conditions. Heat losses to the surroundings are neglected, and the expansion process is assumed to be adiabatic. Under these assumptions, the turbine work output is determined solely by the enthalpy drop of the working fluid across the turbine. The working fluid is treated as an ideal gas mixture with temperature-dependent thermophysical properties. The pressure drop in piping between the combustor outlet and turbine inlet is considered negligible.
A constant turbine isentropic efficiency is assumed based on typical values reported for small-scale gas turbines. This efficiency accounts for aerodynamic, mechanical, and internal flow losses occurring during the expansion process. These assumptions are consistent with those adopted for other system components and ensure coherence throughout the overall system model [93].
The thermodynamic modelling of the gas turbine is based on the conservation of energy applied to an adiabatic steady-flow control volume, combined with the definition of isentropic efficiency to account for irreversibilities during the expansion process. Since the turbine receives the high-temperature exhaust gases directly from the combustor, its inlet conditions are fully determined by the upstream components of the system [93].
The pressure ratio of the turbine is defined as the ratio between the turbine inlet pressure and outlet pressure (Eq.5-39):

$$\beta = \frac{p_{t,in}}{p_{t,out}} \tag{5-38}$$

This pressure ratio represents the driving force for the expansion process and is a key design and operating parameter of the turbine. In the present system, the turbine outlet pressure is assumed to be close to ambient pressure, while the inlet pressure is inherited from the combustor outlet. To evaluate the thermodynamic performance of the turbine, an ideal reference process is first considered [93].

The thermophysical properties of the gas mixture entering the turbine are evaluated based on the chemical composition of the combustion products. The mixture specific heat capacity is calculated using mole-fraction-weighted averaging as previously introduced in Eq. (5.32). From the evaluated mixture molecular weight, the specific gas constant is obtained as (Eq.5-40):

$$R_{mix} = \frac{R_u}{MW_{mix}} \tag{5-39}$$

where R_u is the universal gas constant and MW_{mix} is the molecular weight of the gas mixture. The ratio of specific heats is then evaluated as (Eq.5-41):

$$k = \frac{c_{p,mix}}{c_{p,mix} - R_{mix}} \tag{5-40}$$

The calculated value of $k$is subsequently used in the isentropic expansion relation to determine the ideal turbine outlet temperature. Under the assumption of an isentropic expansion, the outlet temperature corresponding to this ideal process can be calculated using the isentropic relation for an ideal gas mixture (Eq.5-42):

$$T_{t,out,is} = T_{t,in} \times \left(\frac{p_{t,out}}{p_{t,in}}\right)^{\frac{k-1}{k}} \tag{5-41}$$

where $T_{t,in}$ is the turbine inlet temperature, $T_{t,out,is}$ is the isentropic outlet temperature, and $k$is the ratio of specific heats of the gas mixture. The value of k is evaluated based on the composition and temperature of the combustion products entering the turbine. In real turbines, irreversibilities such as friction, flow separation, and shock losses lead to a higher outlet temperature than that predicted by the ideal isentropic expansion [93].

These effects are accounted for through the turbine isentropic efficiency, which is defined as the ratio of the actual enthalpy drop to the ideal isentropic enthalpy drop (Eq.5-43):

$$\eta_t = \frac{T_{t,in} - T_{t,out}}{T_{t,in} - T_{t,out,is}} \tag{5-42}$$

The isentropic efficiency accounts for aerodynamic losses, blade friction, and flow irreversibilities that arise during real expansion. By relating the actual temperature drop to the ideal isentropic temperature drop, the model preserves thermodynamic rigor while maintaining computational simplicity.

This definition provides a convenient way to relate the real turbine behavior to the ideal reference process. Rearranging Equation (5.43) , the actual turbine outlet temperature can be expressed as (Eq.5-44):

$$T_{t,out} = T_{t,in} - \eta_t \left(T_{t,in} - T_{t,out,is}\right) \tag{5-43}$$

Once the inlet and outlet temperatures of the turbine are determined, the mechanical power produced by the turbine can be calculated from the steady-flow energy balance. Neglecting kinetic and potential energy changes, and assuming adiabatic operation, the turbine power output is given by (Eq.5-45):

$$\dot{W}_t = \dot{m}_t \times c_{p,t} \times \left(T_{t,in} - T_{t,out}\right) \tag{5-44}$$

where $\dot{m}_t$ is the mass flow rate of the exhaust gas mixture and $c_{p,t}$ is the specific heat of the mixture evaluated at the mean turbine temperature. In this work, the value of $c_{p,t}$ is obtained using temperature-dependent correlations based on the actual gas composition, ensuring consistency with the combustor and heat exchanger models. The turbine outlet state (State 7) is therefore determined directly from the expansion process and represents the final thermodynamic state of the working fluid before discharge to the environment. The calculated turbine power represents the gross mechanical power available at the turbine shaft. This power is subsequently transmitted to the generator, where it is converted into electrical power after accounting for mechanical and electrical losses, as discussed in the following section [93].

Following the thermodynamic modelling of the gas turbine and the determination of its outlet conditions and mechanical power output, the final stage of the power conversion chain is the electrical generator. The generator is mechanically coupled to the turbine shaft and is responsible for converting the available mechanical power into usable electrical energy. $\dot{W}_t$ denotes the gross mechanical power produced by the turbine prior to compressor power consumption. The compressor is driven directly by the turbine, and only the remaining net shaft power after compressor consumption is available to the generator.

In the present system configuration, the generator does not affect the thermodynamic state of the working fluid; Therefore, the generator model is solved after completion of the thermodynamic cycle calculations and acts solely as an energy-conversion component. However, it plays a crucial role in determining the net electrical output of the SOFC–GT hybrid system. Therefore, the generator model is introduced as an energy conversion block that links the turbine shaft power to the electrical power delivered to the load. The modelling approach adopted for the generator is based on a steady-state energy balance, in which mechanical losses are implicitly accounted for through the generator efficiency. This formulation ensures consistency with the upstream turbine model and allows straightforward integration into the overall system-level performance assessment [93].

5.5.7 Generator Model and Electrical Power Output

The electrical generator represents the final stage of the energy conversion process in the hybrid SOFC–GT system. After thermal energy is converted into mechanical shaft power within the gas turbine, the generator is responsible for transforming this mechanical power into electrical power that can be delivered to the electrical load or auxiliary systems. In the present configuration, the generator is mechanically coupled to the turbine shaft and operates synchronously with the turbine. From a thermodynamic standpoint, the generator does not interact with the working fluid and therefore does not influence the mass or energy balances of the gas path. Instead, its role is confined to the mechanical–electrical energy conversion process. For this reason, the generator is modelled as a lumped energy conversion component operating under steady-state conditions. The electrical power produced by the generator is directly related to the mechanical power available at the turbine shaft. However, not all of the available shaft power can be converted into electrical power because of mechanical and electrical losses within the generator [93]. These losses are accounted for through the generator efficiency, which represents the fraction of shaft power successfully converted into electrical output. Accordingly, the generator electrical power output is calculated using the following relation (Eq.5-46):

$$\dot{W}_{el} = \eta_{gen} \times \dot{W}_{shaft,net} \tag{5-45}$$

where $\dot{W}_{el}$ is the electrical power delivered by the generator, $\dot{W}_{\mathrm{shaft,net}}$is the net shaft power available to the generator, calculated as the difference between the turbine output power and the compressor power consumption, and η_{gen} is the generator efficiency.

In this study, the generator efficiency is assumed to be constant and is selected based on typical values reported for small-scale gas turbine generator systems. The simplicity of this formulation is justified by the system-level nature of the present analysis, in which the objective is to evaluate overall power production rather than detailed electromagnetic behaviour of the generator. This approach ensures consistency with the modelling philosophy adopted for other components of the system and enables transparent coupling between the turbine model and the electrical output of the hybrid system.

5.5.7.1 Overall Electrical Efficiency of the Hybrid System

Following the formulation of the gas turbine and generator models, the final step in the thermodynamic description of the hybrid SOFC–GT system is the definition of the overall electrical performance indicator. Up to this point, the energy conversion processes within each component have been modelled separately: electrochemical conversion in the SOFC, thermal expansion in the turbine, and mechanical-to-electrical conversion in the generator. However, from a system-level perspective, these processes must ultimately be evaluated through a single performance metric that relates the useful electrical output to the chemical energy supplied to the system. The chemical energy input to the hybrid system originates from the fuel stream entering the reformer–SOFC subsystem. Since the fuel undergoes electrochemical and combustion reactions, the appropriate reference for its energy content is the lower heating value (LHV), which represents the usable chemical energy assuming water remains in vapor phase [93]. Accordingly, the total rate of chemical energy supplied to the system is defined as (Eq.5-47):

$$\dot{Q}_{Fuel} = \dot{m}_{Fuel} \times LHV \tag{5-46}$$

where $\dot{m}_{Fuel}$ denotes the fuel mass flow rate $\left(\frac{kg}{s}\right)$ and LHV is the lower heating value $\left(\frac{kJ}{kg}\right)$ of the selected fuel and consequently $\dot{Q}_{Fuel}$ is expressed in kW. This quantity represents the total chemical energy available for conversion within the hybrid architecture and forms the reference basis for defining system efficiency. The net electrical output of the hybrid system consists of two contributions. The primary contribution arises directly from the SOFC stack through electrochemical energy conversion. The secondary contribution is produced by the gas turbine–generator unit, where part of the thermal energy of the exhaust gases is converted into mechanical work and subsequently into electrical power. The net electrical power output of the system can therefore be expressed as (Eq.5-48):

$$\dot{W}_{net} = \dot{W}_{el} + \dot{W}_{SOFC} \tag{5-47}$$

In this relation, $\dot{W}_{SOFC}$ represents the electrical power generated by the fuel cell stack, while $\dot{W}_{el}$corresponds to the electrical power delivered by the generator after accounting for mechanical and conversion losses. Finally, the global net electrical efficiency of the hybrid system is defined as the ratio between the net electrical output and the total chemical energy input (Eq.5-49):

$$\eta_{global} = \frac{\dot{W}_{net}}{\dot{Q}_{Fuel}} \tag{5-48}$$

This efficiency represents the principal system-level performance indicator used throughout the verification and parametric studies presented in the subsequent chapters. At this stage, the above formulation defines the governing performance metric of the hybrid architecture. Its numerical evaluation, sensitivity to operating parameters, and comparison with reference configurations are addressed in the subsequent verification and results chapter.

6. Model Verification and Comparative Performance Analysis

The numerical framework developed in Chapter 5 establishes a unified thermodynamic–electrochemical model for the hybrid SOFC–GT system. However, the reliability of any system-level simulation depends on its ability to reproduce established reference results and to capture physically meaningful performance trends under varying configurations. The present chapter therefore evaluates the developed model through a verification. Rather than redefining the governing equations, the same computational framework is applied to three progressively complex scenarios derived from well-documented literature cases. The analysis proceeds in three stages. First, the model is verified against the NASA baseline architecture [93] to confirm numerical consistency with a recognized aerospace reference. Second, architectural extensions based on the configuration proposed by Wilson et al [94]. are introduced to assess the impact of additional system complexity. Finally, high-altitude and high-power operating conditions are examined using the ProMax-based case to evaluate the model ability to capture performance trends under realistic flight constraints. Through this staged approach, both numerical accuracy and physical robustness of the developed framework are systematically assessed [93, 94].

6.1 Verification Against the NASA Baseline Configuration

The close agreement observed in mass flow distribution, pressure levels, temperature states, electrochemical voltage components, stack power output, and overall system efficiency confirms that the independently developed thermodynamic–electrochemical model successfully reproduces the NASA hybrid SOFC–GT reference case. This analysis establishes a reliable baseline for subsequent comparisons with alternative architectures and operating conditions.

6.1.1 NASA Verification Case and Operating Conditions

The first verification case is based on the NASA reference hybrid SOFC–GT configuration reported by Steffen and Free [93]. Before presenting the verification results, the operating conditions adopted for reconstructing this reference case are summarized in the following tables. These parameters are specific to the NASA verification case and should therefore be regarded as reference operating conditions rather than general model inputs.
The purpose of reporting these data is to demonstrate that the reconstructed thermodynamic state of the system is consistent with the original reference configuration prior to the quantitative verification presented in the following sections. The reported operating conditions include the main heat exchanger characteristics, gas turbine boundary conditions, and generator operating parameters that define the thermodynamic state of the integrated hybrid system.
The operating conditions of the air–air heat exchanger are summarized in Table 6-1. These values define the temperature levels, mass flow rates, and heat exchanger effectiveness used to reproduce the thermal preheating process of the cathode air in the NASA reference configuration.

Table 6-1 Input operating conditions and calculated performance of the compressor and air–air heat exchanger pathway from combustor [93].

Parameter	Type	Hot stream (combustor exhaust gas)	Cold stream (compressed air)	unit
Mass flow rate , ($\dot{m}$)	Input	0.481	0.467	$\left(\frac{kg}{s}\right)$
Inlet temperature , (T_{in})	Input	1563.15	516.15	K
Outlet temperature , (T_{out})	Output	1035.7	1172.15	K
Specific heat capacity ($c_{p,mix}$)	Calculated	1.26	1.04	$\left(\frac{kJ}{kg.K}\right)$
Heat exchanger effectiveness (ε_{AA})	Input (Design parameter)	0.702	0.702	$-$

The reconstructed operating conditions of the air–water heat exchanger are reported in Table 6-2. The calculated heat duty distribution and outlet temperatures confirm the consistency of the thermal recovery process adopted in the reference model.

Table 6-2 Heat duty distribution and outlet conditions of the air–water heat exchanger [93].

Parameter	Status	Hot stream (combustor exhaust gas)	Cold stream (Water)	unit
Mass flow rate , ($\dot{m}$)	Input	0.481	0.0179	$\left(\frac{kg}{s}\right)$
Inlet temperature (T_{in})	Input	1035.25	298.15	K
Outlet temperature (T_{out})	Output	923.45	886.74	K
Sensible heating ,(Q_1)	Output	5.99	$-$	kW
Latent heat of vaporization,(Q_2)	Output	40.4	$-$	kW
Steam superheating,(Q_3)	Output	18.39	$-$	kW
Total heat duty,(Q_{HX})	Output	64.78	64.78	kW
Heat exchanger effectiveness (ε_{Aw})	Specified Input	0.691	0.691	$-$

The operating conditions used for the gas turbine reconstruction are summarized in Table 6-3. These parameters define the inlet pressure, turbine pressure ratio, inlet temperature, expansion process, and resulting shaft power corresponding to the NASA verification case [93].

Table 6-3 Operating conditions and performance of the gas turbine [93].

Parameter	Symbol	Value	Unit	Description
Turbine inlet pressure	$p_{in,t}$	3.34	bar	Pressure at turbine inlet
Turbine outlet pressure	$p_{t,out}$	1	bar	Exhaust pressure
Pressure ratio	β	3.35	$-$	Turbine pressure ratio
Turbine inlet temperature	$T_{in,t}$	923.15	K	From combustor outlet
Isentropic exit temperature	$T_{is,out,t}$	684	K	Ideal expansion
Actual exit temperature	$T_{out,t}$	719.15	K	With efficiency
Isentropic efficiency	η_t	0.85	$-$	Assumed/validated
Mass flow rate	$\dot{m}_t$	0.48	$\frac{kg}{s}$	Exhaust gas flow
Gross turbine power	$\dot{W}_t$	124.32	kW	Shaft power

Finally, the generator operating conditions and electrical power conversion are reported in Table 6-4. These values provide the mechanical-to-electrical power conversion characteristics required to reproduce the net electrical output of the reference system.

Table 6-4 Turbine shaft power and generator electrical output [93].

Parameter	Symbol	Unit	Value
Net shaft power available to generator	$\dot{W}_{shaft,net}$	kW	15.32
Generator efficiency	η_g	$-$	0.9
Generator electrical power	$\dot{W}_{el}$	kW	14
Total net system power	$\dot{W}_{net}$	kW	200
SOFC net electrical power	$\dot{W}_{SOFC}$	kW	186

Since all operating conditions reported in this section correspond to the original NASA verification case, they serve as boundary conditions for the subsequent verification analyses. The quantitative comparison between the reconstructed model and the published reference results is presented in the following subsections, where the electrochemical behaviour, component-level thermodynamic performance, and overall system response are evaluated.

6.1.2 Electrochemical Verification

The first level of activity focuses on the electrochemical behaviour of the SOFC stack. Since the hybrid system performance fundamentally depends on the accurate prediction of cell voltage and associated polarization losses, verification of the electrochemical sub-model is essential before proceeding to thermodynamic assessment. The reversible cell voltage was calculated using the Nernst relation introduced in Chapter 5, accounting for operating temperature and reactant partial pressures at the SOFC inlet. The resulting Nernst potential was then corrected by incorporating activation, ohmic, and concentration losses in order to determine the operating cell voltage. Table 6.5 presents a comparison between the electrochemical parameters calculated in the present model and the values reported in the NASA reference study.

Table 6-5 Electrochemical performance comparison with NASA reference.

Parameter	unit	NASA Reference	Present Model	Error (%)
Nernst Voltage	(V)	0.878	0.871	0.81
Activation Loss	(V)	0.0154	0.0155	0.65
Ohmic Loss	(V)	0.251	0.252	0.4
Concentration Loss	(V)	0.0412	0.0413	0.25

The comparison indicates very close agreement between the present implementation and the NASA reference values. The reversible (Nernst) voltage is reproduced with error of below 1%, confirming correct implementation of the Gibbs free energy formulation and the dependence on reactant partial pressures. Similarly, the individual polarization losses exhibit errors below 1%, demonstrating consistent implementation of the electrochemical kinetic relations and ohmic resistance model. this level of agreement ensures that subsequent power predictions remain physically reliable. Overall, the close correspondence between the calculated and reference electrochemical parameters provides strong confidence in the SOFC sub-model and establishes a validated basis for evaluating the thermodynamic coupling with the gas turbine subsystem. The electrochemical verification therefore confirms that the SOFC formulation has been correctly implemented and reproduces the reference operating behaviour with high accuracy. Since all major electrochemical parameters are predicted within a small error from the reference values, the SOFC sub-model can be considered sufficiently reliable for system-level simulations. Consequently, any remaining discrepancies observed in the hybrid SOFC–GT performance are expected to arise primarily from the thermodynamic interaction between system components rather than from the electrochemical formulation itself.

6.1.3 Component Thermodynamic Verification

The next step is to assess the thermodynamic consistency of the turbomachinery and combustion subsystems. While the previous section verified voltage formation and polarization losses, the present section focuses on the energy conversion processes governing the gas turbine cycle. In a hybrid SOFC–GT architecture, the turbine inlet temperature (TIT), turbine exit temperature, compressor and turbine work, and their respective isentropic efficiencies represent critical thermodynamic indicators. These quantities directly reflect the accuracy of the combustor energy balance, heat exchanger integration, and isentropic expansion modelling. Any inconsistency in mass or energy conservation would manifest as error in these parameters. To verify the correctness of the implemented thermodynamic relations, the present model predictions are compared against the published NASA reference architecture results.

Table 6-6 Thermodynamic components of compressor and turbine verification against NASA reference.

Parameter	Unit	NASA Reference	Present Model	Error (%)
Turbine Inlet Temperature	K	923.15	923.4	0.02
Turbine Exit Temperature	K	719.15	719.9	0.1
Compressor Work	kW	109	109.42	0.42
Turbine Work	kW	124	124.32	0.25
Turbine Efficiency	$(-)$	0.85	0.853	0.35
Compressor Efficiency	$(-)$	0.75	0.755	0.64

The results presented in Table 6-6 indicate very close agreement between the present implementation and the NASA reference data. The turbine inlet temperature (TIT) predicted by the present model $(923.4\,K)$ shows a negligible error of only 0.02% relative to the NASA reference value $(923.15\,K)$. Since TIT is determined by the combustor energy balance and directly depends on the residual chemical energy of the SOFC exhaust, this near-exact agreement confirms that the combustion model and heat release formulation have been implemented correctly.

The turbine exit temperature exhibits a similarly small error of 0.1%, demonstrating accurate application of the isentropic expansion relation combined with the specified turbine adiabatic efficiency. This confirms that the thermodynamic state propagation across the turbine stage is physically consistent and numerically stable. For the compressor work, the predicted value $(109.42\,kW)$ deviates by only 0.42% from the reference $(109\,kW)$,

indicating correct implementation of the compressor pressure ratio and adiabatic efficiency relations. Likewise, the turbine work prediction $(124.32\ kW)$ differs by merely 0.25% from the reference value $(124\ kW)$, confirming that the steady-flow energy equation and enthalpy drop calculations are properly formulated. The reproduced turbine and compressor adiabatic efficiencies $(0.853\ and\ 0.755)$ also remain within 1% error from the reference values, further supporting the internal consistency of the turbomachinery model.
Overall, all thermodynamic parameters exhibit errors well below 1%, which is generally considered excellent agreement for system-level hybrid modeling. This level of consistency confirms that the combustor, compressor, and turbine formulations are correctly coupled with the upstream SOFC model, and that mass and energy conservation are preserved throughout the gas turbine subsystem. The thermodynamic behaviour therefore provides a reliable foundation for proceeding to global system-level performance evaluation.

6.1.4 Global System Performance Verification

While Sections 6.1.1 and 6.1.2 verified the electrochemical and thermodynamic subsystems individually, a hybrid SOFC–GT system must ultimately be assessed at the integrated system level. The overall performance depends not only on the accuracy of each component model, but also on the correct coupling between electrochemical conversion, combustion, turbomachinery expansion, and mechanical-to-electrical transformation.

At the global level, the key performance indicators include:

- Net electrical power output
- SOFC electrical power contribution
- Gas turbine–generator electrical power contribution
- Overall net electrical efficiency

These parameters collectively reflect the combined behaviour of the entire hybrid architecture and therefore provide the final verification step before proceeding to extended case studies.

6.1.4.1 Net Electrical Power

Table 6-7 presents the comparison between the present model and the NASA reference values for system-level power outputs.

Table 6-7 Global electrical performance comparison with NASA reference.

Parameter	Unit	NASA Reference Values	Present Model (output) Result	Error (%)
SOFC Net Electrical Power	kW	186	186.79	0.42
Total Net Electrical Power	kW	200	200.58	0.3
Overall Net Electrical Efficiency	%	40.6	40.63	0.07

The results presented in Table 6-7 indicate very close agreement between the present implementation and the NASA reference data at the system level. The total net electrical power predicted by the present model is 200.58 kW, compared to 200 kW in the reference case, corresponding to an error of only 0.3%. This small discrepancy confirms that the integrated coupling between the SOFC and gas turbine subsystems has been implemented consistently.
The SOFC net electrical power is predicted as $186.79\ kW$, compared to $186\ kW$ in the NASA study, resulting in an error of 0.42%. Since the stack power is directly dependent on the operating cell voltage and fuel utilization factor, this close agreement confirms that the electrochemical formulation and current density implementation remain physically accurate when integrated within the full hybrid system. This difference is still within an acceptable engineering tolerance and is primarily attributed to minor variations in turbine work and generator efficiency propagation through the mechanical power balance.

Finally, the overall net electrical efficiency is predicted as 40.63%, compared to 40.6% in the NASA reference, corresponding to an error of only 0.07%. Because this efficiency represents the ratio between total electrical output and the chemical energy input based on the fuel lower heating value, its accurate reproduction confirms that the global mass and energy balances are satisfied across the entire hybrid architecture. Taken together, these results demonstrate that the developed model reproduces the global thermodynamic performance of the NASA hybrid SOFC–GT configuration with high numerical fidelity. The agreement at the electrochemical, component, and integrated system levels provides strong confidence in the robustness and internal consistency of the implemented computational framework.

6.1.5 Internal Consistency Verification

Beyond comparison with reference numerical results, an additional verification step was performed to ensure that the developed model satisfies fundamental physical conservation principles. First, mass conservation was verified within the reformer and SOFC subsystems. The inlet and outlet mass flow rates of all chemical species were evaluated under steady-state conditions. The results confirmed that the total mass flow is conserved across the reformer and electrochemical sections, indicating that the implemented reaction stoichiometry and fuel utilization relationships (as defined in Section 5.5.1 and 5.5.2) are internally consistent. Second, thermodynamic state consistency was examined by tracking temperature and pressure levels at all defined state points across the system.

The pressure evolution from compressor outlet to combustor and turbine inlet follows the relations previously introduced in Section 5.5.6. Similarly, temperature variations across the combustor and turbine stages remain consistent with the steady-flow energy balance equations formulated in Sections 5.5.4 and 5.5.6. No artificial energy accumulation or pressure discontinuities were observed in the numerical implementation. The continuity of thermodynamic properties across connected components confirms that component-level models are coherently coupled at the system level. This internal verification step strengthens the credibility of the verification process. While agreement with NASA reference data demonstrates external consistency, satisfaction of mass and energy conservation confirms that the model is physically self-consistent and numerically robust.

6.2 Verification Against the Eelman Hybrid SOFC–GT Model

Following the successful verification of the developed model against the NASA NPSS configuration in Section 6.1, the second stage of verification is carried out using the hybrid SOFC–GT system reported by Eelman et al. in Article 8 [95]. Although the Eelman configuration was originally benchmarked against the NASA model, it introduces modifications in fuel representation and flow structure that justify an independent verification step within the present work.

In particular, the aviation fuel is represented through a surrogate mixture composed of n-dodecane ($C_{12}H_{26}$) and m-xylene (C_8H_{10}) , instead of the pseudo-fuel formulation adopted in the NASA reference. While the global thermodynamic architecture remains similar, the reformer inlet composition and the resulting syngas distribution at the SOFC anode are affected by this surrogate approach. Since the electrochemical performance of the SOFC is directly influenced by the H_2/CO ratio and reactant partial pressures, it is necessary to verify that the present model reproduces the reported behavior under these modified conditions. The verification is performed progressively, beginning with the reformer subsystem and subsequently extending to the SOFC electrochemical response and the global system performance [95].

6.2.1 Reformer Inlet Conditions and Fuel Representation

The surrogate fuel composition adopted for this case consists of a fixed molar mixture of n-dodecane and m-xylene selected to preserve the elemental carbon-to-hydrogen ratio and the lower heating value of Jet-A fuel. The reformer operating conditions are summarized below.

Table 6-8 Reformer inlet conditions – Eelman case [95].

Parameter	Unit	Value
Fuel mass flow rate	$\frac{kg}{s}$	0.0115
Steam mass flow rate	$\frac{kg}{s}$	0.0179
Steam to carbon ratio (S/C)	$-$	1.22
Oxygen-to-carbon ratio (O/C)	$-$	0
Reformer temperature	$°C$	900
Reformer pressure	bar	4.5

From the reformer outlet molar flow rates listed in Table 6-8, the hydrogen-to-carbon monoxide (H_2/CO) molar ratio was calculated to be 2.44. Although Wilson et al.[95] do not explicitly report the (H_2/CO) ratio, they provide the individual outlet molar flow rates of hydrogen and carbon monoxide, from which this ratio can be directly calculated.

Therefore, the obtained value is consistent with the reformer outlet composition reported by Wilson et al. Under the operating conditions summarized in Table 6-8, hydrogen accounts for approximately 73% of the reactive fuel mixture entering the SOFC anode. This hydrogen-rich composition results from the combined effects of steam reforming and the water–gas shift reaction, providing a suitable fuel composition for SOFC operation.

The H_2/CO ratio is an important parameter in SOFC analysis because it influences the relative contribution of hydrogen oxidation and carbon monoxide electro-oxidation within the anode. While both species participate in electrochemical conversion, hydrogen oxidation typically governs the stack voltage response under high-temperature equilibrium reforming conditions. Therefore, verifying the reformate composition ensures that the electrochemical operating point of the SOFC is correctly defined. The close numerical agreement between the reformer outlet composition obtained in the present model and the data reported by Wilson et al.[95] confirms that the surrogate fuel representation and equilibrium reforming implementation are consistent. Having established the correctness of the fuel processing stage, the analysis now proceeds to verification of the electrochemical performance of the SOFC stack under the Eelman configuration.

6.2.2 Electrochemical Performance Verification of the SOFC Stack

Following the verification of the reformer outlet composition presented in Section 6.2.1, the electrochemical behaviour of the SOFC stack is now assessed under the Eelman configuration. Since the anode inlet composition directly determines the partial pressures of hydrogen and steam entering the cell, accurate reproduction of the stack voltage components is essential to confirm that the electrochemical sub-model remains valid under the modified fuel representation. The comparison between the electrochemical parameters reported by Wilson et al.[95] and those obtained from the present model is summarized in Table 6-9.

Table 6-9 Electrochemical performance comparison under Eelman configuration.

Parameter	Unit	Eelman Reference Values	Present Model output	Error
Nernst Voltage	V	0.8758	0.874	0.21
Activation Loss	V	0.0155	0.01549	0.6
Ohmic Loss	V	0.251	0.251	0
Concentration Loss	V	0.0412	0.04124	0.09
Operating Cell Voltage	V	0.568	0.566	0.35
Power Density	$\frac{mW}{cm^2}$	284	283.07	0.33

As summarized in Table 6-9, the electrochemical performance predicted by the present model remains in close agreement with the reference results reported for the Eelman configuration, with errors below 1% for all principal electrochemical parameters. Unlike the NASA verification case, this comparison evaluates the capability of the developed model to preserve its predictive accuracy after modifications in both the system architecture and the fuel representation.

The calculated Nernst voltage differs from the reference value by only 0.21%, indicating that the reformer outlet composition and the resulting reactant partial pressures are reproduced consistently. Likewise, the activation, ohmic, and concentration overpotentials are all predicted with errors below 1%, demonstrating that the electrochemical kinetics, electrical resistance model, and mass transport formulation remain valid under the revised operating conditions adopted in the Eelman configuration. In particular, the exact reproduction of the ohmic loss confirms that the implemented temperature-dependent conductivity and area-specific resistance correlations are fully consistent with the reference model.

The combined effect of these voltage-loss components results in an operating cell voltage of $0.566\ V$, corresponding to an error of only 0.35% from the published value. Consequently, the predicted power density also agrees closely with the reference data, differing by only 0.33%, which confirms that the electrical performance of the SOFC stack is accurately reproduced under the modified configuration.

Overall, the verification demonstrates that the electrochemical formulation previously validated using the NASA baseline remains robust when applied to a different hybrid architecture and surrogate fuel representation. The consistent agreement observed across all electrochemical indicators confirms the transferability of the developed modelling framework and provides a reliable basis for the subsequent verification of the thermodynamic behaviour of the complete Eelman hybrid SOFC–GT system.

6.2.3 Turbomachinery Performance and System-Level Energy Closure under the Eelman Configuration

Following the electrochemical verification, the thermodynamic performance of the turbomachinery subsystem is evaluated to determine whether the modified fuel representation affects the overall energy conversion process. Since the compressor and turbine pressure ratios are prescribed design parameters, this analysis focuses on verifying that the revised fuel composition preserves the thermodynamic consistency of the hybrid cycle rather than re-evaluating the component design. For the compressor, the imposed inlet conditions yield a calculated power consumption of $109.56\ kW$, with an isentropic efficiency of 0.7548, in excellent agreement with the reference value reported by Eelman et al. [95]. This confirms that the surrogate fuel implementation does not influence the upstream air path or the compressor thermodynamic behaviour.

The turbine operates under substantially different thermal conditions because of the elevated inlet temperature. To account for the temperature-dependent thermophysical properties of the combustion products, the mixture specific heat capacity was evaluated using the mass-weighted averaging procedure described in Chapter 5. The resulting effective heat capacity at the turbine inlet is $1.24\left(\frac{kJ}{kg.K}\right)$ leading to a predicted turbine power of $123.7(kW)$ and an isentropic efficiency of 0.851, corresponding to an error below 0.24% from the reference configuration. This close agreement confirms that the expansion model remains valid despite the modified fuel representation.

The calculated turbine output exceeds the compressor power requirement, providing a net shaft power of 14.15 (kW). After accounting for the generator efficiency which assumed 0.98 %, this corresponds to an electrical contribution of 13.9 (kW) from the gas turbine subsystem. Combined with the SOFC electrical output, the total net power reaches 198.87 (kW), resulting in an overall electrical efficiency of 40.08%. These results indicate that the modifications introduced in the Eelman configuration do not alter the global thermodynamic behaviour of the hybrid system. Although the fuel representation differs from the NASA baseline, the reconstructed model preserves the overall energy balance, accurately reproduces the turbomachinery performance, and predicts the system electrical efficiency with excellent agreement. The numerical comparison with the reference data is presented in Table 6-10.

Table 6-10 Turbomachinery and global performance under Eelman configuration.

Parameter	Unit	Reference Eelman Values	Present Model output	Error (%)
Compressor Work	kW	109	109.56	0.51
Turbine Work	kW	124	123.7	0.24
Turbine Efficiency	$[-]$	0.85	0.851	0.19
Generator Electrical Power	kW	14	13.9	0.7
Total Net Electrical Power	kW	198.92	198.87	0.03
System Electrical Efficiency	$[-]$	0.401	0.4008	0.05

The results reported in Table 6-10 indicate very close agreement between the present model and the reference data under the Eelman configuration. All evaluated performance indicators exhibit errors below 1%, confirming the numerical consistency of the turbomachinery implementation. The compressor work is reproduced with an error of 0.51%, while the turbine work shows an error of 0.24% relative to the reference value. The turbine adiabatic efficiency differs by only 0.19%, demonstrating that the high-temperature expansion process and associated property evaluation have been implemented correctly within the present framework. The generator electrical power, obtained from the net shaft work and the assumed generator efficiency 0.98 %, exhibits an error of 0.7%, which remains well within acceptable tolerance for integrated hybrid system simulations.

At the system level, the total net electrical power is predicted with remarkable accuracy ($198.87\ kW$ $compared\ to$ $198.92\ kW$), corresponding to an error of only 0.03%. Likewise, the overall system electrical efficiency of 0.4008 closely matches the reference value of 0.401. The consistency observed across component-level and global performance parameters confirms that the thermodynamic coupling between compressor, turbine, generator, and SOFC stack has been preserved under the surrogate fuel representation. Therefore, the introduction of the surrogate fuel formulation and the Mixing Flow assumption does not disturb the integrated energy balance of the hybrid SOFC–GT system. The validated turbomachinery block provides a reliable basis for proceeding toward the analysis of the fully integrated system behaviour under alternative operational conditions.

6.2.4 Structural Robustness of the Model under Modified Fuel Representation

The results obtained under the Eelman configuration provide more than numerical agreement with reference data. They demonstrate that the developed thermodynamic–electrochemical framework remains structurally robust when subjected to a modified fuel representation and altered internal flow structure. The present configuration adopts an explicit surrogate mixture of n-dodecane and m-xylene, leading to a different reformer equilibrium composition and modified SOFC anode inlet conditions. Despite these internal differences, the global performance indicators including compressor work, turbine work, generator output, total net power, and overall electrical efficiency remain in close agreement with the reference configuration.

This observation is particularly significant. The reformer outlet composition directly affects the partial pressures of hydrogen, carbon monoxide, and steam at the SOFC inlet, which in turn influence the electrochemical operating voltage. Any inconsistency in the coupling between chemical equilibrium, electrochemical conversion, and downstream combustion would propagate through the turbine stage and manifest as errors in global power balance. The absence of such errors confirms that the implemented coupling between reformer, SOFC, combustor, and turbomachinery is thermodynamically coherent. Moreover, the use of the Mixing Flow assumption for evaluating turbine inlet properties does not introduce instability at system level. Owing to the high air-to-fuel ratio, the thermophysical properties of the combustion mixture are dominated by the air stream, rendering the turbine expansion process relatively insensitive to minor variations in fuel-derived species concentrations. The close agreement in turbine work and efficiency therefore indicates that the adopted property evaluation method is adequate for system-level analysis without compromising numerical fidelity.

Taken together, these results confirm that the present framework is not tuned to a single fuel formulation or specific architectural layout. Instead, it preserves energy conservation and performance consistency across distinct representations of the same hybrid SOFC–GT concept. This structural robustness is essential before extending the model toward operating scenarios involving different ambient conditions, pressure levels, or power settings. Having established numerical and structural consistency under both the NASA and Eelman configurations, the model can now be extended to operating conditions beyond the original envelope. The following section investigates the ProMax-based configuration, where variations in pressure level and operating constraints provide a further assessment of the model predictive robustness.

6.3 Verification and System-Level Performance Evaluation of the 1-MW ProMax SOFC–GT Configuration under Cruise Conditions

Following the successful verification of the numerical framework against the NASA baseline configuration in Section 6.1 and the structurally modified Eelman architecture in Section 6.2, the present section extends the analysis to a high-altitude, megawatt-class SOFC–GT configuration derived from Wilson et al.[94].

Unlike the previous sections, which focused on benchmark replication and structural robustness verification, this section simultaneously addresses modified operating conditions and system-level performance interpretation. The $1-MW$ ProMax case represents a substantially different operational regime compared to the earlier scenarios. First, the electrical power scale increases to the megawatt level, strengthening the thermodynamic coupling between electrochemical conversion and gas turbine expansion. Second, the system operates under cruise-altitude ambient conditions $(36{,}000\ ft, 10{,}973\ m)$, where reduced inlet pressure and temperature directly influence compressor performance, mass flow rate, combustion characteristics, and turbine inlet conditions. Third, the fuel representation is simplified to pure n-dodecane, and a 70% anode exhaust recycle loop is incorporated, affecting reforming equilibrium, thermal integration, and internal energy redistribution. In addition, the heat exchanger layout and flow routing differ from the baseline configurations, requiring a systematic reconstruction of the gas path and power balance. In contrast to Sections 6.1 and 6.2, where the primary objective was equation-level verification, this section evaluates the predictive capability of the previously validated sub-models under intensified coupling and altered boundary constraints. Verification is performed through comparison with the ProMax reference data, while internal energy conservation, shaft power closure, and electrical power distribution are simultaneously assessed. The following subsections examine, in a structured manner, the operating boundary conditions, thermodynamic reconstruction of the gas path, electrochemical operating state of the SOFC, internal stack energy balance, and finally the global hybrid system efficiency and power distribution.

6.3.1 Operating Scenario Definition and Boundary Conditions

In this case, the ambient pressure and temperature are determined according to the International Standard Atmosphere (ISA) model and serve as the inlet boundary conditions for the compressor stage. Compared to sea-level operation, the significantly reduced ambient pressure alters the inlet air density and directly influences the compressor mass flow rate and the thermodynamic state at the combustor and turbine inlet. These altitude-induced constraints impose a fundamentally different operating regime relative to the previously validated NASA and Eelman cases. Unlike the earlier verification scenarios, which were primarily designed for model verification, the present configuration targets a net electrical output of approximately $1\ MW$. The increased power level intensifies the thermodynamic and electrochemical coupling between the SOFC stack and the gas turbine subsystem, thereby increasing the sensitivity of shaft power balance, turbine inlet temperature (TIT), and internal thermal management. The fuel adopted in this configuration is pure n-dodecane, selected as a surrogate for synthetic aviation fuel while remaining compatible with the thermochemical formulation introduced in Chapter 5. A defining structural feature of the ProMax architecture in Figure (5-3) is the incorporation of a 70% anode exhaust recycle loop. This recycle stream enables internal steam recovery after start-up and significantly affects reforming equilibrium, anode inlet composition, and heat distribution within the SOFC stack. Furthermore, the heat exchanger configuration and flow routing differ from the baseline verification cases, requiring a systematic reconstruction of the temperature and pressure evolution along the gas path. The principal boundary conditions, operating constraints, and design parameters adopted for the $1-MW$ ProMax case are summarised in Table 6-11.

Table 6-11 Operating conditions and boundary parameters for the 1-MW ProMax case.

Parameter	Value	Unit
Cruise Altitude	36000	(ft)
Ambient Pressure (ISA)	0.227	(bar)
Ambient Temperature (ISA)	-56.3	$(°C)$
Air mass flow rate	1.0677	$\left(\frac{kg}{s}\right)$
Fuel Feed	0.02002	$\left(\frac{kg}{s}\right)$
Fuel spray	0.01233	$\left(\frac{kg}{s}\right)$
SOFC Stack Pressure	3.04	(bar)
SOFC Operating Temperature	750	$(°C)$
$\boldsymbol{uf}$	60	%
$\boldsymbol{uair}$	25	%
Reformer Oxygen/Carbon Ratio	$1.8-3.0$ range (allowed to float)	$[-]$

It should be emphasised that this subsection serves to define the operating framework within which the previously verified SOFC–GT model is now evaluated. The subsequent analysis therefore focuses on thermodynamic reconstruction of the gas turbine subsystem, electrochemical operating point determination under modified inlet conditions, and verification of power distribution and energy closure at the integrated system level.

6.3.2 Thermodynamic Reconstruction of the Gas Path

Following the definition of the operating boundary conditions in Section 6.3.1 , the thermodynamic reconstruction of the gas path is carried out to determine the internal state variables and power terms of the turbomachinery subsystem for ProMax configuration. The objective of this subsection is to propagate pressure, temperature, and power consistently from the ambient inlet to the turbine exit under cruise-altitude conditions, ensuring mechanical and thermodynamic closure of the gas turbine block. The reconstruction begins at the compressor inlet, where the ambient conditions corresponding to $36{,}000\ ft$ define the initial state of the air stream. As reported in Table 6-12, the compressor inlet temperature is $-56.32\ °C$ and the corresponding pressure is $0.227\ atm$. Under these conditions, the reduced inlet density directly affects the compression process.

Using the prescribed compressor pressure ratio and adiabatic efficiency, the outlet temperature is obtained from the isentropic compression relation corrected for efficiency. The reconstructed compressor outlet temperature reaches $220.2\ °C$, while the pressure increases to $3.35\ atm$. This state defines the oxidant conditions entering the cathode channel and downstream heat exchanger. Subsequently, the pressure evolution across the cathode, heat exchanger, and combustor is determined by applying the specified pressure losses.

As shown in Table 6-12, the cathode outlet heat exchanger pressure is 3.25 atm and the SOFC cathode pressure outlet is $3.09\ atm$, and after the heat exchanger the pressure reduces to $2.995\ atm$. This value represents the combustor chamber operating pressure and establishes the boundary condition for the combustion and turbine inlet process. On the anode side, the reformer operates at $3.06\ atm$, with pressure losses of 3% in the reformer and 2% in the anode channel, maintaining internal consistency between fuel processing and combustion inlet conditions.

The fuel and recycle streams are then directed toward the combustor, where sufficient thermal input is supplied to reach a turbine inlet temperature (TIT) of $1196\ °C$. Achieving this TIT under altitude-constrained pressure conditions confirms that the combustor provides adequate thermal energy to sustain megawatt-class operation. The turbine expansion is reconstructed using the prescribed turbine pressure ratio and adiabatic efficiency. The resulting turbine exit temperature is $669.8\ °C$. Under these operating conditions, the turbine mechanical power is calculated as $686.72\ kW$, while the compressor requires 301.7 kW. The net shaft power therefore becomes $385.03\ kW$.
When corrected by the generator efficiency, the generator electrical output reaches $377.33\ kW$. Finally, when combined with the SOFC electrical contribution, the total electric power of the hybrid system reaches $996.76\ kW$, which is consistent with the targeted $1 - MW$ class operation. The full set of reconstructed thermodynamic states and power terms is summarised in Table 6-12.

Table 6-12 Thermodynamic reconstruction of the turbomachinery block (1-MW ProMax case).

Parameter	Value	Unit
Compressor Inlet Temperature	-56.32	$(°C)$
Compressor Outlet Temperature	220.2	$(°C)$
Compressor inlet Pressure	0.227	(atm)
Compressor Outlet Pressure	3.35	(atm)
Cathode Heat Exchanger Outlet Pressure	3.25	(atm)
SOFC Cathode Pressure Outlet	3.09	(atm)
Heat Exchanger-1 Outlet Pressure	2.995	(atm)
Combustor Chamber Operating Pressure	2.995	(atm)
Reformer operating pressure	3.06	(atm)
Reformer Pressure losses	3	%
Anode Pressure losses	2	%
Anode operating pressure	3.06	(atm)
Combustor operating pressure	2.995	(atm)
Turbine Exit Temperature	669.8	$(°C)$
$\boldsymbol{Cp_{exhaust\ gas\ turbine}}$	1.26	$\left(\frac{kJ}{kg.K}\right)$
Turbine Power	686.72	(kW)
Compressor Power	301.69	(kW)
Net Shaft Power	385.03	(kW)
Generator net electrical power	377.33	(kW)
Total Electric power	996.76	(kW)

The sequential propagation of pressure and temperature from the ambient inlet to the turbine exit demonstrates that the gas path remains thermodynamically coherent under cruise-altitude conditions. Moreover, the closure of the mechanical shaft power confirms that the turbomachinery subsystem operates consistently within the integrated hybrid architecture. With the gas-path reconstruction completed and mechanically closed, the analysis can now proceed to the evaluation of the SOFC electrochemical operating state under the modified inlet and recycle conditions.

6.3.3 Electrochemical Operating State under ProMax Conditions

Following the reconstruction of the thermodynamic gas path in Section 6.3.2, the electrochemical operating point of the SOFC stack is determined under the cruise-altitude boundary conditions of the $1 - MW$ ProMax configuration. The objective of this subsection is to reconstruct the reversible cell potential and the actual operating voltage using the electrochemical framework established in Chapter 5, and to verify the resulting stack electrical output under recycle-integrated operation. The stack operates at a nominal temperature of $750\ °C$ $(1023.15\ K)$ and a stabilized pressure of approximately $3.06\ atm$. Under these conditions, the anode inlet composition is influenced by the 70% anode exhaust recycle, which modifies the hydrogen-to-steam ratio relative to a once-through configuration. The effective partial pressures of hydrogen, steam, and oxygen are reconstructed from the mass balance results of the anode and cathode streams as described in Section 5.5.

The reversible cell potential is evaluated using the Nernst formulation previously introduced in Eq. (5-16), where the temperature-corrected Gibbs free energy of reaction and the calculated partial pressures are employed. The temperature-dependent Gibbs free energy change at $1023.15\ K$ is obtained from the JANAF-based thermodynamic formulation described in Section 5.5.3. The actual operating voltage is then determined by subtracting the activation, ohmic, and concentration overpotentials according to Eqs. (5-17)–(5-21). The electrochemical parameters (exchange current density, limiting current density, internal current density, charge transfer coefficient, and area-specific resistance) are adopted consistently with the calibrated values introduced in Section 5.5.3.5, ensuring continuity with the validated model structure. At the prescribed current density corresponding to the $1 - MW$ design point, the resulting operating voltage and stack electrical output are reconstructed. The electrochemical efficiency is defined as the ratio of operating voltage to reversible voltage (Eq. 5-25). The complete set of reconstructed electrochemical quantities is summarised in Table 6-13.

Table 6-13 Electrochemical operating point of the SOFC under ProMax conditions.

Parameter	Symbol	Reference	Present Model	Error %	Unit
Operating Temperature	T	1023.15	1023.15	–	(K)
Gibbs free Energy	ΔG°	−196.39	−196.39	–	$\left(\frac{kJ}{mol}\right)$
Hydrogen partial pressure	p_{H_2}	–	0.601	–	(atm)
Steam partial pressure	p_{H_2O}	–	1.907	–	(atm)
Oxygen partial pressure	p_{O_2}	–	0.498	–	(atm)
Reversible Nernst Voltage	V_{rev}	0.95	0.951	0.1	V
Activation Loss	V_{act}	–	0.02	–	V
Ohmic Loss	V_{ohmic}	–	0.075	–	V
Concentration Loss	V_{conc}	–	0.031	–	V
Operating Cell Voltage	V_{Oper}	0.82	0.826	0.7	V
Current Density	i	1250	1250	–	$\left(\frac{mA}{cm^2}\right)$
Power Density	P_d	1025	1025	–	$\left(\frac{mW}{cm^2}\right)$
SOFC Net Electrical Power	P_{SOFC}	615.4	619.43	0.65	%

The close agreement between the reconstructed reversible voltage, operating voltage, and stack electrical output with the ProMax reference data confirms that the electrochemical model maintains consistency under altitude-constrained and recycle-integrated operating conditions. With the electrochemical operating point fully established, the internal energy balance of the SOFC stack can now be evaluated in Section 6.3.4.

6.3.4 SOFC Stack Energy Balance under ProMax Conditions

Following the determination of the electrochemical operating point in Section 6.3.3, the internal energy balance of the SOFC stack is evaluated under the cruise-altitude conditions of the $1 - MW$ ProMax configuration. While the previous section established the reversible voltage, operating voltage, and net electrical power output of the stack, the present section quantifies the thermodynamic consistency of the energy conversion process by evaluating the reaction enthalpy at operating temperature, the internal heat generation rate, and the resulting stack efficiencies. Because the SOFC operates at $1023.15\,K\ (750\,°C)$, all thermodynamic quantities must be evaluated at the actual reaction temperature rather than at standard conditions. The temperature-dependent molar enthalpies of the participating species (H_2, O_2, and H_2O) were calculated using the Shomate polynomial formulation introduced in Chapter 5 (Eq. 5-35), with coefficients obtained from the JANAF/NIST thermochemical database. The reaction enthalpy at operating temperature was then evaluated using the temperature-corrected enthalpy relation described in Chapter 5, ensuring consistency between the thermodynamic and electrochemical blocks of the model. At $1023.15\ K$, the reaction enthalpy of hydrogen oxidation is found to be $-247.85\ kJ/mol$, confirming the strongly exothermic nature of the process under SOFC operating conditions. When multiplied by the corresponding molar fuel flow rate at the design operating point, the total chemical power supplied to the stack equals 963.3 kW.

Since only a fraction of this chemical energy is converted into electrical power (as determined in Section 6.3.3), the remaining portion appears as thermal energy generated within the stack. The heat generation rate is evaluated using the stack energy balance relation presented in Chapter 5 (Eq. 5-24), defined as the difference between the total reaction enthalpy rate and the net SOFC electrical power. Substituting the previously calculated electrical power of $619.4\ kW$ yields a generated heat rate of $343.9\ kW$. This internally generated heat is essential for sustaining the high operating temperature of the SOFC and contributes to the thermal integration of the hybrid SOFC–GT system.

The calculated SOFC energy balance and performance indicators are summarized in Table 6-14.The calculated SOFC energy balance and performance indicators are summarized in Table 6-14.

Table 6-14 SOFC energy balance and performance indicators – ProMax case.

Parameter	Symbol	Reference Promax values	Present Model Output	Error %	Unit
Reaction enthalpy at 1023 K	$\Delta H^{\circ}_{reaction}$	–	-247.85	–	$\left(\frac{kJ}{mol}\right)$
Total chemical input power	ΔH°	–	963.31	–	(kW)
Generated Heat	$\dot{Q}_{gen}$	–	343.88	–	(kW)
Overall Stack Efficiency	$\eta_{Overall}$	52.1	52.08	0.038	%
Fuel-to-Electric Efficiency	η_{SOFC}	69.8	70.02	0.24	%

As shown in Table 6-14, the reconstructed SOFC performance agrees closely with the reference values, confirming the accuracy of the implemented stack energy balance.

6.3.5 Turbine–Generator Power Coupling under ProMax Cruise Conditions

Following the stack-level electrochemical evaluation (Section 6.3.3) and the SOFC internal energy balance (Section 6.3.4), the next step in the hybrid system reconstruction is the thermodynamic assessment of the gas turbine and the subsequent mechanical-to-electrical energy conversion. In the present SOFC–GT architecture, the high-temperature exhaust gases leaving the combustor expand through the turbine, producing mechanical shaft work that simultaneously drives the compressor and the electrical generator.

The turbine thermodynamic reconstruction follows the methodology presented in Section 5.5.6. The inlet and outlet thermodynamic states, together with the turbine performance parameters, are evaluated using the previously established governing equations. The thermophysical properties of the combustion products are obtained from the temperature-dependent Shomate correlations described in Section 5.5.3. The corresponding mixture specific heat capacity is calculated by mole-fraction-weighted averaging and evaluated at the mean turbine temperature. Under the reconstructed operating conditions, the representative specific heat capacity of the exhaust gas mixture is $1.26\ \frac{\mathrm{kJ}}{\mathrm{kg\ K}}$, which is subsequently used in the turbine energy balance.

Under ProMax cruise conditions, the reconstructed turbine expansion produces a gross mechanical power output of $686.72\ kW$. Since the turbine shaft is mechanically coupled to the compressor, the compressor power consumption is subtracted from the turbine output to obtain the net shaft power available for electrical generation. The generator model described in Section 5.5.7 is then employed to convert the net shaft power into electrical power using the prescribed generator efficiency.
Therefore, the gas turbine subsystem delivers $377.33\ kW$ of net electrical power. This recovered electrical contribution constitutes the secondary power-generation pathway of the hybrid SOFC–GT system and, together with the electrochemical power generated by the SOFC stack, determines the overall electrical power output under cruise operating conditions are summarized in Table 6-15.

Table 6-15 Turbine and generator performance under ProMax cruise conditions.

Parameter	Symbol	Reference	Present Model	Error %	Unit
Turbine inlet temperature	$T_{t,in}$	1469.15	1469.15	–	K
Turbine outlet temperature	$T_{t,out}$	943.15	943	0.02	K
Turbine pressure ratio	β_t	12.41	12.41	–	–
Turbine isentropic efficiency	η_t	81	81	–	%
Exhaust gas mass flow rate	$\dot{m}$	–	1.0358	–	$\frac{kg}{s}$
Mixture specific heat	$C_{p,mix}$	–	1.26	–	$\frac{kJ}{kg.K}$
Gross turbine mechanical power	W_t	–	686.72	–	kW
Gross turbine mechanical power	W_{comp}	–	301.69	–	kW
Net shaft power	W_{shaft}	–	385.03	–	kW
Generator electrical output	W_{gen}	381	377.33	0.96	kW

6.3.6 System-Level Electrical Performance of the Hybrid Configuration

Following the independent reconstruction of the SOFC stack electrochemical performance (Section 6.3.3), the internal energy balance of the fuel cell (Section 6.3.4), and the thermodynamic modelling of the turbine–generator subsystem (Section 6.3.5), the final step in the cruise-condition analysis is the evaluation of the overall electrical efficiency of the integrated SOFC–GT system. The overall electrical efficiency of the integrated SOFC–GT system is evaluated using the methodology presented in Section 5.5.7.

Under cruise operating conditions, the total fuel input includes both the primary fuel supplied to the SOFC and the supplementary fuel injected into the combustor. Using the reconstructed total fuel mass flow rate and the adopted lower heating value of n-dodecane ($44{,}000\ kJ/kg$), the chemical energy input rate is determined. Substituting the previously calculated net electrical contributions of the SOFC stack and the gas turbine subsystem into the system efficiency relation yields an overall electrical efficiency of 70.02%. This value shows an error of only 0.24% from the ProMax reference efficiency of 69.8%, demonstrating strong agreement between the reconstructed thermodynamic model and the benchmark configuration. The close correspondence confirms that the coupling between electrochemical conversion and thermal energy recovery has been consistently captured, and that no energy imbalance propagates across subsystem boundaries. From a system-design perspective, this result verifies the internal coherence of the hybrid architecture under high-altitude cruise constraints and validates the adopted modelling framework across electrochemical, thermodynamic, and mechanical domains. Table 6-16 summarizes the overall electrical performance of the hybrid SOFC–GT system under cruise operating conditions.

Table 6-16 Overall hybrid system electrical performance at cruise condition.

Parameter	Symbol	Reference	Present Model	Error %	Unit
Total fuel mass flow rate	$\dot{m}$	–	0.03235	–	$\left(\frac{kg}{s}\right)$
Total chemical energy input	$\dot{Q}_{fuel}$	–	1423.4	–	kW
Total net electrical power	W_{net}	996.4	996.76	0.03	kW
Global electrical efficiency	η_{global}	69.8	70.02	0.24	$[-]$

6.3.7 Verification and Physical Consistency Assessment of the Hybrid Model

This section verifies the physical consistency of the reconstructed hybrid SOFC–GT model under cruise operating conditions. Using Eqs. (5-47)–(5-49), the calculated global electrical efficiency is 70.02%, compared with the ProMax reference value of 69.8%, corresponding to an error of 0.24%. This close agreement confirms that the reconstructed model provides a physically consistent representation of the integrated system. The remaining difference is mainly attributed to the simplified assumptions adopted for the turbine–generator subsystem.

6.3.8 Thermodynamic Hierarchy and Hybridization Insight

Although the hybrid SOFC–GT system achieves a fuel-to-electricity efficiency of approximately 70.3% at cruise altitude, the importance of this result lies not merely in the numerical value itself, but in how this efficiency is structurally constructed within the hybrid architecture. At the selected operating point, approximately 44% of the fuel chemical energy is converted directly into electricity through the electrochemical pathway of the SOFC stack. An additional ~27% is recovered through the gas turbine via thermal cascading of high-temperature exhaust gases. This distribution reveals a clear hierarchical structure: the SOFC functions as the primary conversion mechanism, while the turbine operates as a secondary, yet thermodynamically essential, recovery stage. Hybridization in this configuration therefore enhances system performance not by replacing the electrochemical pathway, but by structurally extending it. A counterfactual perspective further clarifies the role of integration. In the absence of the turbine subsystem, the system efficiency would collapse to approximately the standalone SOFC efficiency (~44%). The observed increase to nearly 70.3% therefore represents an absolute efficiency gain of roughly 27 percentage points attributable to bottoming-cycle integration. The percentage contributions are calculated by normalizing each electrical output with respect to the fuel chemical input based on LHV.
This quantifies the real thermodynamic contribution of hybridization and demonstrates that the turbine is not merely auxiliary but strategically embedded within the energy cascade.
From an internal performance standpoint, the relatively high electrochemical efficiency indicates that activation and ohmic voltage losses remain controlled at the selected current density. The system does not operate near limiting current constraints or severe concentration polarization. As a result, dominant irreversibilities are more likely concentrated in combustion processes, gas mixing, heat exchange interactions, and turbomachinery aerodynamic losses rather than intrinsic electrochemical degradation.

Figure 6-1 shows the hierarchical distribution of fuel chemical energy under cruise conditions, normalized with respect to fuel lower heating value (LHV) in order to isolate structural conversion hierarchy independent of absolute power scale.

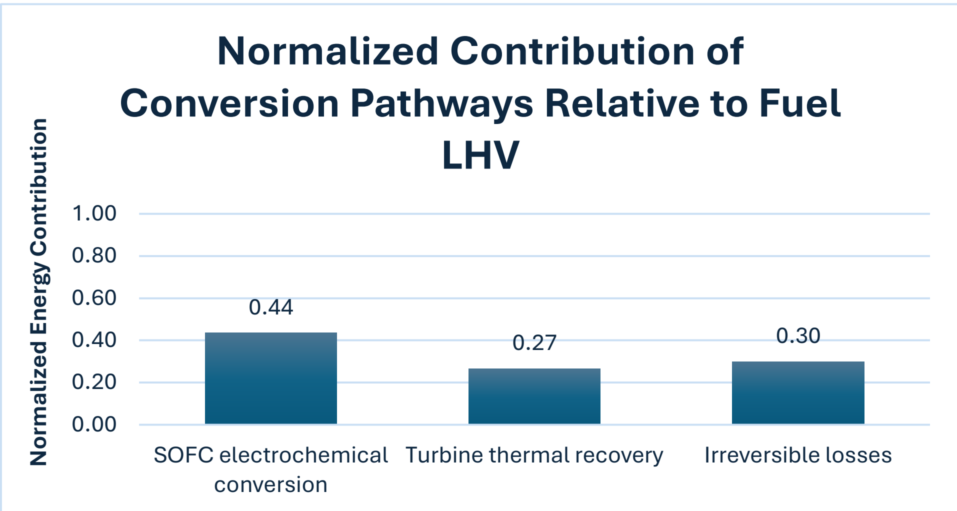

Figure 6-1 Hierarchical distribution of fuel chemical energy under cruise conditions, normalized with respect to fuel lower heating value (LHV).

As illustrated in Figure 6-1, the electrochemical pathway remains the dominant conversion mechanism, while turbine integration structurally elevates overall system efficiency through thermal cascading. The figure provides a normalized visualization of the internal energy hierarchy, clarifying the contribution of hybridization beyond simple numerical efficiency reporting. This layered structure demonstrates that the system is not electrochemical-limit constrained under cruise conditions; rather, the remaining improvement potential is largely associated with balance-of-plant losses and distributed thermodynamic irreversibilities. Consequently, future efficiency gains are more likely to emerge from enhanced thermal integration, turbomachinery refinement, and reduction of auxiliary losses than from further increases in stack voltage alone. The present configuration may therefore be interpreted as a thermodynamically coherent hybrid architecture in which electrochemical dominance is preserved while thermal recovery elevates overall system performance in a structurally optimized manner.

6.4 Comparative Performance Assessment

The reconstructed hybrid SOFC–GT model is compared with a reference configurations reported in the literature the ProMax-based model developed by Wilson et al. The comparison focuses on the global electrical efficiency obtained under comparable cruise operating conditions.

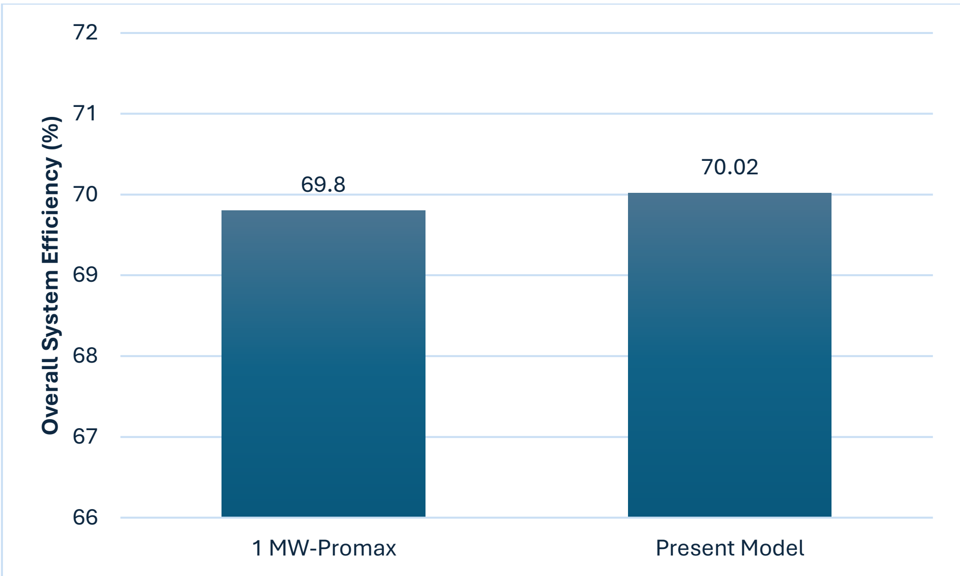

Figure 6-2 Comparison of the global electrical efficiency predicted by the present model with the ProMax reference (Wilson et al.)

As illustrated in Figure 6-2, the present model predicts a global electrical efficiency of 70.02%, compared with 69.8% for the ProMax reference model. The error from the ProMax result is only 0.24%, indicating excellent agreement between the reconstructed model and the reference simulation. The remaining difference is mainly attributed to the simplified turbine–generator representation adopted in the present model. Overall, the comparison demonstrates that the proposed model reproduces the expected system performance while remaining consistent with published reference studies. While Fig. 6-2 verify the reconstructed model against the primary reference configurations, a broader comparison with other published small-scale SOFC–GT systems is presented to evaluate whether the predicted efficiency remains consistent with the general performance trends reported in the literature.

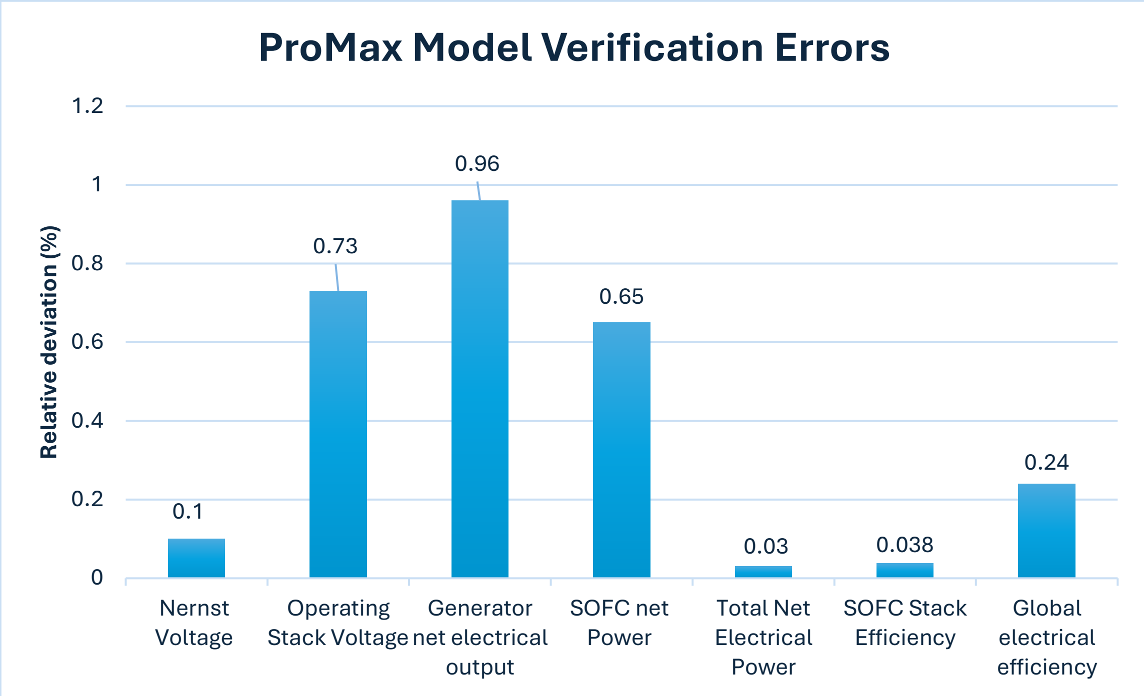

Figure 6-3 Error of key performance indicators relative to the ProMax reference configuration.

Figure 6-3 evaluates numerical robustness through error analysis relative to the ProMax reference configuration. All key performance indicators, including stack voltage, generator electrical output, total net electrical power, and global electrical efficiency, exhibit errors below 1%. The slightly higher error observed in generator output can be attributed to the assumption of constant isentropic efficiency and lumped mechanical losses, whereas the reference model may incorporate temperature-dependent or component-resolved loss formulations.

No parameter tuning or empirical correction factors were introduced to enforce agreement. The error magnitude lies within typical modeling uncertainty bounds reported in hybrid SOFC–GT simulation studies and confirms structural integrity of the integrated model. Overall, the comparative assessment demonstrates that the present cruise-altitude hybrid configuration preserves electrochemical dominance, achieves thermodynamically bounded turbine recovery, reproduces literature architectures with high numerical fidelity, and maintains predictive consistency across different scales. The results indicate that the model is structurally coherent, physically plausible, and architecturally balanced rather than numerically calibrated to a specific case.

6.5 Overall System Performance and Physical Interpretation

This chapter evaluated the verification and performance assessment of the developed SOFC–GT numerical framework using three representative hybrid configurations: the NASA baseline architecture, the modified Eelman configuration, and a 1 MW ProMax-based cruise operating case. The close agreement with published reference data demonstrates that the proposed methodology provides a physically consistent representation of coupled electrochemical and thermodynamic processes over different architectures and operating conditions. In addition to the verification results, the results showed the mechanisms responsible for the observed improvement in system performance. The increase in global electrical efficiency was not caused by an increase in the intrinsic electrochemical performance of the SOFC stack, which remained the dominant power-producing component throughout all operating conditions. Instead, the improvement resulted from a more effective utilisation of the available fuel energy through thermodynamic integration between the SOFC and the gas turbine.

The hybrid architecture recovered part of the high-temperature exhaust energy that would otherwise leave the system unused. Without consuming additional fuel, the recovered thermal energy was converted into approximately $377\ kW$ of additional electrical power through the turbine-generator subsystem. Consequently, the chemical energy supplied to the system was utilised more effectively, leading to higher overall fuel utilisation and a corresponding reduction in thermodynamic losses. This finding also explains the difference observed between the reference configurations. While the original NASA architecture achieved an overall electrical efficiency close to 64.7%, the reconstructed cruise-scale configuration reached approximately 70.02%. This improvement was mainly due to more effective thermal energy recovery, improved fuel utilisation, and better integration between the electrochemical and thermodynamic subsystems, rather than modifications to the SOFC electrochemistry itself.

The results also showed that hybridization should not be interpreted as the simple combination of two independent power-producing units. Instead, the gas turbine acts as a secondary energy recovery device, converting residual exhaust enthalpy into useful power and reducing the exergy that would otherwise be rejected to the environment. As a result, the hybrid configuration improves overall efficiency by reducing irreversible losses instead of increasing primary energy consumption. Overall, the results demonstrate that the proposed modelling framework combines numerical reliability with physical interpretability. In addition to reproducing published reference cases with errors below one percent, the model explains how energy is distributed, recovered, and utilised throughout the integrated SOFC–GT architecture. This capability makes the framework a robust platform for the analysis and future optimisation of hydrogen-fuelled hybrid propulsion systems for aerospace applications.

7. Conclusions

This thesis addressed the development and verification of a physics-based numerical model for the analysis of hybrid Solid Oxide Fuel Cell–Gas Turbine (SOFC–GT) systems intended for high-efficiency aerospace power generation. Unlike commercial simulation software, the proposed model was developed directly from the governing thermodynamic, electrochemical, and component performance equations, providing an independent engineering framework capable of describing the coupled behaviour of the complete hybrid system. The model integrates fuel processing, SOFC electrochemistry, combustion, heat exchangers, turbomachinery, and electrical generation within a unified numerical methodology.
The work began with a comprehensive review of fuel cell technologies and their applications in land, marine, and aerospace sectors. Particular attention was devoted to hybrid SOFC–GT architectures because of their capability to combine efficient electrochemical energy conversion with high-temperature waste-heat recovery. This review established the scientific background required to identify the most appropriate system architecture, modelling assumptions, and verification strategy adopted throughout the thesis.
Based on this foundation, a complete system-level numerical model was formulated using the conservation equations of mass, species, and energy together with electrochemical relations describing the SOFC stack and performance models for each auxiliary component. Rather than treating the components independently, the methodology represented the entire hybrid power plant as an integrated thermodynamic system in which the interaction between electrochemical conversion, thermal energy recovery, and mechanical power generation could be analysed simultaneously.

A major contribution of this work is the systematic verification methodology adopted for the developed model. Instead of validating the numerical implementation against a single reference, three independent benchmark configurations were selected to evaluate different aspects of the modelling framework. The first verification reproduced the NASA baseline SOFC–GT architecture and demonstrated that the developed equations accurately reconstructed the thermodynamic states, electrochemical operating conditions, and global electrical performance reported in the reference study. The second verification considered the modified hybrid configuration proposed by Eelman et al., where different fuel representation and thermal integration strategies were employed. The successful reproduction of this case demonstrated that the proposed methodology is sufficiently robust to accommodate changes in system architecture without requiring modifications to the underlying physical formulation. The third verification extended the analysis to a 1 MW SOFC–GT configuration operating under representative cruise conditions. This case required complete reconstruction of the gas path, electrochemical operating point, SOFC energy balance, turbine-generator coupling, and overall electrical performance. In addition to reproducing the published operating conditions, this verification provided a detailed thermodynamic interpretation of the energy conversion processes governing the hybrid system.

For all three verification cases, the predicted thermodynamic, electrochemical, and system-level performance parameters showed errors below 1% compared with the published reference data. This level of agreement confirms not only the numerical accuracy of the developed model but also its internal physical consistency, demonstrating that the governing conservation equations correctly describe the coupled interactions between all major system components. Beyond the verification process itself, the results provide important engineering insight into the mechanisms responsible for the high efficiency of hybrid SOFC–GT systems. The analyses demonstrate that the increase in global electrical efficiency does not originate from improvements in the intrinsic electrochemical performance of the SOFC stack. Instead, the higher efficiency is achieved through effective thermodynamic integration between the fuel cell and the gas turbine. The SOFC remains the primary power-producing component, while the gas turbine converts part of the high-temperature exhaust energy into additional electrical power, thereby increasing overall fuel utilisation. Under the representative cruise operating conditions investigated in this work, the verified model predicts a global electrical efficiency of approximately 70%, confirming the effectiveness of this integrated energy conversion strategy.

From a scientific perspective, the principal contribution of this thesis is therefore not only the development of a numerical model, but the establishment of a physically consistent and independently verified modelling framework capable of reproducing different SOFC–GT hybrid architectures using a common set of governing equations. The successful verification against three independent reference configurations demonstrates that the proposed methodology is sufficiently general for analysing hybrid systems operating under different fuels, layouts, and boundary conditions. Overall, the objectives established at the beginning of this research have been successfully achieved. A comprehensive literature review was completed, an independent numerical model was developed, its predictive capability was verified through three representative case studies, and the physical mechanisms governing hybrid SOFC–GT performance were systematically interpreted. The modelling framework developed in this thesis therefore provides a reliable engineering tool for future research, preliminary system design, and performance optimisation of advanced hydrogen-fuelled SOFC–GT hybrid systems for aerospace applications.

8. Bibliography

1. IPCC, *AR6 Synthesis Report: Climate Change 2023.* Intergovernmental Panel on Climate Change, 2023.
2. UNFCCC, *COP28 UAE Consensus: Official Outcome Documents.* UNFCCC, 2023.
3. Nunes, L.J., *The rising threat of atmospheric CO2: a review on the causes, impacts, and mitigation strategies.* Environments, 2023. **10**(4): p. 66.
4. Lackner, K.S., et al., *The urgency of the development of CO2 capture from ambient air.* Proceedings of the National Academy of Sciences, 2012. **109**(33): p. 13156–13162.
5. Ritchie, H.R., Max. *Global greenhouse gas emissions by sector*. 2020 19 March 2026]; Available from: https://ourworldindata.org/co2-and-greenhouse-gas-emissions.
6. Agency, I.E., *World Energy Outlook 2023,STEPS scenario.* 2023.
7. Kaya, Y.Ç. and H. Kaya, *Global Energy Policy: A Legal Perspective on Renewable Energy Initiatives.* Sustainability, 2025. **17**(9): p. 3991.
8. Mor, S., et al., *Kyoto protocol and Paris agreement: Transition from bindings to pledges–A Review.* Millennial Asia, 2024. **15**(4): p. 690–711.
9. Nations, U., *Kyoto protocol to the united nations framework convention on climate change.* 1998.
10. Grubb, M., *The Economics of the Kyoto Protocol,.* World Economics,, 2003. **vol. 4(3)**: p. pages 143–189.
11. Davies, P., *The Collapse of the Kyoto Protocol and the Struggle to Slow Global Warming. By DAVID G. VICTOR [Princeton, Princeton University Press, 2004, 224 pp, ISBN 0691120269, Paperback,£ 11.95, previously published in Hardback, 2001, 160 pp, ISBN 0691088705,£ 26.95].* Journal of Environmental Law, 2006. **18**(2): p. 328–330.
12. Agency, I.E., *World Energy Outlook 2023 , APS and STEPS scenarios.* 2023, International Energy Agency.
13. Masson-Delmotte, V., et al., *Climate change 2021: the physical science basis.* Contribution of working group I to the sixth assessment report of the intergovernmental panel on climate change, 2021. **2**(1): p. 2391.
14. Von Stein, J., *The international law and politics of climate change: Ratification of the United Nations Framework Convention and the Kyoto Protocol.* Journal of Conflict Resolution, 2008. **52**(2): p. 243–268.
15. Bhuiyan, M.M.H. and Z. Siddique, *Hydrogen as an alternative fuel: A comprehensive review of challenges and opportunities in production, storage, and transportation.* International Journal of Hydrogen Energy, 2025. **102**: p. 1026–1044.
16. Alreshidi, M.A., et al., *Hydrogen in transport: a review of opportunities, challenges, and sustainability concerns.* RSC advances, 2025. **15**(29): p. 23874–23909.
17. Höhne, N., et al., *The rules for land use, land use change and forestry under the Kyoto Protocol—lessons learned for the future climate negotiations.* environmental science & policy, 2007. **10**(4): p. 353–369.
18. Sethia, H. and A. Priyam, *Review on hydrogen fuel cells as an alternative fuel.* Next Energy, 2025. **9**: p. 100460.
19. Fu, Z., et al., *Fuel cell and hydrogen in maritime application: A review on aspects of technology, cost and regulations.* Sustainable Energy Technologies and Assessments, 2023. **57**: p. 103181.

20. O'hayre, R., et al., *Fuel cell fundamentals*. 2016: John Wiley & Sons.
21. EG&G Technical Services, I., *Fuel Cell Handbook* (Seventh Edition), ed. U.C.N. DE-AM26-99FT40575. 2004: U.S. Department of Energy Office of Fossil Energy National Energy Technology Laboratory 427.
22. Ebrahimi, M., et al., *A review on ionic liquids-based membranes for middle and high temperature polymer electrolyte membrane fuel cells (PEM FCs).* International journal of molecular sciences, 2021. **22**(11): p. 5430.
23. Barbir, F., *PEM fuel cells: theory and practice*. 2023: Academic press.
24. Yu, W.-L., et al., *Implementation of Accurate Parameter Identification for Proton Exchange Membrane Fuel Cells and Photovoltaic Cells Based on Improved Honey Badger Algorithm.* Micromachines, 2024. **15**(8).
25. Karami, N., *Control of a hybrid system based PEMFC and photovoltaic panels*. 2013, Universite d'Aix-Marseille, Ecole Doctorale en Mathematiques et Informatique ….
26. Maaruf, M., et al., *Advanced control strategies for fuel cell hybrid electric vehicles-A review.* Energy Conversion and Management: X, 2025: p. 101354.
27. Guo, Y.-F., H.-C. Chen, and F.-C. Wang, *The development of a hybrid PEMFC power system.* International Journal of Hydrogen Energy, 2015. **40**(13): p. 4630–4640.
28. Damo, U., et al., *Solid oxide fuel cell hybrid system: A detailed review of an environmentally clean and efficient source of energy.* Energy, 2019. **168**: p. 235–246.
29. Nikiforakis, I., S. Mamalis, and D. Assanis, *Understanding solid oxide fuel cell hybridization: a critical review.* Applied Energy, 2025. **377**: p. 124277.
30. Xu, J., et al., *Comprehensive thermodynamic performance evaluation of a novel dual-shaft solid oxide fuel cell hybrid propulsion system.* Aerospace, 2025. **12**(1): p. 59.
31. Andaloro, L., et al., *Study and design of a hybrid electric vehicle (Lithium Batteries-PEM FC).* International Journal of Hydrogen Energy, 2017. **42**(5): p. 3166–3184.
32. Dudek, M., et al., *Hybrid fuel cell–battery system as a main power unit for small unmanned aerial vehicles (UAV).* International journal of electrochemical science, 2013. **8**(6): p. 8442–8463.
33. Kerviel, A., et al., *An evaluation of turbocharging and supercharging options for high-efficiency fuel cell electric vehicles.* Applied Sciences, 2018. **8**(12): p. 2474.
34. Fattoruso, O., *Study and modelling of a fuel cell air supply system with turbocharger for a regional hybrid electric aircraft*. 2023, Politecnico di Torino.
35. Showers, S.O. and A.K. Raji, *State-of-the-art review of fuel cell hybrid electric vehicle energy management systems.* AIMS Energy, 2022.
36. Han, K., et al. *Optimization of energy management system for fuel-cell/battery hybrid power in unmanned aerial vehicle*. in *2019 22nd international conference on electrical machines and systems (ICEMS)*. 2019. IEEE.
37. *PEMFC System Controls: Transients, Load-Following And Degradation Minimization*. SEP 15, 2025; Available from: https://eureka.patsnap.com/report-pemfc-system-controls-transients-load-following-and-degradation-minimization.
38. Wang, X., et al., *Review and Outlook of Fuel Cell Power Systems for Commercial Vehicles, Buses, and Heavy Trucks.* Sustainability, 2025. **17**(13): p. 6170.

39. Pérez-Trujillo, J.P., et al., *Thermoeconomic comparison of a molten carbonate fuel cell and a solid oxide fuel cell system coupled with a micro gas turbine as hybrid plants.* Energy Conversion and Management, 2023. **276**: p. 116533.
40. Brouwer, J., *Hybrid Gas Turbine Fuel Cell Systems*. Gas Turbine Handbook.
41. McLarty, D., J. Brouwer, and S. Samuelsen, *Fuel cell–gas turbine hybrid system design part I: Steady state performance.* Journal of Power Sources, 2014. **257**: p. 412–420.
42. Leal, E.M., B.E.S. Silva, and A.M.L. Junior, *Analysis of a Hybrid Molten Carbonate Fuel Cell and Gas Turbine Cycle.*
43. Roberts, R.A., et al., *Dynamic simulation of carbonate fuel cell-gas turbine hybrid systems.* J. Eng. Gas Turbines Power, 2006. **128**(2): p. 294–301.
44. Lukas, M. and K. Lee, *Model-Based Analysis for the Control of Molten Carbonate Fuel Cell Systems.* Fuel Cells, 2005. **5**(1): p. 115–125.
45. Sundmacher, K., et al., *Molten carbonate fuel cells.* Wiley-VCH google schola Blomen, LJMJ/1993/Fuel Cell Systems/Plenum google schola 김범주/2009/5kW 용융탄산염 연료전지 (MCFC) 이젝터 설계 및 시험/한국수소및신에너지학회논문집, 2007. **20**(1): p. 31–37.
46. Chen, Z., et al., *Optimization Design of SOFC-GT Hybrid Power System for Aviation Application.* Energies, 2024. **17**(15): p. 3681.
47. Peyrani, G., et al., *Solid oxide fuel cells for aviation: A comparative evaluation against alternative propulsion technologies.* Etransportation, 2025. **24**: p. 100408.
48. Turner, C., *Integration of a microtubular solid oxide fuel cell into a mini-UAV: Design and simulation of power system architecture*. 2010, SAE Technical Paper.
49. Köhler, P., J. Hollmann, and S. Kabelac, *Solid Oxide Fuel Cell-Gas Turbine (SOFC-GT) Hybrid Engines for Aircraft Propulsion: Comprehensive Thermodynamic System Study and Analysis of High-Temperature Heat Exchangers for Heat Integration.* Available at SSRN 5497576, 2025.
50. Ferrari, M.L., L. Mantelli, and M. Pascenti, *Emulation tests of dynamics and control for a turbocharged SOFC system.* Applied Thermal Engineering, 2025. **258**: p. 124514.
51. Hohloch, M., A. Huber, and M. Aigner, *Analysis of operational strategies of a SOFC/micro gas turbine hybrid power plant.* Journal of Engineering for Gas Turbines and Power, 2018. **140**(8): p. 081703.
52. Run-Peng, Q., et al. *Comparative analysis of SOFC-MGT top-level and new bottom-level system performance*. in *E3S Web of Conferences*. 2021. EDP Sciences.
53. Yuan, Q., et al., *Performance analysis and optimization of SOFC/GT hybrid systems: a review.* Energies, 2024. **17**(5): p. 1265.
54. Cable, T.L. and S.W. Sofie, *A symmetrical, planar SOFC design for NASA's high specific power density requirements.* Journal of Power Sources, 2007. **174**(1): p. 221–227.
55. Alsamri, K., et al. *Dynamic modeling of Hydrogen SOFC/GT powered Aircraft with integration analysis*. in *AIAA SCITECH 2024 Forum*. 2024.
56. Braun, R., M. Gummalla, and J. Yamanis, *System architectures for solid oxide fuel cell-based auxiliary power units in future commercial aircraft applications.* 2009.
57. Azizi, M.A. and J. Brouwer, *Progress in solid oxide fuel cell-gas turbine hybrid power systems: System design and analysis, transient operation, controls and optimization.* Applied energy, 2018. **215**: p. 237–289.

58. Ferrari, M.L., M. Pascenti, and A. Abrassi. *Test rig for emulation of turbocharged SOFC Plants*. in *E3S Web of Conferences*. 2019. EDP Sciences.
59. Tsourapas, V., J. Sun, and A. Stefanopoulou. *Incremental step reference governor for load conditioning of hybrid fuel cell and gas turbine power plants*. in *2008 American Control Conference*. 2008. IEEE.
60. Mantelli, L., et al., *Fuel flexibility for a turbocharged SOFC system.* Energy Procedia, 2019. **158**: p. 1974–1979.
61. McLarty, D., J. Brouwer, and S. Samuelsen, *Hybrid fuel cell gas turbine system design and optimization.* Journal of Fuel Cell Science and Technology, 2013. **10**(4): p. 041005.
62. System, S.W.H.S.G.D. *Microtubular Cell Design, Integrated Planar (Segmented-Cell-In-Series) Design*. Available from: https://ebrary.net/203886/engineering/microtubular_cell_design.
63. Lin, W., J. Yuan, and B. Sundén. *Waste heat recovery system for fuel cell system*. in *International Green Energy Conference*. 2010.
64. Chinda, P. and P. Brault, *The hybrid solid oxide fuel cell (SOFC) and gas turbine (GT) systems steady state modeling.* International Journal of Hydrogen Energy, 2012. **37**(11): p. 9237–9248.
65. Köhler, P., J. Hollmann, and S. Kabelac, *Hydrogen-fueled Solid Oxide Fuel Cell-Gas Turbine (SOFC-GT) hybrid engines for aircraft propulsion: Comprehensive thermodynamic heat integration study.* Energy Conversion and Management: X, 2026: p. 101883.
66. Cao, Y., et al., *Waste heat recovery of a combined solid oxide fuel cell-gas turbine system for multi-generation purposes.* Applied Thermal Engineering, 2021. **198**: p. 117463.
67. Najafi, B., et al., *Exergetic, economic and environmental analyses and multi-objective optimization of an SOFC-gas turbine hybrid cycle coupled with an MSF desalination system.* Desalination, 2014. **334**(1): p. 46–59.
68. Minh, N.Q., *Solid oxide fuel cell technology—features and applications.* Solid State Ionics, 2004. **174**(1-4): p. 271–277.
69. Wang, Z., et al., *Evaluating fuel cell power systems for coastal and inland waterway vessels: Technical and economic perspectives.* Energy Conversion and Management, 2025. **323**: p. 119200.
70. Mehrabian, M.J., H. Hooshmand, and M.H.K. Manesh, *Ammonia-fueled solid oxide fuel cells for maritime applications: A 4E and risk assessment with multi-objective optimization and intelligent control.* Renewable Energy, 2025: p. 124432.
71. Di Micco, S., et al., *Multi-Fuel SOFC System Modeling for Ship Propulsion: Comparative Performance Analysis and Feasibility Assessment of Ammonia, Methanol and Hydrogen as Marine Fuels.* Journal of Marine Science and Engineering, 2025. **13**(10): p. 1960.
72. Van Biert, L., et al., *A review of fuel cell systems for maritime applications.* Journal of Power Sources, 2016. **327**: p. 345–364.
73. Van Veldhuizen, B., et al., *Solid oxide fuel cells for marine applications.* International Journal of Energy Research, 2023. **2023**(1): p. 5163448.
74. DNV, G., *Study on the use of fuel cells in shipping.* Retrieved from European Maritime Safety Agency (EMSA), 2017.

75. Li, Y., et al., *Life-Cycle Assessment of an Ammonia-Fueled SOFC Container Ship: Identifying Key Impact Drivers and Environmental Advantages over Diesel-Powered Vessels.* Journal of Marine Science and Engineering, 2025. **13**(10): p. 1873.
76. Dai, Y., et al., *A comprehensive 6E analysis and optimization of a SOFC-based trigeneration system model for marine applications.* Energy Conversion and Management: X, 2025: p. 101327.
77. Mashamba, T.M., et al., *Characteristic investigation of a novel aircraft SOFC/GT hybrid system under varying operational parameters.* Applied Sciences, 2024. **14**(8): p. 3504.
78. Gu, X., et al., *Analysis of a gas turbine auxiliary power unit system based on a fuel cell combustor.* International Journal of Hydrogen Energy, 2023. **48**(4): p. 1540–1551.
79. Seitz, A., et al., *Initial assessment of a fuel cell—gas turbine hybrid propulsion concept.* Aerospace, 2022. **9**(2): p. 68.
80. Waters, D.F., L.M. Pratt, and C.P. Cadou, *Gas turbine/solid oxide fuel cell hybrids for aircraft propulsion and power.* Journal of Propulsion and Power, 2021. **37**(3): p. 349–361.
81. Kotas, T.J., *The exergy method of thermal plant analysis*. 2012: Paragon Publishing.
82. Campanari, S. and M. Gazzani, *High efficiency SOFC power cycles with indirect natural gas reforming and CO2 capture.* Journal of Fuel Cell Science and Technology, 2015. **12**(2): p. 021008.
83. Ferrari, M.L., et al., *Hybrid systems based on solid oxide fuel cells: modelling and design*. 2017: John Wiley & Sons.
84. Kuterbekov KA, N.A., Bekmyrza KZ, Pavzderin NB, Kabyshev AM, Kubenova MM, Kabdrakhimova GD, Aidarbekov N., *Classification of Solid Oxide Fuel Cells.* Nanomaterials (Basel). 2022 Mar. **24;12(7):1059.**
85. Meadowcroft, A.D., et al., *Testing micro-tubular SOFCs in unmanned air vehicles (UAVs).* Electrochemical Society Transactions, 2013. **57**(1): p. 451–457.
86. Pratt, J.W. and L.E. Klebanoff, *Feasibility of the SF-BREEZE: a zero-emission, hydrogen fuel cell, high-speed passenger ferry.* 2016.
87. Di Micco, S., et al., *Advancing Sustainable Propulsion Solutions for Maritime Applications: Numerical and Experimental Assessments of a Methanol HT-PEMFC System.* Energies, 2025. **18**(19): p. 5119.
88. Balsamo, F., et al. *A case study on high-temperature fuel cells for hybrid electric ship propulsion*. in *2023 IEEE International Conference on Electrical Systems for Aircraft, Railway, Ship Propulsion and Road Vehicles & International Transportation Electrification Conference (ESARS-ITEC)*. 2023. IEEE.
89. Ahn, J., et al., *Molten carbonate fuel cell (MCFC)-based hybrid propulsion systems for a liquefied hydrogen tanker.* International Journal of Hydrogen Energy, 2018. **43**(15): p. 7525–7537.
90. Terzi, B., et al. *Modeling Methodology for PEM Fuel Cells as Auxiliary Power Units in Aircraft Applications*. in *AIAA AVIATION FORUM AND ASCEND 2025*. 2025.
91. Ji, Z., et al., *Thermodynamic performance comparisons of ideal brayton cycles integrated with high temperature fuel cells as power sources on aircraft.* Sustainability, 2023. **15**(3): p. 2805.
92. Kazula, S., S. de Graaf, and L. Enghardt, *Review of fuel cell technologies and evaluation of their potential and challenges for electrified propulsion systems in*

commercial aviation. Proceedings of Global Power and Propulsion Society, 2022: p. 1–13.

93. Freeh, J.E., J.W. Pratt, and J. Brouwer. *Development of a Solid-Oxide Fuel Cell/Gas Turbine Hybrid System Model for Aerospace Applications*. in *ASME Turbo Expo 2004: Power for Land, Sea, and Air*. 2004.
94. Wilson, J.A., et al., *Hybrid solid oxide fuel cell/gas turbine model development for electric aviation.* Energies, 2022. **15**(8): p. 2885.
95. Wilson JA, W.Y., Carroll J, Raush J, Arkenberg G, Dogdibegovic E, Swartz S, Daggett D, Singhal S, Zhou X-D., *Hybrid Solid Oxide Fuel Cell/Gas Turbine Model Development for Electric Aviation.* Energies, 2022. **15(8):2885**.